

UNIVERSITÀ
DEGLI STUDI
DI PADOVA

Sede Amministrativa: Università degli Studi di Padova

Dipartimento di Biologia

CORSO DI DOTTORATO DI RICERCA IN: BIOSCIENZE E BIOTECNOLOGIE
CURRICULUM: BIOLOGIA CELLULARE
CICLO: XXIX

PHARMACOLOGY, BIOCHEMISTRY AND BIOMEDICAL APPLICATIONS OF PLANT STILBENES

Coordinatore: Ch.mo Prof. Paolo Bernardi

Supervisore: Dr. Mario Zoratti

Dottorando: Martina La Spina

Ad Antonio

Contents:

Riassunto **1**

Summary **7**

Introduction **13**

Chapter 1: Amino acid carbamates as prodrugs of Resveratrol **23**

Chapter 2: Synthesis and evaluation as prodrugs of hydrophilic carbamate ester analogues of Resveratrol **35**

Chapter 3: Pharmacokinetics and tissue distribution of Pterostilbene in the rat **49**

Chapter 4: New natural amino acid-bearing prodrugs boost Pterostilbene's oral pharmacokinetic and distribution profile **65**

Chapter 5: Transcription factor EB is a crucial transducer of the biomedical activity of the natural compound Pterostilbene **107**

Chapter 6: Pterostilbene partially rescues the phenotype of Collagen VI dystrophic zebrafish morphants **139**

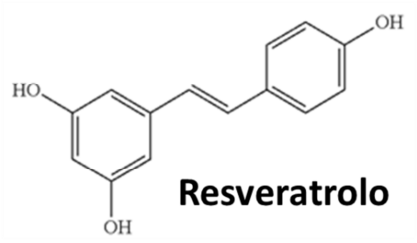
Chapter 7: Pterostilbene improves cognitive performance in aged rats: a mechanistic pilot study **153**

Abbreviations **175**

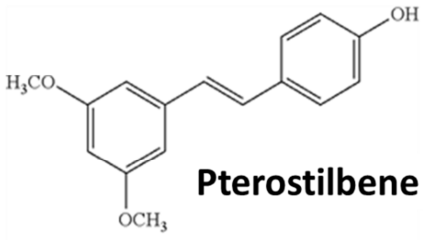
Ringraziamenti **179**

Riassunto:

Questa tesi riguarda la ricerca che ho condotto su aspetti della farmacologia e delle attività biologiche di due stilbeni, il Resveratrolo (Rv) e lo Pterostilbene (Pt), componenti polifenoliche principali rispettivamente della vite e dei mirtilli.



Resveratrolo



Pterostilbene

Negli ultimi anni queste due molecole hanno attirato l'attenzione della comunità scientifica grazie alle loro attività biologiche di rilievo per molte settori della medicina. Numerosi studi descrivono le loro azioni protettive nei confronti di sindromi metaboliche, contro il cancro e la neurodegenerazione. Al giorno d'oggi, questi effetti non vengono attribuiti tanto alle loro proprietà antiossidanti quanto alla loro capacità di modulare, direttamente o indirettamente, l'attività di proteine-chiave in vie di segnalazione intracellulare tra loro interconnesse. Un punto importante è che non sono stati riportati effetti collaterali negativi del loro utilizzo.

Nonostante questi aspetti positivi, Rv e Pt presentano dei punti deboli. Entrambi sono soggetti ad un intenso metabolismo di fase II che ne limita significativamente la biodisponibilità. Inoltre, mentre molto lavoro è stato condotto con il fine di elucidare i meccanismi di azione del Rv, quelli dello Pt rimangono ancora in gran parte da chiarire.

Durante il mio corso di dottorato, mi sono occupata di entrambe queste problematiche. Descrivo di seguito:

1) I tentativi effettuati per aumentare la biodisponibilità del Rv e dello Pt
2) Gli studi dei processi intracellulari innescati dallo Pt e la valutazione del suo potenziale terapeutico in due modelli *in vivo*

1) Per far fronte al problema della scarsa biodisponibilità sono stati adottati diversi metodi. Il mio gruppo di ricerca è ricorso alla produzione di pro-farmaci.

Nel caso dei polifenoli, un buon pro-farmaco implica l'utilizzo di gruppi protettori per mascherare i gruppi ossidrilici tipici di queste molecole e per evitare le modifiche metaboliche da parte degli enzimi coniugativi di fase II. Tali sostituenti, chiamati "pro-moieties", sono legati chimicamente alla struttura stilbenica in modo reversibile nelle condizioni fisiologiche d'impiego. Essi assumono particolare importanza per l'assorbimento dei composti, mentre la tipologia del legame è cruciale affinché le molecole attive vengano rigenerate con cinetiche adeguate.

Noi abbiamo voluto creare dei pro-farmaci da somministrare oralmente. Pertanto essi dovevano essere relativamente stabili nel tratto gastro-intestinale e più labili negli altri compartimenti biologici (fluidi corporei e organi).

Quando ho iniziato la mia esperienza nel gruppo di ricerca del Dott. Mario Zoratti, erano stati sintetizzati dei derivati del Rv come esteri carbammici N,N-bisostituiti recanti come sostituenti (pro-moieties) PEG 350 o gruppi glicosidici. Questi pro-farmaci aumentavano la scarsa solubilità in acqua del composto fenolico, ma si sono rivelati troppo stabili in ambiente fisiologico per essere utilizzati come pro-drugs. Abbiamo quindi deciso di creare dei derivati carbamoilici N-monosostituiti che si prevedeva sarebbero stati meno stabili. Un aspetto importante è che questa struttura chimica è essenzialmente stabile in acido, mentre può essere idrolizzata a pH vicino alla neutralità o basico. In un primo set di composti si sono utilizzati come pro-moieties degli aminoacidi. Oltre ad aumentare la solubilità in acqua, ci si aspettava che gli aminoacidi potessero essere riconosciuti da specifici sistemi di trasporto espressi a livello degli enterociti favorendo l'assorbimento intestinale della molecola. In un altro gruppo di derivati carbamoilici N-monosostituiti, tutti e tre, due o uno solo degli ossigeni fenolici del Resveratrolo sono stati decorati con gruppi poliossidrilati (diidrossipropil o 6-deossigalattosil). In questo caso si sperava che i trasportatori di zuccheri potessero intervenire per facilitarne l'assorbimento attraverso l'epitelio intestinale. Come ci si attendeva, tutti i composti sintetizzati venivano idrolizzati con cinetiche compatibili con la loro utilizzazione come pro-drugs. L'assorbimento dopo somministrazione orale invece è risultato essere insoddisfacente, senza alcuna evidenza di un coinvolgimento di traslocatori di membrana. Il Rv galattosilato non ha raggiunto la circolazione sistemica in nessun caso. I risultati migliori sono stati ottenuti con i derivati amminoacidici mono-sostituiti. Ipotizziamo quindi che la struttura estesa e tripartita dei prodrugs con protezione completa interferisca con il

riconoscimento ed il trasporto da parte dei sistemi di membrana. Tutte le procedure sintetiche, la caratterizzazione e la valutazione farmacocinetica di queste famiglie di composti sono già state pubblicate. Gli articoli relativi sono inclusi in questa tesi come capitoli 1 e 2.

Dopo aver completato il lavoro coi pro-farmaci del Rv, ho iniziato un nuovo progetto riguardante lo Pt. Questo ha rappresentato il principale tema delle ricerche del mio programma di PhD.

Poiché lo Pt era stato poco studiato da un punto di vista farmacologico, ne abbiamo dapprima valutato la distribuzione nel sangue e negli organi (capitolo 3). Abbiamo quindi messo a punto un metodo per la quantificazione di questa molecola e suoi metaboliti negli organi di ratto. Il protocollo che abbiamo sviluppato ha permesso di preservare la stabilità del composto e di ottenere un'estrazione quantitativa dello Pt e dei suoi metaboliti dalle matrici biologiche.

Le analisi HPLC/UV hanno rivelato che, in seguito ad una somministrazione singola di una dose pari a 88µmoli/Kg di peso corporeo, i livelli di Pt in diversi organi erano maggiori rispetto a quelli riscontrati nel sangue, raggiungendo valori nell'ambito di varie nmoli/gr (µM). Inoltre, lo Pt-4'-solfato è stato identificato come la principale specie metabolica. I suoi livelli erano più alti rispetto a quelli dello Pt in tutti gli organi presi in considerazione tranne che nel cervello. Alla luce di questi risultati, abbiamo lavorato ulteriormente per cercare di limitare le modificazioni metaboliche da parte degli enzimi di fase II.

Ho quindi sfruttato l'esperienza acquisita dal lavoro con i pro-farmaci del Rv e in collaborazione con il gruppo di ricerca della Prof. Paradisi del Dipartimento di Scienze Chimiche dell'Università di Padova, abbiamo sintetizzato e caratterizzato una serie di derivati dello Pt recanti amminoacidi come pro-moieties, collegate all'ossidrile in posizione 4' tramite un legame carbammico mono-sostituito. Le cinetiche di idrolisi di questi composti sono risultate adatte per il loro utilizzo. I derivati con catene laterali idrofobiche si sono distinti per gli elevati livelli di Pterostilbene rigenerato nel sangue dopo somministrazione intra-gastrica ai ratti. Abbiamo pertanto selezionato il più promettente tra questi composti e ne abbiamo controllato la distribuzione negli organi, seguendo lo stesso protocollo utilizzato per lo Pt. In questo caso, il pro-farmaco *per se* è stato identificato come la specie predominante in tutti gli organi eccetto che nel cervello, ma soprattutto, i livelli di Pt rilasciati sono risultati notevolmente maggiori, e

quelli di solfato minori, se paragonati a quelli ottenuti somministrando la molecola originaria (capitolo 4).

2) Come accennato in precedenza, i meccanismi intracellulari alla base degli effetti benefici dello Pt non sono stati ancora completamente delucidati. Alcune ricerche suggeriscono che le sue proprietà potrebbero essere attribuite all'induzione dell'autofagia. Ho quindi deciso di indagare questo aspetto (capitolo 5).
   L'autofagia è una via di degradazione la cui errata regolazione è associata a varie condizioni patologiche. Il Prof. Ballabio ed i suoi collaboratori hanno dimostrato che questo processo è regolato principalmente dal Fattore di Trascrizione EB (TFEB), inibito da mTORC1. Ho quindi voluto verificare gli effetti dello Pt su questo fattore di trascrizione. Ho dimostrato che questo polifenolo è in grado di stimolare l'attività di TFEB inducendo la sua migrazione nel nucleo e promuovendo la sua espressione. In accordo con quanto osservato, lo Pt ha provocato un aumento della lipidazione della proteina LC3 e dei livelli di espressione di alcuni geni lisosomiali target di TFEB. È stata valutata anche l'efficacia dei due metaboliti principali dello Pt, Pt-4'-solfato e DiidroPt, poiché essi rappresentano le specie principali ritrovate in circolo dopo somministrazione dello Pt. Mentre il primo composto è risultato essere inerte, il secondo si è mostrato attivo come lo Pt, ma a concentrazioni più alte.
   Ulteriori studi sono stati effettuati per esplorare le vie di segnalazione a monte di questi fenomeni. Misurazioni basate sull'utilizzo di sonde FRET hanno messo in evidenza che lo Pt incrementa la concentrazione di cAMP e attiva CREB. Come riportato in precedenti lavori, questo nucleotide ciclico può indurre indirettamente l'attivazione dell'AMPK, noto antagonista di mTORC1. La stimolazione di questo asse di segnalazione cellulare potrebbe quindi essere alla base dell'attivazione del TFEB. In accordo con questa ipotesi, abbiamo osservato una riduzione dell'attività chinasica di mTORC1. Trattamenti farmacologici volti ad aumentare le concentrazioni di cAMP o attivare l'AMPK si sono tuttavia rivelati meno efficaci dello Pt indicando che questo polifenolo induce la migrazione di TFEB al nucleo modulando diverse vie di segnalazione cellulare. La traslocazione nucleare di TFEB, oltre ad essere sotto il controllo di mTORC1, può anche essere regolata dalla Calcineurina. Di recente, è stato dimostrato che questa fosfatasi può essere attivata da ROS esogeni ed endogeni. Nel contesto di queste ricerche, ho evidenziato che lo Pt aumenta la produzione mitocondriale di queste specie e che questo fenomeno è correlato alla migrazione del

TFEB. Alla luce di ciò, è possibile ipotizzare che questa rappresenti una via alternativa attraverso la quale lo Pterostilbene influenza la localizzazione subcellulare del fattore di trascrizione (capitolo 5).

Lo stabilirsi dell'azione pro-autofagica dello Pt in cellule in coltura mi ha spinto a saggiare il suo potenziale terapeutico per il trattamento delle distrofie muscolari da carenza di Collagene VI. Queste malattie sono caratterizzate principalmente dall'accumulo di mitocondri non funzionali. Concomitanti difetti del processo autofagico aggravano ulteriormente le condizioni patologiche e conducono alla morte di tipo apoptotico delle miofibrille.

Come indicato dalla letteratura scientifica, l'utilizzo di un morfolino antisenso è attualmente la strategia migliore per ottenere un fenotipo marcato di distrofie muscolari da carenza di Collagene VI in zebrafish. Abbiamo quindi iniettato specifici oligonucleotidi antisenso diretti contro l'esone 9 dell'mRNA codificante per il Collagene VI nelle uova fecondate di tali pesci. In questo modo abbiamo indotto una delezione "in frame" della regione N-terminale del dominio a tripla elica della molecola di Collagene VI e una profonda alterazione della struttura delle fibre muscolari.

I dati che ho ottenuto indicano che il trattamento con lo Pt induce un recupero pari a più del 30% nella struttura delle fibre muscolari ed un notevole aumento dell'attività motoria. Questa parte del progetto è stata svolta in collaborazione con il Prof. Bernardi e il Dott. Marco Schiavone del Dipartimento di Scienze Biomediche dell'Università di Padova. Nonostante i nostri risultati non dimostrino direttamente che il miglioramento delle condizioni patologiche sia dovuto all'induzione dell'autofagia, è plausibile che la stessa serie di eventi che si verificano *in vitro* possano aver luogo anche *in vivo*. A supporto di questa ipotesi, abbiamo verificato che lo Pt è in grado di aumentare i livelli di una proteina mCherry la cui espressione è posta sotto il controllo di elementi influenzati dal cAMP (CRE) in una linea transgenica reporter di zebrafish (questo modello è stato generato dalla Dott.ssa Patrizia Porazzi e dalla Prof.ssa Natascia Tiso del Dipartimento di Biologia dell'Università di Padova). Tali fenomeni necessitano di essere ulteriormente approfonditi (capitolo 6).

Infine, durante il mio percorso di dottorato, ho preso parte ad un altro progetto ancora in corso nel mio laboratorio di ricerca. Le analisi farmacocinetiche condotte in ratti hanno riportato che lo Pt è particolarmente abbondante nel cervello. Questa evidenza è in linea con diversi studi che dimostrano la capacità del polifenolo di migliorare le

prestazioni di animali anziani in test comportamentali. I meccanismi molecolari alla base di questi effetti sono stati poco caratterizzati anche in questo contesto. Il lavoro che ho condotto *in vitro*, e confermato in zebrafish, dimostra che lo Pt è in grado di indurre un aumento di cAMP attivando CREB. È stato dimostrato che questo fattore di trascrizione svolge un ruolo cruciale per il consolidamento della memoria perché in grado di promuovere la neurogenesi in soggetti adulti a livello del giro dentato, una parte dell'ippocampo. La memoria, insieme ad altre funzioni cognitive, peggiora notevolmente con l'invecchiamento.

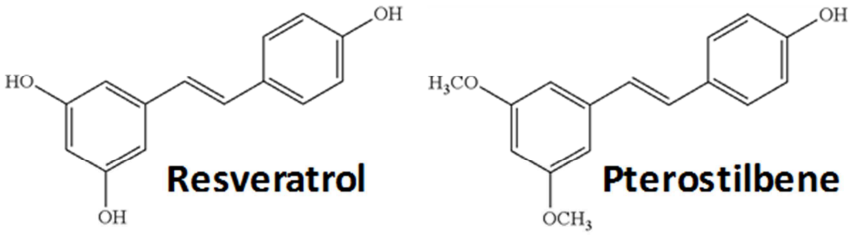
Alla luce di ciò, in collaborazione con la Prof.ssa Nicoletta Berardi ed il gruppo di ricerca del Dott. Alessandro Sale (Istituto di Neuroscienze - Pisa), abbiamo messo a punto un lavoro sperimentale volto a valutare cambiamenti molecolari nel giro dentato e nell'ippocampo in seguito ad un eventuale miglioramento cognitivo in ratti anziani da parte dello Pt (capitolo 7).

I risultati che abbiamo ottenuto hanno confermato che, dopo somministrazione cronica di questo composto, gli animali dimostrano un miglioramento della memoria. Inoltre, nonostante la statistica necessiti di essere ampliata aggiungendo più individui, sia analisi Western blot che RT-qPCR suggeriscono che tale trattamento ha indotto una up-regolazione di CREB. Allo stesso tempo, è stato misurato un aumento della massa mitocondriale. Questi effetti sono più evidenti a livello del giro dentato piuttosto che nella parte restante dell'ippocampo e suggeriscono fortemente il verificarsi di processi di rimodellamento neuronale. Nonostante ciò, non sono state riportate differenze nei livelli di PSD95. Per le prossime analisi saranno presi in considerazione marker diversi di plasticità sinaptica.

In conclusione, le ricerche che ho condotto hanno permesso di delineare uno dei meccanismi responsabili delle proprietà dello Pt e di incrementare la sua biodisponibilità. Pertanto, essi potrebbero esse utili per lo sviluppo di futuri trattamenti terapeutici o preventivi.

Summary:

This thesis reports the research I conducted on aspects of the pharmacology and biological activities of two natural stilbenes, Resveratrol (Rv) and Pterostilbene (Pt), major polyphenolic components of grapevines and blueberries respectively.



Over the years, these two molecules have drawn attention from the scientific community thanks to their beneficial bioactivities, relevant for many areas of health care. Numerous papers describe their protective roles against the metabolic syndrome, cancer development and neurodegeneration. These striking effects nowadays are not exclusively attributed to their redox properties but also to their capacity to modulate, directly or indirectly, the activities of key proteins of interconnected cellular signalling networks. Importantly, no noxious side effects have been reported.

However, in spite of their positive features, Rv and Pt are not free of shortcomings. They are subjected to an intensive phase II metabolism, largely limiting their bioavailability. Moreover, while much research has been carried out to elucidate the molecular mechanisms of action of Rv, those of Pt still largely remain to be established.

During my PhD program, I addressed both these themes. I describe below:

1) the attempts to increase the bioavailability of Rv and Pt
2) my investigations on intracellular processes affected by Pt as well as the demonstration of its therapeutic potential in two different *in vivo* models

1) A variety of approaches has been developed to overcome the poor bioavailability of many drugs. My research group turned to the development of prodrugs for oral administration.

   In the case of polyphenols, a useful prodrug implies the use of protecting groups to mask the characteristic hydroxyl groups and to avoid metabolic transformations by

phase II conjugative enzymes. These substituents, technically defined as pro-moieties, are attached to the backbone of the molecule through a chemical bond which can be broken in the relevant physiological environment.

The choice of the pro-moiety is important for the process of absorption from the intestinal tract. The type of linkage is crucial to achieve "cargo" regeneration with appropriate kinetics. We created prodrugs for oral administration. Thus, they ought to exhibit relative stability in the gastro-intestinal tract and lability in other biological compartments (body fluids and organs).

When I joined the group of Dr. Mario Zoratti, N,N-disubstituted carbamoyl derivatives of Rv bearing a PEG 350 or a sugar pro-moiety had been created. Although they increased the poor water solubility of the natural compound, these prodrugs were too stable under physiological conditions. Thus, we moved to the N-monosubstituted carbamoyl bond, expected to be less stable, for new prodrugs. Importantly, this type of chemical bond is essentially stable in acid, while it can be more easily lysed at neutral or basic pH values. A first set of compounds incorporated amino acids as pro-moieties. We hypothesized that in addition to increasing water solubility, amino acids might be recognized and transported by specific carrier systems, expressed in the enterocytes, and thus favor the intestinal absorption of the molecules. In another set of N-monosubstituted carbamoyl derivatives polyhydroxylated groups (dihydroxypropyl or 6-deoxygalactose) were attached to all three, two or one phenolic oxygen(s) of Rv. In this case, the hope was that sugar transporters might intervene to facilitate absorption through the intestinal epithelium. All synthetized compounds displayed hydrolysis kinetics suitable for their use as prodrugs. However, absorption after oral administration to rats turned out to be rather unsatisfactory, with no evidence of an involvement of membrane carriers. In no case did galactosylated Rv derivatives reach the bloodstream of rats. The best results were obtained by administering mono-substituted aminoacid derivatives. We speculate that the extended, three-pronged structure of the fully protecting prodrugs might interfere with recognition and transport. All synthesis procedures and the characterization and pharmacokinetic evaluation of these families of compounds have been already published. The papers are included in this thesis as chapters 1 and 2.

Once completed the assessment of Rv prodrugs, I started a new research project involving Pterostilbene, a more compact and possibly more effective compound than Resveratrol. This represented the main theme of my PhD program investigations.

As Pt was still poorly defined from a pharmacological point of view, we first evaluated its distribution in blood and organs after oral administration (see chapter 3). Thus, we developed an appropriate method for the quantification of the molecule and its metabolites in organs after administration to rats. The resulting protocol preserves stability and allows the quantitative extraction and clarification from biological matrices of Pt itself and its metabolites, and their quantitative analysis by HPLC/UV. We used this method to determine the levels of these compounds in the blood and several other organs as a function of time after administration as a single intra-gastric dose of 88μmoles/kg of body weight. Pterostilbene levels in several organs turned out to be much higher than those measured in blood, reaching nmoles/gr (μM)-range concentrations. Moreover, Pt-4'-Sulfate was identified as the major metabolic species. Its levels were higher than those of Pt in all tissues examined except the brain. In light of this, we next aimed to prevent metabolic modifications by phase II conjugative enzymes.

I exploited the experience derived from the work with the prodrugs of Rv and in collaboration with the research group of Prof. Paradisi of the Department of Chemical Sciences of the University of Padua, we developed and characterized a collection of Pt prodrugs bearing amino acids as pro-moieties, linked to the Pt 4'-OH via an N-monosubstituted carbamate ester group. The rates of hydrolysis of all compounds fell in a range suitable for their use. Derivatives with hydrophobic aminoacid side chains were notable for the high levels of Pterostilbene they regenerated in blood after intra-gastric administration. We selected the most promising one and we measured its levels in rat organs, following the same methodology developed for Pterostilbene. This time, the pro-drug itself was the major specie measured in all organs considered (except the brain) but, most importantly, the levels of (regenerated) Pterostilbene were drastically increased and those of its sulfate decreased in comparison with the administration of the polyphenol as such (see chapter 4).

2) As mentioned above, the intracellular processes underlying Pt benefits are still largely undefined. Several papers suggest that the induction of autophagy may contribute importantly. I decided to investigate this aspect.

Autophagy is a catabolic pathway whose dysregulation is associated with various pathological conditions. As discovered by Prof. Ballabio and co-workers it is mainly controlled by transcription factor EB (TFEB), normally inhibited by mTORC1. Thus, I

evaluated the effect of Pt on the autophagy master regulator. We demonstrated that this polyphenol stimulates TFEB activity by promoting its translocation to the nucleus as well as its expression. Accordingly, Pt induced an increase of LC3B protein, an autophagy marker, and an up-regulation of TFEB lysosomal target genes. These investigations have been extended to two Pt major metabolites, Pt-4'-Sulfate and DiHydroPt, as they are the main species formed upon ingestion of the natural compound. Interestingly, while the former was ineffective, the reduced form showed an activity similar to that of the parent compound but required higher concentrations.

Further studies have been carried out to clarify the upstream signalling cascade. FRET-sensor based measurements have shown that Pt is able to modestly increase the concentration of cAMP, followed by the activation of CREB. This cyclic nucleotide has been previously reported to indirectly activate AMPK, a well-recognized mTORC1 antagonist. Thus, the enhancement of this cellular axis may be responsible for the activation of TFEB. Accordingly, we observed a reduction of the activity of the mammalian target of the rapamycin. However, pharmacological interventions expected to drastically increase cAMP and AMPK activity were less effective than Pt, suggesting that this phenolic compound promotes TFEB nuclear migration by modulating more than one signalling pathway. In addition to mTORC1 inhibition, the activation of TFEB is mediated by Calcineurin. Recently, it has been demonstrated that both endogenous and exogenous ROS may promote the activity of this phosphatase.

We observed in *in vitro* studies with cultured cells that indeed Pt increased the production of these species by mitochondria and that this phenomenon is related to TFEB migration. In light of this, it is possible to speculate that this may represent an alternative way through which this phenolic compound perturbs TFEB intracellular localization (see chapter 5).

The establishment of the capability of Pt to induce autophagy in cultured cells led me to test Pt as a potential therapeutic treatment for Collagen VI (ColVI) muscular dystrophies. These disorders are mainly characterized by the presence of dysfunctional mitochondria. The concomitant deficiency of the autophagic process results in the exacerbation of the pathological conditions since the apoptotic death of myofibers occurs.

As known from the literature, the use of an antisense morpholino is nowadays the best strategy to obtain zebrafish animal models with a strong phenotype of ColVI-related

muscle dystrophy. Therefore, we injected into fertilized eggs a designed oligonucleotide, specifically directed against the ColVI exon 9 splicing region. This results in a frame-shift deletion of the N-terminal region of the ColVIa1 triple helical domain and therefore in a strong impairment of the organization of the muscular fibers.

The data I have obtained using this model indicate that Pt treatment induces a recovery of muscular structure by more than 30%, as well as a clear recovery of motor activity.This part of the project has been carried out in collaboration with Prof. Paolo Bernardi and Dr. Marco Schiavone of the University of Padua. Although these results do not provide evidence that the amelioration of the dystrophic phenotype is due to the induction of autophagy, it is credible to suppose that the same cascade of events enhanced *in vitro* by Pt may be relevant also *in vivo*. Supporting this hypothesis, Pt provoked a significant increase of a mCherry protein, whose expression is under control of cAMP responsive elements (CRE) in a zebrafish transgenic reporter (this model has been generated by Dr. Patrizia Porazzi and Prof. Natascia Tiso of the University of Padua). Further investigations need to be performed (see chapter 6).

Finally, during my graduate training I have also participated in another project still ongoing in my research laboratory. The pharmacokinetic study we performed in rats showed that Pt was particularly abundant in the brain. This observation is consistent with several papers showing a role of this phenolic compound in ameliorating performance of old rodents in behavioral tests. However, also in this context, the mechanisms accounting for these effects have been poorly characterized. My *in vitro* data, confirmed later in zebrafish, suggest that Pt may activate CREB following an increase of cAMP. This transcription factor has been demonstrated to play a crucial role in memory consolidation as it promotes neurogenesis in the dentate gyrus, a sub-area of the hippocampus, in adult individuals. Memory, among other functions, undergoes deterioration in old age.

In light of this, we set up an experimental work (see chapter 7), in collaboration with Prof. Nicoletta Berardi and the research group of Dr. Alessandro Sale, aimed to evaluate the molecular changes in the dentate gyrus and the hippocampus related to the recovery of cognitive impairments in old rats by Pt, if any. The results confirmed that after chronic administration of Pt aged animal presented a remarkable improvement in memory-related behavioral tasks. Moreover, although statistics need to be improved by adding more animals, Western blot and gene expression analyses

suggest that the treatment up-regulates the activity of transcription factor CREB. An increase of mitochondrial mass has been also measured. These effects were more evident in the dentate gyrus if compared to the remaining hippocampus and strongly support the occurrence of neuronal remodeling processes. However, no differences in PSD95 levels have been observed. Further markers of synaptic plasticity will need to be taken into account in future investigations.

Concluding, the studies I carried out have outlined one of the mechanisms accounting for the striking properties of the Pt, characterized its organ pharmacokinetics in the rat and allowed to boost its bioavailability. Thus, they may be helpful for the development of Pt-based therapeutic/preventive treatments.

Introduction

Polyphenols are natural compounds synthesized by plants as secondary metabolites as they confer protection against a variety of stressful conditions such as UV radiations, pathogen infections, parasites, and herbivorous predators [1-3]. They are defined, as the name suggests, by the presence of multiple hydroxyl groups bound to aromatic structures (generally phenyl rings). The term is often loosely applied also to mono-phenols of plant origin (e.g., Pterostilbene).

According to their chemical structure, polyphenols can be divided in different classes, some of which are exemplified in **Fig.1** [3-6].

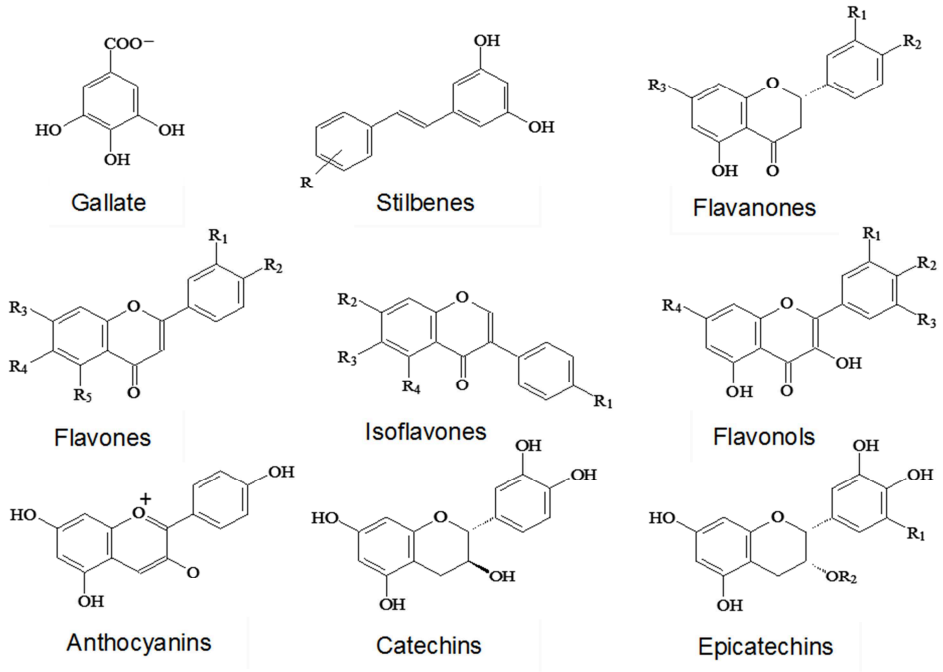


Fig.1: Some of the most common polyphenol families found in plants.

Polyphenols are widely distributed in a variety of foods typical of the human diet such as fruits, vegetables, spices, herbs and extracts/beverages derived from them, e.g. tea, and contribute to their organoleptic properties [5, 7-10].

Multiple lines of research have established that these molecules may prevent the onset of several human pathological conditions as well as hinder their progression [11-18]. A short and partial list of the major health problems includes several cancers, diabetes and the metabolic syndrome, cardiovascular dysfunctions, inflammation in its various manifestations (e.g. rheumatoid arthritis, inflammatory bowel disease), neurodegeneration,

cognitive decline in aging, *H. pylori*-linked gastric disorders, allergy. Importantly, no toxic effects have been associated to their consumption. Their pharmacology is complicated by the extensive metabolism they undergo in enterocytes and the liver (largely sulfation and glucuronidation by Phase II metabolism enzymes) and also in the gut, due to the reactions carried out by the intestinal flora.

My PhD studies focused on two of these molecules, Resveratrol (Rv) and its di-methylated analogue Pterostilbene (Pt), belonging to the stilbene family.

Resveratrol has been mainly found in grapes. Its fame may be ascribed to the so-called "French paradox", which emphasizes the link between a moderate consumption of red wine and a lower incidence of cardiovascular diseases [19-24].

Rv has been classically defined as an anti-oxidant compound since it is able to scavenge hydroxyl, superoxide and others radical species preventing peroxidation of cell membranes and DNA damage [25-27]. However, it is unlikely that this mechanism of action may be relevant *in vivo*. Indeed Rv is characterized by a poor bioavailability (discussed below) and thus it is not expected to reach concentrations comparable to those of endogenous antioxidants such as glutathione, thioredoxin, NADH. [28-31]. Instead, it has been shown that, depending on factors such as its concentration, the pH, the presence of metal ions capable of sustaining redox cycles, Rv may promote a mild oxidative stress to indirectly enhance intracellular defense systems and to confer protection against more severe perturbations [29, 32-39]. This polyphenol may also interact with and inhibit several ROS-producing enzymes [31, 40, 41].

The virtues of Rv cannot be exclusively ascribed to its capability to counteract oxidative stress. Indeed, this molecule shows a pleiotropic activity as it modulates the expression and the activities of many key intracellular "players" [42-46].

Among them, the competitive binding (vs. cAMP) to several classes of phosphodiesterases (PDEs) is noteworthy. In particular, Park et al. in 2012 have demonstrated that Rv inhibits PDE1, PDE3 and PDE4. Consequently, the intracellular amount of this second messenger increases and leads to the indirect activation of AMPK through the EPAC-CAMKK axis [47, 48].

AMPK activation may have multiple consequences in different contexts. Together with PGC-1α, it remarkably decreases lipogenesis in adipocytes or promotes their apoptotic death. On the other hand, in light of its antagonistic relationship with mTORC1, AMPK may induce autophagy and thus the degradation of toxic protein aggregates and damaged

organelles, typical hallmarks of neurodegenerative disorders. Accordingly, Rv shows beneficial effects against metabolic disorders and a neuroprotective role [49-54].

Furthermore, this natural compound inhibits cyclooxygenases (COX) and lipoxygenases (LOX) as well as activation of the transcription factor NF-kB, mitigating inflammatory processes involved in the pathogenesis of cancer and cardio-vascular diseases [55-58].

Pt is the major phenolic component of the blueberries [59-62]. This compound has come to attention more recently, therefore, its pharmacological traits as well as its mechanisms of action are still largely undefined. However, it manifests health-promoting properties similar to those of Rv. It induces apoptotic cell death in tumoral cell lines and shows a hypolipidemic action [63-65]. Remarkably, it is more effective than Rv in counteracting the progressive cognitive decline associated with aging and neurodegeneration [66-68]. This might be due to the presence of methylether groups in place of two of the hydroxyls, which confer a higher lipophilicity to the molecule allowing it to cross biological membranes more easily [69, 70].

In light of the potentially beneficial properties of Rv and Pt many therapeutic applications have been proposed. Unfortunately, they have been limited because of low bioavailability, a common hallmark of all polyphenols [4, 71, 72].

Once ingested, the fates followed by these compounds within the body are notably intricate (**Fig.2**). The small intestine absorbs just a fraction of the total dietary intake since they are recognized as xenobiotics. This percentage is subjected to biotransformation, first in enterocytes, then, and mostly, in hepatocytes. The free hydroxyls are preferential sites of action of conjugative enzymes mediating methylation, sulfation and glucoronidation [73, 74]. Metabolites are then liberated in the systemic circulation and reach tissues and internal organs.

The remaining part not absorbed by the small intestine accumulates in the colon where undergoes enzymatic modifications by bacteria. The reduction of the double bound joining the two aromatic rings often occurs in the case of stilbenes [75, 76]. Microbial metabolites may be, in turn, absorbed and conveyed to organs or excreted [77-80].

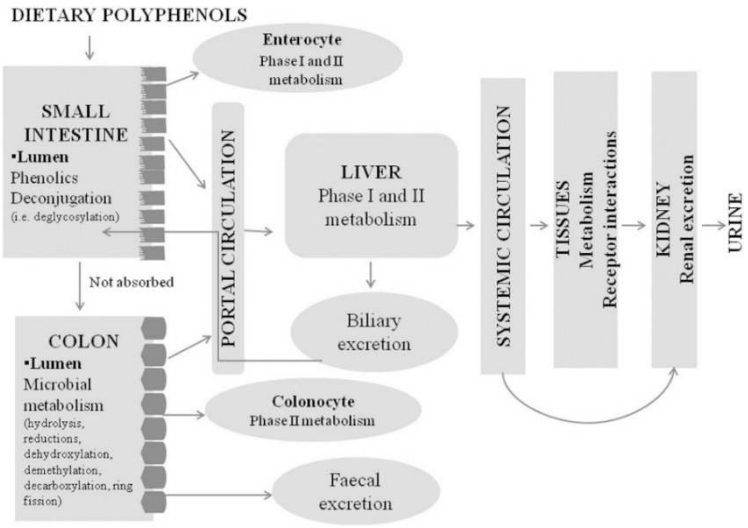


Fig.2: After assumption of polyphenols from foods, they are poorly absorbed and progressively undergo enzymatic modifications, absorption and elimination. From Cardona et al., 2013.

In light of the above, the real effectiveness that Rv and Pt can manifest *in vivo* is still questionable. The vast majority of their behaviors and the molecular interactions have been documented in *in vitro* studies by using elevated concentrations. Moreover, as metabolites are the main species present in the body after polyphenols ingestion, several authors suspect they might be really responsible for the effectiveness of polyphenols in general [78, 81-84].

Therefore, the development of appropriate systems aimed to boost their bioavailability as well as a better outlining of the molecular mechanisms of action of stilbenes and their metabolites represent relevant challenges for the entire scientific community.

The project and its aims

My PhD work mainly concerned the improvement of Rv and Pt efficacy.

As first aim, we attempted to increase the bioavailability of Rv, by developing oral prodrugs. The strategy implied the modification of the original molecule. More in detail, to prevent metabolic modifications, specific substituents, defined as pro-moieties, have been attached to the phenolic oxygens through a chemical bond (**Fig.3**). The latter ought to manifest a moderate stability for the appropriate regeneration of the parent compound.

The prodrug approach is an alternative to other delivery methods such as polymeric nanoparticles, micelles and liposomes or specific carrier systems. It involves the manipulation of the chemical-physical properties of the compounds. In this regard, a key

role is played by pro-moieties. Their choice has been motivated by the desire to favor the absorption into the enterocytes through endogenous membrane transport systems, and to avoid the formation of noxious by-products. Furthermore, we tried to increase the water solubility of these natural compounds, a convenient practical feature in particular for administration.

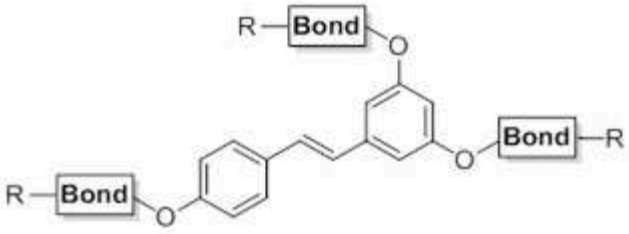


Fig.3: Sketch of a prodrug of Resveratrol

Specific Rv derivatives have been synthesized, in collaboration with the research group of Prof. Paradisi of the Department of Chemistry of the University of Padua. I participated to the assessment of their solubility and hydrolytic properties as well as to the delineation of their pharmacokinetic profiles during the first months of my research. These investigations and their outcomes are described in chapters 1 and 2 of this thesis.

A second part of the project was intended to further our understanding of the bioactivities of Pt and of the underlying mechanisms. Its pharmacokinetic properties were preliminary evaluated. This part of the work is reported in chapter 3. Next, to strengthen its potentialities, we moved back to the synthesis of prodrugs, whose characterizations are shown in chapter 4. On the other hand, I wanted to investigate the physiological processes Pt mediates. The structural analogy with Rv suggested that it might act in a similar manner. Rv has been reported to promote autophagy. The occurrence of this intracellular catabolic pathway might explain, at least in part, the multiplicity of the actions ascribed to its di-methylated cousin. Therefore, as illustrated in chapter 5, we explored the induction of this biological phenomenon by Pt and its main metabolites through *in vitro* investigations. Finally, thanks to the knowledge learned, we set out two different *in vivo* studies to evaluate the therapeutic effectiveness of Pt in two different models. In particular, as my research group is part of the Institute of Neuroscience of the National Council of Research, we examined the actions of Pt in the nervous system. These investigations, still ongoing, are reported in chapters 6 and 7.

References

1. Frohnmeyer, H. and D. Staiger, *Ultraviolet-B radiation-mediated responses in plants. Balancing damage and protection.* Plant Physiol, 2003. **133**(4): p. 1420-8.
2. Asensi, M., et al., *Natural polyphenols in cancer therapy.* Crit Rev Clin Lab Sci, 2011. **48**(5-6): p. 197-216.
3. Dai, J. and R.J. Mumper, *Plant phenolics: extraction, analysis and their antioxidant and anticancer properties.* Molecules, 2010. **15**(10): p. 7313-52.
4. Brglez Mojzer, E., et al., *Polyphenols: Extraction Methods, Antioxidative Action, Bioavailability and Anticarcinogenic Effects.* Molecules, 2016. **21**(7).
5. Li, A.N., et al., *Resources and biological activities of natural polyphenols.* Nutrients, 2014. **6**(12): p. 6020-47.
6. Tsao, R., *Chemistry and biochemistry of dietary polyphenols.* Nutrients, 2010. **2**(12): p. 1231-46.
7. Islam, M.A. and F. Alam, *Dietary Phytochemicals: Natural Swords Combating Inflammation and Oxidation-Mediated Degenerative Diseases.* 2016. **2016**: p. 5137431.
8. Fresco, P., et al., *The anticancer properties of dietary polyphenols and its relation with apoptosis.* Curr Pharm Des, 2010. **16**(1): p. 114-34.
9. Bravo, L., *Polyphenols: chemistry, dietary sources, metabolism, and nutritional significance.* Nutr Rev, 1998. **56**(11): p. 317-33.
10. Manach, C., et al., *Polyphenols: food sources and bioavailability.* Am J Clin Nutr, 2004. **79**(5): p. 727-47.
11. Pandey, K.B. and S.I. Rizvi, *Plant polyphenols as dietary antioxidants in human health and disease.* Oxid Med Cell Longev, 2009. **2**(5): p. 270-8.
12. Manach, C., A. Mazur, and A. Scalbert, *Polyphenols and prevention of cardiovascular diseases.* Curr Opin Lipidol, 2005. **16**(1): p. 77-84.
13. Scalbert, A., et al., *Dietary polyphenols and the prevention of diseases.* Crit Rev Food Sci Nutr, 2005. **45**(4): p. 287-306.
14. Rodriguez-Mateos, A., et al., *Bioavailability, bioactivity and impact on health of dietary flavonoids and related compounds: an update.* Arch Toxicol, 2014. **88**(10): p. 1803-53.
15. Hussain, T. and B. Tan, *Oxidative Stress and Inflammation: What Polyphenols Can Do for Us?* 2016. **2016**: p. 7432797.
16. Abdal Dayem, A., et al., *The Anti-Cancer Effect of Polyphenols against Breast Cancer and Cancer Stem Cells: Molecular Mechanisms.* Nutrients, 2016. **8**(9).
17. Niedzwiecki, A., et al., *Anticancer Efficacy of Polyphenols and Their Combinations.* Nutrients, 2016. **8**(9).
18. Lewandowska, H., et al., *The role of natural polyphenols in cell signaling and cytoprotection against cancer development.* J Nutr Biochem, 2016. **32**: p. 1-19.
19. Weiskirchen, S. and R. Weiskirchen, *Resveratrol: How Much Wine Do You Have to Drink to Stay Healthy?* Adv Nutr, 2016. **7**(4): p. 706-18.
20. Biagi, M. and A.A. Bertelli, *Wine, alcohol and pills: What future for the French paradox?* Life Sci, 2015. **131**: p. 19-22.
21. Artero, A., et al., *The impact of moderate wine consumption on health.* Maturitas, 2015. **80**(1): p. 3-13.
22. Yang, X., X. Li, and J. Ren, *From French Paradox to cancer treatment: anti-cancer activities and mechanisms of resveratrol.* Anticancer Agents Med Chem, 2014. **14**(6): p. 806-25.
23. Latruffe, N. and J.P. Rifler, *Bioactive polyphenols from grapes and wine emphasized with resveratrol.* Curr Pharm Des, 2013. **19**(34): p. 6053-63.

24. Catalgol, B., et al., *Resveratrol: French paradox revisited.* Front Pharmacol, 2012. **3**: p. 141.
25. Lorenz, P., et al., *Oxyresveratrol and resveratrol are potent antioxidants and free radical scavengers: effect on nitrosative and oxidative stress derived from microglial cells.* Nitric Oxide, 2003. **9**(2): p. 64-76.
26. Leonard, S.S., et al., *Resveratrol scavenges reactive oxygen species and effects radical-induced cellular responses.* Biochem Biophys Res Commun, 2003. **309**(4): p. 1017-26.
27. Huang, Y.T., et al., *Resveratrol alleviates the cytotoxicity induced by the radiocontrast agent, ioxitalamate, by reducing the production of reactive oxygen species in HK-2 human renal proximal tubule epithelial cells in vitro.* Int J Mol Med, 2016. **37**(1): p. 83-91.
28. Kursvietiene, L., et al., *Multiplicity of effects and health benefits of resveratrol.* Medicina (Kaunas), 2016. **52**(3): p. 148-55.
29. Plauth, A., et al., *Hormetic shifting of redox environment by pro-oxidative resveratrol protects cells against stress.* Free Radic Biol Med, 2016. **99**: p. 608-622.
30. Biasutto, L., I. Szabo, and M. Zoratti, *Mitochondrial effects of plant-made compounds.* Antioxid Redox Signal, 2011. **15**(12): p. 3039-59.
31. Jang, J.Y., et al., *Resveratrol inhibits collagen-induced platelet stimulation through suppressing NADPH oxidase and oxidative inactivation of SH2 domain-containing protein tyrosine phosphatase-2.* Free Radic Biol Med, 2015. **89**: p. 842-51.
32. Plauth, A., et al., *Data of oxygen- and pH-dependent oxidation of resveratrol.* Data Brief, 2016. **9**: p. 433-437.
33. Khan, H.Y., et al., *Plant polyphenol induced cell death in human cancer cells involves mobilization of intracellular copper ions and reactive oxygen species generation: a mechanism for cancer chemopreventive action.* Mol Nutr Food Res, 2014. **58**(3): p. 437-46.
34. Ahmad, A., et al., *Prooxidant activity of resveratrol in the presence of copper ions: mutagenicity in plasmid DNA.* Toxicol Lett, 2005. **159**(1): p. 1-12.
35. Galati, G., et al., *Prooxidant activity and cellular effects of the phenoxyl radicals of dietary flavonoids and other polyphenolics.* Toxicology, 2002. **177**(1): p. 91-104.
36. Bonnefont-Rousselot, D., *Resveratrol and Cardiovascular Diseases.* Nutrients, 2016. **8**(5).
37. Bayele, H.K., E.S. Debnam, and K.S. Srai, *Nrf2 transcriptional derepression from Keap1 by dietary polyphenols.* Biochem Biophys Res Commun, 2016. **469**(3): p. 521-8.
38. Reinisalo, M., et al., *Polyphenol Stilbenes: Molecular Mechanisms of Defence against Oxidative Stress and Aging-Related Diseases.* Oxid Med Cell Longev, 2015. **2015**: p. 340520.
39. Bjorklund, G. and S. Chirumbolo, *Role of oxidative stress and antioxidants in daily nutrition and human health.* Nutrition, 2016.
40. Whitehouse, S., et al., *Resveratrol, piperine and apigenin differ in their NADPH-oxidase inhibitory and reactive oxygen species-scavenging properties.* Phytomedicine, 2016. **23**(12): p. 1494-1503.
41. Xia, N., et al., *Antioxidant effects of resveratrol in the cardiovascular system.* Br J Pharmacol, 2016.
42. Pirola, L. and S. Frojdo, *Resveratrol: one molecule, many targets.* IUBMB Life, 2008. **60**(5): p. 323-32.
43. Diaz-Gerevini, G.T., et al., *Beneficial action of resveratrol: How and why?* Nutrition, 2016. **32**(2): p. 174-8.

44. Britton, R.G., C. Kovoor, and K. Brown, *Direct molecular targets of resveratrol: identifying key interactions to unlock complex mechanisms.* Ann N Y Acad Sci, 2015. **1348**(1): p. 124-33.
45. Tennen, R.I., E. Michishita-Kioi, and K.F. Chua, *Finding a target for resveratrol.* Cell, 2012. **148**(3): p. 387-9.
46. Kulkarni, S.S. and C. Canto, *The molecular targets of resveratrol.* Biochim Biophys Acta, 2015. **1852**(6): p. 1114-23.
47. Park, S.J., et al., *Resveratrol ameliorates aging-related metabolic phenotypes by inhibiting cAMP phosphodiesterases.* Cell, 2012. **148**(3): p. 421-33.
48. Wan, D., et al., *Resveratrol provides neuroprotection by inhibiting phosphodiesterases and regulating the cAMP/AMPK/SIRT1 pathway after stroke in rats.* Brain Res Bull, 2016. **121**: p. 255-62.
49. Bitterman, J.L. and J.H. Chung, *Metabolic effects of resveratrol: addressing the controversies.* Cell Mol Life Sci, 2015. **72**(8): p. 1473-88.
50. Wang, S., et al., *Novel insights of dietary polyphenols and obesity.* J Nutr Biochem, 2014. **25**(1): p. 1-18.
51. Chung, J.H., *Metabolic benefits of inhibiting cAMP-PDEs with resveratrol.* Adipocyte, 2012. **1**(4): p. 256-258.
52. Pallas, M., et al., *Resveratrol: new avenues for a natural compound in neuroprotection.* Curr Pharm Des, 2013. **19**(38): p. 6726-31.
53. Porquet, D., et al., *Dietary resveratrol prevents Alzheimer's markers and increases life span in SAMP8.* Age (Dordr), 2013. **35**(5): p. 1851-65.
54. Tang, B.L., *Resveratrol is neuroprotective because it is not a direct activator of Sirt1-A hypothesis.* Brain Res Bull, 2010. **81**(4-5): p. 359-61.
55. Nakata, R., S. Takahashi, and H. Inoue, *Recent advances in the study on resveratrol.* Biol Pharm Bull, 2012. **35**(3): p. 273-9.
56. Das, S. and D.K. Das, *Anti-inflammatory responses of resveratrol.* Inflamm Allergy Drug Targets, 2007. **6**(3): p. 168-73.
57. de la Lastra, C.A. and I. Villegas, *Resveratrol as an anti-inflammatory and anti-aging agent: mechanisms and clinical implications.* Mol Nutr Food Res, 2005. **49**(5): p. 405-30.
58. Kundu, J.K., Y.K. Shin, and Y.J. Surh, *Resveratrol modulates phorbol ester-induced pro-inflammatory signal transduction pathways in mouse skin in vivo: NF-kappaB and AP-1 as prime targets.* Biochem Pharmacol, 2006. **72**(11): p. 1506-15.
59. Kosuru, R., et al., *Promising therapeutic potential of pterostilbene and its mechanistic insight based on preclinical evidence.* Eur J Pharmacol, 2016. **789**: p. 229-43.
60. Estrela, J.M., et al., *Pterostilbene: Biomedical applications.* Crit Rev Clin Lab Sci, 2013. **50**(3): p. 65-78.
61. McCormack, D. and D. McFadden, *Pterostilbene and cancer: current review.* J Surg Res, 2012. **173**(2): p. e53-61.
62. McCormack, D. and D. McFadden, *A review of pterostilbene antioxidant activity and disease modification.* Oxid Med Cell Longev, 2013. **2013**: p. 575482.
63. Guo, L., et al., *Pterostilbene inhibits hepatocellular carcinoma through p53/SOD2/ROS-mediated mitochondrial apoptosis.* Oncol Rep, 2016.
64. Dong, J., H. Guo, and Y. Chen, *Pterostilbene induces apoptosis through caspase activation in ovarian cancer cells.* Eur J Gynaecol Oncol, 2016. **37**(3): p. 342-7.
65. Dhar, S., et al., *Dietary pterostilbene is a novel MTA1-targeted chemopreventive and therapeutic agent in prostate cancer.* Oncotarget, 2016. **7**(14): p. 18469-84.
66. Poulose, S.M., et al., *Effects of pterostilbene and resveratrol on brain and behavior.* Neurochem Int, 2015. **89**: p. 227-33.

67. Cherniack, E.P., *A berry thought-provoking idea: the potential role of plant polyphenols in the treatment of age-related cognitive disorders.* Br J Nutr, 2012. **108**(5): p. 794-800.
68. Chang, J., et al., *Low-dose pterostilbene, but not resveratrol, is a potent neuromodulator in aging and Alzheimer's disease.* Neurobiol Aging, 2012. **33**(9): p. 2062-71.
69. Walle, T., *Methylation of dietary flavones greatly improves their hepatic metabolic stability and intestinal absorption.* Mol Pharm, 2007. **4**(6): p. 826-32.
70. Cichocki, M., et al., *Pterostilbene is equally potent as resveratrol in inhibiting 12-O-tetradecanoylphorbol-13-acetate activated NFkappaB, AP-1, COX-2, and iNOS in mouse epidermis.* Mol Nutr Food Res, 2008. **52 Suppl 1**: p. S62-70.
71. Marin, L., et al., *Bioavailability of dietary polyphenols and gut microbiota metabolism: antimicrobial properties.* 2015. **2015**: p. 905215.
72. Biasutto, L., et al., *Improving the efficacy of plant polyphenols.* Anticancer Agents Med Chem, 2014. **14**(10): p. 1332-42.
73. Rotches-Ribalta, M., et al., *Pharmacokinetics of resveratrol metabolic profile in healthy humans after moderate consumption of red wine and grape extract tablets.* Pharmacol Res, 2012. **66**(5): p. 375-82.
74. Vitaglione, P., et al., *Bioavailability of trans-resveratrol from red wine in humans.* Mol Nutr Food Res, 2005. **49**(5): p. 495-504.
75. Bode, L.M., et al., *In vivo and in vitro metabolism of trans-resveratrol by human gut microbiota.* Am J Clin Nutr, 2013. **97**(2): p. 295-309.
76. Rotches-Ribalta, M., et al., *Gut and microbial resveratrol metabolite profiling after moderate long-term consumption of red wine versus dealcoholized red wine in humans by an optimized ultra-high-pressure liquid chromatography tandem mass spectrometry method.* J Chromatogr A, 2012. **1265**: p. 105-13.
77. Cardona, F., et al., *Benefits of polyphenols on gut microbiota and implications in human health.* J Nutr Biochem, 2013. **24**(8): p. 1415-22.
78. Ozdal, T., et al., *The Reciprocal Interactions between Polyphenols and Gut Microbiota and Effects on Bioaccessibility.* Nutrients, 2016. **8**(2): p. 78.
79. Del Rio, D., et al., *Dietary (poly)phenolics in human health: structures, bioavailability, and evidence of protective effects against chronic diseases.* Antioxid Redox Signal, 2013. **18**(14): p. 1818-92.
80. Yu, C., et al., *Human, rat, and mouse metabolism of resveratrol.* Pharm Res, 2002. **19**(12): p. 1907-14.
81. Del Rio, D., G. Borges, and A. Crozier, *Berry flavonoids and phenolics: bioavailability and evidence of protective effects.* Br J Nutr, 2010. **104 Suppl 3**: p. S67-90.
82. Bolca, S., T. Van de Wiele, and S. Possemiers, *Gut metabotypes govern health effects of dietary polyphenols.* Curr Opin Biotechnol, 2013. **24**(2): p. 220-5.
83. Tomas-Barberan, F.A., M.V. Selma, and J.C. Espin, *Interactions of gut microbiota with dietary polyphenols and consequences to human health.* Curr Opin Clin Nutr Metab Care, 2016. **19**(6): p. 471-476.
84. Stevens, J.F. and C.S. Maier, *The Chemistry of Gut Microbial Metabolism of Polyphenols.* Phytochem Rev, 2016. **15**(3): p. 425-444.

www.nature.com/scientificreports

SCIENTIFIC REPORTS

OPEN

Amino Acid Carbamates As Prodrugs Of Resveratrol

Andrea Mattarei[1,*], Michele Azzolini[2,3,4,*], Martina La Spina[3], Mario Zoratti[2,3], Cristina Paradisi[1] & Lucia Biasutto[2,3]

Received: 18 June 2015
Accepted: 21 September 2015
Published: 14 October 2015

Resveratrol (3, 5, 4′-trihydroxy-*trans*-stilbene), a plant polyphenol, has important drug-like properties, but its pharmacological exploitation *in vivo* is hindered by its rapid transformation via phase II conjugative metabolism. One approach to bypass this problem relies on prodrugs. We report here the synthesis, characterization, stability and *in vivo* pharmacokinetic behaviour of prodrugs of resveratrol in which the OH groups are engaged in an N-monosubstituted carbamate ester (-OC(O)NHR) linkage with a natural amino acid (Leu, Ile, Phe, Thr) to prevent conjugation and modulate the physicochemical properties of the molecule. We also report a convenient, high-yield protocol to obtain derivatives of this type. The new carbamate ester derivatives are stable at pH 1, while they undergo slow hydrolysis at physiological pH and hydrolyse with kinetics suitable for use in prodrugs in whole blood. After administration to rats by oral gavage the isoleucine-containing prodrug was significantly absorbed, and was present in the bloodstream as non-metabolized unaltered or partially deprotected species, demonstrating effective shielding from first-pass metabolism. We conclude that prodrugs based on the N-monosubstituted carbamate ester bond have the appropriate stability profile for the systemic delivery of phenolic compounds.

Resveratrol (trans-3,5,4′-trihydroxystilbene), is a naturally occurring phytoalexin produced by some plants (e.g. *V. vinifera*) in response to stresses[1]. It exhibits a range of activities of biomedical interest, including lifespan extension in model systems[2], protection of the cardiovascular apparatus[3–6], anti-inflammatory activity[3], improvement of glucose handling in diabetes[7,8], decrease of fat and cholesterol load[9–12], improvements of functionality in aging[2,13–15], neuroprotection[16], cancer chemoprevention[17,18] and potentiation of chemotherapy[19,20].

The efficacy of orally administered resveratrol depends on its absorption, metabolism, and tissue distribution. Clinical studies with humans reported mostly small effects, and sometimes controversial results[21,22]. Beneficial effects *in vivo* are in fact limited by low bioavailability. Thus, for example, administration of even very large doses (2.5–5.0 g) to volunteers resulted in circulating levels of non-metabolized resveratrol so low as to be considered insufficient for any bioactivity[23]. Resveratrol, like other polyphenols, is rapidly converted to phase II metabolites (mainly glucuronides and sulfates) during absorption and first pass through the liver. These hydrophilic metabolites are re-exported to the intestinal lumen by enterocyte ABC transporters, and/or rapidly excreted with faeces and urine[23,24]. Nonetheless, given their preponderance, their bioactivities are now under investigation to verify whether they may account for resveratrol's effects. The available data suggest that a level of activity may well be maintained in specific contexts (e.g.[25–28]), but conjugation often determines at least a partial loss of bioefficacy[29–34]. Retention of bioactivity *in vivo* may be due in part to the metabolites acting as a temporary reservoir from which the more active species may be regenerated through the activity of enzymes such as glucuronidases and sulfatases[35,36]. While investigation of these aspects continues, a reduction or delay of phase II metabolism remains a primary target for the biomedical exploitation of resveratrol.

[1]University of Padova, Department of Chemical Sciences, Via F. Marzolo 1, 35131 Padova, Italy. [2]CNR Neuroscience Institute, Viale G. Colombo 3, 35121 Padova, Italy. [3]University of Padova, Department of Biomedical Sciences, Viale G. Colombo 3, 35121 Padova, Italy. [4]NÓOS srl, via Campello sul Clitunno 34, 00181 Roma, Italy. *These authors contributed equally to this work. Correspondence and requests for materials should be addressed to A.M. (email: andrea.mattarei@unipd.it)

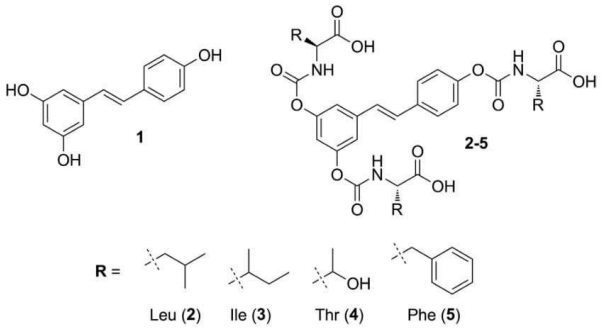


Figure 1. Resveratrol (1) and new amino acid substituted prodrugs (2–5).

One of the strategies used to prevent drug metabolism and enhance bioavailability and effectiveness is based on prodrugs. In a successful resveratrol prodrug, the natural active compound is protected against phase II metabolism by having the reactive hydroxyl groups masked as suitably reversible derivatives (-OH → -OXR). The capped hydroxyl functionalities (-OXR) should withstand the processes of absorption, first pass through the liver and distribution. Once in the bloodstream, the prodrug should then release the active natural compound, resveratrol (-OXR → -OH). Appropriate regeneration kinetics may provide a form of sustained delivery, a possibly convenient alternative to other approaches such as slow-release capsules. Optimal prodrug performance is sought by modulating its physicochemical properties using the best combination of X, the reversible protecting linkage (ester, carbamate, acetal, …), and of R, the promoiety. The type of linkage X is mostly relevant for prodrug persistence whereas the promoiety R may determine its solubility in aqueous media and partitioning between aqueous and lipidic (membrane) phases. One crucial additional requirement is that hydrolysis of the prodrug produce, besides the original active natural compound, safe by-products.

The carbamoyl moiety provides a versatile protecting group for phenols (-OH → -OC(=O)NR′R″)[37,38], which allows fine-tuning of the properties of the molecule since the two substituents on nitrogen, R′ and R″, can be tailored to modulate the stability and physicochemical properties of the resulting prodrug. Several prodrugs have been developed to improve oral bioavailability of phenolic compounds[39–41] but surprisingly there are only few examples of carbamate ester prodrugs of polyphenols. Mulholland *et al.*[42] reported a water-soluble glycine N-monosubstituted carbamate ester prodrug (QC12) of the flavonoid quercetin. The advantage of QC12 was its high aqueous solubility. Quercetin-amino acid N-monosubstituted carbamate esters were also synthesized by Kim *et al.*[43] and showed remarkable increases in water solubility, stability, and cell permeability compared with the parent polyphenol. We have previously reported that N,N-disubstituted carbamoyl derivatives of resveratrol are too stable under physiological conditions to be of practical use as prodrugs[44]. We therefore turned our attention to N-monosubstituted carbamoyl derivatives -OC(=O)NHR and report here the synthesis and the properties of a family of new prodrugs in which three units of a natural amino acid are linked to resveratrol via carbamoyl derivatization of the three hydroxyl groups (Fig. 1).

Use of amino acids as promoieties in prodrug design has been recently reviewed[45]. Their presence increases water solubility, and they are considered to be safe hydrolysis by-products. Moreover, we reasoned that prodrugs incorporating suitable amino acids in the promoieties might be recognized and transported by the various epithelial amino acid[46] and peptide[47–49] carrier systems. We selected Leu, Ile and Phe (Fig. 1) because intestinal epithelia are well provided with carriers of neutral/large amino acids. These are, in particular, known substrates of the LAT (Large-neutral Amino acid Transporters or L-type Amino acid Transporters)[50] systems, with affinities in the μM range. Amino acid transporters LAT1 and LAT2 have been previously exploited for the transport/absorption of drugs; they are especially useful for the permeation of the blood brain barrier[51–53]. We also included threonine as a "control" amino acid because it is not efficiently transported by LAT (although it is a known substrate of the ASCT2 system)[46].

The performance of the new derivatives **2–5** was assessed by kinetic studies of hydrolysis in aqueous media under different pH conditions of physiological relevance (strongly acidic, as in the stomach, and near neutral, as in the intestine) as well as in blood. Pharmacokinetic experiments in rats were also performed in order to evaluate *in vivo* absorption, stability and metabolism of these new prodrugs.

Results & Discussion

Synthesis. Synthesis of N-monosubstituted carbamate esters is usually carried out in two steps: reaction of the desired primary amine with phosgene or its equivalent to give a reactive isocyanate derivative, followed by coupling of this intermediate with the phenolic function[54]. These procedures, however, led to

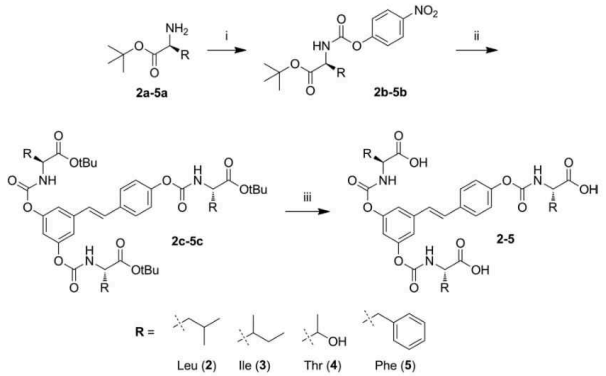


Figure 2. Synthesis of resveratrol N-monosubstituted carbamate ester prodrugs. *Reagents and conditions*: (i) bis-(4-nitrophenyl) carbonate, DMAP, ACN, 50 °C, 3 h; (ii) resveratrol (1), ACN, DMAP, 50 °C, 24 h; (iii) DCM/TFA 1:1, TIPS, from 0 °C to r.t., 1.5 h.

the desired trisubstituted resveratrol derivatives in low yields, probably due to the high reactivity of the isocyanate group promoting side reactions of polymerization entraining the stilbene C-C double bond. In this study, therefore, we utilized and optimized an alternative approach via an activated 4-nitrophenyl carbamate intermediate[43]. By this route, outlined in Fig. 2, we prepared N-monosubstituted resveratrol carbamate esters **2**–**5** in fair overall yields.

The procedure involves conversion of the C-protected amino acids **2a**–**5a** into the corresponding activated 4-nitrophenyl carbamates **2b**–**5b**. After isolation, these intermediates are treated with resveratrol to afford the product of transesterification, the *t*-butyl protected resveratrol amino acid carbamate ester conjugates **2c**–**5c** in good to excellent yields under mild conditions. The desired final products **2**–**5** are readily obtained by removal of the *t*-butyl protecting group by treatment with TFA.

Hydrolysis studies. The hydrolytic reactivity of the new derivatives **2**–**5** was tested in aqueous solutions mimicking gastric and intestinal pH and also in blood. All compounds turned out to be highly stable at pH values close to that of the human stomach, no reaction occurring over 24 hours at 37 °C in 0.1 N HCl, and they underwent slow hydrolysis at near-neutral pH (pH 6.8, representing intestinal pH) thus ensuring protection of the phenolic moieties from first pass metabolism during absorption in the gastrointestinal tract. In contrast all the synthesized prodrugs hydrolyzed in murine whole blood, with kinetics suitable for use as prodrugs.

Hydrolysis of derivatives **2**–**5** to resveratrol proceeds stepwise through intermediates in which initially one and then two protecting groups have been sequentially removed, as shown in Fig. 3. There are two possible isomeric disubstituted intermediates and, likewise, two monosubstituted intermediates. By HPLC-UV and HPLC-MS analyses in most cases we were able to detect and separate all of them. However, to simplify the kinetic analysis of the data we considered each pair of isomeric intermediates, resulting from the first and second hydrolysis steps, as a single species, i.e. the two disubstituted and the two monosubstituted intermediates were handled as species **II** and **I**, respectively (Fig. 3). Fitting of the experimental data was then performed considering consecutive pseudo first order reactions and using a set of equations analogous to those described by Kozerski *et al.*[55]

Examples are shown in Fig. 4, which reports the results of kinetic and product analysis for hydrolysis of derivatives **3** (a, b) and **5** (c, d) in aqueous PBS 0.1 M, at pH 6.8 and 37 °C (a, c) and in rat blood (b, d).

The full set of kinetic results obtained for hydrolysis of derivatives **2**–**5** according to the procedures described above is presented in Table 1 and, graphically, in Fig. 5.

The stability of our derivatives **2**–**5** in acidic solution and their reactivity at higher pH's are consistent with a mechanism of base catalyzed hydrolysis of carbamates proceeding via deprotonation and elimination to give an isocyanate intermediate which rapidly adds water and decomposes releasing carbon dioxide and the amino acid (Fig. 6)[56].

The data show that hydrolysis is much faster in blood, suggesting the involvement of enzymes. This notion is reinforced by the variability of the rates from one compound to the other. Hansen[38] and co-workers have demonstrated that the predominant rate-accelerating component of plasma (human in that study) is albumin.

Pharmacokinetics studies. Derivatives **2**–**5** were then tested for their *in vivo* absorption and metabolism by performing pharmacokinetic studies after oral administration to rats. Each compound was

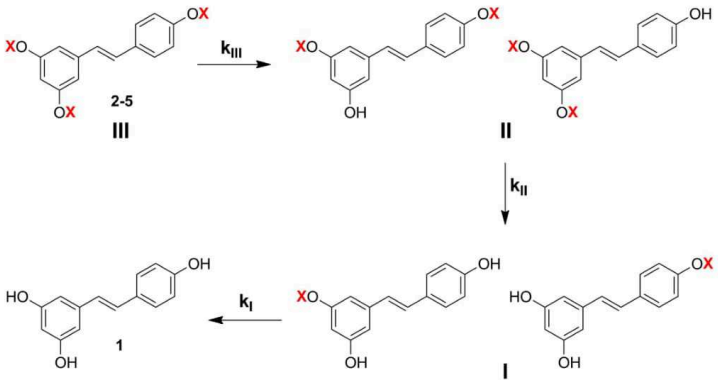


Figure 3. Stepwise hydrolysis of 2–5 to resveratrol (1) and simplified kinetic treatment.

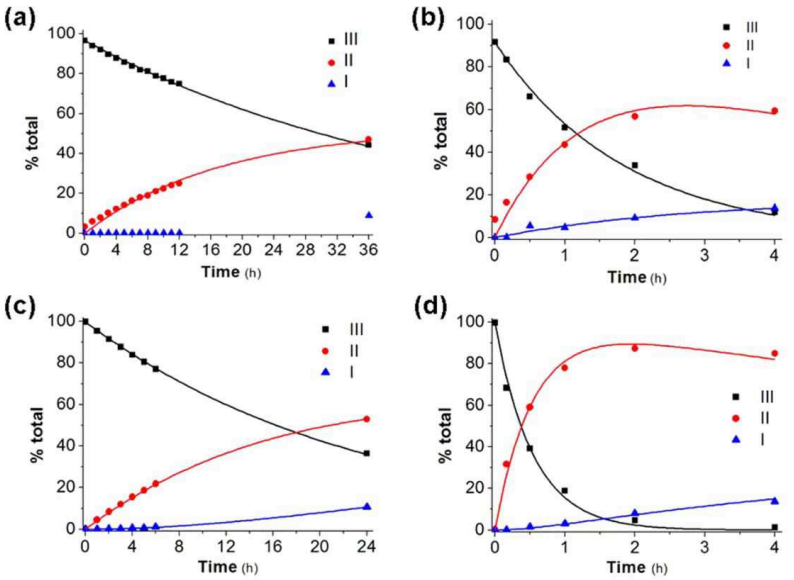


Figure 4. Kinetics and products of hydrolysis of derivatives 3 (a,b) and 5 (c,d): (a) and (c): aqueous PBS 0.1 M at pH 6.8 and 37 °C; (b) and (d): rat blood. The experimental data were processed and fitted as described in the text, with reference to Fig. 3. Please note that the abscissa scale varies among panels.

administered as a single intragastric bolus, in an equimolar dose/kg body weight (88 μmol/kg). Blood samples were taken at different time points over a 24 h period, treated and analyzed as described in the Materials and Methods section. Each experiment was replicated at least 3 times.

Contrary to our expectations the linkage of resveratrol through the N-monosubstituted carbamate ester to amino acids resulted in poor absorption of the prodrugs after oral administration. We can only speculate that this result is probably due to the excessive hydrophilicity conferred by the three carboxylic ionisable groups present in the derivatives, which hinder permeation of lipophilic biomembranes. It is furthermore evident that these trisubstituted prodrugs were not readily recognized and/or transported by aminoacid carriers. The best results were obtained with the isoleucine derivative, **3**, as summarized in

Derivative	$t_{1/2}$ (h)	PBS 0.1 M, pH 6.8, 37 °C			Blood			
		$10^2 * k_{III}$ (h^{-1})	$10^2 * k_{II}$ (h^{-1})	$10^2 * k_I$ (h^{-1})	$t_{1/2}$ (h)	k_{III} (h^{-1})	k_{II} (h^{-1})	k_I (h^{-1})
2	>24	1.98 ± 0.03	0.9 ± 0.2	*	1	0.57 ± 0.06	ND#	ND#
3	>24	2.21 ± 0.02	0.4 ± 0.4	*	1	0.63 ± 0.04	0.12 ± 0.03	0.4 ± 0.1
4	15	5.30 ± 0.08	1.4 ± 0.1	0.6 ± 0.1	0,17	3.9 ± 0.2	0.057 ± 0.006	0.45 ± 0.09
5	17	4.25 ± 0.02	1.36 ± 0.04	0.2 ± 0.1	0,3	1.86 ± 0.06	0.056 ± 0.007	0.09 ± 0.02

Table 1. Observed pseudo first-order rate constants for hydrolysis of resveratrol derivatives 2–5 in aqueous PBS 0.1 M at pH 6.8 and 37 °C and in rat blood. Values ± standard error are reported as obtained from the fit of all the available data. *k_I not determined; monosubstituted derivative detected only at the latest time point. #k_{II} and k_I not determined because of co-elution of di- and mono-substituted derivatives with matrix background interfering peaks.

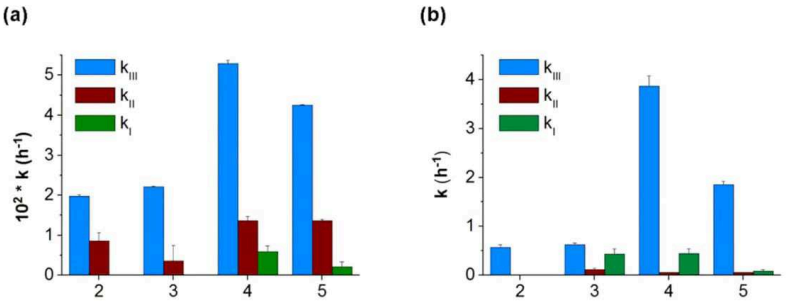


Figure 5. Observed pseudo first order rate constant for hydrolysis of resveratrol derivatives: (a) PBS 0.1 M, pH 6.8, 37 °C, (b) rat blood. Please note the different ordinate scales in (**a**,**b**).

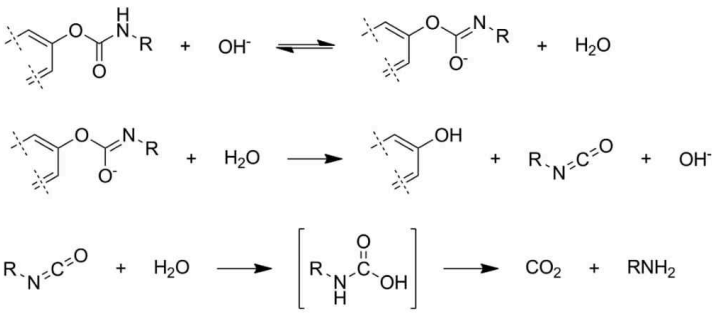


Figure 6. Mechanism of base-induced hydrolysis of carbamates 2–5.

Fig. 7. About one hour after oral administration the concentration of this prodrug in blood was higher than 0.5 μM and remained around this level for several hours (Fig. 7). Disubstituted hydrolysis products (**II**, Fig. 3) were also present, indicating the bioreversibility of the carbamate linker also *in vivo* and, interestingly, their level was about as high as that of their precursor, the trisubstituted derivative **3**. Notably, neither sulfated nor glucuronidated species appeared in the bloodstream confirming the protection by the N-monosubstituted carbamate linker from first pass metabolism during absorption.

The concentration of tri- and di- substituted carbamate-Ile resveratrol prodrugs was substantially maintained for at least 8 hours, i.e. ample time for equilibration with organs. This behaviour may be due to the fact that the derivative is constantly absorbed from the intestinal mucosa and/or that it is slowly cleared from the body. Resveratrol (**1**) and monosubstituted carbamate-Ile (**I**) were not detected in the

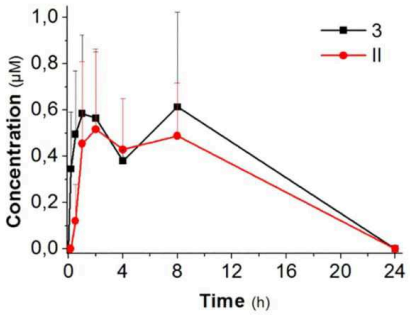


Figure 7. Blood pharmacokinetic profile after oral administration of derivative 3. Data represent average values +s.d. N = 3.

bloodstream probably because the blood concentration of these species were too low for reliable measurement. Nature and levels of the species found in blood may not be representative of the nature and levels of stilbenoid species in other organs: the hydrophilicity of the amino acid-decorated compounds is expected to result in their enrichment in blood, while less hydrophilic molecules, e.g. resveratrol itself, are expected to associate with membrane-rich compartments[57,58].

In any case, the prodrug appears to perform as a slow-action vehicle providing a sustained delivery of precursor. By comparison, blood concentration of resveratrol after oral administration of an equimolar amount of resveratrol itself peaks at approximately 1 μM after only about 10 minutes from administration, and rapidly declines. Phase II metabolites peak (~10 μM) at about 1 h, and then decline by 80–90% over the next 7 hours[59].

In contrast with the behaviour of **3**, administration of compounds **4** and **5** did not result in the appearance in blood samples of detectable amounts of either resveratrol, products of partial hydrolysis (**II** and **I**) or any metabolites. Similar results were also obtained with **2**, although in this case the presence of very small amounts of partially hydrolyzed derivatives (**II** and **I**) cannot be excluded due to interfering co-eluting peaks due to the matrix.

Conclusions

The N-monosubstituted carbamate bond is a convenient linker for prodrugs of resveratrol[60] which has been coupled in this study with amino acid promoieties. All synthesized compounds have good solubility and stability properties in aqueous media and in blood for use as resveratrol prodrugs. *In vivo* pharmacokinetic studies revealed an interesting behaviour of the isoleucine derivative **3**, which acts as a slow-action vehicle providing a sustained delivery of the prodrug and partially hydrolysed unconjugated species, indicating protection from first pass metabolism during absorption. However, the choice of amino acid as promoieties proved to be unsatisfactory in terms of absorption of the prodrug, probably due to the excessive hydrophilicity of the resulting prodrugs bearing three ionisable groups, and because carrier-mediated uptake apparently did not take place to a significant extent. Possibly the prodrugs were too large and ramified to be handled by the transporters. As a future development of this work, we aim to seek a better performing promoiety in order to improve absorption.

Methods

Chemistry. *Materials and instrumentation.* Resveratrol was purchased from Waseta Int. Trading Co. (Shangai, P.R.China). Other starting materials and reagents were purchased from Aldrich, Fluka, Merck-Novabiochem, Riedel de Haen, J.T. Baker, Cambridge Isotope Laboratories Inc., Acros Organics, Carlo Erba and Prolabo, and were used as received. TLCs were run on silica gel supported on plastic (Macherey-Nagel Polygram®SIL G/UV_{254}, silica thickness 0.2 mm) and visualized by UV detection. Flash chromatography was performed on silica gel (Macherey-Nagel 60, 230–400 mesh granulometry (0.063–0.040 mm)) under air pressure. The solvents were analytical or synthetic grade and were used without further purification. ^{1}H NMR spectra were recorded with a Bruker AC250F spectrometer operating at 250 MHz and a Bruker AVII500 spectrometer operating at 500 MHz. Chemical shifts (δ) are given in ppm relative to the signal of the solvent. HPLC-UV analyses were performed with an Agilent 1290 Infinity LC System (Agilent Technologies), equipped with binary pump and a diode array detector (190–500 nm). HPLC/ESI-MS analyses and mass spectra were performed with a 1100 Series Agilent Technologies system, equipped with binary pump (G1312A) and MSD SL Trap mass spectrometer (G2445D SL) with ESI source. ESI-MS positive spectra of reaction intermediates and final purified products were obtained from solutions in acetonitrile, eluting with a water:acetonitrile, 1:1 mixture containing 0.1% formic acid.

High resolution mass measurements were obtained using a Mariner ESI-TOF spectrometer (PerSeptive Biosystems). HPLC-MS analysis was used to confirm purity (>95% in all cases).

Synthesis of derivatives 2–5. *General procedure for the preparation of activated 4-nitrophenyl urethanes (**2b-5b**, Fig. 2).* A solution of amino acid t-butyl ester (**2a–5a**) (8.2 mmol, 1.0 eq.) and DMAP (2.00 g, 16.4 mmol, 2.0 eq.) in acetonitrile (15 mL) was added dropwise to a solution of bis(4-nitrophenyl) carbonate (2.74 g, 9.0 mmol, 1.1 eq.) in acetonitrile (15 mL) and the resulting solution was stirred at 50 °C for 3 hours. The reaction mixture was then diluted in DCM (150 mL) and washed with 0.5 N HCl (100 mL). The aqueous layer was washed with DCM (5 × 100 mL) and all the organic fractions were collected, dried over $MgSO_4$ and filtered. The solvent was evaporated under reduced pressure and the residue was purified by flash chromatography.

*Tert-butyl 4-methyl-2-(((4-nitrophenoxy)carbonyl)amino)pentanoate (**2b**).* Purified by flash chromatography using DCM:Acetone:Hexane = 8:0.5:1.5 as eluent. The first two spots were collected and the solvent was evaporated under reduced pressure, then the residue was absorbed on silica and purified by flash chromatography using Hexane:Ethyl Ether = 6.5:3.5 as eluent. 65% yield as a pale yellow oil. ^{1}H-NMR (250 MHz, $CDCl_3$) δ (ppm): 0.97–1.01 (m, 6 H, 2 × -CH-CH_3), 1.49 (s, 1 H, -CH-CH_3), 1.52–1.85 (m, 11 H, 3 × -C-CH_3 and -CH-CH_2-), 4.27–4.36 (m, 1 H, NH-CH-), 5.56 (d, 1 H, -CH-NH-, $^3J_{H\text{-}H}$ = 8.5 Hz), 7.33 (d, 2 H, Ar-H, $^3J_{H\text{-}H}$ = 9.25 Hz), 8.24 (d, 2 H, Ar-H, $^3J_{H\text{-}H}$ = 9.25 Hz); ^{13}C-NMR (62.9 MHz, $CDCl_3$) δ (ppm): 171.7, 155.8, 152.7, 125.1, 122.0, 82.5, 53.2, 42.0, 28.0, 27.9, 24.9, 22.8, 22.0. ESI-MS (ion trap): m/z 353 $[M+H]^+$; HRMS (ESI+): *m/z* 353.1720 $[M+H]^+$, calcd for $C_{17}H_{25}N_2O_6$: 353.1713.

*Tert-butyl 3-methyl-2-(((4-nitrophenoxy)carbonyl)amino)pentanoate (**3b**).* Purified by flash chromatography using DCM:Acetone:Hexane = 8:0.5:1.5. 93% yield as a pale yellow oil. ^{1}H-NMR (300 MHz, $CDCl_3$) δ (ppm): 0.95–1.38 (m, 5 H, -CH_2-CH_3, CH_3-CH_2-), 1.52 (s, 9 H, 3 × -C-CH_3), 1.87–2.04 (m, 1 H, -CH-CH_2-), 4.29 (dd, 1 H, -CH-NH-, $^3J_{H\text{-}H}$ = 8.7, 4.3 Hz), 5.76 (d, 1 H, -CH-NH-, $^3J_{H\text{-}H}$ = 8.6 Hz), 7.32–7.37 (d, 2 H, Ar-H, $^3J_{H\text{-}H}$ = 9.25 Hz), 8.22–8.28 (d, 2 H, Ar-H, $^3J_{H\text{-}H}$ = 9.25 Hz); ^{13}C-NMR (300 MHz, $CDCl_3$) δ(ppm): 172.2, 157.6, 154.6, 145.5, 126.8, 123.7, 84.3, 79.2, 78.8, 78.3, 60.5, 29.8, 26.9, 17.1, 13.4. ESI-MS (ion trap): m/z 353 $[M+H]^+$. ESI-MS (ion trap): m/z 353 $[M+H]^+$; HRMS (ESI+): *m/z* 353.1724 $[M+H]^+$, calcd for $C_{17}H_{25}N_2O_6$: 353.1713.

*Tert-butyl 3-(tert-butoxy)-2-(((4-nitrophenoxy)carbonyl)amino)butanoate (**4b**).* Purified by flash chromatography using DCM:Acetone:Hexane = 8:0.5:1.5 as eluent. 93% yield as a pale yellow oil. ^{1}H-NMR (250 MHz, $CDCl_3$) δ (ppm): 1.19 (s, 9 H, 3 × C-CH_3), 1.28 (d, 3 H, -CH-CH_3, $^3J_{H\text{-}H}$ = 6.3 Hz), 1.49 (s, 9 H, 3 × -C-CH_3), 4.05–4.17 (m, 1 H, -O-CH-), 4.22–4.33 (m, 1 H, NH-CH-), 5.94 (d, 1 H, CH-NH-, $^3J_{H\text{-}H}$ = 9.5 Hz), 7.35 (d, 2 H, Ar-H, $^3J_{H\text{-}H}$ = 9.25 Hz), 8.27 (d, 2 H, Ar-H, $^3J_{H\text{-}H}$ = 9.25 Hz); ^{13}C-NMR (62.9 MHz, $CDCl_3$) δ(ppm): 169.7, 156.2, 153.8, 144.9, 125.2, 122.2, 82.5, 74.2, 67.2, 60.8, 28.9, 28.3, 21.4. ESI-MS (ion trap): m/z 397 $[M+H]^+$. HRMS (ESI+): *m/z* 397.1977 $[M+H]^+$, calcd for $C_{19}H_{29}N_2O_7$: 397.1975.

*Tert-butyl 2-(((4-nitrophenoxy)carbonyl)amino)-3-phenylpropanoate (**5b**).* Purified by flash chromatography using DCM:Acetone = 9:1 as eluent. 81% yield as a pale yellow oil. 1H-NMR (250 MHz, CDCl3) δ (ppm): 1.54 (s, 9 H, 3 × -C-CH_3), 3.05–3.35 (m, 2 H, 2 × C-CH_2), 4.70 (dd, 1 H, -NH-CH-CH_2- J = 14.7, 6.5 Hz), 6.33 (d, 1 H, -NH-, J = 8.3 Hz), 7.22–7.45 (m, 7 H, Ar-H), 8.23 (d, 2 H, Ar-H, $^3J_{H\text{-}H}$ = 15.5 Hz); 13C-NMR (62.9 MHz, CDCl3) δ (ppm): 170.4, 155.8, 152.6, 144.6, 136.0, 129.5, 128.1, 127.5, 124.9, 121.9, 82.7, 55.6, 38.2, 27.3. ESI-MS (ion trap): m/z 387 $[M+H]^+$. HRMS (ESI+): *m/z* 387.1547 $[M+H]^+$, calcd for $C_{20}H_{23}N_2O_6$: 387.1556.

*General procedure for the preparation of 3,4′,5-N-monosubstituted-resveratrol carbamate esters (**2c–5c**).* A solution of resveratrol (0.24 g, 1.1 mmol, 1.0 eq.) and DMAP (0.52 g, 4.2 mmol, 4.0 eq.) in ACN (15 mL) was added to a solution of the activated 4-nitrophenyl urethane (**2b**–**5b**) (4.8 mmol, 4.5 eq) in ACN (5 mL) and the resulting mixture was allowed to react under vigorous stirring at 50 °C for 24 h. The reaction mixture was diluted with DCM (150 mL) and washed with 0.5 N HCl (100 mL). The aqueous layer was washed with DCM (5 × 75 mL) and all the organic fractions were collected, dried over $MgSO_4$ and filtered. The solvent was evaporated under reduced pressure and the residue was purified by flash chromatography.

*(E)-di-tert-butyl 2,2′-((((5-(4-(((1-(tert-butoxy)-4-methyl-1-oxopentan-2-yl)carbamoyl)oxy)styryl)-1,3-phenylene)bis(oxy))bis(carbonyl))bis(azanediyl))bis(4-methylpentanoate) (**2c**).* Purified by flash chromatography using $CHCl_3$ as eluent. 55% yield as a colourless oil. ^{1}H-NMR (250 MHz, $CDCl_3$) δ (ppm): 0.93 (m, 18 H, 6 × CH-CH_3), 1.44 (s, 27 H, 9 × -C-CH_3), 1.48–1.53 (m, 9 H, 3 × CH_3-CH and 3 × -CH-CH_2), 4.23–4.32 (m, 3 H, 3 × -NH-CH), 5.64 (m, 3 H, 3 × -NH-), 6.80–7.07 (m, 7 H, H-4, H-3′, H-5′, H-2, H-6, H-7, H-8), 7.47 (d, 2 H, $^3J_{H\text{-}H}$ = 8.5 Hz, H-2′, H-6′); ^{13}C-NMR (62.9 MHz, $CDCl_3$) δ (ppm): 172.1, 172.3, 154.0, 153.7, 151.4, 150.5, 139.0, 134.0, 129.2, 134.0, 129.2, 127.3, 127.0, 121.7, 116.4, 114.2, 82.0, 53.1,

41.9, 27.9, 24.8, 22.8, 21.9. ESI-MS (ion trap): m/z 868 $[M+H]^+$. HRMS (ESI+): *m/z* 868.4966 $[M+H]^+$, calcd for $C_{47}H_{70}N_3O_{12}$: 868.4959.

*(E)-di-tert-butyl 2,2′-((((5-(4-(((1-(tert-butoxy)-3-methyl-1-oxopentan-2-yl)carbamoyl)oxy)styryl)-1,3-phenylene)bis(oxy))bis(carbonyl))bis(azanediyl))bis(3-methylpentanoate) (**3c**).* Purified by flash chromatography using Hexane: EtOAc = 8:2. The first spot was separated and the remaining spots were collected and the solvent was evaporated under reduced pressure, then purified by flash chromatography using DCM:Hexane:EtOAc = 7:2:1. 60% yield as a colourless oil. ^{1}H-NMR (300 MHz, $CDCl_3$) δ (ppm): 0.87–1.05 (m, 18 H, 3 × CH_2-CH_3, 3 × CH-CH_3), 1.12–1.33 (m, 6 H, 3 × CH-CH_2-CH_3), 1.49 (s, 27 H, 9 × C-CH_3), 1.87–2.00 (m, 3 H, 3 × CH-CH-CH_3), 4.11 (q, 1 H, -NH-C*H*-CH-, $^3J_{H\text{-}H}$ = 7.1 Hz), 4.23–4.33 (m, 2 H, 2 × -NH-C*H*-CH-), 5.79 (d, 3 H, 3 × -N*H*-, $^3J_{H\text{-}H}$ = 8.7 Hz), 6.82–7.30 (m, 7 H, H-4, H-3′, H-5′, H-2, H-6, H-7, H-8), 7.43 (d, 2 H, $^3J_{H\text{-}H}$ = 8.5 Hz, H-2′, H-6′); ^{13}C-NMR (300 MHz, $CDCl_3$) δ(ppm): 170.7, 170.6, 154.1, 153.7, 151.4, 150.6, 139.1, 134.0, 129.2, 127.3, 116.3, 114.2, 82.1, 58.6, 38.2, 27.9, 25.1, 15.3, 11.6. ESI-MS (ion trap): m/z 868 $[M+H]^+$. HRMS (ESI+): *m/z* 868.4966 $[M+H]^+$, calcd for $C_{47}H_{70}N_3O_{12}$: 868.4959.

*(E)-di-tert-butyl 2,2′-((((5-(4-(((1,3-di-tert-butoxy-1-oxobutan-2-yl)carbamoyl)oxy)styryl)-1,3-phenylene)bis(oxy))bis(carbonyl))bis(azanediyl))bis(3-(tert-butoxy)butanoate) (**4c**).* Purified by flash chromatography using DCM:ethyl ether = 95:5 as eluent. 58% yield as a colourless oil. ^{1}H-NMR (250 MHz, $CDCl_3$) δ (ppm): 1.15 (s, 27 H, 9 × C-CH_3), 1.23 (d, 9 H, 3 × CH-CH_3, $^3J_{H\text{-}H}$ = 6.2 Hz), 1.45 (s, 27 H, 9 × C-CH_3), 4.04–4.25 (m, 6 H, 3 × CH_3-C*H* and 3 × NH-C*H*), 5.78 (d, 3 H, 3 × -N*H*-, $^3J_{H\text{-}H}$ = 9.5 Hz), 6.85–7.30 (m, 7 H, H-4, H-3′, H-5′, H-2, H-6, H-7, H-8), 7.43 (d, 2 H, $^3J_{H\text{-}H}$ = 8.5 Hz, H-2′, H-6′); ^{13}C-NMR (62.9 MHz, $CDCl_3$) δ (ppm): 169.6, 154.7, 154.3, 151.4, 150.5, 139.0, 133.9, 129.1, 127.3, 127.1, 121.6, 116.2, 114.1, 81.9, 81.8, 73.7, 66.9, 60.3, 28.5, 27.9, 20.8. ESI-MS (ion trap): m/z 1001 $[M+H]^+$. HRMS (ESI+): *m/z* 1000.5754 $[M+H]^+$, calcd for $C_{53}H_{82}N_3O_{15}$: 1000.5746.

*(E)-di-tert-butyl 2,2′-((((5-(4-(((1-(tert-butoxy)-1-oxo-3-phenylpropan-2-yl)carbamoyl)oxy)styryl)-1,3-phenylene)bis(oxy))bis(carbonyl))bis(azanediyl))bis(3-phenylpropanoate) (**5c**).* Purified by flash chromatography using Hexane:Diethyl ether = 7:3 as eluent until the exit of 4-nitrophenol from the column, and Hexane:Diethyl ether:EtOAc = 5:3.5:1.5 thereafter. 57% yield as a colourless oil. ^{1}H-NMR (250 MHz, $CDCl_3$) δ (ppm): 1.41 (s, 27 H, 3 × -C-CH_3), 3.02–3.30 (m, 6 H, 3 × Ph-CH_2), 4.16 (q, 1 H, NH-C*H*-CH_2, $^3J_{H\text{-}H}$ = 7.1 Hz), 4.64 (q, 2 H, 2 × NH-C*H*-CH_2, $^3J_{H\text{-}H}$ = 6.2 Hz), 5.79 (m, 3 H, 3 × -N*H*-), 6.81–7.56 (m, 24 H, Ar-*H*); ^{13}C-NMR (62.9 MHz, $CDCl_3$) δ (ppm): 170.6, 154.0, 153.7, 151.6, 150.8, 139.4, 136.2, 128.8, 128.7, 127.7, 127.3, 122.0, 116.7, 114.5, 82.8, 55.6, 38.6, 28.2. ESI-MS (ion trap): m/z 970 $[M+H]^+$. HRMS (ESI+): *m/z* 970.4499 $[M+H]^+$, calcd for $C_{56}H_{64}N_3O_{12}$: 970.4490

*General procedure for the tert-butyl ester deprotection in resveratrol-amino acid carbamoyl conjugates (**2**–**5**).* The t-butyl protected resveratrol-amino acid carbamoyl conjugate (**2c**–**5c**) (1.12 mmol) was dissolved in 10 mL of DCM at 0 °C. 500 μL of TIPS and 10 mL of TFA were then added and the reaction mixture was stirred at room temperature under nitrogen overnight. The solvent and residual TFA were removed under reduced pressure. The residue was triturated with toluene (3 × 5 mL), and the solvent was removed under reduced pressure. The product was purified by preparative reverse phase HPLC.

*(E)-2,2′-((((5-(4-(((1-carboxy-3-methylbutyl)carbamoyl)oxy)styryl)-1,3-phenylene)bis(oxy))bis(carbonyl))bis(azanediyl))bis(4-methylpentanoic acid) (**2**).* Purified using a reverse-phase preparative HPLC column (ACE 5AQ 150 mm × 21.2 mm from 7.5% to 38% of ACN in water in 14.5 minutes). 89% yield as a white powder after freeze-drying. ^{1}H-NMR (250 MHz, DMSO-d_6) δ (ppm): 0.89–0.94 (m, 18 H, 3 × -CH(CH_3)$_2$), 1.45–1.81 (m, 9 H, 3 × -CH-CH_2- and 3 × $(CH_3)_2$C*H*-), 3.98–4.07 (m, 3 H, -NH-C*H*-), 6.76 (t, 1 H, $^4J_{H\text{-}H}$ = 2 Hz, H-4), 7.10–7.38 (m, 6 H, H-3′, H-5′, H-2, H-6, H-7, H-8), 7.63 (d, 2 H, H-2′, H-6′, $^3J_{H\text{-}H}$ = 8.7 Hz), 8.12–8.21 (m, 3 H, 3 × -N*H*-); ^{13}C-NMR (250 MHz, DMSO-d_6) δ(ppm): 174.1, 174.0, 154.4, 154.2, 151.6, 150.7, 139.1, 133.7, 129.3, 127.6, 126.8, 121.9, 116.3, 114.4, 52.5, 39.6, 24.4, 23.0, 21.2. ESI-MS (ion trap): m/z 700 $[M+H]^+$. HRMS (ESI+): *m/z* 700.3092 $[M+H]^+$, calcd for $C_{35}H_{46}N_3O_{12}$: 700.3081.

*(E)-2,2′-((((5-(4-(((1-carboxy-2-methylbutyl)carbamoyl)oxy)styryl)-1,3-phenylene)bis(oxy))bis(carbonyl))bis(azanediyl))bis(3-methylpentanoic acid) (**3**).* Purified using a reverse-phase preparative HPLC column (ACE 5AQ 150 mm × 21.2 mm from 40% to 70% of ACN in water in 11 minutes). 93% yield as a white powder after freeze-drying. ^{1}H-NMR (300 MHz, DMSO) δ (ppm): 0.86–0.95 (m, 18H, 3 × -CH_2-CH_3 and 3 × -CH-CH_3), 1.21–1.55 (m, 6H, 3 × -CH-CH_2), 1.80–1.91 (m, 3 H, -CH-C*H*-CH_3), 3.89–4.13 (m, 3 H, 3 × NH-C*H*-CH), 6.77 (t, 1 H, $^4J_{H\text{-}H}$ = 2 Hz, H-4), 7.06–7.37 (m, 6 H, H-3′, H-5′, H-2, H-6, H-7, H-8), 7.63 (d, 2 H, H-2′, H-6′, $^3J_{H\text{-}H}$ = 8.7 Hz), 8.04 (d, 1 H, -N*H*-, $^3J_{H\text{-}H}$ = 8.4 Hz), 8.10 (d, 2 H, 2 × -N*H*-, $^3J_{H\text{-}H}$ = 8.4 Hz); ^{13}C-NMR (300 MHz, DMSO) δ(ppm): 175.1, 175.0, 156.7, 156.5, 153.8, 152.9, 141.3, 135.8, 131.5, 129.8, 124.1, 118.4, 97.3, 61.0, 38.3, 26.9, 17.8, 13.5. ESI-MS (ion trap): m/z 700 $[M+H]^+$. HRMS (ESI+): *m/z* 700.3075 $[M+H]^+$, calcd for $C_{35}H_{46}N_3O_{12}$: 700.3081.

(E)-2,2′-((((5-(4-(((1-carboxy-2-hydroxypropyl)carbamoyl)oxy)styryl)-1,3-phenylene)bis(oxy))bis(carbonyl))bis(azanediyl))bis(3-hydroxybutanoic acid) (**4**). Purified using a reverse-phase preparative HPLC column (ACE 5AQ 150 mm × 21.2 mm from 7.5% to 38% of ACN in water in 14.5 minutes). 91% yield as a white powder after freeze-drying. ^{1}H-NMR (250 MHz, DMSO-d_6) δ (ppm): 1.17–1.19 (m, 9 H, 3 × -CH-C*H*$_3$), 4.00–4.23 (m, 6 H, 3 × CH_3-C*H*- and 3 × NH-C*H*-), 6.80 (t, 1 H, $^{4}J_{H\text{-}H}$ = 2 Hz, H-4), 7.01–7.39 (m, 6 H, H-3′, H-5′, H-2, H-6, H-7, H-8), 7.61–7.72 (m, 5 H, 3 × -N*H*- and H-2′, H-6′); ^{13}C-NMR (250 MHz, DMSO-d_6) δ(ppm):172.1, 172.1, 154.8, 154.6, 151.7, 150.8, 139.2, 133.8, 129.4, 127.7, 126.9, 122.0, 116.4, 114.6, 66.5, 60.4, 48.7, 20.5. ESI-MS (ion trap): m/z 664 $[M+H]^+$. HRMS (ESI+): *m/z* 664.1993 $[M+H]^+$, calcd for $C_{29}H_{34}N_3O_{12}$: 664.1990.

(E)-2,2′-((((5-(4-(((1-carboxy-2-phenylethyl)carbamoyl)oxy)styryl)-1,3-phenylene)bis(oxy))bis(carbonyl))bis(azanediyl))bis(3-phenylpropanoic acid) (**5**). Purified using a reverse-phase preparative HPLC column (ACE 5AQ 150 mm × 21.2 mm from 35% to 65% of ACN in water in 13 minutes). 91% yield as a white powder after freeze-drying. 1H-NMR (250 MHz, DMSO-d_6) δ (ppm): 2.86–3.19 (m, 6 H, 3 × Ph-C*H*$_2$), 4.21–4.30 (m, 3H, 3 × -NH-C*H*-CH$_2$), 6.47 (t, 1 H, $^{4}J_{H\text{-}H}$ = 2 Hz, H-4), 6.91–7.33 (m, 21 H, Ar-*H* and H-3′, H-5′, H-2, H-6, H-7, H-8), 7.58 (d, 2 H, H-2′, H-6′, $^{3}J_{H\text{-}H}$ = 8.7 Hz), 8.20–8.29 (m, 3H, 3 × -N*H*-); 13C-NMR (62.9 MHz, DMSO-d_6) δ (ppm): 173.0, 154.3, 154.0, 151.5, 150.7, 139.1, 137.8, 137.8, 133.6, 129.3, 128.3, 127.6, 126.6, 121.8, 116.1, 114.2, 55.8, 55.0, 36.6; ESI-MS (ion trap): m/z 802 $[M+H]^+$. HRMS (ESI+): *m/z* 802.2604 $[M+H]^+$, calcd for $C_{44}H_{40}N_3O_{12}$: 802.2612.

Stability under physiologically relevant conditions. The stability of all new compounds was tested in aqueous media imitating gastric (0.1 N HCl, NormaFix) and intestinal (0.1 M PBS buffer, pH 6.8) conditions. A 5 μM solution of the compound was prepared from a 5 mM stock solution in DMSO, and incubated at 37 °C for 24 hours; samples withdrawn at different times were analysed by HPLC-UV. Hydrolysis products were identified by HPLC/ESI-MS analysis of selected samples. Non-linear curve fitting was performed using Origin 8.0 data analysis software, using the equations described in[55,61].

Stability in rat whole blood. Rats were anesthetised and blood was withdrawn from the jugular vein, and transferred into tubes containing heparin. Blood samples (1 mL) were spiked with 5 μM compound (dilution from a 5 mM stock solution in DMSO), and incubated at 37 °C for 4 hours (the maximum period allowed by blood stability). Aliquots were taken after 10 min, 30 min, 1 h, 2 h and 4 h and treated as described below (blood sample treatment and analysis). Cleared blood samples were finally subjected to HPLC-UV analysis.

Blood sample treatment and analysis. Before starting the treatment, 4,4′-dihydroxybiphenyl was added as internal standard to a carefully measured blood volume (25 μM final concentration). 0.1 vol of 0.6 M TEA (pH 8.0) and 4 vol of MeOH were then added to the blood samples, which were then sonicated (2 min) and centrifuged (12,000 g, 7 min, 4 °C). The supernatant was finally collected and stored at −20 °C. Before analysis, MeOH was evaporated off at room temperature using a Univapo 150H (UniEquip) vacuum concentrator centrifuge, and up to 40 μL of ACN were added to precipitate residual proteins. After centrifugation (12,000 g, 5 min, 4 °C), cleared samples were directly subjected to HPLC-UV analysis. Metabolites and hydrolysis products were identified by comparison of chromatographic retention time with true samples or by HPLC/ESI-MS analysis.

Internal standard recovery from the treatment used to extract resveratrol-AA derivatives was 91.8 ± 10.7%. The recovery of **3**, expressed as ratio to the recovery of internal standard, was 0.633 ± 0.088. Recoveries of partially protected (disubstituted) derivatives (Fig. 7) were assumed to be the same as those of the corresponding fully substituted prodrug. Knowledge/assumption of these ratios allowed us to determine the unknown amount of analyte in a blood sample by measuring the recovery of internal standard[57].

Since sample treatment includes an evaporation/concentration step, LOD and LOQ were determined relatively to the analytical part of the method (HPLC/UV analysis). The prodrugs have the same absorption coefficient of resveratrol itself within experimental error; LOD and LOQ were thus the same of resveratrol (i.e., 0.04 and 0.12 μM, respectively[58]), and quantification of the analytes in blood samples was done using the same calibration curve of resveratrol (y = 5.3085 x), taking into account the recovery ratio.[57]

Pharmacokinetics studies. Derivatives **2–5** were administered to overnight-fasted male Wistar rats from the facility of the Department of Biomedical Sciences, University of Padova, as a single intragastric dose (88 μmol/Kg, dissolved in 250 μl DMSO). Blood samples were obtained by the tail bleeding technique: before drug administration, rats were anesthetised with isoflurane and the tip of the tail was cut off; blood samples (80–100 μL each) were then taken from the tail tip at different time points after drug administration. Blood was collected in heparinised tubes, kept in ice and treated as described above within 10 min.

All experiments involving animals were approved by the University of Padova Ethical Committee for Experimentation on Animals (CEASA) and performed with the supervision of the University Central Veterinary Service, in compliance with Italian Law DL 116/92, embodying UE Directive 86/609.

References

1. Jeandet, P. *et al.* Biosynthesis, metabolism, molecular engineering, and biological functions of stilbene phytoalexins in plants. *Biofactors* **36,** 331–341, doi: 10.1002/biof.108 (2010).
2. Agarwal, B. & Baur, J. A. Resveratrol and life extension. *Ann N Y Acad Sci* **1215,** 138–143, doi: 10.1111/j.1749-6632.2010.05850.x (2011).
3. Csiszar, A. Anti-inflammatory effects of resveratrol: possible role in prevention of age-related cardiovascular disease. *Ann N Y Acad Sci* **1215,** 117–122, doi: 10.1111/j.1749-6632.2010.05848.x (2011).
4. Kroon, P. A., Iyer, A., Chunduri, P., Chan, V. & Brown, L. The cardiovascular nutrapharmacology of resveratrol: pharmacokinetics, molecular mechanisms and therapeutic potential. *Curr Med Chem* **17,** 2442–2455, doi: 10.2174/092986710791556032 (2010).
5. Khurana, S., Venkataraman, K., Hollingsworth, A., Piche, M. & Tai, T. C. Polyphenols: benefits to the cardiovascular system in health and in aging. *Nutrients* **5,** 3779–3827, doi: 10.3390/nu5103779 (2013).
6. Raederstorff, D., Kunz, I. & Schwager, J. Resveratrol, from experimental data to nutritional evidence: the emergence of a new food ingredient. *Ann N Y Acad Sci* **1290,** 136–141, doi: 10.1111/nyas.12147 (2013).
7. Szkudelski, T. & Szkudelska, K. Anti-diabetic effects of resveratrol. *Ann N Y Acad Sci* **1215,** 34–39, doi: 10.1111/j.1749-6632.2010.05844.x (2011).
8. Liu, K., Zhou, R., Wang, B. & Mi, M. T. Effect of resveratrol on glucose control and insulin sensitivity: a meta-analysis of 11 randomized controlled trials. *Am J Clin Nutr* **99,** 1510–1519, doi: 10.3945/ajcn.113.082024 (2014).
9. Baile, C. A. *et al.* Effect of resveratrol on fat mobilization. *Ann N Y Acad Sci* **1215,** 40–47, doi: 10.1111/j.1749-6632.2010.05845.x (2011).
10. Wang, S. *et al.* Novel insights of dietary polyphenols and obesity. *J Nutr Biochem* **25,** 1–18, doi: 10.1016/j.jnutbio.2013.09.001 (2014).
11. Andrade, J. M. *et al.* Resveratrol increases brown adipose tissue thermogenesis markers by increasing SIRT1 and energy expenditure and decreasing fat accumulation in adipose tissue of mice fed a standard diet. *Eur J Nutr*, doi: 10.1007/s00394-014-0655-6 (2014).
12. Andrade, J. M. *et al.* Resveratrol attenuates hepatic steatosis in high-fat fed mice by decreasing lipogenesis and inflammation. *Nutrition* **30,** 915–919, doi: 10.1016/j.nut.2013.11.016 (2014).
13. Biasutto, L., Szabo, I. & Zoratti, M. Mitochondrial effects of plant-made compounds. *Antioxid Redox Signal* **15,** 3039–3059, doi: 10.1089/ars.2011.4021 (2011).
14. Park, S. J. *et al.* Resveratrol ameliorates aging-related metabolic phenotypes by inhibiting cAMP phosphodiesterases. *Cell* **148,** 421–433, doi: 10.1016/j.cell.2012.01.017 (2012).
15. Foti Cuzzola, V., Ciurleo, R., Giacoppo, S., Marino, S. & Bramanti, P. Role of resveratrol and its analogues in the treatment of neurodegenerative diseases: focus on recent discoveries. *CNS Neurol Disord Drug Targets* **10,** 849–862, doi: 10.2174/187152711798072310 (2011).
16. Quincozes-Santos, A. & Gottfried, C. Resveratrol modulates astroglial functions: neuroprotective hypothesis. *Ann N Y Acad Sci* **1215,** 72–78, doi: 10.1111/j.1749-6632.2010.05857.x (2011).
17. Aggarwal, B. B. *et al.* Role of resveratrol in prevention and therapy of cancer: preclinical and clinical studies. *Anticancer Res* **24,** 2783–2840 (2004).
18. Vanden Berghe, W. Epigenetic impact of dietary polyphenols in cancer chemoprevention: lifelong remodeling of our epigenomes. *Pharmacol Res* **65,** 565–576, doi: 10.1016/j.phrs.2012.03.007 (2012).
19. Kaminski, B. M., Steinhilber, D., Stein, J. M. & Ulrich, S. Phytochemicals resveratrol and sulforaphane as potential agents for enhancing the anti-tumor activities of conventional cancer therapies. *Curr Pharm Biotechnol* **13,** 137–146, doi: 10.2174/138920112798868746 (2012).
20. Gupta, S. C., Kannappan, R., Reuter, S., Kim, J. H. & Aggarwal, B. B. Chemosensitization of tumors by resveratrol. *Ann N Y Acad Sci* **1215,** 150–160, doi: 10.1111/j.1749-6632.2010.05852.x (2011).
21. Cottart, C. H., Nivet-Antoine, V. & Beaudeux, J. L. Review of recent data on the metabolism, biological effects, and toxicity of resveratrol in humans. *Mol Nutr Food Res* **58,** 7–21, doi: 10.1002/mnfr.201200589 (2014).
22. Subramanian, L. *et al.* Resveratrol: challenges in translation to the clinic–a critical discussion. *Clin Cancer Res* **16,** 5942–5948, doi: 10.1158/1078-0432.ccr-10-1486 (2010).
23. Walle, T. Bioavailability of resveratrol. *Ann N Y Acad Sci* **1215,** 9–15, doi: 10.1111/j.1749-6632.2010.05842.x (2011).
24. Yu, C. *et al.* Human, rat, and mouse metabolism of resveratrol. *Pharm Res* **19,** 1907–1914, doi: 10.1023/A:1021414129280 (2002).
25. Bresciani, L. *et al.* Bioaccumulation of resveratrol metabolites in myocardial tissue is dose-time dependent and related to cardiac hemodynamics in diabetic rats. *Nutr Metab Cardiovasc Dis* **24,** 408–415, doi: 10.1016/j.numecd.2013.09.008 (2014).
26. Walker, J. *et al.* Resveratrol and its metabolites inhibit pro-inflammatory effects of lipopolysaccharides in U-937 macrophages in plasma-representative concentrations. *Food Funct* **5,** 74–84, doi: 10.1039/c3fo60236b (2014).
27. Eseberri, I., Lasa, A., Churruca, I. & Portillo, M. P. Resveratrol metabolites modify adipokine expression and secretion in 3T3-L1 pre-adipocytes and mature adipocytes. *PLoS One* **8,** e63918, doi: 10.1371/journal.pone.0063918 (2013).
28. Lasa, A., Churruca, I., Eseberri, I., Andres-Lacueva, C. & Portillo, M. P. Delipidating effect of resveratrol metabolites in 3T3-L1 adipocytes. *Mol Nutr Food Res* **56,** 1559–1568, doi: 10.1002/mnfr.201100772 (2012).
29. Kenealey, J. D. *et al.* Resveratrol metabolites do not elicit early pro-apoptotic mechanisms in neuroblastoma cells. *J Agric Food Chem* **59,** 4979–4986, doi: 10.1021/jf104901g (2011).
30. Lu, D. L. *et al.* Influence of glucuronidation and reduction modifications of resveratrol on its biological activities. *Chembiochem* **14,** 1094–1104, doi: 10.1002/cbic.201300080 (2013).
31. Calamini, B. *et al.* Pleiotropic mechanisms facilitated by resveratrol and its metabolites. *Biochem J* **429,** 273–282, doi: 10.1042/bj20091857 (2010).
32. Hoshino, J. *et al.* Selective synthesis and biological evaluation of sulfate-conjugated resveratrol metabolites. *J Med Chem* **53,** 5033–5043, doi: 10.1021/jm100274c (2010).
33. Herath, W., Khan, S. I. & Khan, I. A. Microbial metabolism. Part 14. Isolation and bioactivity evaluation of microbial metabolites of resveratrol. *Nat Prod Res* **27,** 1437–1444, doi: 10.1080/14786419.2012.722089 (2013).
34. Ruotolo, R. *et al.* Anti-estrogenic activity of a human resveratrol metabolite. *Nutr Metab Cardiovasc Dis* **23,** 1086–1092, doi: 10.1016/j.numecd.2013.01.002 (2013).
35. Patel, K. R. *et al.* Sulfate metabolites provide an intracellular pool for resveratrol generation and induce autophagy with senescence. *Sci Transl Med* **5,** 205ra133, doi: 10.1126/scitranslmed.3005870 (2013).
36. Andreadi, C., Britton, R. G., Patel, K. R. & Brown, K. Resveratrol-sulfates provide an intracellular reservoir for generation of parent resveratrol, which induces autophagy in cancer cells. *Autophagy* **10,** 524–525, doi: 10.4161/auto.27593 (2014).
37. Ghosh, A. K. & Brindisi, M. Organic Carbamates in Drug Design and Medicinal Chemistry. *J Med Chem*, doi: 10.1021/jm501371s (2015).
38. Hansen, J., Mørk, N. & Bundgaard, H. Phenyl carbamates of amino acids as prodrug forms for protecting phenols against first-pass metabolism. *Int J Pharm* **81,** 253–261, doi: 10.1016/0378-5173(92)90017-V (1992).

39. Biasutto, L. & Zoratti, M. Prodrugs of quercetin and resveratrol: a strategy under development. *Curr Drug Metab* **15,** 77–95, doi: 10.2174/1389200214666131211160005 (2014).
40. Ferriz, J. M. & Vinsova, J. Prodrug design of phenolic drugs. *Curr Pharm Des* **16,** 2033–2052, doi: 10.2174/138161210791293042 (2010).
41. Dhareshwar, S. & Stella, V. In *Prodrugs* Vol. V *Biotechnology: Pharmaceutical Aspects* eds Valentino J Stella *et al.*) Ch. 21, 731–799 (Springer New York, 2007).
42. Mulholland, P. J. *et al.* Pre-clinical and clinical study of QC12, a water-soluble, pro-drug of quercetin. *Ann Oncol* **12,** 245–248, doi: 10.1023/A:1008372017097 (2001).
43. Kim, M. K., Park, K. S., Yeo, W. S., Choo, H. & Chong, Y. *In vitro* solubility, stability and permeability of novel quercetin-amino acid conjugates. *Bioorg Med Chem* **17,** 1164–1171, doi: 10.1016/j.bmc.2008.12.043 (2009).
44. Mattarei, A. *et al.* New water-soluble carbamate ester derivatives of resveratrol. *Molecules* (*Basel, Switzerland)* **19,** 15900–15917, doi: 10.3390/molecules191015900 (2014).
45. Vig, B. S., Huttunen, K. M., Laine, K. & Rautio, J. Amino acids as promoieties in prodrug design and development. *Adv Drug Deliver Rev* **65,** 1370–1385, doi:10.1016/j.addr.2012.10.001 (2013).
46. Broer, S. Amino acid transport across mammalian intestinal and renal epithelia. *Physiol Rev* **88,** 249–286, doi: 10.1152/physrev.00018.2006 (2008).
47. Brandsch, M. Drug transport via the intestinal peptide transporter PepT1. *Curr Opin Pharmacol* **13,** 881–887, doi: 10.1016/j.coph.2013.08.004 (2013).
48. Estudante, M., Morais, J. G., Soveral, G. & Benet, L. Z. Intestinal drug transporters: an overview. *Adv Drug Deliver Rev* **65,** 1340–1356, doi: 10.1016/j.addr.2012.09.042 (2013).
49. Tamai, I. Oral drug delivery utilizing intestinal OATP transporters. *Adv Drug Deliver Rev* **64,** 508–514, doi: 10.1016/j.addr.2011.07.007 (2012).
50. del Amo, E. M., Urtti, A. & Yliperttula, M. Pharmacokinetic role of L-type amino acid transporters LAT1 and LAT2. *Eur J Pharm Sci* **35,** 161–174, doi: 10.1016/j.ejps.2008.06.015 (2008).
51. Gynther, M. *et al.* Large neutral amino acid transporter enables brain drug delivery via prodrugs. *J Med Chem* **51,** 932–936, doi: 10.1021/jm701175d (2008).
52. Peura, L. *et al.* Large amino acid transporter 1 (LAT1) prodrugs of valproic acid: new prodrug design ideas for central nervous system delivery. *Mol Pharm* **8,** 1857–1866, doi: 10.1021/mp2001878 (2011).
53. Peura, L. *et al.* Design, synthesis and brain uptake of LAT1-targeted amino acid prodrugs of dopamine. *Pharm Res* **30,** 2523–2537, doi: 10.1007/s11095-012-0966-3 (2013).
54. Wu, X., Cheng, L., Xiang, D. & Wei, Y. Syntheses of Carbamate Derivatives of Quercetin by Reaction with Amino Acid Ester Isocyanates. *Lett Org Chem* **2,** 535–538, doi: 10.2174/1570178054640796 (2005).
55. Kozerski, G. E., Gallavan, R. H. & Ziemelis, M. J. Investigation of trialkoxysilane hydrolysis kinetics using liquid chromatography with inductively coupled plasma atomic emission spectrometric detection and non-linear regression modeling. *Anal Chim Acta* **489,** 103–114, doi: 10.1016/S0003-2670(03)00710-4 (2003).
56. Adams, P. & Baron, F. A. Esters of Carbamic Acid. *Chem Rev* **65,** 567–602, doi: 10.1021/cr60237a002 (1965).
57. Azzolini, M. *et al.* Pharmacokinetics and tissue distribution of pterostilbene in the rat. *Mol Nutr Food Res* **58,** 2122–2132, doi: 10.1002/mnfr.201400244 (2014).
58. Biasutto, L., Marotta, E., Garbisa, S., Zoratti, M. & Paradisi, C. Determination of quercetin and resveratrol in whole blood–implications for bioavailability studies. Molecules (*Basel, Switzerland)* **15,** 6570–6579, doi: 10.3390/molecules15096570 (2010).
59. Biasutto, L. *et al.* Soluble polyphenols: synthesis and bioavailability of 3,4′,5-tri(alpha-D-glucose-3-O-succinyl) resveratrol. *Bioorg Med Chem Lett* **19,** 6721–6724, doi: 10.1016/j.bmcl.2009.09.114 (2009).
60. Mattarei, A. *et al.* New derivatives of resveratrol. (2014). European Patent Application EP2774915. Application Number EP20140157948. Filing date 03/05/2014. Publication Date 09/10/2014.
61. Mattarei, A. *et al.* Acetal derivatives as prodrugs of resveratrol. *Mol Pharm* **10,** 2781–2792, doi: 10.1021/mp400226p (2013).

Acknowledgements

This work was supported by grants from the Fondazione Cassa di Risparmio di Padova e Rovigo (CARIPARO) ("Developing a Pharmacology of Polyphenols"), from the Italian Ministry of the University and Research (PRIN n. 20107Z8XBW_004), and by the CNR Project of Special Interest on Aging.

Author Contributions

A.M., C.P., M.Z. and L.B. designed the study and wrote the manuscript; A.M. carried out the syntheses; M.A., L.B. and M.L.S. performed the hydrolysis studies and pharmacokinetics experiments. All authors reviewed the manuscript.

Additional Information

Competing financial interests: The authors have applied for a patent covering the compounds described in this paper.

How to cite this article: Mattarei, A. *et al.* Amino Acid Carbamates As Prodrugs Of Resveratrol. *Sci. Rep.* **5**, 15216; doi: 10.1038/srep15216 (2015).

This work is licensed under a Creative Commons Attribution 4.0 International License. The images or other third party material in this article are included in the article's Creative Commons license, unless indicated otherwise in the credit line; if the material is not included under the Creative Commons license, users will need to obtain permission from the license holder to reproduce the material. To view a copy of this license, visit http://creativecommons.org/licenses/by/4.0/

molecular pharmaceutics

Article

pubs.acs.org/molecularpharmaceutics

Synthesis and Evaluation as Prodrugs of Hydrophilic Carbamate Ester Analogues of Resveratrol

Michele Azzolini,[†,‡,⊥] Andrea Mattarei,[§,⊥] Martina La Spina,[†] Ester Marotta,[§] Mario Zoratti,[†,∥] Cristina Paradisi,[§] and Lucia Biasutto*[,†,∥]

[†]Department of Biomedical Sciences, University of Padova, viale G. Colombo 3, 35131 Padova, Italy

[‡]NÓOS Srl, via Campello sul Clitunno 34, 00181 Roma, Italy

[§]Department of Chemical Sciences, University of Padova, via Marzolo 1, 35121 Padova, Italy

[∥]CNR Neuroscience Institute, viale G. Colombo 3, 35131 Padova, Italy

ABSTRACT: Resveratrol (3,5,4′-trihydroxy-*trans*-stilbene) is an unfulfilled promise for health care: its exploitation is hindered by rapid conjugative metabolism in enterocytes and hepatocytes; low water solubility is a serious practical problem. To advantageously modify the physicochemical properties of the compound we have developed prodrugs in which all or part of the hydroxyl groups are linked via an N-monosubstituted carbamate ester bond to promoieties derived from glycerol or galactose, conferring higher water solubility. Kinetic studies of hydrolysis in aqueous solutions and in blood indicated that regeneration of resveratrol takes place in an appropriate time frame for delivery via oral administration. Despite their hydrophilicity some of the synthesized compounds were absorbed in the gastrointestinal tract of rats. In these cases the species found in blood after administration of a bolus consisted mainly of partially deprotected resveratrol derivatives and of the products of their glucuronidation, thus providing proof-of-principle evidence of behavior as prodrugs. The soluble compounds largely reached the lower intestinal tract. Upon administration of resveratrol, the major species found in this region was dihydroresveratrol, produced by enzymes of the intestinal flora. In experiments with a fully protected (trisubstituted) deoxygalactose containing prodrug, the major species were the prodrug itself and partially deprotected derivatives, along with small amounts of dihydroresveratrol. We conclude that the N-monosubstituted carbamate moiety is suitable for use in prodrugs of polyphenols.



KEYWORDS: *resveratrol, bioavailability, prodrugs, carbamate ester, pharmacokinetics, galactose, glycerol*

■ INTRODUCTION

Resveratrol (3,5,4′-trihydroxy-*trans*-stilbene) is well-known to the public as a "natural drug", potentially useful on major health battlefields: afflictions of the cardiovascular system,[1−3] neurodegeneration,[4−7] aging,[8,9] diabetes, obesity, metabolic syndrome,[10−12] and cancer.[13,14]

This multiplicity of potential biomedical effects stems from the impact resveratrol has on the activity of apical or key proteins in interconnected cellular signaling networks. Among its major effects observed *in vitro*, resveratrol inhibits phosphodiesterases, leading to an increase of cellular cAMP.[15,16] Signaling along the cAMP-AMPK-mTORC1 axis is thought to largely account for the antagonistic activity of resveratrol vs metabolic syndrome.[17,18] Modulation of this pathway,[19] but also of others, e.g., the activity of MTA1[20] and of microRNAs,[21,22] is important in cancer. After much debate, a consensus now seems to have been reached that resveratrol also induces upregulation of SIRT1, an important NAD-dependent histone deacetylase.[23,24] Enhancement of SIRT1 activity has pleiotropic epigenetic effects, reportedly culminating in life extension and health improvement in mice.[25,26] Another, interwined[27−29] major way resveratrol acts is by antagonizing inflammation.[30,31] Chronic inflammation is well recognized to be a factor in carcinogenesis.[32−34] A relevant example is provided by the frequent insurgence of polyposis and colon cancer in humans[35−37] and laboratory animals[38,39] affected by inflammatory bowel disease. Resveratrol has been reported to be beneficial in rodent models of colitis, polyposis, and colon cancer induced by sodium dextran sulfate (DSS) or azoxymethane + DSS.[40−44]

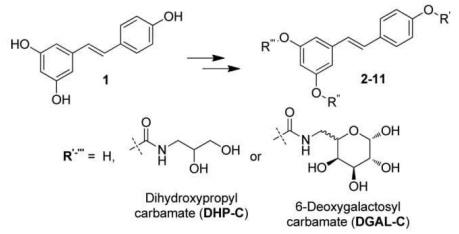
Resveratrol is not, however, free of shortcomings. The major one is its built-in propensity, common to all polyphenols, to undergo Phase II metabolic conjugation to give sulfated and glucuronidated derivatives.[45−50] In addition resveratrol undergoes reduction of the double bond plus other transformations by the colonic flora.[51,52] It has therefore often been pointed out[53] that the results of studies carried out *in vitro* with high concentrations of unmodified resveratrol may be of little pharmacological or nutritional relevance. Another unfavorable characteristic of resveratrol is its low water solubility.

Received: June 12, 2015
Revised: July 28, 2015
Accepted: August 7, 2015
Published: August 7, 2015

ACS Publications © 2015 American Chemical Society

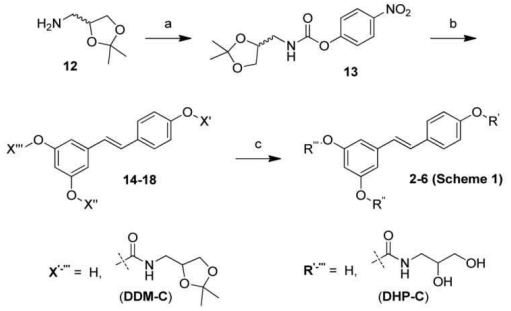
DOI: 10.1021/acs.molpharmaceut.5b00464
Mol. Pharmaceutics 2015, 12, 3441−3454

Scheme 1. Molecular Structure of Resveratrol (1, *trans*-3,5,4′-Trihydroxy Stilbene) and Its Carbamate Ester Derivatives Synthesized in This Work (2−11)



	R’	R’’	R’’’
2	DHP-C	H	H
3	H	DHP-C	H
4	DHP-C	DHP-C	H
5	H	DHP-C	DHP-C
6	DHP-C	DHP-C	DHP-C
7	DGAL-C	H	H
8	H	DGAL-C	H
9	DGAL-C	DGAL-C	H
10	H	DGAL-C	DGAL-C
11	DGAL-C	DGAL-C	DGAL-C

Scheme 2. Synthesis of Derivatives 2−6[a]



	X’	X’’	X’’’
14	DDM-C	H	H
15	H	DDM-C	H
16	DDM-C	DDM-C	H
17	H	DDM-C	DDM-C
18	DDM-C	DDM-C	DDM-C

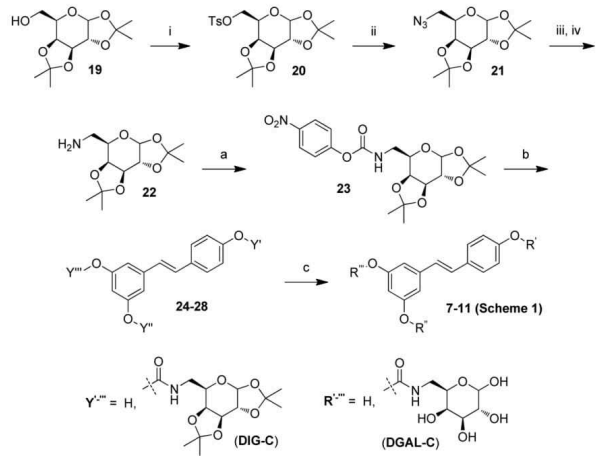
[a]Reagents and conditions: (a) bis(4-nitrophenyl) carbonate, DMAP, THF, RT, 3 h; (b) resveratrol (1), pyridine, DMAP, 70 °C, 16 h; (c) trifluoroacetic acid/water 9:1, RT, 1.5 h.

A variety of formulations and nanostructured delivery systems are being tested with the goal of overcoming these obstacles.[54,55] Another approach relies on the construction of prodrugs, i.e., reversible derivatives with favorable physicochemical properties, which can offer initial protection from metabolism and regenerate the active compound with appropriate kinetics.[55,56] As the molecular mechanisms of action are clarified and polyphenols tend to be viewed more and more as drugs rather than as nutrients, it seems well justified to apply this strategy and to develop a pharmacology of bioactive natural compounds. Indeed, in view of the many-fold activities and possible applications of resveratrol there is a need for customized delivery vehicles and/or chemical elaborations to best achieve the specific task at hand. Thus, returning to the example of the use of resveratrol against colitis and associated pathologies, specific delivery to the colon has been obtained using a formulation (Ca pectinate beads)[57] or sophisticated prodrugs comprising a glucose moiety linked to resveratrol via a glycosidic bond and an hydrocarbon chain linked to the sugar ring by an ester bond.[58] In addition to the acetal bond system,[58,59] other groups including carboxyester, sulfonate, and carbonate have been tested as protective, reversible capping groups for the hydroxyls of resveratrol. However, none of them has proven satisfactory.[55,56]

The carbamoyl ester linkage is a promising alternative.[60] A first family of resveratrol prodrugs was produced and tested, in which the phenolic OH groups are masked as −O−C(═O)−N(CH_3)R where R is a methoxypolyethylene glycol-350 (mPEG-350) or a butyl-glucosyl group.[61] These derivatives are highly soluble in aqueous media but too stable to be used as prodrugs.[61] N-monosubstituted carbamates are expected to undergo faster hydrolysis.[62] Here we report the synthesis and characterization of mono-, di-, and trisubstituted resveratrol derivatives incorporating promoieties imparting water solubility (dihydroxypropyl and 6-deoxygalactosyl moieties) linked via N-monosubstituted carbamate ester bonds to the phenolic oxygens of resveratrol. The kinetics and products of hydrolysis have been studied, and the fate of the prodrugs after oral administration to rats has been investigated. The results indicate that these new compounds may be useful for all applications in which water solubility and protection from metabolism and oxidation are important.

DOI: 10.1021/acs.molpharmaceut.5b00464
Mol. Pharmaceutics 2015, 12, 3441−3454

Scheme 3. Synthesis of Derivatives 7−11[a]



	Y'	Y''	Y'''
24	DIG-C	H	H
25	H	DIG-C	H
26	DIG-C	DIG-C	H
27	H	DIG-C	DIG-C
28	DIG-C	DIG-C	DIG-C

[a]Reagents and conditions: (i) tosyl chloride, pyridine, DMAP, from 0 °C to RT, 5 h; (ii) sodium azide, DMSO, 160 °C, 1.5 h; (iii) triphenylphosphine, THF, RT, 4 h; (iv) water, reflux, 16 h; (a) bis(4-nitrophenyl) carbonate, DMAP, THF, RT, 3 h; (b) resveratrol (**1**), pyridine, DMAP, 70 °C, 16 h; (c) trifluoroacetic acid/water 9:1, RT, 1.5 h.

■ RESULTS AND DISCUSSION

Synthesis. The new derivatives of resveratrol (**1**) synthesized in this work, compounds **2**−**11**, are shown in Scheme 1.

The synthesis of **2**-**6** is outlined in Scheme 2. The starting material for the dihydroxypropyl carbamate (**DHP**-**C**) moiety was commercially available, 2,2-dimethyl-1,3-dioxolane-4-methanamine (**12**), which was allowed to react with bis(4-nitrophenyl) carbonate in the presence of 4-(dimethylamino)-pyridine (DMAP) to give the corresponding activated urethane (**13**) in good yield. Compound **13** was added in slight excess to resveratrol (**1**) in pyridine and in the presence of DMAP and allowed to react at 70 °C to obtain a mixture of all the possible mono-, di-, and tri-substituted resveratrol derivatives (**14**−**18**). The last step consisted in the removal of the isopropylidene protecting groups, freeing the hydroxyl functions necessary to enhance the solubility in water of the final products (**2**−**6**), which were finally isolated by preparative reverse-phase HPLC. Purity was in all cases >95%, as assessed by HPLC-UV analysis.

The synthesis of derivatives **7**−**11** (Scheme 3) was somewhat more complex because the starting reagent, amine (**22**), is not commercially available and had to be synthesized. The starting material in this case was 1,2:3,4-di-*O*-isopropylidene-α-D-galactopyranose (**19**), possessing one free hydroxyl group, which was esterified with tosyl chloride to obtain compound **20**. The tosylate group of **20** was easily displaced in the second step by sodium azide giving the azide (**21**) in nearly quantitative yield. Azide **21** was then reduced under Staudinger reaction conditions to give the desired primary amine (**22**) in excellent yield. The subsequent synthetic steps are equivalent to those reported above for derivatives (**2**−**6**), and consisted in the production of the active urethane (**23**) followed by transesterification with resveratrol to give a mixture of all the possible mono-, di-, and tri-substituted resveratrol derivatives (**24**−**28**). Cleavage of the isopropylidene protecting groups afforded the desired resveratrol-6-deoxy-galactosyl carbamate ester conjugates (**7**−**11**), which were isolated by preparative HPLC.

Log P_{ow}, Solubility, and TPSA. The octanol/water partition coefficient, water solubility, and the polar surface area were estimated for all new compounds synthesized (Table 1) (see Experimental Section). The molecular polar surface area is the sum of the surfaces of polar atoms (primarily oxygen, nitrogen, and their hydrogens) in a molecule, as calculated from molecular models taking into account atomic dimensions (modeled as spheres).[63,64] The ability to permeate cell membranes is considered to be inversely related to this parameter, which is instead positively linked to water solubility.

Table 1. Log P_{ow}, Water Solubility, and Topological PSA Values of Resveratrol and Its Carbamate Ester Derivatives[a]

compd	log P_{ow}	PSA (Å^2)	solubility (g/L)
resveratrol (**1**)	2.69 ± 0.12[b,59]	60.68	0.039 ± 0.009[b,59]
2	1.57	119.24	0.049
3	1.57	119.24	0.054
4	0.15	177.80	0.12
5	0.15	177.80	0.13
6	−1.27	236.36	0.20
7	0.52	168.93	1.38
8	0.52	168.93	1.51
9	−1.94	277.18	2.53
10	−1.94	277.18	2.80
11	−4.34	385.43	>4.22[b]

[a]Algorithm-predicted values unless otherwise indicated. [b]Experimental value.

Hydrolysis Studies. All the compounds proved to be stable over a 24 h period in acidic solution (0.1 N HCl) at 37 °C. In contrast, they underwent hydrolysis of the carbamoyl bond in 0.1 M PBS buffer at pH 6.8 and 37 °C. Kinetic results obtained

DOI: 10.1021/acs.molpharmaceut.5b00464
Mol. Pharmaceutics 2015, 12, 3441−3454

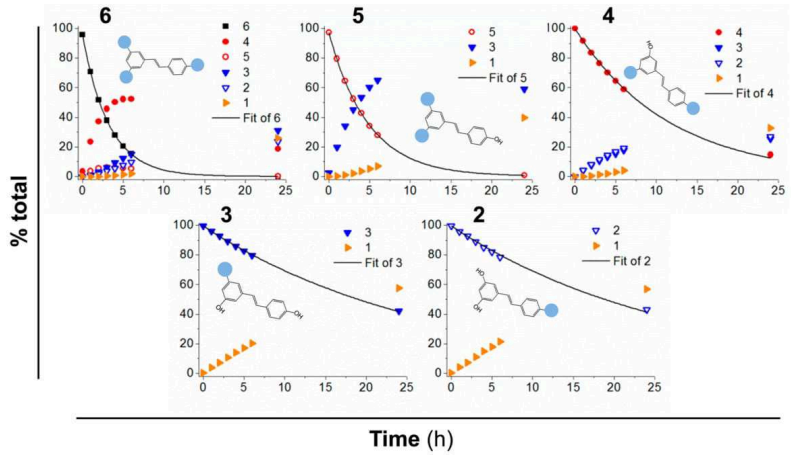


Figure 1. Hydrolysis of resveratrol dihydroxypropyl carbamate ester derivatives (**2**–**6**) in PBS 0.1 M, pH 6.8, 37 °C. Hydrolysis of the trisubstituted compound **6** forms disubstituted isomers **4** and **5**. In turn, hydrolysis of **4** leads to a mixture of monosubstituted isomers **2** and **3**, while **5** can only give rise to **3**. Finally, hydrolysis of either **2** or **3** yields resveratrol, **1**. Data are expressed as % of the initially loaded compound. The fit is for pseudo-first order kinetics.

Table 2. Rate Constants (k) for Hydrolysis of Resveratrol Derivatives 2−11 in Aqueous PBS 0.1 M, at pH 6.8 and 37°C

Substitution pattern	Compound	$10^2 \cdot k$ (h^{-1})	Compound	$10^2 \cdot k$ (h^{-1})
	**6**	30.72 ± 0.08	**11**	32.9 ± 0.3
	**5**	20.63 ± 0.09	**10**	23.8 ± 0.7
	**4**	8.7 ± 0.1	**9**	8.8 ± 0.1
	**3**	3.62 ± 0.03	**8**	3.15 ± 0.03
	**2**	3.66 ± 0.08	**7**	3.69 ± 0.09

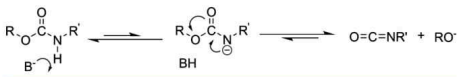
with the dihydroxypropyl carbamate ester derivatives **2**-**6** are shown in Figure 1, which reports time profiles for reactants, intermediates, and products. The experimental data of reactant conversion are nicely fitted by a first order exponential decay equation, from which rate constants (k) for hydrolysis of **2**–**6** were derived.

Similar behavior was observed with the 6-deoxygalactosyl carbamate ester derivatives **7**–**11** (kinetic plots not shown). The pseudo-first order hydrolysis rate constants obtained in all these kinetic experiments are collected in Table 2. As was reasonably expected, hydrolysis of multifunctional derivatives proceeds in a stepwise manner. Thus, reaction of the trisubstituted derivative **6** leads to disubstituted resveratrols **4** and **5**, which in turn hydrolyze to the monosubstituted compounds **2** and **3** (Figure 1). Interestingly, the data in Table 2 show that different isomers undergo hydrolysis at different rates. Specifically, if one considers the disubstituted isomers (3,4′- vs 3,5-; i.e., **4** vs **5**, **9** vs **10**), it appears that the presence of two carbamoyl moieties in the same ring (at positions 3 and 5) accelerates the hydrolysis process. This conclusion is consistent with the product distribution observed in the hydrolysis of the trisubstituted derivatives **6** and **11**. In both cases, the 3,4′-isomers, **4** and **9**, are present in larger amounts with respect to the more reactive 3,5-isomers, **5** and **10**, respectively.

When only one carbamoyl function is present in the molecule, the rate of its hydrolysis is not affected by the specific position occupied (see the similar reactivity of 4′- and 3-monosubstituted derivatives, **2** vs **3** and **7** vs **8** in Table 2).

Our results are consistent with a base catalyzed mechanism of hydrolysis proceeding via deprotonation and release of an isocyanate reactive intermediate, as sketched in Scheme 4.[65]

Scheme 4. Mechanism of Base Catalyzed Hydrolysis of N-Monosubstituted Carbamate Esters



This mechanism is not viable under acidic conditions, which accounts for the observation that derivatives **2**–**11** are stable in acidic solutions. It is also obviously not viable for

DOI: 10.1021/acs.molpharmaceut.5b00464
Mol. Pharmaceutics 2015, 12, 3441−3454

N,N-disubstituted carbamate esters, which accounts for the observation that N,N-disubstituted analogues of **2**–**11** were found to be stable also in neutral and basic solutions.[61]

To verify whether these derivatives would withstand long-term storage in aqueous formulations we followed the hydrolysis of compound **11** in citrate buffer (5 mM each) at pH 5.0 and 6.0, at 4 °C and at room temperature, over several months. The results (Figure 2) indicate that indeed hydrolysis is very slow under these conditions.

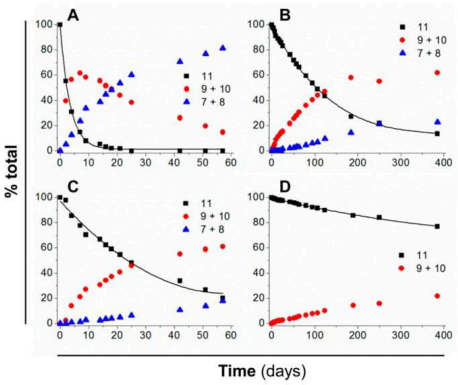


Figure 2. Long-term stability of **11** against hydrolysis in aqueous citrate buffer. (A) pH 6, room temperature (RT); (B) pH 6, 4 °C; (C) pH 5, RT; (D) pH 5, 4 °C.

Hydrolysis in Blood. Hydrolysis in blood (Figure 3) was faster than in PBS pH 6.8. Reaction rates were similar for dihydroxypropyl and 6-deoxygalactosyl carbamate ester derivatives. As found for reaction in aqueous PBS solutions, hydrolysis in blood is favored by the presence of two carbamoyl groups on the same ring. Thus, reaction of **5** and **10** is faster than that of their isomers **4** and **9**, respectively. In the case of monosubstituted derivatives, the rate of hydrolysis depends on the substitution position, the compounds substituted in 4′ reacting markedly more rapidly than their 3-substituted isomers (see Figure 3 and Table 3). This indicates the involvement of a regioselective (enzymatic) hydrolysis mechanism since in aqueous buffered solutions the rates are similar for isomeric monosubstituted pairs (**2** and **3**, **7** and **8**).

Plasma albumin has carbamoyl esterase activity,[66,67] and it has been reported to be the main component of plasma catalyzing hydrolysis of phenolic carbamate esters.[68]

Pharmacokinetic Studies. *In vitro* stability studies thus indicated that the rate of hydrolysis of the carbamoyl bond in our new resveratrol derivatives is of the correct order of magnitude for application as prodrugs. We therefore proceeded to investigate the behavior of our compounds in pharmacokinetics studies *in vivo*.

Dihydroxypropyl Carbamate Ester Derivatives. Following administration of a single intragastric bolus, the monosubstituted derivatives were readily absorbed but also extensively metabolized. Low concentrations of the unmodified derivative were detected in blood, together with considerably higher amounts of glucuronides(s). Remarkably, sulfated metabolites were below detection limits in all cases. An example is shown in Figure 4, which shows the HPLC-UV chromatogram of a blood sample withdrawn 2 h after oral administration of **2**. The major metabolite was identified from its ESI mass spectra (Figure 4B,C) and assigned to the product of monoglucuronidation still bearing the protecting carbamoyl group (Scheme 5).

HPLC–UV–ESI/MS analysis showed that the other monosubstituted derivative **3** produced instead two different isomeric monoglucuronidated metabolites, both still bearing the protective carbamoyl group (Scheme 5).

It was not possible to attribute the two peaks observed in HPLC–UV and HPLC–MS chromatograms to the two isomeric glucuronides formed from **3**. Therefore, they are referred to by their chromatographic retention times (r.t.), which under

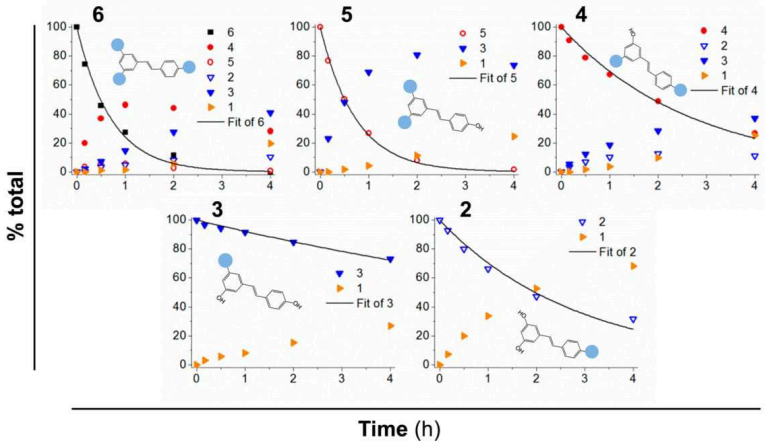


Figure 3. Hydrolysis of resveratrol dihydroxypropyl carbamates (**2**–**6**) in rat blood. Data are expressed as % of the initially loaded compound.

DOI: 10.1021/acs.molpharmaceut.5b00464
Mol. Pharmaceutics 2015, 12, 3441–3454

Table 3. Rate Constants (k) for Hydrolysis of Resveratrol Derivatives 2−11 in Rat Blood, at 37°C

Pattern of substitution	Compound	$10^2 \cdot k$ (h^{-1})	Compound	$10^2 \cdot k$ (h^{-1})
	6	140 ± 10	11	390 ± 50
	5	136 ± 4	10	110 ± 20
	4	36 ± 2	9	34 ± 2
	3	8.1 ± 0.3	8	11.4 ± 0.9
	2	35 ± 3	7	70 ± 6

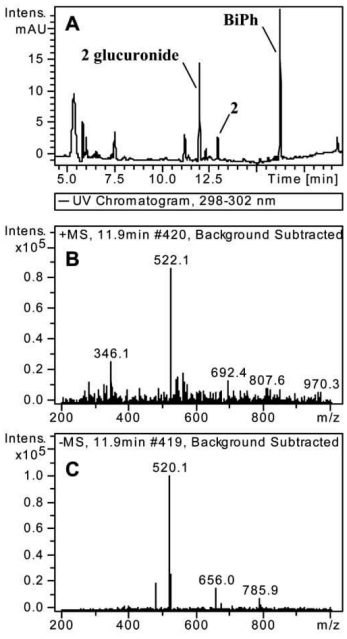


Figure 4. HPLC−UV−MS analysis of a blood sample taken 2 h after administration of **2**. (A) UV chromatogram, recorded at 300 nm; "BiPh" stands for 4,4′-dihydroxybiphenyl, which was used as internal standard. (B,C) ESI mass spectra of the metabolite, acquired in the positive (B) and negative (C) ion current mode, respectively.

our standard analysis protocol were 2.38 and 3.08 min, respectively. The isomer with the retention time of 2.38 min, which is very similar to that (2.35 min) of the monoglucuronidated metabolite formed from **2**, probably also has a similar structure, i.e., it most likely carries the glucuronic acid moiety in position 4′. It follows that in the metabolite with r.t. 3.08 the two substituents probably occupy positions 3 and 5.

In pharmacokinetic experiments, for both **2** and **3**, the overall concentration of stilbenic compounds was reached approximately 1 h after administration (Figure 5). However, interestingly, the two isomers have different kinetic profiles: thus, **2** and its metabolite persisted in the bloodstream for a significantly longer time than **3** and its metabolites.

The tri- and disubstituted derivatives (**4**−**6**) were poorly absorbed. The relative amount of nonconjugated vs conjugated (glucuronidated) derivatives in the bloodstream was inversely correlated to the number of protected hydroxyls in the original prodrug. This suggests that partially protected resveratrol still functions as a substrate for glucuronosyl transferases.

When **6** was administered, the intact derivative rapidly reached the bloodstream and underwent hydrolysis to the 3,4′-disubstituted derivative (**4**). In addition, metabolites **2**-glucuronide and **3**-glucuronide with r.t. 3.08 min (Scheme 5) were also detected and reached maximum concentration at later times (t_{max} at 8 and 2 h, respectively).

Absorption of disubstituted derivatives was rapid, with the unmodified prodrug peaking in blood about 30 min after gavage. Administration of the 3,4′-(dihydroxypropyl) derivative (**4**) resulted in detectable levels of **2**-glucuronide and of **3**-glucuronide with r.t. 2.38 min; no other intermediate products were detected. However, administration of the 3,5-(dihydroxypropyl) isomer (**5**) resulted in appearance of **3** and of its glucuronide with r.t. 2.38 min.

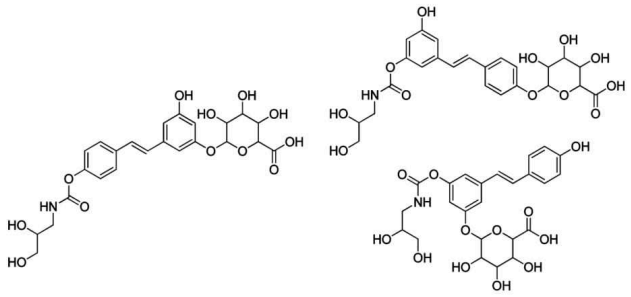
6-Deoxygalactosyl Carbamate Ester Derivatives. Pharmacokinetic determinations provided no evidence of absorption for 3,4′,5- and 3,5-derivatives (**11** and **10**) after oral administration.

Figure 6 shows the pharmacokinetic profiles of 3,4′-, 3-, and 4′-substituted derivatives (**9**, **8**, and **7**, respectively). Compounds were generally poorly absorbed. Absorption of **9** was rapid, reaching 10 min after administration a low peak blood concentration, which then remained approximately constant for up to 2 h. Derivative **8** reached an early peak in blood, with the concentration decaying in an approximately exponential manner to undetectable levels after about 4 h. The 4′-substituted derivative (**7**) again differed significantly from its isomer: it showed a delayed absorption with the maximum concentration of total species in blood reached at approximately 2 h after administration. Metabolites or resveratrol could not be reliably identified in any pharmacokinetic run with deoxygalactosyl carbamate ester derivatives.

Intestinal Levels. The highly soluble derivative **11** did not enter systemic circulation after oral administration. Poor intestinal absorption may however be expected to result in high levels in the lumen of the lower intestinal tract, suggesting possible applications for the treatment of intestinal disorders. After chronic administration, a striking difference was observed

DOI: 10.1021/acs.molpharmaceut.5b00464
Mol. Pharmaceutics 2015, 12, 3441−3454

Scheme 5. Glucuronidated Metabolites Formed from 2 and 3



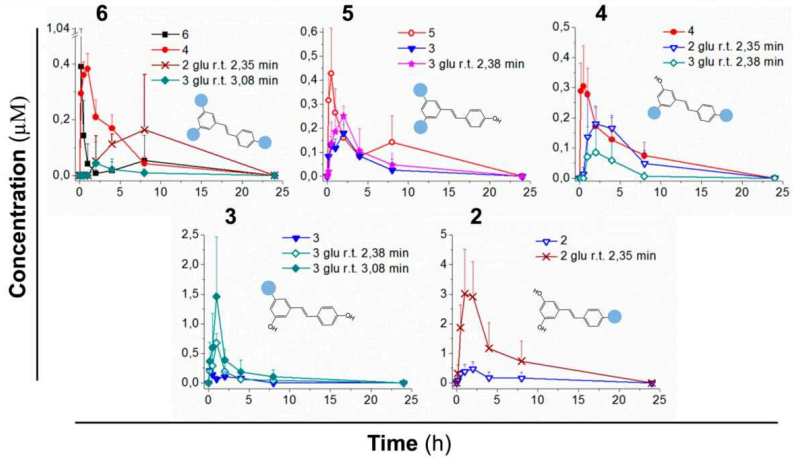


Figure 5. Blood pharmacokinetic profiles after oral administration of resveratrol derivatives (**2**–**6**). Data represent average values + standard deviation. $N = 3$ in all cases.

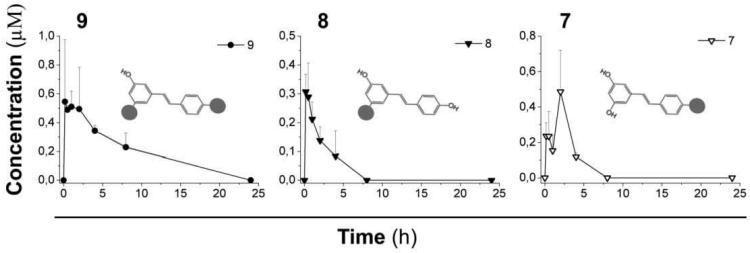


Figure 6. Blood pharmacokinetic profiles after oral administration of resveratrol 6-deoxygalactosyl derivatives **7**–**9**. Data represent average values + standard deviation. $N = 3$ in all cases.

in the intestinal fate of resveratrol and **11**: in the colon and cecum the former was present mainly as its bacterial metabolite dihydroresveratrol (Figure 7), while the latter was mainly present as partially hydrolyzed derivatives (Figure 8). Low amounts of resveratrol and dihydroresveratrol were also detected.

DOI: 10.1021/acs.molpharmaceut.5b00464
Mol. Pharmaceutics 2015, 12, 3441−3454

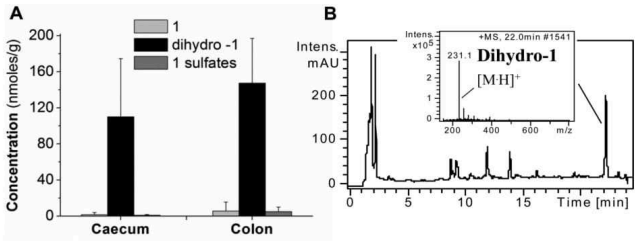


Figure 7. Resveratrol and its metabolites in the lower intestine of rats after chronic administration. (A) Amounts of resveratrol (**1**), dihydroresveratrol (**dihydro-1**), and resveratrol sulfates (**1-sulfates**) in cecum and colon after 48 h of chronic treatment with approximately 220 μmol/kg × day of resveratrol. (B) HPLC-UV chromatogram (286 nm) and ESI mass spectrum of dihydroresveratrol (insert).

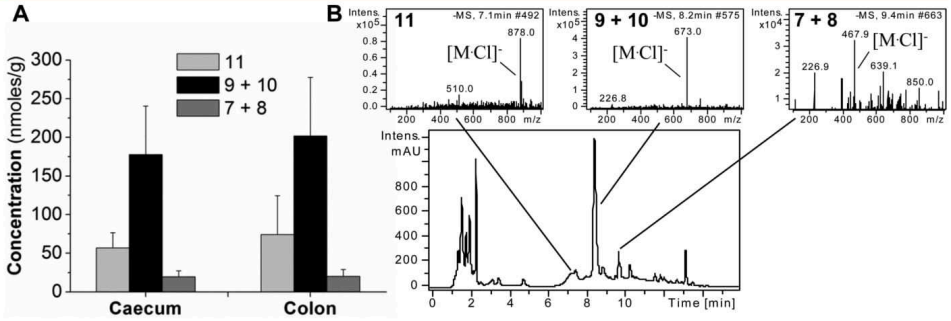


Figure 8. Compound **11** and derived species in the lower intestine of rats after chronic administration. (A) Amounts of resveratrol derivatives in cecum and colon after 48 h of chronic treatment with approximately 220 μmol/kg × day of **11**. (B) HPLC-UV chromatogram (286 nm) and ESI mass spectra of **11** and its hydrolysis products (inserts).

■ CONCLUSIONS

The new resveratrol derivatives we developed have properties and reactivity that match expectations for their use as prodrugs. In particular, they are stable in acid solution and can therefore survive the gastric stage. In near-neutral solution and blood the rate of hydrolysis is conveniently slow.

The behavior of these prodrugs vis-à-vis absorption from the intestine is bound to depend on the properties of the chosen promoieties. While water solubility is desirable for obvious practical reasons, high hydrophilicity is known to hinder biomembrane permeation due to the hydrophobic barrier formed by the hydrocarbon chains of phospholipids. Accordingly, while in *in vivo* experiments dihydroxypropyl derivatives were absorbed, and monosubstituted ones (**2**, **3**) satisfactorily so, derivatives comprising the more hydrophilic 6-deoxygalactose moiety (**7**−**11**) performed poorly in this respect. Solute carriers might intervene to aid translocation, but apparently **7**−**11** are not recognized and/or transported by intestinal glucose carriers.

The trisubstituted compound **11** is the most soluble and was not absorbed in the gastrointestinal tract; however, interestingly, chronic administration of this compound resulted in its accumulation in the lower intestine. The presence in colon and cecum of partially hydrolyzed derivatives of **11** points to protracted release of resveratrol, which is rapidly reduced to dihydroresveratrol by bacterial enzymes. These findings suggest a possible use of glycosyl−resveratrol derivatives for the treatment of colitis and prevention of colon cancer.

Unmodified resveratrol was below detection limits in the bloodstream in all cases, undoubtedly reflecting the powerful phase II metabolism of the liver. Blood however is well suited to accommodate hydrophilic compounds such as glucuronides (and, to an extent, our prodrugs), and the composition of prodrug-derived species in other organs may well be different. Important interorgan variations have been reported in the case of pterostilbene and its metabolites.[69,70]

■ EXPERIMENTAL SECTION

Materials. Resveratrol was purchased from Waseta Int. Trading Co. (Shangai, P.R.China). Other starting materials and reagents were purchased from Sigma-Aldrich, Fluka, Merck-Novabiochem, Riedel de Haen, J.T. Baker, Cambridge Isotope Laboratories Inc., Acros Organics, Carlo Erba, and Prolabo, and were used as received. ^{1}H and ^{13}C NMR spectra were recorded with a Bruker AC250F spectrometer and a Bruker Avance DMX 600. Chemical shifts (δ) are given in ppm relative to the signal of the solvent. TLCs were run on silica gel supported on plastic (Macherey-Nagel PolygramSIL G/UV$_{254}$, silica thickness 0.2 mm) and visualized by UV detection, ninhydrin reaction or $KMnO_4$ oxidation. Flash chromatography was performed on silica gel (Macherey-Nagel 60, 230−400 mesh granulometry (0.063−0.040 mm)) under air pressure. The solvents were analytical or synthetic grade and were used without further

DOI: 10.1021/acs.molpharmaceut.5b00464
Mol. Pharmaceutics 2015, 12, 3441−3454

purification. Preparative HPLC was performed using a Shimadzu LC-8A equipped with a UV/vis detector SPD-20A Prominence and a reverse phase column (ACE 5AQ (150 × 21.2 mm)).

Animals. Adult male Wistar rats (approximately 400 g body weight) from the facility of the Department of Biomedical Sciences were used for pharmacokinetic experiments. All experiments involving animals were performed after approval by the University of Padova Ethical Committee for Experimentation on Animals (CEASA) (Permit Number: 80/2011) and of the Italian Ministry of Health, and with the supervision of the Central Veterinary Service of the University of Padova, in compliance with Italian Law DL 116/92, embodying UE Directive 86/609.

Synthetic Procedures. Please refer to the Results sections for an outline of the general strategy. Synthetic targets (compounds **2**−**11**) as well as some intermediates were purified by preparative HPLC. For all new compounds purity was >95%, as assessed by HPLC-UV analysis.

*[N-(2,2-Dimethyl-1,3-dioxolane-4-methan)-carbamoyl]-4-nitrophenol (**13**).* Bis-4-(nitrophenyl) carbonate (3.47 g, 11.4 mmol, 1 equiv) in 20 mL of anhydrous THF and DMAP (2.79 g, 22.8 mmol, 2 equiv) were mixed in a 100 mL round-bottom flask with a magnetic stirrer under N_2. 2,2-Dimethyl-1,3-dioxolane-4-methanamine (**12**, 1.5 g, 11.4 mmol, 1 equiv) in THF (20 mL) was then added dropwise at RT. After 3 h the mixture was taken up in EtOAc (150 mL), transferred to a 500 mL separation funnel, and washed with 0.5 M HCl (3 × 150 mL). The organic phase was then dried over $MgSO_4$ and filtered. The solvent was evaporated under reduced pressure, and the residue was purified by flash chromatography on silica gel (eluent: CH_2Cl_2/EtOAc, 9.5:0.5) to afford **13** (75% yield). ^{1}H NMR (250 MHz, $CDCl_3$) δ (ppm): 1.38 (s, 3H, $-CH_3$), 1.48 (s, 3H, $-CH_3$), 3.28−3.61 (m, 2H, $-NH-CH_2$), 3.70−4.14 (m, 2H, $-CH_2-$), 4.28−4.37 (m, 1H, $-CH-$), 7.32 (d, 2H, Ar−*H*, $^3J_{H-H}$: 9.25 Hz), 8.25 (d, 2H, Ar−*H*, $^3J_{H-H}$: 9.25 Hz); ^{13}C NMR (62.9 MHz, $CDCl_3$) δ (ppm): 155.7, 153.3, 144.7, 125.1, 121.9, 109.6, 74.2, 66.5, 43.6, 26.7, 25.0; ESI-MS (ion trap): m/z 297 $[M + H]^+$.

*(4′-Mono-, 3-Mono-, 3,4′-Di-, 3,5-Di-, 3,4′,5-Tri-) [N-(2,2-dimethyl-1,3-dioxolane-4-methan)-carbamoyl]-resveratrol (**14**−**18**).* Compound **13** (1.24 g, 4.2 mmol, 2.6 equiv) and pyridine (10 mL) were placed in a 100 mL round-bottom flask with magnetic stirrer and under N_2. Resveratrol (**1**, 0.37 g, 1.6 mmol, 1.0 equiv) and DMAP (0.79 g, 6.4 mmol, 4.0 equiv) in pyridine (10 mL) was added, and the reaction was allowed to proceed at 70 °C overnight. The mixture was then taken up with 150 mL of EtOAc, transferred to a separation funnel, and washed with 0.5 M HCl (5 × 150 mL). The organic phase was then dried over $MgSO_4$ and filtered. The solvent was evaporated under reduced pressure. The resulting solid was purified by flash chromatography (eluent: CH_2Cl_2/acetone, 7.5:2.5) to afford 0.57 g of a mixture of **14**−**18** used as such for the subsequent synthetic step. ESI-MS (ion trap): **14**, **15**, m/z 386 $[M + H]^+$; **16**, **17**, m/z 543 $[M + H]^+$; **18**, m/z 700 $[M + H]^+$.

*(4′-Mono-, 3-Mono-, 3,4′-Di-, 3,5-Di-, 3,4′,5-Tri-)[N-(2,3-Dihydroxypropyl)-carbamoyl]-resveratrol Conjugates (**2**−**6**).* The mixture (**14**−**18**, 0.57 g) obtained in the previous step was added to a solution of TFA/water (90:10, 5 mL). The resulting mixture was vigorously stirred for 1.5 h at RT and then dried under vacuum. The residue was then separated by preparative HPLC (from 0% to 40% ACN in 17 min) and lyophilized to afford derivatives: **2** (0.129 g, cumulative yield of the final two steps: 23%), **3** (0.068 g, cumulative yield of the final two steps: 12%), **4** (0.135 g, cumulative yield of the final two steps: 18%), **5** (0.038 g, cumulative yield of the final two steps: 5%), and **6** (0.085 g, cumulative yield of the final two steps: 9%).

Compound **2**: ^{1}H NMR (250 MHz, DMSO-d_6) δ (ppm): 2.95−3.25 (m, 2H, $-CH_2-$), 3.35 (d, 2H, $^3J_{H-H}$ = 5.25 Hz, $-CH_2-$), 3.51−3.66 (m, 1H, $-CH-$), 6.17 (t, 1H, $^4J_{H,H}$ = 2.0 Hz, H-4), 6.45 (d, 2H, $^4J_{H,H}$ = 2.0 Hz, H-2, H-6), 7.03−7.10 (m, 4H, H-3′, H-5′, H-7, H-8), 7.57 (d, 2H, $^3J_{H-H}$ = 8.5 Hz, H-2′, H-6′), 7.65 (t, 1H, $^3J_{H-H}$ = 5.75 Hz, −N−*H*. ^{13}C NMR (62.9 MHz, DMSO-d_6) δ (ppm): 158.5, 154.5, 150.5, 138.8, 133.8, 128.6, 127.2, 127.1, 121.9, 104.7, 102.3, 70.3, 63.8, 44.1. ESI-MS (ion trap): m/z 346 $[M+ H]^+$.

Compound **3**: ^{1}H NMR (250 MHz, DMSO-d_6) δ (ppm): 2.93−3.23 (m, 2H, $-CH_2-$), 3.34 (d, 2H, $^3J_{H-H}$ = 5.25 Hz, $-CH_2-$), 3.52−3.61 (m, 1H, $-CH-$), 6.38 (t, 1H, $^4J_{H,H}$ = 2.0 Hz, H-4), 6.73−6.78 (m, 4H, H-2, H-6, H-3′, H-5′), 6.90 (d, 1H, $^3J_{H-H}$ = 16.5, H-7), 7.07 (d, 1H, $^3J_{H-H}$ = 16.5, H-8), 7.42 (d, 2H, $^3J_{H-H}$ = 8.75, H-2′, H-6′), 7.58 (t, 2H, $^3J_{H-H}$ = 5.75 Hz, 2 × −N−*H*). ^{13}C NMR (62.9 MHz, DMSO-d_6) δ (ppm): 158.0, 157.4, 154.5, 152.2, 139.3, 128.9, 128.0, 127.8, 124.6, 115.5, 110.0, 109.7, 107.8, 70.3, 63.8, 44.0. ESI-MS (ion trap): m/z 346 $[M+ H]^+$.

Compound **4**: ^{1}H NMR (250 MHz, DMSO-d_6) δ (ppm): ^{1}H NMR (250 MHz, DMSO-d_6) δ (ppm): 2.95−3.25 (m, 4H, 2 × $-CH_2-$), 3.36 (d, 4H, $^3J_{H-H}$ = 5.25 Hz, 2 × $-CH_2-$), 3.53−3.62 (m, 2H, $-CH-$), 6.41−6.43 (m, 1H, H-4), 6.77−6.80 (m, 2H, H-2, H-6), 7.02−7.19 (m, 4H, H-3′, H-5′, H-7, H-8), 7.52−7.61 (m, 4H, 2 × −N*H*−, H-2′, H-6′). ^{13}C NMR (62.9 MHz, DMSO-d_6) δ (ppm): 158.1, 154.5, 154.4, 152.2, 150.6, 138.7, 133.6, 128.0, 127.6, 127.3, 121.9, 110.3, 110.1, 108.4, 70.2, 70.3, 63.7, 44.0. ESI-MS (ion trap): m/z 463 $[M + H]^+$.

Compound **5**: ^{1}H NMR (250 MHz, $CDCl_3$) δ (ppm): ^{1}H NMR (250 MHz, DMSO-d_6) δ (ppm): 2.96−3.25 (m, 4H, 2 × $-CH_2-$), 3.36 (d, 4H, $^3J_{H-H}$ = 5.25 Hz, 2 × $-CH_2-$), 3.54−3.63 (m, 2H, 2 × $-CH-$), 6.64−6.80 (m, 3H, H-4, H-2, H-6), 6.97−7.24 (m, 4H, H-3′, H-5′, H-7, H-8), 7.40 (d, 2H, $^3J_{H-H}$ = 8.5 Hz, H-2′, H-6′), 7.70 (t, 2H, $^3J_{H-H}$ = 5.75 Hz, 2 × −N−*H*). ^{13}C NMR (62.9 MHz, DMSO-d_6) δ (ppm): 157.6, 154.3, 151.8, 139.4, 130.0, 128.2, 127.7, 123.7, 115.8, 115.6, 114.0, 70.3, 63.8, 44.2. ESI-MS (ion trap): m/z 463 $[M + H]^+$.

Compound **6**: ^{1}H NMR (250 MHz, $CDCl_3$) δ (ppm): ^{1}H NMR (250 MHz DMSO-d_6) δ (ppm): 2.94−3.25 (m, 6H, 3 × $-CH_2-$), 3.35 (d, 6H, $^3J_{H-H}$ = 5.25 Hz, 3 × $-CH_2-$), 3.53−3.62 (m, 3H, 3 × $-CH-$), 6.78 (t, 1H, $^4J_{H,H}$ = 2.0 Hz, H-4), 7.10−7.36 (m, 6H, H-2, H-6, H-3′, H-5′, H-7, H-8), 7.59−7.74 (m, 5H, H-2′, H-6′, 3 × −N−*H*). ^{13}C NMR (62.9 MHz, DMSO-d_6) δ (ppm): 154.4, 154.2, 151.7, 150.8, 138.8, 133.5, 129.1, 127.5, 126.7, 122.0, 116.2, 114.6, 70.3, 63.8, 44.1. ESI-MS (ion trap): m/z 580 $[M + H]^+$.

*(1,2:3,4-Di-O-isopropylidene-6-O-(p-toluensulfonate))-α-D-galactopiranose (**20**).* Pyridine (3.1 mL, 38.4 mmol, 2.0 equiv) and DMAP (3.51 g, 28.7 mmol, 1.5 equiv) were added to a solution of 1,2:3,4-di-*O*-isopropylidene-α-D-galactopiranose (**19**, 5.0 g, 19.2 mmol, 1.0 equiv) in CH_2Cl_2 (20 mL), and the mixture was stirred at 0 °C for 15 min. A solution of tosyl chloride (5.49 g, 28.7 mmol, 1.5 equiv) in CH_2Cl_2 (20 mL) was then added dropwise, and the mixture was stirred at room temperature for 5 h. After adding H_2O (30 mL), the mixture was diluted in CH_2Cl_2 (150 mL) and washed with 0.5 N HCl (5 × 100 mL). The organic layer was dried over $MgSO_4$ and filtered. The solvent was evaporated under reduced pressure, and the residue was purified by flash chromatography

DOI: 10.1021/acs.molpharmaceut.5b00464
Mol. Pharmaceutics 2015, 12, 3441−3454

(eluent: CH_2Cl_2/EtOAc, 9:1) to afford 7.33 g of **20** (92% yield). ^{1}H NMR (250 MHz, $CDCl_3$) δ (ppm): 1.26 (s, 3H, −C−CH_3), 1.30 (s, 3H, −C−CH_3), 1.33 (s, 3H, −C−CH_3), 1.49 (s, 3H, −C−CH_3), 2.43 (s, 3H, Ar−CH_3), 4.00−4.20 (m, 4H, H-4, H-5, H-6), 4.28 (dd, 1H, $^3J_{3-2}$ = 2.5 Hz, $^3J_{3-4}$ = 2.5 Hz, H-3), 4.57 (dd, 1H, $^3J_{2-1}$ = 2.5 Hz, H-2), 5.44 (d, 1H, $^3J_{1-2}$ = 5 Hz, H-1), 7.32 (d, 2H, Ar−*H*, $^3J_{H-H}$ = 10 Hz), 7.80 (d, 2H, $^3J_{H-H}$ = 7.5 Hz). ^{13}C NMR (62.9 MHz, $CDCl_3$) δ (ppm): 144.7, 132.7, 129.7, 128.0, 109.5, 108.9, 96.0, 70.4, 70.3, 70.3, 68.1, 65.8, 25.9, 25.7, 24.9, 24.3, 21.6. ESI-MS (ion trap): m/z 415 $[M + H]^+$.

*(1,2:3,4-Di-O-isopropylidene-6-deoxy-azido)-α-D-galactopiranose (**21**).* Sodium azide (5.84 g, 89.8 mmol, 5.0 equiv) was added to a solution of **20** (7.22 g, 17.4 mmol, 1.0 equiv) in DMSO (40 mL), and the mixture was stirred at 160 °C for 1.5 h under nitrogen. The resulting mixture was poured into ice water (500 mL) and extracted with EtOAc (2 × 250 mL). The organic layer was dried over $MgSO_4$ and filtered. The solvent was evaporated under reduced pressure, and the residue was purified by flash chromatography (eluent: CH_2Cl_2/EtOAc, 97:3) to afford 4.60 g of **11** (93% yield). ^{1}H NMR (250 MHz, $CDCl_3$) δ (ppm): 1.33 (s, 6H, 2 × −C−CH_3), 1.44 (s, 3H, −C−CH_3), 1.53 (s, 3H, −C−CH_3), 3.34 (dd, 1H, $^2J_{6*-6}$ = 12.5 Hz, $^3J_{6*-5}$ = 5 Hz, H-6*), 3.50 (dd, 1H, $^2J_{6-6*}$ = 12.5 Hz, $^3J_{6-5}$ = 7.5 Hz, H-6), 3.87−3.93 (m, 1H, H-5), 4.18 (dd, 1H, $^3J_{4-3}$ = 2.5 Hz, $^3J_{4-5}$ = 7.5 Hz, H-4), 4.31 (dd, 1H, $^3J_{3-2}$ = 2.5 Hz, $^3J_{3-4}$ = 2.5 Hz, H-3), 4.61 (dd, 1H, $^3J_{2-1}$ = 7.5 Hz, $^3J_{2-3}$ = 2.5 Hz, H-2), 5.53 (d, 1H, $^3J_{1-2}$ = 5 Hz, H-1). ^{13}C NMR (62.9 MHz, $CDCl_3$) δ (ppm): 109.5, 108.7, 96.3, 71.0, 70.7, 70.3, 66.9, 50.6, 25.9, 25.9, 24.8, 24.3. ESI-MS (ion trap): m/z 286 $[M + H]^+$.

*(1,2:3,4-Di-O-isopropylidene-6-deoxy-amino)-α-D-galactopiranose (**22**).* A solution of triphenylphosphine (5.49 g, 20.9 mmol, 1.3 equiv) in THF (35 mL) was added dropwise to a solution of **21** (4.60 g, 16.1 mmol, 1.0 equiv) in THF (60 mL), and the mixture was stirred at RT for 4 h under nitrogen. Distilled water (25 mL) was then added, and the resulting mixture was heated to reflux and vigorously stirred for 15 h. Solvents were removed under vacuum, and the residue was purified by flash chromatography (eluent: CH_2Cl_2/MeOH, 95:5 + 1% of triethylamine) to afford 4.05 g of **22** (97% yield). ^{1}H NMR (250 MHz, $CDCl_3$) δ (ppm): 1.32 (s, 6H, 2 × −C−CH_3), 1.34 (s, 2H, −NH_2), 1.43 (s, 3H, −C−CH_3), 1.51 (s, 3H, −C−CH_3), 2.82 (dd, 1H, $^2J_{6*6}$ = 15 Hz, $^3J_{6*-5}$ = 5 Hz, H-6*), 2.95 (dd, 1H, $^2J_{6-6*}$ = 12.5 Hz, $^3J_{6-5}$ = 7.5 Hz, H-6), 3.65−3.71 (m, 1H, H-5), 4.21 (dd, 1H, $^3J_{4-3}$ = 7.5 Hz, $^3J_{4-5}$ = 2.5 Hz, H-4), 4.30 (dd, 1H, $^3J_{3-2}$ = 5 Hz $^3J_{3-4}$ = 2.5 Hz, H-3), 4.58 (dd, 1H, $^3J_{2-1}$ = 10 Hz, $^3J_{2-3}$ = 2.5 Hz, H-2), 5.53 (d, 1H, $^3J_{1-2}$ = 2.5 Hz, H-1). ^{13}C NMR (62.9 MHz, $CDCl_3$) δ (ppm): 109.1, 108.4, 96.3, 71.7, 70.7, 70.5, 69.4, 42.3, 26.0, 25.9, 24.9, 24.3. ESI-MS (ion trap): m/z 260 $[M + H]^+$.

*[N-(1,2:3,4-Di-O-isopropylidene-6-deoxy-α-D-galactopyranosyl)-carbamoyl]-4-nitrophenol (**23**).* A solution of **22** (1.0 g, 3.9 mmol, 1.0 equiv) in THF (15 mL) was added dropwise to a solution of bis (4-nitrophenyl) carbonate (1.17 g, 3.9 mmol, 1.0 equiv) and DMAP (1.01 g, 7.8 mmol, 2.0 equiv) in THF (20 mL), and the mixture was stirred at RT for 5 h. The resulting mixture was diluted in EtOAc (150 mL) and washed with 0.5 N HCl (3 × 100 mL). The organic layer was dried over $MgSO_4$ and filtered. The solvent was evaporated under reduced pressure, and the residue was purified by flash chromatography (eluent: CH_2Cl_2/hexane, 75:25) to afford 1.27 g of **23** (78% yield). ^{1}H NMR (250 MHz, $CDCl_3$) δ (ppm): 1.34 (s, 3H, −C−CH_3), 1.35 (s, 3H, −C−CH_3), 1.46 (s, 3H, −C−CH_3), 1.51 (s, 3H, −C−CH_3), 3.34−3.44 (m, 1H, H-6*), 3.55−3.65 (m, 1H, H-6), 3.95−4.01 (m, 1H, H-5), 4.23 (dd, 1H, $^3J_{4-3}$ = 10 Hz, $^3J_{4-5}$ = 2.5 Hz, H-4), 4.34 (dd, 1H, $^3J_{3-2}$ = 2.5 Hz, $^3J_{3-4}$ = 5 Hz, H-3), 4.63 (dd, 1H, $^3J_{2-1}$ = 7.5 Hz, $^3J_{2-3}$ = 2.5 Hz, H-2), 5.55 (d, 1H, $^3J_{1-2}$ = 5 Hz, H-1), 5.60 (dd, 1H, $^3J_{NH-6*}$ = 7.5 Hz, J_{NH-6} = 5 Hz, −N*H*), 7.28−7.32 (m, 2H, H-2′, H-6′), 8.21−8−25 (m, 2H, H-3′, H-5′). ^{13}C NMR (250 MHz, $CDCl_3$) δ (ppm): 155.9, 153.3, 144.7, 125.0, 121.9, 109.5, 108.8, 96.3, 71.5, 70.7, 70.4, 66.0, 41.8, 26.0, 25.9, 24.9, 24.3. ESI-MS (ion trap): m/z 425 $[M + H]^+$.

*(4′-Mono-, 3-Mono-, 3,4′-Di-, 3,5-Di-, 3,4′,5-Tri-)-[N-(1,2:3,4-di-O-isopropylidene-6-deoxy-α-D-galactopyranosyl)-carbamoyl]-resveratrol (**24**−**28**).* A solution of resveratrol (0.15 g, 0.66 mmol, 1.0 equiv) and DMAP (0.32 g, 2.64 mmol, 4.0 equiv) in pyridine (10 mL) was added to a solution of **23** (1.13 g, 2.7 mmol, 4.0 equiv) in pyridine (10 mL), and the resulting mixture was allowed to react under vigorous stirring at 70 °C for 16 h. The reaction mixture was then diluted in EtOAc (200 mL) and washed with 0.5 N HCl (5 × 150 mL). The organic layer was dried over $MgSO_4$ and filtered. The solvent was evaporated under reduced pressure, and the residue was purified by flash chromatography using EtOAc/hexane 5.5:4.5 as eluent to afford 0.39 g of a mixture of **24**−**28** used as such for the subsequent synthetic step. ESI-MS (ion trap): **24**, **25**, m/z 514 $[M + H]^+$; **26**, **27**, m/z 799 $[M + H]^+$; **28**, m/z 1084 $[M + H]^+$.

*(4′-Mono-, 3-Mono-, 3,4′-Di-, 3,5-Di-, 3,4′,5-Tri-)-[N-(6-deoxy-galactosyl)-carbamoyl]-resveratrol (**7**−**11**).* The mixture (**24**−**28**, 0.39 g) obtained in the previous step was added to a solution of TFA/water (90:10, 3 mL) and vigorously stirred at RT. After 1.5 h the resulting mixture was precipitated with 40 mL of diethyl ether, the material was centrifuged, and the solvent was decanted. The white powder obtained was then washed with diethyl ether three more times to eliminate traces of TFA. The residue was then dried under vacuum, separated by preparative HPLC (from 0% to 38% ACN in 17 min), and lyophilized to afford derivatives: **7** (0.040 g, cumulative yield of the final two steps: 14%), **8** (0.023 g, cumulative yield of the final two steps: 8%), **9** (0.093 g, cumulative yield of the final two steps: 22%), **10** (0.025 g, cumulative yield of the final two steps: 6%), and **11** (0.094 g, cumulative yield of the final two steps: 17%).

Compound **7**: ^{1}H NMR (600 MHz, DMSO-d_6) δ(ppm): 8.00 (t, 1H, J_{NH-6*} = J_{NH-6} = 6 Hz, −N*H*−), 7.56 (d, 2H, $J_{2''-3''}$ = 12 Hz, H-2″, 6″), 7.07 (d, 2H, $J_{3''-2''}$ = 6 Hz, H-3″, 5″), 7.10−7.31 (m, 2H, H-8, 9), 6.43 (s, 2H, H-2′, 6′), 6.15 (s, 1H, H-4′), 4.89−5.00 (m, 1H, H-1), 4.24−3.17 (m, 12H, H-2, 3, 4, 5, 6, 6*, 6 O*H*). ^{13}C NMR (151 MHz, DMSO-d_6) δ (ppm): 158.6, 154.5, 150.5, 138.8, 133.9, 128.7, 127.3, 127.1, 121.9, 104.7, 102.4, 97.6, 92.7, 73.3, 72.4, 71.9, 69.5, 69.2, 68.9, 68.6, 68.0, 41.8, 41.6. ESI-MS (ion trap): m/z 434 $[M + H]^+$.

Compound **8**: ^{1}H NMR (600 MHz, DMSO-d_6) δ (ppm): 7.68 (t, 1H, J_{NH-6*} = J_{NH-6} = 6 Hz, −N*H*−), 7.41 (d, 2H, $J_{2''-3''}$ = 6 Hz, H-2″, 6″), 6.16−7.08 (m, 7H, H-3″,5″, 2′, 4′, 6′, 8, 9), 3.17−4.95(m, 13H, H-1, 2, 3, 4, 5, 6, 6*,6 O*H*). ^{13}C NMR (151 MHz, DMSO-d_6) δ (ppm): 158.5, 157.9, 154.9, 152.6, 139.8, 129.4, 128.4, 128.3, 125.0, 115.9, 115.5, 115.1, 114.8, 110.4, 110.2, 108.2, 97.9, 93.1, 73.7, 72.8, 72.3, 69.9, 69.6, 69.3, 69.0, 68.5, 42.1, 42.0. ESI-MS (ion trap): m/z 434 $[M + H]^+$.

Compound **9**: ^{1}H NMR (600 MHz, DMSO-d_6) δ (ppm): 7.71 (m, 2H, −N*H*−), 7.58 (d, 2H, $J_{2''-3''}$ = 6 Hz, H-2″, 6″), 7.08−7.18 (m, 4H, H-3″5″, 8, 9), 6.81 (s, 1H, H-2′), 6.79 (s, 1H, H-4′), 6.41 (s, 1H, H-6′), 4.94−5.01 (m, 2H, 2 × H-1),

DOI: 10.1021/acs.molpharmaceut.5b00464
Mol. Pharmaceutics 2015, 12, 3441−3454

3.18−4.26 (m, 22H, 2 × H-1, 2, 3, 4, 5, 6, 6*, 8 O*H*). ^{13}C NMR (151 MHz, DMSO-d_6) δ (ppm): 158.2, 154.5, 154.5, 152.3, 150.6, 138.9, 133.7, 128.2, 127.7, 127.4, 121.9, 110.4, 110.2, 108.4, 101.7, 97.5, 97.5, 92.7, 82.6, 82.2, 76.2, 73.3, 73.3, 72.4, 72.4, 72.0, 71.9, 69.5, 69.2, 68.9, 68.6, 68.1, 68.0, 41.7, 41.6. ESI-MS (ion trap): m/z 639 $[M + H]^+$.

Compound **10**: ^{1}H NMR (600 MHz, DMSO-d_6) δ (ppm): 7.74 (t, 2H, $J_{NH-6*} = J_{NH-6}$ = 6 Hz, −N*H*−), 7.42 (d, 2H, $J_{2''-3''}$ = 6 Hz, H-2″, 6″), 6.97−7.18 (m, 4H, H-3″S″, 8, 9), 6.79 (s, 1H, H-2′), 6.76(s, 1H, H-4′), 3.07−4.24 (m, 23H, H-6′, 2 × H-1, 2, 3, 4, 5, 6, 6*, 8 O*H*). ^{13}C NMR (151 MHz, DMSO-d_6) δ (ppm): 157.6, 154.3, 154.2, 151.7, 151.7, 130.1, 130.0, 128.2, 127.8, 115.6, 115.3, 97.5, 97.5, 92.7, 73.3, 73.3, 72.4, 71.9, 71.9, 69.4, 69.3, 68.9, 68.8, 68.6, 68.0, 41.8, 41.7, 41.6. ESI-MS (ion trap): m/z 639 $[M + H]^+$.

Compound **11**: ^{1}H NMR (600 MHz, DMSO-d_6) δ (ppm): 7.68−7.81 (m, 3H, −N*H*−), 7.60 (d, 2H, $J_{2''-3''}$ = 6 Hz, H-2″, 6″), 7.11−7.33 (m, 6H, H-3″S″, 8, 9, 2′, 6′), 6.78 (s, 1H, H-4′), 2.98−4.95 (m, 33H, 3 × H-1, 2, 3, 4, 5, 6, 6*, 12 O*H*). ^{13}C NMR (151 MHz, DMSO-d_6) δ (ppm): 154.4, 154.2, 151.7, 150.8, 138.9, 134.5, 133.5, 129.2, 127.5, 126.7, 122.0, 116.3, 101.7, 97.5, 92.7, 82.6, 82.1, 76.1, 73.3, 72.4, 71.9, 69.4, 69.2, 68.9, 68.6, 68.0, 68.0, 41.8, 41.7. ESI-MS (ion trap): m/z 845 $[M + H]^+$.

Log P_{ow}, Solubility, and TPSA. Unless otherwise indicated, the log P_{ow} and solubility values reported are predictions obtained using the software ALOGPS 2.1 (available at Virtual Computational Chemistry Laboratory, http://www.vcclab.org). "Topological" Polar Surface Area[63] values were predicted using the Molinspiration Property Calculator (www.molinspiration.com).

HPLC-UV Analysis. Samples (2 μL) were analyzed by HPLC/UV (1290 Infinity LC System, Agilent Technologies) using a reverse phase column (Zorbax RRHD Eclipse Plus C18, 1.8 μm, 50 × 2.1 mm i.d.; Agilent Technologies) and a UV diode array detector (190−500 nm). Solvents A and B were water containing 0.1% trifluoroacetic acid (TFA) and acetonitrile, respectively. The gradient for B was as follows: 2% (0.5 min), from 2% to 10% in 0.3 min, then from 10% to 18% in 1.7 min, then from 18% to 28% in 0.5 min, 28% for 0.5 min then from 28% to 100% in 1.8 min; the flow rate was 0.6 mL/min. The eluate was preferentially monitored at 286, 300, and 320 nm (corresponding to absorbance maxima of the internal standard, derivatives, and resveratrol, respectively). The column compartment was thermostated at 35 °C.

HPLC/ESI-MS Analysis. HPLC/ESI-MS analyses and mass spectra were performed with a 1100 Series Agilent Technologies system, equipped with binary pump (G1312A) and MSD SL Trap mass spectrometer (G2445D SL) with ESI source operating in full-scan positive or negative ion mode, with nebulizer pressure 70 psi, dry gas flow 12 L/min, and dry gas temperature 350 °C. ESI-MS positive mass spectra of reaction intermediates and final purified products were obtained by flow injection analysis of solutions in acetonitrile, eluting with a water/acetonitrile, 1:1 mixture containing 0.1% formic acid. HPLC/ESI-MS was also performed on selected samples from hydrolysis studies and pharmacokinetics. Samples (20 μL) were analyzed using a reversed phase column (Synergi-MAX, 4 μm, 150 × 4.6 mm i.d.; Phenomenex, Castel Maggiore (BO), Italy). Solvents A and B were water containing 0.1% TFA or 5 mM NH_4OAc and acetonitrile, respectively. The gradient for B was as follows: 10% for 2 min, from 10% to 35% in 20 min, from 35% to 100% in 20 min, then 100% for 2 min; the flow rate was 1 mL/min. The eluate was preferentially monitored at 286, 300, and 320 nm. MS analysis was performed with an ESI source operating in full-scan positive or negative ion mode.

Hydrolysis Reactions. The chemical stability of all new compounds was tested in aqueous media approximating gastric (0.1 N HCl, NormaFix) and intestinal (0.1 M PBS buffer, pH 6.8) pH values. A 5 μM solution of the compound was prepared from a 5 mM stock solution in DMSO and incubated at 37 °C for 24 h; samples withdrawn at different times were analyzed by HPLC-UV. Hydrolysis products were identified by comparison of chromatographic retention time with authentic standards. Nonlinear curve fitting was performed using Origin 8.0 data analysis software; the hydrolysis reaction rate constants (k) of the starting compounds were calculated through interpolation of data with the equation for pseudo-first order reactions:

$$[C] = [C]_0 \cdot e^{-kt}$$

where $[C]$ is concentration of the compound, $[C]_0$ is concentration of the compound at the initial time t_0, and t is time.

To evaluate its long-term stability under mildly acidic conditions, we stored compound **11** dissolved in citrate buffer (5 mM)/sucrose (5 mM) solution, pH 5.0, at 4 °C or RT, following the disappearance of **11** by HPLC analysis of samples taken at intervals over a period of several months.

Hydrolysis in Blood. Rats were anesthetized, and blood was withdrawn from the jugular vein and collected into heparinized test tubes. Blood samples (1 mL) were spiked with compound (5 μM; dilution from a 5 mM stock solution in DMSO), and incubated at 37 °C for 4 h (the maximum period allowed by blood stability). Aliquots were taken after 10 min, 30 min, 1 h, 2 h, and 4 h and treated as described below. Cleared blood samples were finally subjected to HPLC-UV analysis.

Blood Sample Treatment and Analysis. Before starting the treatment, 4,4′-dihydroxybiphenyl was added as internal standard to a carefully measured blood volume (25 μM final concentration). Blood was then stabilized with a freshly prepared 10 mM solution of ascorbic acid (0.1 vol) and acidified with 0.6 M acetic acid (0.1 vol); after mixing, an excess of acetone (4 vol) was added, followed by sonication (2 min) and centrifugation (12,000g, 7 min, 4 °C). The supernatant was finally collected and stored at −20 °C. Before analysis, acetone was allowed to evaporate at room temperature using a Univapo 150H (UniEquip) vacuum concentrator centrifuge, and up to 40 μL of ACN were added to precipitate residual proteins. After centrifugation (12,000g, 5 min, 4 °C), cleared samples were directly subjected to HPLC-UV analysis. Metabolites and hydrolysis products were identified by HPLC/ESI-MS analysis and/or comparison of chromatographic retention time with true samples.

The recovery yields of resveratrol and its metabolites have been reported previously.[71,72] For the new prodrugs the corresponding recoveries, expressed as ratio to the recovery of internal standard, were as follows: **2**, 0.75 ± 0.12; **3**, 0.75 ± 0.10; **4**, 0.98 ± 0.08; **5**, 1.02 ± 0.03; **6**, 0.85 ± 0.11; **7**, 1.36 ± 0.12; **8**, 1.10 ± 0.25; **9**, 0.68 ± 0.07; **10**, 0.67 ± 0.07; **11**, 0.90 ± 0.10 (N = 4 or 5 for all derivatives; mean values ± standard deviation). Recovery ratios of glucuronides were approximated as follows: for the glucuronide of **2** (retention time 2.35 min) the ratio used was that of compound **4**, which has the same substitution pattern; for the two glucuronides of **3** (r.t. 2.38 and 3.08 min) the ratio was assumed to be 1.0 since the recovery ratios of both isomeric prodrugs carrying two protecting groups

DOI: 10.1021/acs.molpharmaceut.5b00464
Mol. Pharmaceutics 2015, 12, 3441−3454

(**4** and **5**) were not significantly different from 1. Knowledge or assumption of these ratios allowed us to determine the unknown amount of analyte in a blood sample by quantifying the recovered internal standard.[69]

Pharmacokinetics Studies. Derivatives **2**−**11** were administered to overnight-fasted male rats as a single intragastric dose (88 μmol/kg, dissolved in 250 μL DMSO). Blood samples were obtained by the tail bleeding technique: before drug administration, rats were anesthetized with isoflurane and the tip of the tail was cut off; blood samples (80−100 μL each) were then taken from the tail tip at different time points after drug administration. Blood was collected in heparinized tubes, kept in ice, and treated as described below within 10 min.

Intestinal Accumulation and Distribution. Resveratrol or **11** were chronically administered to rats for 48 h. The beverage for the treatments was 5 mM citrate buffer with sucrose (5 mM), pH 5, supplemented with the compound at a concentration calculated to provide a daily intake of approximately 220 μmol/kg × day. Preliminary experiments showed that this solution was well-liked by rats, which drank an average of about 35 mL daily (hence, e.g., the concentration of resveratrol or derivative was 2.51 mM for a 400-g rat). The slightly acidic pH ensured the stability of the carbamoyl derivative (see above). In the case of resveratrol, 2-hydroxypropyl-β-cyclodextrin (HP-β-CD) was used to allow its solubilization: resveratrol and HP-β-CD were mixed in a 1:3 ratio in citrate buffer and stirred overnight.

At the end of the treatment, the treatment solution was replaced with tap water; 1 h later, animals were sacrificed, and the intestine explanted and cut into 10 cm-long segments. The luminal content of each segment was collected, 100 mg were weighed, H_2O (1 vol) was added, and the mixture was homogenized by vortexing (2 min). Samples were then stabilized and extracted adding 10 mM ascorbic acid (0.1 vol), 0.6 M acetic acid (0.1 vol) and acetonitrile (3 vol), vortexed (2 min), sonicated (2 min), and centrifuged (12,000g, 7 min, 4 °C); the supernatant was collected, concentrated, and finally analyzed via HPLC-UV and LC-ESI/MS.

Statistics. All experiments were performed at least in triplicate. Averages ± SD are presented. Significance in comparisons was assessed using the Wilcoxon Rank Test.

■ AUTHOR INFORMATION

Corresponding Author

*E-mail: lucia.biasutto@cnr.it. Tel: +39 049 8276483. Fax: +39 049 8276049.

Author Contributions

⊥These authors contributed equally to the paper and share first authorship. The manuscript was written through contributions of all authors. All authors have given approval to the final version of the manuscript.

Notes

The authors declare the following competing financial interest(s): The authors have applied for a patent covering the compounds described in this paper.

■ ACKNOWLEDGMENTS

We thank Mr. M. Ghidotti for technical help, Dr. Stefano Pluda for help with some of the syntheses, Dr. Alice Bradaschia for help with some of the pharmacokinetics, and NÔOS Srl for generous support and consultations. This work was supported by grants from the Fondazione Cassa di Risparmio di Padova e Rovigo (CARIPARO) ("Developing a Pharmacology of Polyphenols"), from the Italian Ministry of the University and Research (PRIN n. 20107Z8XBW_004), and by the CNR Project of Special Interest on Aging.

■ ABBREVIATIONS USED

AMPK, 5′ adenosine monophosphate-activated protein kinase; cAMP, 3′-5′-cyclic adenosine monophosphate; DDM-C, (2,2-dimethyl-1,3-dioxolane-4-methan)-carbamoyl; DGAL-C, 6-deoxygalactosyl carbamoyl; DHP-C, dihydroxypropyl carbamoyl; DIG-C, (1,2:3,4-di-*O*-isopropylidene-α-D-galactopyranosyl)-carbamoyl; DMAP, 4-(dimethylamino)pyridine; MTA1, metastasis-associated protein 1; mTORC1, mammalian target of rapamycin complex 1; PBS, phosphate buffered saline; PSA, polar surface area; SIRT1, SIRTuin (silent mating type information regulation 2 homologue) 1

■ REFERENCES

(1) Khurana, S.; Venkataraman, K.; Hollingsworth, A.; Piche, M.; Tai, T. C. Polyphenols: benefits to the cardiovascular system in health and in aging. *Nutrients* **2013**, *5*, 3779−827.

(2) Mattison, J. A.; Wang, M.; Bernier, M.; Zhang, J.; Park, S. S.; Maudsley, S.; An, S. S.; Santhanam, L.; Martin, B.; Faulkner, S.; Morrell, C.; Baur, J. A.; Peshkin, L.; Sosnowska, D.; Csiszar, A.; Herbert, R. L.; Tilmont, E. M.; Ungvari, Z.; Pearson, K. J.; Lakatta, E. G.; de Cabo, R. Resveratrol prevents high fat/sucrose diet-induced central arterial wall inflammation and stiffening in nonhuman primates. *Cell Metab.* **2014**, *20*, 183−90.

(3) Wong, R. H.; Coates, A. M.; Buckley, J. D.; Howe, P. R. Evidence for circulatory benefits of resveratrol in humans. *Ann. N. Y. Acad. Sci.* **2013**, *1290*, 52−8.

(4) Bigford, G. E.; Del Rossi, G. Supplemental substances derived from foods as adjunctive therapeutic agents for treatment of neurodegenerative diseases and disorders. *Adv. Nutr.* **2014**, *5*, 394−403.

(5) Li, F.; Gong, Q.; Dong, H.; Shi, J. Resveratrol, a neuroprotective supplement for Alzheimer's disease. *Curr. Pharm. Des.* **2012**, *18*, 27−33.

(6) Pallas, M.; Porquet, D.; Vicente, A.; Sanfeliu, C. Resveratrol: new avenues for a natural compound in neuroprotection. *Curr. Pharm. Des.* **2013**, *19*, 6726−31.

(7) Porquet, D.; Grinan-Ferre, C.; Ferrer, I.; Camins, A.; Sanfeliu, C.; Del Valle, J.; Pallas, M. Neuroprotective role of trans-resveratrol in a murine model of familial Alzheimer's disease. *J. Alzheimers Dis* **2014**, *42*, 1209−20.

(8) Marchal, J.; Pifferi, F.; Aujard, F. Resveratrol in mammals: effects on aging biomarkers, age-related diseases, and life span. *Ann. N. Y. Acad. Sci.* **2013**, *1290*, 67−73.

(9) Witte, A. V.; Kerti, L.; Margulies, D. S.; Floel, A. Effects of resveratrol on memory performance, hippocampal functional connectivity, and glucose metabolism in healthy older adults. *J. Neurosci.* **2014**, *34*, 7862−70.

(10) Hausenblas, H. A.; Schoulda, J. A.; Smoliga, J. M. Resveratrol treatment as an adjunct to pharmacological management in type 2 diabetes mellitus-systematic review and meta-analysis. *Mol. Nutr. Food Res.* **2015**, *59*, 147.

(11) Timmers, S.; Hesselink, M. K.; Schrauwen, P. Therapeutic potential of resveratrol in obesity and type 2 diabetes: new avenues for health benefits? *Ann. N. Y. Acad. Sci.* **2013**, *1290*, 83−9.

(12) Wang, S.; Moustaid-Moussa, N.; Chen, L.; Mo, H.; Shastri, A.; Su, R.; Bapat, P.; Kwun, I.; Shen, C. L. Novel insights of dietary polyphenols and obesity. *J. Nutr. Biochem.* **2014**, *25*, 1−18.

(13) Shukla, Y.; Singh, R. Resveratrol and cellular mechanisms of cancer prevention. *Ann. N. Y. Acad. Sci.* **2011**, *1215*, 1−8.

DOI: 10.1021/acs.molpharmaceut.5b00464
Mol. Pharmaceutics 2015, 12, 3441−3454

(14) Yang, X.; Li, X.; Ren, J. From French Paradox to cancer treatment: anti-cancer activities and mechanisms of resveratrol. *Anti-Cancer Agents Med. Chem.* **2014**, *14*, 806−25.
(15) Biasutto, L.; Mattarei, A.; Zoratti, M. Resveratrol and health: the starting point. *ChemBioChem* **2012**, *13*, 1256−9.
(16) Park, S. J.; Ahmad, F.; Philp, A.; Baar, K.; Williams, T.; Luo, H.; Ke, H.; Rehmann, H.; Taussig, R.; Brown, A. L.; Kim, M. K.; Beaven, M. A.; Burgin, A. B.; Manganiello, V.; Chung, J. H. Resveratrol ameliorates aging-related metabolic phenotypes by inhibiting cAMP phosphodiesterases. *Cell* **2012**, *148*, 421−33.
(17) Wilson, C. M.; Magnaudeix, A.; Yardin, C.; Terro, F. Autophagy dysfunction and its link to Alzheimer's disease and type II diabetes mellitus. *CNS Neurol. Disord.: Drug Targets* **2014**, *13*, 226−46.
(18) Widlund, A. L.; Baur, J. A.; Vang, O. mTOR: more targets of resveratrol? *Expert Rev. Mol. Med.* **2013**, *15*, e10.
(19) Chen, S.; Zhu, X.; Lai, X.; Xiao, T.; Wen, A.; Zhang, J. Combined Cancer Therapy with Non-Conventional Drugs: All Roads Lead to AMPK. *Mini-Rev. Med. Chem.* **2014**, *14*, 642−54.
(20) Dhar, S.; Kumar, A.; Li, K.; Tzivion, G.; Levenson, A. S. Resveratrol regulates PTEN/Akt pathway through inhibition of MTA1/HDAC unit of the NuRD complex in prostate cancer. *Biochim. Biophys. Acta, Mol. Cell Res.* **2015**, *1853*, 265−75.
(21) Dhar, S.; Hicks, C.; Levenson, A. S. Resveratrol and prostate cancer: promising role for microRNAs. *Mol. Nutr. Food Res.* **2011**, *55*, 1219−29.
(22) Phuah, N. H.; Nagoor, N. H. Regulation of microRNAs by natural agents: new strategies in cancer therapies. *BioMed Res. Int.* **2014**, *2014*, 804510.
(23) Hubbard, B. P.; Sinclair, D. A. Small molecule SIRT1 activators for the treatment of aging and age-related diseases. *Trends Pharmacol. Sci.* **2014**, *35*, 146−54.
(24) Sinclair, D. A.; Guarente, L. Small-molecule allosteric activators of sirtuins. *Annu. Rev. Pharmacol. Toxicol.* **2014**, *54*, 363−80.
(25) Mercken, E. M.; Mitchell, S. J.; Martin-Montalvo, A.; Minor, R. K.; Almeida, M.; Gomes, A. P.; Scheibye-Knudsen, M.; Palacios, H. H.; Licata, J. J.; Zhang, Y.; Becker, K. G.; Khraiwesh, H.; Gonzalez-Reyes, J. A.; Villalba, J. M.; Baur, J. A.; Elliott, P.; Westphal, C.; Vlasuk, G. P.; Ellis, J. L.; Sinclair, D. A.; Bernier, M.; de Cabo, R. SRT2104 extends survival of male mice on a standard diet and preserves bone and muscle mass. *Aging Cell* **2014**, *13*, 787−96.
(26) Mitchell, S. J.; Martin-Montalvo, A.; Mercken, E. M.; Palacios, H. H.; Ward, T. M.; Abulwerdi, G.; Minor, R. K.; Vlasuk, G. P.; Ellis, J. L.; Sinclair, D. A.; Dawson, J.; Allison, D. B.; Zhang, Y.; Becker, K. G.; Bernier, M.; de Cabo, R. The SIRT1 activator SRT1720 extends lifespan and improves health of mice fed a standard diet. *Cell Rep.* **2014**, *6*, 836−43.
(27) Chen, C. C.; Lin, J. T.; Cheng, Y. F.; Kuo, C. Y.; Huang, C. F.; Kao, S. H.; Liang, Y. J.; Cheng, C. Y.; Chen, H. M. Amelioration of LPS-induced inflammation response in microglia by AMPK activation. *BioMed Res. Int.* **2014**, *2014*, 692061.
(28) Grahame Hardie, D. AMP-activated protein kinase: a key regulator of energy balance with many roles in human disease. *J. Intern. Med.* **2014**, *276*, 543.
(29) Park, D. W.; Jiang, S.; Liu, Y.; Siegal, G. P.; Inoki, K.; Abraham, E.; Zmijewski, J. W. GSK3beta-dependent inhibition of AMPK potentiates activation of neutrophils and macrophages and enhances severity of acute lung injury. *Am. J. Physiol Lung Cell Mol. Physiol* **2014**, *307*, L735−45.
(30) Gupta, S. C.; Tyagi, A. K.; Deshmukh-Taskar, P.; Hinojosa, M.; Prasad, S.; Aggarwal, B. B. Downregulation of tumor necrosis factor and other proinflammatory biomarkers by polyphenols. *Arch. Biochem. Biophys.* **2014**, *559*, 91−9.
(31) Renaud, J.; Martinoli, M. G. Resveratrol as a protective molecule for neuroinflammation: a review of mechanisms. *Curr. Pharm. Biotechnol.* **2014**, *15*, 318−29.
(32) Kundu, J. K.; Surh, Y. J. Inflammation: gearing the journey to cancer. *Mutat. Res., Rev. Mutat. Res.* **2008**, *659*, 15−30.
(33) Mariani, F.; Sena, P.; Roncucci, L. Inflammatory pathways in the early steps of colorectal cancer development. *World J. Gastroenterol* **2014**, *20*, 9716−31.
(34) Sethi, G.; Shanmugam, M. K.; Ramachandran, L.; Kumar, A. P.; Tergaonkar, V. Multifaceted link between cancer and inflammation. *Biosci. Rep.* **2012**, *32*, 1−15.
(35) Conteduca, V.; Sansonno, D.; Russi, S.; Dammacco, F. Precancerous colorectal lesions (Review). *Int. J. Oncol.* **2013**, *43*, 973−84.
(36) Janakiram, N. B.; Rao, C. V. The role of inflammation in colon cancer. *Adv. Exp. Med. Biol.* **2014**, *816*, 25−52.
(37) Alguel, H.; Rasch, S. A clinical perspective on the role of chronic inflammation in gastrointestinal cancer. *Clin. Exp. Gastroenterol.* **2014**, *7*, 261−72.
(38) Kanneganti, M.; Mino-Kenudson, M.; Mizoguchi, E. Animal models of colitis-associated carcinogenesis. *J. Biomed. Biotechnol.* **2011**, *2011*, 342637.
(39) Neurath, M. F. Animal models of inflammatory bowel diseases: illuminating the pathogenesis of colitis, ileitis and cancer. *Dig Dis* **2012**, *30*, 91−4.
(40) Cui, X.; Jin, Y.; Hofseth, A. B.; Pena, E.; Habiger, J.; Chumanevich, A.; Poudyal, D.; Nagarkatti, M.; Nagarkatti, P. S.; Singh, U. P.; Hofseth, L. J. Resveratrol suppresses colitis and colon cancer associated with colitis. *Cancer Prev. Res.* **2010**, *3*, 549−59.
(41) Juan, M. E.; Alfaras, I.; Planas, J. M. Colorectal cancer chemoprevention by trans-resveratrol. *Pharmacol. Res.* **2012**, *65*, 584−91.
(42) Larrosa, M.; Yanez-Gascon, M. J.; Selma, M. V.; Gonzalez-Sarrias, A.; Toti, S.; Ceron, J. J.; Tomas-Barberan, F.; Dolara, P.; Espin, J. C. Effect of a low dose of dietary resveratrol on colon microbiota, inflammation and tissue damage in a DSS-induced colitis rat model. *J. Agric. Food Chem.* **2009**, *57*, 2211−20.
(43) Sanchez-Fidalgo, S.; Cardeno, A.; Villegas, I.; Talero, E.; de la Lastra, C. A. Dietary supplementation of resveratrol attenuates chronic colonic inflammation in mice. *Eur. J. Pharmacol.* **2010**, *633*, 78−84.
(44) Sharma, M.; Mohapatra, J.; Wagh, A.; Patel, H. M.; Pandey, D.; Kadam, S.; Argade, A.; Deshpande, S. S.; Shah, G. B.; Chatterjee, A.; Jain, M. R. Involvement of TACE in colon inflammation: a novel mechanism of regulation via SIRT-1 activation. *Cytokine* **2014**, *66*, 30−9.
(45) Delmas, D.; Aires, V.; Limagne, E.; Dutartre, P.; Mazue, F.; Ghiringhelli, F.; Latruffe, N. Transport, stability, and biological activity of resveratrol. *Ann. N. Y. Acad. Sci.* **2011**, *1215*, 48−59.
(46) Muzzio, M.; Huang, Z.; Hu, S. C.; Johnson, W. D.; McCormick, D. L.; Kapetanovic, I. M. Determination of resveratrol and its sulfate and glucuronide metabolites in plasma by LC-MS/MS and their pharmacokinetics in dogs. *J. Pharm. Biomed. Anal.* **2012**, *59*, 201−8.
(47) Rotches-Ribalta, M.; Andres-Lacueva, C.; Estruch, R.; Escribano, E.; Urpi-Sarda, M. Pharmacokinetics of resveratrol metabolic profile in healthy humans after moderate consumption of red wine and grape extract tablets. *Pharmacol. Res.* **2012**, *66*, 375−82.
(48) Vitaglione, P.; Sforza, S.; Galaverna, G.; Ghidini, C.; Caporaso, N.; Vescovi, P. P.; Fogliano, V.; Marchelli, R. Bioavailability of trans-resveratrol from red wine in humans. *Mol. Nutr. Food Res.* **2005**, *49*, 495−504.
(49) Walle, T. Bioavailability of resveratrol. *Ann. N. Y. Acad. Sci.* **2011**, *1215*, 9−15.
(50) Yu, C.; Shin, Y. G.; Chow, A.; Li, Y.; Kosmeder, J. W.; Lee, Y. S.; Hirschelman, W. H.; Pezzuto, J. M.; Mehta, R. G.; van Breemen, R. B. Human, rat, and mouse metabolism of resveratrol. *Pharm. Res.* **2002**, *19*, 1907−14.
(51) Bode, L. M.; Bunzel, D.; Huch, M.; Cho, G. S.; Ruhland, D.; Bunzel, M.; Bub, A.; Franz, C. M.; Kulling, S. E. In vivo and in vitro metabolism of trans-resveratrol by human gut microbiota. *Am. J. Clin. Nutr.* **2013**, *97*, 295−309.
(52) Rotches-Ribalta, M.; Urpi-Sarda, M.; Llorach, R.; Boto-Ordonez, M.; Jauregui, O.; Chiva-Blanch, G.; Perez-Garcia, L.; Jaeger, W.; Guillen, M.; Corella, D.; Tinahones, F. J.; Estruch, R.; Andres-Lacueva, C. Gut and microbial resveratrol metabolite profiling after moderate

DOI: 10.1021/acs.molpharmaceut.5b00464
Mol. Pharmaceutics 2015, 12, 3441−3454

long-term consumption of red wine versus dealcoholized red wine in humans by an optimized ultra-high-pressure liquid chromatography tandem mass spectrometry method. *J. Chromatogr A* **2012**, *1265*, 105−13.
(53) Visioli, F. The resveratrol fiasco. *Pharmacol. Res.* **2014**, *90*, 87.
(54) Amri, A.; Chaumeil, J. C.; Sfar, S.; Charrueau, C. Administration of resveratrol: What formulation solutions to bioavailability limitations? *J. Controlled Release* **2012**, *158*, 182−93.
(55) Biasutto, L.; Mattarei, A.; Sassi, N.; Azzolini, M.; Romio, M.; Paradisi, C.; Zoratti, M. Improving the efficacy of plant polyphenols. *Anti-Cancer Agents Med. Chem.* **2014**, *14*, 1332−42.
(56) Biasutto, L.; Zoratti, M. Prodrugs of quercetin and resveratrol: a strategy under development. *Curr. Drug Metab.* **2014**, *15*, 77−95.
(57) Abdin, A. A. Targeting sphingosine kinase 1 (SphK1) and apoptosis by colon-specific delivery formula of resveratrol in treatment of experimental ulcerative colitis in rats. *Eur. J. Pharmacol.* **2013**, *718*, 145−53.
(58) Larrosa, M.; Tome-Carneiro, J.; Yanez-Gascon, M. J.; Alcantara, D.; Selma, M. V.; Beltran, D.; Garcia-Conesa, M. T.; Urban, C.; Lucas, R.; Tomas-Barberan, F.; Morales, J. C.; Espin, J. C. Preventive oral treatment with resveratrol pro-prodrugs drastically reduce colon inflammation in rodents. *J. Med. Chem.* **2010**, *53*, 7365−76.
(59) Mattarei, A.; Azzolini, M.; Carraro, M.; Sassi, N.; Zoratti, M.; Paradisi, C.; Biasutto, L. Acetal derivatives as prodrugs of resveratrol. *Mol. Pharmaceutics* **2013**, *10*, 2781−92.
(60) Ferriz, J. M.; Vinsova, J. Prodrug design of phenolic drugs. *Curr. Pharm. Des.* **2010**, *16*, 2033−52.
(61) Mattarei, A.; Carraro, M.; Azzolini, M.; Paradisi, C.; Zoratti, M.; Biasutto, L. New water-soluble carbamate ester derivatives of resveratrol. *Molecules* **2014**, *19*, 15900−17.
(62) Vacondio, F.; Silva, C.; Mor, M.; Testa, B. Qualitative structure-metabolism relationships in the hydrolysis of carbamates. *Drug Metab. Rev.* **2010**, *42*, 551−89.
(63) Ertl, P.; Rohde, B.; Selzer, P. Fast calculation of molecular polar surface area as a sum of fragment-based contributions and its application to the prediction of drug transport properties. *J. Med. Chem.* **2000**, *43*, 3714−7.
(64) Palm, K.; Stenberg, P.; Luthman, K.; Artursson, P. Polar molecular surface properties predict the intestinal absorption of drugs in humans. *Pharm. Res.* **1997**, *14*, 568−71.
(65) Williams, A. Alkaline hydrolysis of substituted phenyl N-phenylcarbamates. Structure-reactivity relationships consistent with an E1cB mechanism. *J. Chem. Soc., Perkin Trans. 2* **1972**, 808−812.
(66) Sogorb, M. A.; Alvarez-Escalante, C.; Carrera, V.; Vilanova, E. An in vitro approach for demonstrating the critical role of serum albumin in the detoxication of the carbamate carbaryl at in vivo toxicologically relevant concentrations. *Arch. Toxicol.* **2007**, *81*, 113−9.
(67) Sogorb, M. A.; Vilanova, E. Serum albumins and detoxication of anti-cholinesterase agents. *Chem.-Biol. Interact.* **2010**, *187*, 325−9.
(68) Hansen, K. T.; Faarup, P.; Bundgaard, H. Carbamate ester prodrugs of dopaminergic compounds: synthesis, stability, and bioconversion. *J. Pharm. Sci.* **1991**, *80*, 793−8.
(69) Azzolini, M.; La Spina, M.; Mattarei, A.; Paradisi, C.; Zoratti, M.; Biasutto, L. Pharmacokinetics and tissue distribution of pterostilbene in the rat. *Mol. Nutr. Food Res.* **2014**, *58*, 2122−32.
(70) Deng, L.; Li, Y.; Zhang, X.; Chen, B.; Deng, Y. UPLC-MS method for quantification of pterostilbene and its application to comparative study of bioavailability and tissue distribution in normal and Lewis lung carcinoma bearing mice. *J. Pharm. Biomed. Anal.* **2015**, *114*, 200−207.
(71) Biasutto, L.; Marotta, E.; Bradaschia, A.; Fallica, M.; Mattarei, A.; Garbisa, S.; Zoratti, M.; Paradisi, C. Soluble polyphenols: synthesis and bioavailability of 3,4′,5-tri(alpha-D-glucose-3-O-succinyl) resveratrol. *Bioorg. Med. Chem. Lett.* **2009**, *19*, 6721−4.
(72) Biasutto, L.; Marotta, E.; Garbisa, S.; Zoratti, M.; Paradisi, C. Determination of quercetin and resveratrol in whole blood−implications for bioavailability studies. *Molecules* **2010**, *15*, 6570−9.

DOI: 10.1021/acs.molpharmaceut.5b00464
Mol. Pharmaceutics 2015, 12, 3441−3454

2122 DOI 10.1002/mnfr.201400244 *Mol. Nutr. Food Res.* 2014, *58*, 2122–2132

RESEARCH ARTICLE

Pharmacokinetics and tissue distribution of pterostilbene in the rat

Michele Azzolini[1], Martina La Spina[1,2], Andrea Mattarei[2,3], Cristina Paradisi[3], Mario Zoratti[1,2] and Lucia Biasutto[1,2]

[1] Department of Biomedical Sciences, University of Padova, Padova, Italy
[2] CNR Neuroscience Institute, Padova, Italy
[3] Department of Chemical Sciences, University of Padova, Padova, Italy

Scope: Pterostilbene (Pt) is emerging as an important health-promoting natural compound. Pharmacokinetic studies so far have focused on plasma levels, while Pt distribution in tissues is most relevant for biological action. This study determined tissue distribution of Pt and its major metabolite, pterostilbene-4′-sulfate (Pt-S), in rats after oral administration.
Methods and results: Upon intravenous (iv) administration (88 μmol/kg), Pt was cleared from blood with a half-life of 1.8 ± 0.3 h. Oral administration (same dose) resulted in moderate Pt bioavailability (~35%) and in an increased abundance of Pt-S in blood ($AUC_{Pt}/AUC_{Pt\text{-}S}$ ~0.75 and ~0.05 after iv or oral administration, respectively). Pt-S was the major species in all organs except the brain, where intact Pt was predominant ($AUC_{Pt}/AUC_{Pt\text{-}S}$ ~5). Both Pt and Pt-S peaked in all tissues at approximately 2 h. The highest levels (~200 nmoles/g for Pt-S and 40 nmoles/g for Pt) were measured in the liver, the lowest (≤7 nmol/g) in skeletal muscles and testes.
Conclusion: AUC_{Pt} was ~2- to ~25-fold higher in tissues than in blood; this may explain its bioactivity despite barely detectable blood levels. Of particular interest is the high fraction of nonmetabolized Pt in the brain, given the reports of its activity at the level of the central nervous system.

Received: April 9, 2014
Revised: July 15, 2014
Accepted: July 17, 2014

Keywords:
Area under the curve / LC / Pharmacokinetics / Pterostilbene / Tissue distribution

Additional supporting information may be found in the online version of this article at the publisher's web-site

1 Introduction

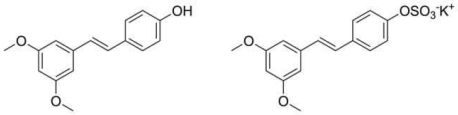
An already substantial and rapidly growing literature describes the favorable effects of pterostilbene (*trans*-3,5-dimethoxy-4′-hydroxystilbene; Pt) on processes and conditions of physiological and medical relevance [1–3]. This phytoalexin—found in blueberries, deerberries [4, 5], grapes [6], and in plants used by ayurvedic medicine [7]—acts as an anti-inflammatory compound [8–10], with a consequent positive impact on inflammation-associated pathologies, such as cancer [11,12] and neurodegeneration [13]. Pt exhibits chemopreventive [4,11,14] and chemotherapeutic properties [15–19]; it is cardioprotective [20] and antidiabetic [21, 22]. It reportedly exerts anti-aging and neuroprotective effects, effectively reversing cognitive behavioral deficits in aging rats [23, 24], and positively modulating markers of cellular stress, inflammation, and Alzheimer's disease pathology in a mouse model of aging [13]. These effects were associated with normalized expression of peroxisome proliferator-activated receptor alpha (PPARalpha), which is downregulated in senescent mice [13]. At a molecular level, Pt was reported to activate transcription factor Nrf2 [12,25], thus promoting the downstream anti-oxidant response [26, 27]. In a mouse model of chemically induced colon carcinogenesis, Pt was shown to inhibit multiple signaling pathways: Wnt/β-catenin, Ras, PI3K/Akt, EGFR [28]. Furthermore, Pt was reported to inhibit tumor growth through metastasis-associated protein 1 (MTA1) [15], and to inhibit phosphorylation of protein kinase C-β2

Correspondence: Dr. Lucia Biasutto, CNR Neuroscience Institute, Viale G. Colombo 3, 35121 Padova, Italy
E-mail: lucia.biasutto@cnr.it
Fax: +39-0498276040

Abbreviations: **AUC**, area under the curve; **HP-β-CD**, 2-hydroxypropyl-β-cyclodextrin; **iv**, intravenous; **Pt**, pterostilbene; **Pt-S**, pterostilbene-4′-sulfate

© 2014 WILEY-VCH Verlag GmbH & Co. KGaA, Weinheim

Mol. Nutr. Food Res. 2014, *58*, 2122–2132



Pterostilbene (Pt) **Pterostilbene-4'-sulfate** (Pt-S)

Figure 1. Chemical structure of Pterostilbene (Pt) and Pterostilbene-4′-sulfate (Pt-S).

(PKC-β2), decreasing expression of its downstream target genes, which include proinflammatory inducible nitric oxide synthase (iNOS), cyclooxygenase-2 (COX-2), and aldose reductase (AR) [12]. Pt was also found to inhibit the catalytic activity of CYP1A1 and CYP1B1 in vitro, at sub-μM K_i values. These enzymes are inducible, extra-hepatic forms of cytochrome P450, and are responsible for converting polycyclic aromatic hydrocarbons, heterocyclic amines, and estradiol to potentially carcinogenic metabolites [29].

What makes Pt particularly interesting, compared to its nonmethylated analog resveratrol, is the ability to reach higher plasma levels after oral administration [30]. An analogous improvement is shown also by other methylated polyphenols [31]. Interestingly, methylation often does not abolish but rather even potentiates the biological activity of the compounds (e.g. [10, 31]), possibly because it increases lipophilicity. Thus methylated polyphenols are very promising pharmacological agents. Determination of levels and distribution/accumulation of Pt and its metabolites in tissues is of crucial importance to understand its therapeutic potential. However, studies on Pt absorption and metabolism were all focused only on plasma levels of Pt and its metabolites [30, 32–34]. Orally administered pterostilbene was shown to be mainly sulfated in rats; pterostilbene-4′-glucuronide can also be produced, but its abundance is very low compared to the sulfate and also to pterostilbene itself [30]. Peak plasma concentrations of both Pt and its metabolites were reached 2–4 h after oral administration. To our knowledge, no pharmacokinetic studies investigated tissue levels of Pt, with the only exception of [13] which observed its presence in the brain of mice fed for 8 weeks with 120 mg pterostilbene/kg of diet.

We thus developed a method to extract and quantify Pt and its main in vivo metabolite, pterostilbene-4′sulfate (Pt-S; [30]) (Fig. 1), from various tissues. We then applied the method in pharmacokinetic studies in the rat model, and assessed blood and tissue levels of Pt and its metabolite(s) at different time points after administration of a single intragastric dose of Pt.

The dosage we used was 88 μmoles/kg, i.e. 22.5 mg/kg of pterostilbene. This is similar to dosages used in other pharmacokinetic studies in the rat [33, 34], and is roughly equivalent to the administration of 250 mg to an average human ([33] and refs. therein). Such an amount can hardly be obtained from food; for example, pterostilbene content is estimated to be 100–520 ng/g in blueberries [5, 35], one of the richest sources of this compound. However, it may well be clinically relevant, since administering this dose daily to volunteers reportedly lowered blood pressure [36]. Furthermore, it seems safe to consider it nontoxic since consumption of 22.5 mg/kg twice daily for 30 days by rats did not cause any evident ill effects (not shown). Oral administration of 125 mg twice daily for 6–8 weeks to humans [37] and of up to 3 g/kg/day for 28 days to mice [38] was also reported to be innocuous.

2 Materials and methods

2.1 Chemicals

Pterostilbene was purchased from Wonda Science (Changzhou, Jiang, People's Republic of China, batch n. WF12062501). Other materials were purchased from Sigma/Aldrich/Fluka/Riedel de-Haen (Milan, Italy) and Merck-Novabiochem (Milan, Italy), and were used as received.

2.2 Animals

Adult male Wistar rats (approximately 400 g body weight) from the facility of the Department of Biomedical Sciences were used for the pharmacokinetic experiments. All experiments involving animals were performed after approval by the University of Padova Ethical Committee for Experimentation on Animals (CEASA) (Permit Number: 80/2011) and of the Italian Ministry of Health, and with the supervision of the Central Veterinary Service of the University of Padova, in compliance with Italian Law DL 116/92, embodying UE Directive 86/609.

2.3 Synthesis of pterostilbene-4′-sulfate

Pterostilbene-4′-sulfate is the main in vivo phase II metabolite of Pt in rats [30]. We thus chemically synthesized it as an analytical standard, adapting an existing synthetic protocol [39, 40]. The crude reaction mixture was diluted with brine and washed with methylene chloride. Combined organic fractions were then concentrated under reduced pressure (500 mbar, 40°C) and the resulting mixture was applied to a column of cation-exchange resin (Dowex 50WX8-200, K^+ form) prepared as described in [41]. Fractions containing the product were combined and concentrated. The Pt-S potassium salt was finally purified through reversed phase preparative HPLC (ACE 5 AQ, 150 × 21.2 mm, Advanced Chromatography Technologies, Aberdeen, Scotland; acetonitrile/water, from 10% to 60% acetonitrile in 20 min, 17 mL/min, 280 nm). Details about the synthetic protocols and spectroscopic data can be found in the Supporting Information.

© 2014 WILEY-VCH Verlag GmbH & Co. KGaA, Weinheim

2.4 Calibration/standard curves

Standard solutions of Pt and Pt-S in acetonitrile (in the concentration range 0.15–500 μM) were analyzed by HPLC/UV as described below; peak area at the maximum absorption wavelength (320 nm for Pt and 300 nm for Pt-S) was plotted against concentration to establish the correlation between peak area and amount analyzed.

2.5 HPLC analysis

Samples (2 μL) were analyzed by HPLC/UV (1290 Infinity LC System, Agilent Technologies) using a reverse phase column (Zorbax RRHD Eclipse Plus C18, 1.8 μm, 50 × 2.1 mm id; Agilent Technologies) and a UV diode array detector (190–500 nm). Solvents A and B were water containing 0.1% TFA and acetonitrile, respectively. The gradient for B was as follows: 10% for 0.5 min, then from 10 to 100% in 3.5 min, 100% for 1 min; the flow rate was 0.6 mL/min. The eluate was preferentially monitored at 286, 300, and 320 nm (corresponding to absorbance maxima of the internal standard, Pt-S and Pt, respectively). The temperature of the column was kept at 35°C.

2.6 HPLC/ESI-MS analysis

HPLC/ESI-MS was performed on selected samples with a 1100 Series system (Agilent Technologies). Samples (20 μL) were analyzed using a reversed phase column (Synergi-MAX, 4 μm, 150 × 4.6 mm id; Phenomenex, Castel Maggiore (BO), Italy). Solvents A and B were water containing 0.1% TFA and acetonitrile, respectively. The gradient for B was as follows: 10% for 2 min, from 10 to 100% in 20 min, then 100% for 2 min; the flow rate was 1 mL/min. The eluate was preferentially monitored at 286, 300, and 320 nm. MS analysis was performed with an ESI source operating in full-scan positive ion mode, applying the following ESI parameters: capillary 3762.30 V, skimmer 19.18 V, cap exit 50.00 V, nebulizer pressure 70 psi, dry gas flow 12 L/min, dry gas temperature 350°C.

2.7 Pharmacokinetic studies

2.7.1 Intravenous administration

Pt was injected in the tail vein of three rats as a single intravenous bolus (88 μmol/kg body weight, 22.5 mg/kg; injection volume: 200 μL). Because of the limited aqueous solubility of Pt, the dose was solubilized using 2-hydroxypropyl-β-cyclodextrin (HP-β-CD). Briefly, Pt and HP-β-CD were mixed in a 1:3 ratio in 5 mL of 9% NaCl solution; the solution was then sterile-filtered before injection. Serial blood samples were collected in heparinized tubes before and at different times after administration (5, 10, and 30 min; 1, 1.5, 2, 3, 4, 5, 6, 9, and 12 h); samples were kept in ice and treated as described below within 10 min.

2.7.2 Oral administration

Pt was administered to overnight-fasted rats as a single intragastric dose (88 μmol/kg body weight, dissolved in 250 μL DMSO). At different times after Pt administration (0.5, 2, 4, 8, 12, and 16 h), animals were anesthetized with isoflurane and sacrificed (N = 3 or 4 for each time point). Blood was collected in heparinized tubes, kept in ice and treated as described below within 10 min. Brain, lungs, heart, liver, kidneys, testes, and skeletal muscles (soleus, gastroctemius, and anterior tibialis) were explanted, weighed, and immediately frozen in liquid nitrogen; treatments were then performed as described below. The area under the curve (AUC) values were calculated using the trapezoidal rule.

2.8 Treatment of blood and tissue samples

2.8.1 Blood

Blood aliquots (100 μL) were treated as described in [42]. Briefly, after addition of the internal standard (4,4′-dihydroxybiphenyl; dilution from a 50 × stock solution in acetonitrile, 25 μM final concentration), samples were stabilized with a freshly prepared 10 mM solution of ascorbic acid (10 μL) and acidified with 0.6 M acetic acid (10 μL); after mixing, an excess of acetone (400 μL) was added, followed by sonication (2 min) and centrifugation (12 000 g, 7 min, 4°C). An accurately measured portion of the supernatant was finally collected and stored at –20°C. Before analysis, acetone was allowed to evaporate at room temperature using a Univapo 150 H (UniEquip) vacuum concentrator centrifuge, and up to 40 μL of acetone were added to precipitate residual proteins. After centrifugation (12 000 g, 5 min, 4°C), cleared samples were analyzed by HPLC/UV. The concentration of analytes in the original sample was determined as described in Supporting Information.

2.8.2 Tissues

One gram of thawed tissue was mixed with 1 mL of D-PBS (Euroclone), and homogenized with a motorized polypropylene pestel (Sigma) (for brain and testes) or with an Ultra-Turrax T25 homogenizer (Janke & Kunkel) (for all other tissues). Two hundred milligrams of tissue homogenate were transferred into a vial and spiked with the internal standard (4,4′-dihydroxybiphenyl, dilution from a 50 × stock solution in acetonitrile, 25 nmol/g tissue final concentration). Ten microliters of a freshly prepared 10 mM solution of ascorbic acid, 10 μL of 4.35 M acetic acid, and 500 μL of acetone were added. Samples were vortexed (2 min), sonicated (2 min), and then centrifuged (12 000 × *g*, 7 min, 4°C). An accurately

© 2014 WILEY-VCH Verlag GmbH & Co. KGaA, Weinheim

measured portion of the supernatant was finally collected and stored at –20°C. Further processing and analysis was carried out as described above for blood samples.

2.8.3 Recovery yields

To establish the recovery yields of Pt and Pt-S from blood and organs, the protocols for the treatment of blood or tissues were applied to samples spiked with a known amount of Pt or Pt-S.

One milliliter of blood (from an untreated animal) was spiked with 5 nmoles of Pt or Pt-S (dilution from a 1000× stock solution in DMSO). One hundred sixty microliters aliquots were then taken and processed as described above.

One gram of tissue (from an untreated animal) was mixed with 1 mL of PBS containing 5 nmoles of Pt or Pt-S (dilution from a 100 × stock solution in DMSO), and homogenized. Two hundred milligrams aliquots of the homogenate were then taken and processed as described above. Recoveries of Pt, Pt-S, and internal standard were determined as described in Supporting Information.

2.9 Pharmacokinetic analysis

Mean blood concentrations of pterostilbene were plotted versus time. Pharmacokinetic parameters were determined by noncompartmental analysis, using PKSolver 2.0 [43]. Absolute bioavailability for oral administration was calculated as $F(\%) = AUC_{0\text{-}t}(\text{oral})/AUC_{0\text{-}t}(\text{iv}) \times 100$; since the same Pt dose was used for intravenous and oral administration, no dose correction was applied. Pt blood concentration was close to 0 at 16 h or 12 h after oral or iv administration, respectively; $AUC_{0\text{-}t}$ thus approaches $AUC_{0\text{-}\infty}$ in both cases.

3 Results

3.1 Development of protocols for blood and tissue sample analysis

The general protocol developed for blood and tissue treatment was adapted from [42]; it includes acidification of the sample, addition of an antioxidant (ascorbic acid) to preserve compound stability, and addition of organic solvent followed by sonication to ensure compound extraction and protein denaturation. The samples are then cleared of cell/tissue debris and denaturated proteins by centrifugation, and the supernatant concentrated and analyzed by HPLC/UV. Treatment of tissue homogenates required some adjustments of the original method; since samples are more dense than blood, an additional vortexing before sonication was required to ensure an efficient mixing and extraction. Furthermore, increased sample acidification was necessary to improve recovery of the analytes, allowing disruption of polyphenol–protein binding [44].

The main metabolite of Pt in the rat, pterostilbene-4′-sulfate (Pt-S), was synthesized and used as analytical standard. Recovery yields of Pt and Pt-S from organs (brain, lungs, liver, kidneys, heart, testes, skeletal muscles) and blood were evaluated treating and analyzing samples spiked with a known amount of the analyte (5 nmoles/g tissue or 5 nmoles /mL blood) and of the internal standard (4, 4′-dihydroxy biphenyl, 25 nmol/g tissue, or 25 nmol/mL blood). Pt, Pt-S, and internal standard were quantified at 320, 300, or 286 nm, respectively (corresponding to their absorbance maxima). Selectivity at these wavelengths was evaluated; HPLC/UV chromatograms show that both analytes, as well as the internal standard, are well resolved and free from interfering background peaks due to the matrix (blood or tissues) (Fig. 2). Figure 2 shows HPLC/UV chromatograms of "blank" tissue lysates of liver and kidneys (traces "a"), which are the organs with the most conspicuous background signal(s), compared to lysates spiked with Pt (traces "b") or Pt-S (traces "c").

The recovery yield ratio of Pt and Pt-S to the internal standard was satisfyingly reproducible (Table 1). Intraday precision, expressed as coefficient of variation (CV), was 10% at most in all cases, with exception of Pt in brain, where the CV was about 15%; interday precision was also within 10%, with exception of Pt in brain and liver, where the CV was about 15% (Table 1). HPLC analysis of standard solutions of Pt and Pt-S showed that these analytes (at their maximum UV absorption wavelengths, which are 320 and 300 nm, respectively) have the same calibration curve ($y = 4.96\,x$, where y is the peak area at the maximum absorption wavelength and x is the concentration in μM units). LOD and LOQ of the analytical part of the method were calculated measuring the average background response at 320 and 300 nm in 30 different HPLC runs, at the retention time of the analytes (2.93 and 2.33 min for Pt and Pt-S, respectively) and over a time lapse of 0.04 min, which is the typical peak width of the analytes at low concentrations (< 1 μM). LOD and LOQ were taken to be 3 or 10 times, respectively, the background response. Interpolating the data in the calibration curve, we obtained LOD and LOQ values of 0.05 and 0.15 μM, respectively, for both Pt and Pt-S. LOQ was confirmed analyzing three solutions at the LOQ concentration; peak area fitted well within the calibration curve.

3.2 Pharmacokinetics

The method was then applied to pharmacokinetic studies; intravenous administration of a single Pt bolus (88 μmol/kg, 22.5 mg/kg) to rats resulted in a bi-exponential decay of Pt levels in blood (i.e. a rapid distribution phase followed by a prolonged elimination phase) (Fig. 3A), in accordance with previous studies [32–34]. Pharmacokinetic parameters for Pt, obtained using noncompartmental analysis, are presented in Fig. 3B. Two-compartment analysis was also performed, but the values obtained in this case were affected by a much higher uncertainty due to the rapidity of the first

© 2014 WILEY-VCH Verlag GmbH & Co. KGaA, Weinheim

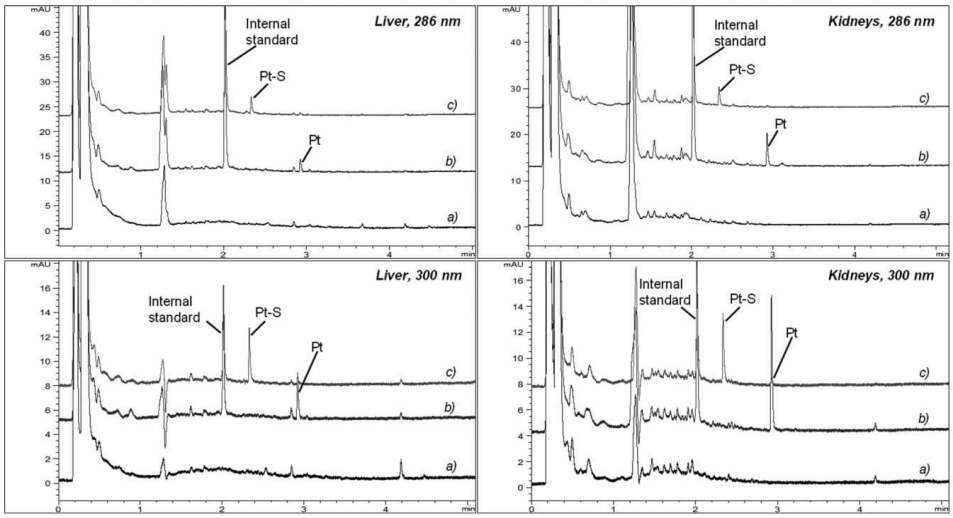


Figure 2. HPLC/UV chromatograms (286 and 300 nm) of extracts of liver and kidney lysates. (a) "blank" tissue lysate; (b) tissue lysate spiked with 5 nmol/g Pt; (c) tissue lysate spiked with 5 nmol/g Pt-S.

process. Pt-S was the only detectable metabolite in circulation; it was progressively generated, reaching the maximum concentration (11.7 ± 3.2 μM) 2 h after injection of the Pt bolus. Its $AUC_{0\text{-}12h}$ was slightly higher than that of Pt itself (52.1 ± 14.7 nmol/mL × h versus 38.8 ± 5.3 nmol/mL × h, respectively).

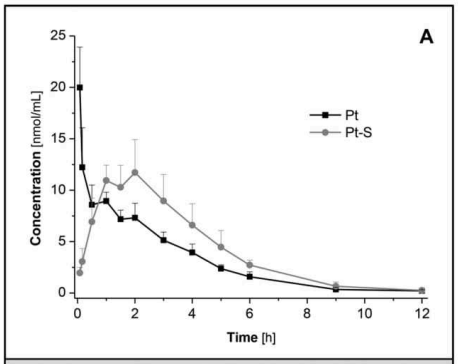
For the evaluation of oral bioavailability, blood samples were taken at preestablished times after administration of the same Pt dosage by oral gavage and analyzed (see Materials and methods). To study tissue distribution, rats were sacrificed, organs were explanted at different times after oral administration, and tissue levels of Pt and its metabolite(s) were determined. Measured concentrations of both Pt and Pt-S were above the LOQ in all samples in the 0.5 –12 h interval. Analytes were quantified according to their calibration curve, adjusting the result for the recovery of each analyte, determined on the basis of the recovery of the internal standard and of the known recovery ratio between analyte and internal standard (see Supporting Information for details). Figure 4 illustrates time-concentration profiles of Pt and Pt-S in blood and tissues, and Fig. 5 reports $AUC_{0\text{-}16h}$ values, C_{max} and t_{max} for both Pt and Pt-S in all analyzed tissues (N = 3 or 4 for each time point). A residual amount of blood in explanted tissues is expected if they are collected without perfusion; in rats, this amount has been estimated to account for a fraction of organ weight comprised between 1 or 2% (in muscles and brain, respectively) and 13% (in lungs and heart) [45]. The residual blood is thus not expected to significantly

Table 1. Recovery of Pt and Pt-S from blood and tissues

Tissue	Analyte/internal standard recovery ratio[a)]		Interday precision (CV)	
	Pt	Pt-S	Pt	Pt-S
Blood	0.841 ± 0.028	0.922 ± 0.056	3.3	6.1
Brain	0.732 ± 0.115	0.853 ± 0.087	15.7	10.2
Lungs	0.636 ± 0.062	0.633 ± 0.034	9.8	5.4
Heart	0.752 ± 0.085	0.497 ± 0.028	11.3	5.6
Liver	0.716 ± 0.104	0.610 ± 0.064	14.6	10.4
Kidneys	0.697 ± 0.048	0.597 ± 0.042	6.8	7.1
Testes	0.676 ± 0.064	0.720 ± 0.076	9.4	10.5
Muscles	0.708 ± 0.053	0.597 ± 0.051	7.5	8.6

a) N ≥ 4 for each condition. Mean values ± SD are shown.

© 2014 WILEY-VCH Verlag GmbH & Co. KGaA, Weinheim



Parameter	Value	B
$AUC_{0\text{-}12h}$ [(nmol/mL)×h]	38.8 ± 5.3	
$t_{1/2}$ [h]	1.8 ± 0.3	
CL [L/h/kg]	2.3 ± 0.3	
V_{ss} [L/kg]	6.1 ± 1.0	
C_0 [nmol/mL]	35.6 ± 17.2	
λ_z [1/h]	0.39 ± 0.07	
MRT [h]	2.7 ± 0.3	

Figure 3. Pharmacokinetic profile of Pt after intravenous administration. (A) Concentration versus time profiles of Pt and Pt-S in blood. Reported are mean values ± SD (N = 3). (B) Intravenous pharmacokinetic parameters for Pt.

affect the assessment of analytes in any given tissue sample; we thus decided to collect tissues without perfusion, immediately freezing them in liquid nitrogen after explantation. Our approximation was validated a posteriori by the experimental results; in fact, the relative abundance of Pt and Pt-S in blood turned out to be very different from that found in all other tissues.

Absolute oral bioavailability for Pt, calculated as the percentage ratio between $AUC_{0\text{-}t}$(oral) and $AUC_{0\text{-}t}$(iv) in blood, was about 35%. No major differences were observed in the t_{max}; both pterostilbene and its sulfate, in all organs, reached a maximum concentration about 2 h after administration. The pharmacokinetic profile was very different in blood compared to the other tissues: Pt levels were the lowest among the tissues analyzed ($C_{max} = 1.5 \pm 1.0$ μM), and the difference between the AUCs of intact Pt versus its sulfate was the highest ($AUC_{0\text{-}16h}$ for Pt-S was about 20 times that for Pt). At all times, Pt levels were higher in any given organ than in blood, but the relative amounts of Pt and Pt-S differed depending on tissue. $AUC_{0\text{-}16h}$ for Pt-S was significantly higher than that for Pt in lungs, heart, liver, kidneys, and testes. On the contrary, brain displayed an higher $AUC_{0\text{-}16h}$ for nonmetabolized Pt compared to the sulfate, while the differences were nonsignificant in skeletal muscles. The highest amounts per gram of Pt were detected in the liver, followed by kidneys, lungs, and brain. Also Pt-S levels were highest in the liver, followed by kidneys, lungs, and blood. The other possible phase II metabolite of Pt, pterostilbene-4′-glucuronide [30], was detected only in the liver, and was present in very low amounts (at most 1% of the total amount of recovered analytes; 98% were Pt and Pt-S) (Fig. 6). Another 1% of analytes found in the liver extracts showed the characteristic absorption spectrum of stilbenes, but remained unidentified. The latter might be phase II metabolites (i.e. sulfates or glucuronides) of demethylated and/or hydroxylated pterostilbene (as reported by [46]). In all other organs however these putative metabolites were below detection limit.

4 Discussion

Our results confirm the observations by others that pterostilbene is readily transformed into phase II conjugates after oral administration [30]. This metabolism is due to enzymatic activities in hepatocytes as well as enterocytes; the relevance of the latter is made evident by the different blood $AUC_{Pt}/AUC_{Pt\text{-}S}$ ratios obtained after intravenous or oral administration (approx. 0.75 versus 0.05, respectively). In rats, the sulfate is by far the predominant metabolite, with a small amount of glucuronide being found only in liver. It should be pointed out however that there may be marked differences in the relative relevance of these conjugative processes depending on the species and also on factors such as dosage (see, e.g. in the case of resveratrol, [47, 48] and Table 1 in [49]).

It has been suggested that DMSO, used as vehicle for oral administration, may enhance absorption ([50]; but to the contrary see, e.g. [51]). However such an effect, if present, seems to have little relevance in our study since the absolute bioavailability value we calculated is intermediate between values already present in the literature and obtained administering aqueous solutions/suspensions (with HP-β-CD, carboxymethylcellulose, or methylcellulose) [30, 32, 33].

To our knowledge, this is the first extensive study of the tissue distribution of Pt and its metabolites at different times after oral administration. Pharmacokinetic data already present in the literature largely concern plasma levels [30, 32–34]. We found that Pt, as well as its main metabolite, Pt-S, is not evenly distributed in the body after oral administration. The different concentrations, as well as the different relative abundance, of Pt and Pt-S in blood versus tissues confirm the notion that analysis of blood—and even more so of plasma [42]—may not be considered as representative for the whole organism. Pt and its metabolite(s) (in this case mainly Pt-S) have different lipophilicity/hydrophilicity, and this may account for variations in their relative abundance in tissues. Soluble metabolites are expected to be enriched in aqueous environments, while the less hydrophilic parent compound may associate more readily with tissues, depending on characteristics such as lipid content and accessibility. This

© 2014 WILEY-VCH Verlag GmbH & Co. KGaA, Weinheim

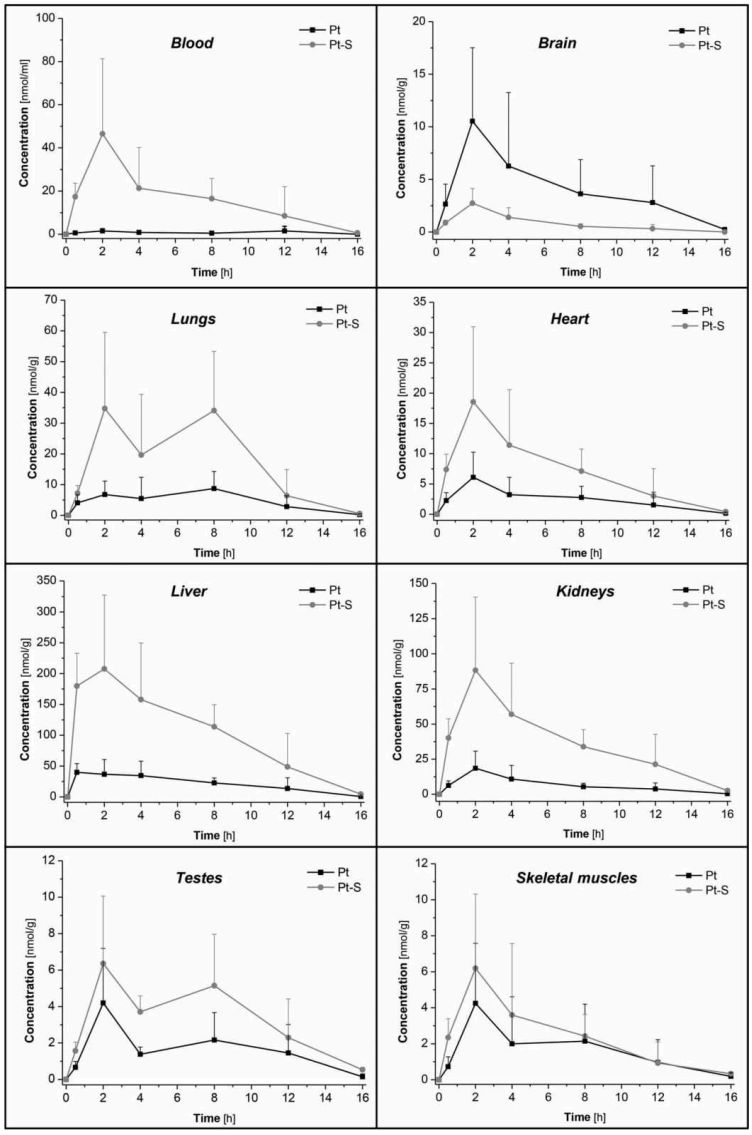


Figure 4. Concentration versus time profiles of Pt and Pt-S in blood and tissues. A single intragastric dose of pterostilbene (88 μmoles/kg body weight) was administered to rats at time 0. Reported are mean values ± SD (N = 3 or 4).

© 2014 WILEY-VCH Verlag GmbH & Co. KGaA, Weinheim

A

Tissue	$AUC_{0\text{-}16h}$ [(nmol/g) x h]		C_{max} [nmol/g]		t_{max} [h]	
	Pt	*Pt-S*	*Pt*	*Pt-S*	*Pt*	*Pt-S*
Blood	13.7 ± 6.6	263.6 ± 76.6	1.5 ± 1.0 / 1.5 ± 2.1	46.5 ± 34.8	2	2
Brain	66.1 ± 22.4	13.2 ± 3.0	10.5 ± 7.0	2.7 ± 1.4	2	2
Lungs	79.0 ± 24.9	289.9 ± 80.5	6.8 ± 4.4 / 8.7 ± 5.5	34.7 ± 24.8 / 34.1 ± 19.3	2 / 8	2 / 8
Heart	40.0 ± 11.5	115.4 ± 30.6	6.1 ± 4.2	18.5 ± 12.4	2	2
Liver	351.6 ± 82.3	1674.2 ± 316.4	39.7 ± 14.2	207.6 ± 119.8	0.5 - 4	2
Kidneys	108.6 ± 30.3	591.6 ± 125.9	18.5 ± 12.2	88.3 ± 52.2	2	2
Testes	26.9 ± 7.3	54.1 ± 11.2	4.2 ± 3.0 / 2.2 ± 1.5	6.4 ± 3.7 / 5.1 ± 2.8	2 / 8	2 / 8
Muscles	27.0 ± 9.9	38.1 ± 11.3	4.2 ± 3.3	6.2 ± 4.1	2	2

B

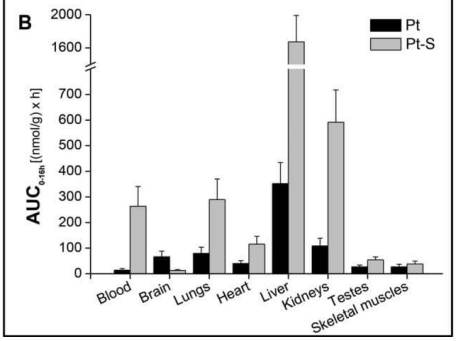


Figure 5. Pharmacokinetic parameters for Pt and Pt-S in blood and tissues. (A) AUC, C_{max}, and t_{max} values for Pt and Pt-S in blood and organs. For blood, concentrations are expressed in nmol/mL units (i.e. μM). (B) AUC values are plotted for various organs, with comparison between Pt and Pt-S.

idea is supported by the observation that blood (which has an abundant aqueous component) shows the lowest $AUC_{Pt}/AUC_{Pt\text{-}S}$ ratio (about 0.05), while the brain, which is particularly rich in lipids, is the tissue with the highest $AUC_{Pt}/AUC_{Pt\text{-}S}$ ratio (about 5). This observation has logical implications for the in vivo biological activity of pterostilbene; of particular interest is the high percentage of non-metabolized Pt in the brain, given the reports of its activity on the central nervous system [13, 24].

Since Pt-S can reach high levels in various tissues, elucidation of the activity of Pt-S would be very interesting. No studies are available at the moment on the possible biological activity of Pt-S or Pt-glucuronide, and are clearly needed. Studies of the effects of metabolites of resveratrol have indicated that conjugation with sulfate or glucuronyl groups may alter the efficacy of the natural compound, often decreasing it. For example, sulfation of resveratrol in either position 3 or 4′ reduces inhibition of COX-1 and -2, as well as inhibition of Quinone Reductase 2 [41, 52]. A level of activity is nonetheless retained by metabolites. A recent study [48] for example reports that prolonged (6 weeks) administration of a relatively low (5 mg/kg × day) dose of resveratrol to diabetic rats led to the progressive appearance of approximately 0.07 nmoles/g of reveratrol sulfate and glucuronide in the heart tissue, while resveratrol itself was absent. Clear protective effects on hemodynamic function could be measured.

Another emerging aspect of relevance here is that phase II metabolites may act as a source of the natural compound, which can be regenerated from them thanks to enzymatic activities. This phenomenon is well known for flavonoids, regenerated from their glucuronides through the intervention of β-glucuronidase [53, 54]. Similar processes also take place with resveratrol glucuronides and sulfates [55, 56].

Supporting Information Table 1 summarizes pharmacokinetic data for resveratrol (from literature) and Pt (from the present work). The comparison indicates that in organs higher concentrations of the unmodified molecule can be reached in the case of pterostilbene than in the case of resveratrol.

When resveratrol was orally administered to rats at the same dose we used in this study with pterostilbene (88 μmol/kg, 20mg/kg), tissue levels of resveratrol were always below 1 nmol/g [57]. In contrast, nonmetabolized Pt found during our work was much higher: maximum concentrations ranged from 4.2 ± 3.0 nmol/g (in testes) to 39.7 ± 14.2 nmol/g (in the liver). Interestingly, t_{max} was considerably higher when Pt was administered, compared to resveratrol (2 h versus 5–15 min, respectively). Furthermore, tissue levels of resveratrol and metabolites were reported to be much lower than those of Pt and its metabolite(s), even if resveratrol was administered intravenously [44] or orally at higher dosages (219 μmol/kg [55] or 438 μmol/kg [58] instead of 88 μmol/kg). These higher levels may be attributed to a higher lipophilicity of Pt compared to resveratrol, which favours intestinal absorption and, more generally, permeation of biomembranes. Also the presence in the molecule of only one hydroxyl (instead of three, in resveratrol) gives the compound an intrinsic advantage in phase II conjugative reactions. Note however that absolute oral bioavailability, calculated as the ratio of $AUC_{0\text{-}t}$(oral) to $AUC_{0\text{-}t}$(iv) in blood, may actually be comparable or even higher for resveratrol than for Pt, because of resveratrol's low $AUC_{0\text{-}t}$(iv) values [30, 59–61].

In summary, this work shows that pterostilbene levels much higher than those found in blood are reached in some tissues and may in fact be adequate to explain effects probably mediated largely by regulation of epigenetic processes. This may help explain the apparent paradox of pterostilbene bioactivity in the face of low blood or plasma concentrations. The results of this study thus concur with those of functional and biochemical investigations to support the potential of pterostilbene for biomedical applications. It is now relevant to explore the "bioaccumulation" of pterostilbene and its metabolite(s) upon prolonged administration of relatively low levels, mimicking intake obtainable through the diet.

© 2014 WILEY-VCH Verlag GmbH & Co. KGaA, Weinheim

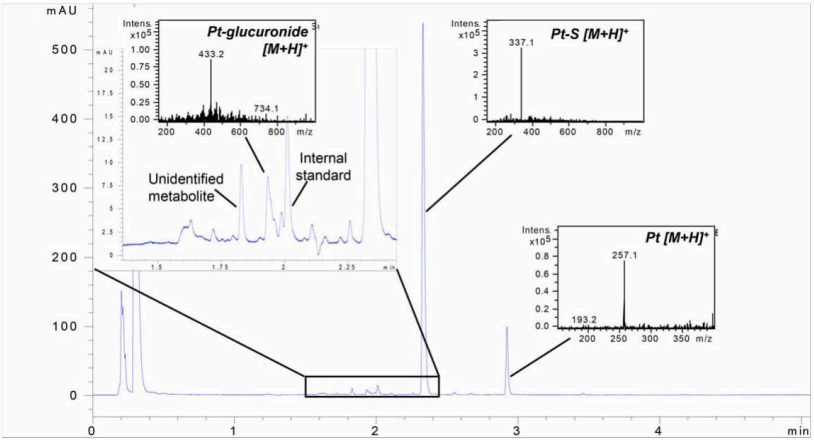


Figure 6. HPLC/UV and ESI-MS analysis of a sample from pharmacokinetic studies. A representative chromatogram (300 nm) of liver extract (2 h after Pt administration). Inserts represent an enlargement of the indicated part of the chromatogram, and ESI + mass spectra for Pt, Pt-S, and Pt-glucuronide.

We thank Mr. M. Ghidotti for technical help. This work was supported by grants from the Fondazione Cassa di Risparmio di Padova e Rovigo (CARIPARO) ("Developing a Pharmacology of Polyphenols"), from the Italian Ministry of the University and Research (PRIN n. 20107Z8XBW_004), and by the CNR Project of Special Interest on Aging.

The authors have declared no conflict of interest

5 References

[1] McCormack, D., McFadden, D., A review of pterostilbene antioxidant activity and disease modification. *Oxid. Med. Cell Longev.* 2013, *2013*, 575482.

[2] Pterostilbene. Monograph. *Altern. Med. Rev.* 2010, *15*, 159–163.

[3] Estrela, J. M., Ortega, A., Mena, S., Rodriguez, M. L. et al., Pterostilbene: Biomedical applications. *Crit. Rev. Clin. Lab. Sci.* 2013, *50*, 65–78.

[4] Paul, S., DeCastro, A. J., Lee, H. J., Smolarek, A. K. et al., Dietary intake of pterostilbene, a constituent of blueberries, inhibits the beta-catenin/p65 downstream signaling pathway and colon carcinogenesis in rats. *Carcinogenesis* 2010, *31*, 1272–1278.

[5] Rimando, A. M., Kalt, W., Magee, J. B., Dewey, J. et al., Resveratrol, pterostilbene, and piceatannol in vaccinium berries. *J. Agric. Food Chem.* 2004, *52*, 4713–4719.

[6] Schmidlin, L., Poutaraud, A., Claudel, P., Mestre, P. et al., A stress-inducible resveratrol O-methyltransferase involved in the biosynthesis of pterostilbene in grapevine. *Plant Physiol.* 2008, *148*, 1630-1639.

[7] Paul, B., Masih, I., Deopujari, J., Charpentier, C., Occurrence of resveratrol and pterostilbene in age-old darakchasava, an ayurvedic medicine from India. *J. Ethnopharmacol.* 1999, *68*, 71–76.

[8] Paul, S., Rimando, A. M., Lee, H. J., Ji, Y. et al., Anti-inflammatory action of pterostilbene is mediated through the p38 mitogen-activated protein kinase pathway in colon cancer cells. *Cancer Prev. Res. (Phila)* 2009, *2*, 650–657.

[9] McCormack, D., McDonald, D., McFadden, D., Pterostilbene ameliorates tumor necrosis factor alpha-induced pancreatitis in vitro. *J. Surg. Res.* 2012, *178*, 28–32.

[10] Cichocki, M., Paluszczak, J., Szaefer, H., Piechowiak, A. et al., Pterostilbene is equally potent as resveratrol in inhibiting 12-O-tetradecanoylphorbol-13-acetate activated NFkappaB, AP-1, COX-2, and iNOS in mouse epidermis. *Mol. Nutr. Food Res.* 2008, *52* (Suppl 1), S62–S70.

[11] Tsai, M. L., Lai, C. S., Chang, Y. H., Chen, W. J. et al., Pterostilbene, a natural analogue of resveratrol, potently inhibits 7,12-dimethylbenz[a]anthracene (DMBA)/12-O-tetradecanoylphorbol-13-acetate (TPA)-induced mouse skin carcinogenesis. *Food Funct. 2012*, *3*, 1185–1194.

[12] Chiou, Y. S., Tsai, M. L., Nagabhushanam, K., Wang, Y. J. et al., Pterostilbene is more potent than resveratrol in preventing azoxymethane (AOM)-induced colon tumorigenesis via activation of the NF-E2-related factor 2 (Nrf2)-mediated antioxidant signaling pathway. *J. Agric. Food Chem.* 2011, *59*, 2725-2733.

[13] Chang, J., Rimando, A., Pallas, M., Camins, A. et al., Low-dose pterostilbene, but not resveratrol, is a potent neuromodulator in aging and Alzheimer's disease. *Neurobiol. Aging* 2012, *33*, 2062–2071.

© 2014 WILEY-VCH Verlag GmbH & Co. KGaA, Weinheim

[14] Suh, N., Paul, S., Hao, X., Simi, B. et al., Pterostilbene, an active constituent of blueberries, suppresses aberrant crypt foci formation in the azoxymethane-induced colon carcinogenesis model in rats. *Clin. Cancer Res.* 2007, *13*, 350-355.

[15] Li, K., Dias, S. J., Rimando, A. M., Dhar, S. et al., Pterostilbene acts through metastasis-associated protein 1 to inhibit tumor growth, progression and metastasis in prostate cancer. *PLoS One* 2013, *8*, e57542.

[16] Kapoor, S., Pterostilbene and its emerging antineoplastic effects: a prospective treatment option for systemic malignancies. *Am. J. Surg.* 2013, *205*, 483.

[17] Mak, K. K., Wu, A. T., Lee, W. H., Chang, T. C. et al., Pterostilbene, a bioactive component of blueberries, suppresses the generation of breast cancer stem cells within tumor microenvironment and metastasis via modulating NF-kappaB/microRNA 448 circuit. *Mol. Nutr. Food Res.* 2013, *57*, 1123–1134.

[18] McCormack, D., McFadden, D., Pterostilbene and cancer: current review. *J. Surg. Res.* 2012, *173*, e53–e61.

[19] Mena, S., Rodriguez, M. L., Ponsoda, X., Estrela, J. M. et al., Pterostilbene-induced tumor cytotoxicity: a lysosomal membrane permeabilization-dependent mechanism. *PLoS One* 2012, *7*, e44524.

[20] Rimando, A. M., Nagmani, R., Feller, D. R., Yokoyama, W., Pterostilbene, a new agonist for the peroxisome proliferator-activated receptor alpha-isoform, lowers plasma lipoproteins and cholesterol in hypercholesterolemic hamsters. *J. Agric. Food Chem.* 2005, *53*, 3403–3407.

[21] Manickam, M., Ramanathan, M., Jahromi, M. A., Chansouria, J. P. et al., Antihyperglycemic activity of phenolics from *Pterocarpus marsupium*. *J. Nat. Prod.* 1997, *60*, 609–610.

[22] Pari, L., Satheesh, M. A., Effect of pterostilbene on hepatic key enzymes of glucose metabolism in streptozotocin- and nicotinamide-induced diabetic rats. *Life Sci.* 2006, *79*, 641-645.

[23] Joseph, J. A., Fisher, D. R., Cheng, V., Rimando, A. M. et al., Cellular and behavioral effects of stilbene resveratrol analogues: implications for reducing the deleterious effects of aging. *J. Agric. Food Chem.* 2008, *56*, 10544-10551.

[24] Cherniack, E. P., A berry thought-provoking idea: the potential role of plant polyphenols in the treatment of age-related cognitive disorders. *Br. J. Nutr.* 2012, *108*, 794–800.

[25] Ramkumar, K. M., Sekar, T. V., Foygel, K., Elango, B. et al., Reporter protein complementation imaging assay to screen and study Nrf2 activators in cells and living animals. *Anal. Chem.* 2013, *85*, 7542–7549.

[26] Kundu, J. K., Surh, Y. J., Nrf2-Keap1 signaling as a potential target for chemoprevention of inflammation-associated carcinogenesis. *Pharm. Res.* 2010, *27*, 999–1013.

[27] Copple, I. M., The Keap1-Nrf2 cell defense pathway—a promising therapeutic target? *Adv. Pharmacol.* 2012, *63*, 43–79.

[28] Chiou, Y. S., Tsai, M. L., Wang, Y. J., Cheng, A. C. et al., Pterostilbene inhibits colorectal aberrant crypt foci (ACF) and colon carcinogenesis via suppression of multiple signal transduction pathways in azoxymethane-treated mice. *J. Agric. Food Chem.* 2010, *58*, 8833–8841.

[29] Mikstacka, R., Przybylska, D., Rimando, A. M., Baer-Dubowska, W., Inhibition of human recombinant cytochromes P450 CYP1A1 and CYP1B1 by trans-resveratrol methyl ethers. *Mol. Nutr. Food. Res.* 2007, *51*, 517–524.

[30] Kapetanovic, I. M.,Muzzio, M., Huang, Z., Thompson, T. N. et al., Pharmacokinetics, oral bioavailability, and metabolic profile of resveratrol and its dimethylether analog, pterostilbene, in rats. *Cancer Chemother. Pharmacol.* 2011, *68*, 593–601.

[31] Walle, T., Methylation of dietary flavones greatly improves their hepatic metabolic stability and intestinal absorption. *Mol. Pharm.* 2007, *4*, 826–832.

[32] Lin, H. S., Yue, B. D., Ho, P. C., Determination of pterostilbene in rat plasma by a simple HPLC-UV method and its application in pre-clinical pharmacokinetic study. *Biomed. Chromatogr.* 2009, *23*, 1308–1315.

[33] Yeo, S. C., Ho, P. C., Lin, H. S., Pharmacokinetics of pterostilbene in Sprague–Dawley rats: the impacts of aqueous solubility, fasting, dose escalation, and dosing route on bioavailability. *Mol. Nutr. Food Res.* 2013, *57*, 1015–1025.

[34] Remsberg, C. M., Yanez, J. A., Ohgami, Y., Vega-Villa, K. R. et al., Pharmacometrics of pterostilbene: preclinical pharmacokinetics and metabolism, anticancer, antiinflammatory, antioxidant and analgesic activity. *Phytother. Res.* 2008, *22*, 169–179.

[35] Neto, C. C., Cranberry and blueberry: evidence for protective effects against cancer and vascular diseases. *Mol. Nutr. Food Res.* 2007, *51*, 652–664.

[36] Riche, D. M., Deschamp, D., Griswold, M. E., McEwen, C. L. et al., Impact of pterostilbene on blood pressure and other metabolic parameters in adults. *Hypertension* 2012, *60*, A617.

[37] Riche, D. M., McEwen, C. L., Riche, K. D., Sherman, J. J. et al., Analysis of safety from a human clinical trial with pterostilbene. *J. Toxicol.* 2013, *2013*, 463595.

[38] Ruiz, M. J., Fernandez, M., Pico, Y., Manes, J. et al., Dietary administration of high doses of pterostilbene and quercetin to mice is not toxic. *J. Agric. Food Chem.* 2009, *57*, 3180–3186.

[39] Gottumukkala, V. S., Hindupur, R. M., Masna, M., Novel stilbene analogs. Patent WO 2010/046926 A2. 2010.

[40] Iwuchukwu, O. F., Sharan, S., Canney, D. J., Nagar, S., Analytical method development for synthesized conjugated metabolites of trans-resveratrol, and application to pharmacokinetic studies. *J. Pharm. Biomed. Anal.* 2012, *63*, 1–8.

[41] Hoshino, J., Park, E. J., Kondratyuk, T. P., Marler, L. et al., Selective synthesis and biological evaluation of sulfate-conjugated resveratrol metabolites. *J. Med. Chem.* 2010, *53*, 5033–5043.

[42] Biasutto, L., Marotta, E., Garbisa, S., Zoratti, M. et al., Determination of quercetin and resveratrol in whole blood—implications for bioavailability studies. *Molecules* 2010, *15*, 6570–6579.

[43] Zhang, Y., Huo, M., Zhou, J., Xie, S., PKSolver: an add-in program for pharmacokinetic and pharmacodynamic data analysis in Microsoft Excel. *Comput. Methods Programs Biomed.* 2010, *99*, 306–314.

© 2014 WILEY-VCH Verlag GmbH & Co. KGaA, Weinheim

[44] Juan, M. E., Maijo, M., Planas, J. M., Quantification of trans-resveratrol and its metabolites in rat plasma and tissues by HPLC. *J. Pharm. Biomed. Anal.* 2010, *51*, 391–398.

[45] de Boer, V. C., Dihal, A. A., van der Woude, H., Arts, I. C. et al., Tissue distribution of quercetin in rats and pigs. *J. Nutr.* 2005, *135*, 1718–1725.

[46] Shao, X., Chen, X., Badmaev, V., Ho, C. T. et al., Structural identification of mouse urinary metabolites of pterostilbene using liquid chromatography/tandem mass spectrometry. *Rapid Commun. Mass. Spectrom.* 2010, *24*, 1770–1778.

[47] Dellinger, R. W., Garcia, A. M., Meyskens, F. L., Jr., Differences in the glucuronidation of resveratrol and pterostilbene: altered enzyme specificity and potential gender differences. *Drug Metab. Pharmacokinet.* 2014, *29*, 112–119.

[48] Bresciani, L., Calani, L., Bocchi, L., Delucchi, F. et al., Bioaccumulation of resveratrol metabolites in myocardial tissue is dose-time dependent and related to cardiac hemodynamics in diabetic rats. *Nutr. Metab. Cardiovasc. Dis.* 2014, *24*, 408–415.

[49] Menet, M. C., Marchal, J., Dal-Pan, A., Taghi, M. et al., Resveratrol metabolism in a non-human primate, the grey mouse lemur (*Microcebus murinus*), using ultra-high-performance liquid chromatography-quadrupole time of flight. *PLoS One* 2014, *9*, e91932.

[50] Hashimoto, H., Tokunaka, S., Sasaki, M., Nishihara, M. et al., Dimethylsulfoxide enhances the absorption of chemotherapeutic drug instilled into the bladder. *Urol. Res.* 1992, *20*, 233–236.

[51] Zhou, Y., Li, W., Chen, L., Ma, S. et al., Enhancement of intestinal absorption of akebia saponin D by borneol and probenecid in situ and in vitro. *Environ. Toxicol. Pharmacol.* 2010, *29*, 229–234.

[52] Calamini, B., Ratia, K., Malkowski, M. G., Cuendet, M. et al., Pleiotropic mechanisms facilitated by resveratrol and its metabolites. *Biochem. J.* 2010, *429*, 273–282.

[53] Menendez, C., Duenas, M., Galindo, P., Gonzalez-Manzano, S. et al., Vascular deconjugation of quercetin glucuronide: the flavonoid paradox revealed? *Mol. Nutr. Food Res.* 2011, *55*, 1780–1790.

[54] Terao, J., Murota, K., Kawai, Y., Conjugated quercetin glucuronides as bioactive metabolites and precursors of aglycone in vivo. *Food Funct.* 2011, *2*, 11–17.

[55] Abd El-Mohsen, M., Bayele, H., Kuhnle, G., Gibson, G. et al., Distribution of [3H]trans-resveratrol in rat tissues following oral administration. *Br. J. Nutr.* 2006, *96*, 62–70.

[56] Patel, K. R., Andreadi, C., Britton, R. G., Horner-Glister, E. et al., Sulfate metabolites provide an intracellular pool for resveratrol generation and induce autophagy with senescence. *Sci. Transl. Med.* 2013, *5*, 205ra133.

[57] Asensi, M., Medina, I., Ortega, A., Carretero, J. et al., Inhibition of cancer growth by resveratrol is related to its low bioavailability. *Free Radic. Biol. Med.* 2002, *33*, 387–398.

[58] Liang, L., Liu, X., Wang, Q., Cheng, S. et al., Pharmacokinetics, tissue distribution and excretion study of resveratrol and its prodrug 3,5,4′-tri-O-acetylresveratrol in rats. *Phytomedicine* 2013, *20*, 558–563.

[59] Marier, J. F., Vachon, P., Gritsas, A., Zhang, J. et al., Metabolism and disposition of resveratrol in rats: extent of absorption, glucuronidation, and enterohepatic recirculation evidenced by a linked-rat model. *J. Pharmacol. Exp. Ther.* 2002, *302*, 369–373.

[60] Colom, H., Alfaras, I., Maijo, M., Juan, M. E. et al., Population pharmacokinetic modeling of trans-resveratrol and its glucuronide and sulfate conjugates after oral and intravenous administration in rats. *Pharm. Res.* 2011, *28*, 1606–1621.

[61] Das, S., Lin, H. S., Ho, P. C., Ng, K. Y., The impact of aqueous solubility and dose on the pharmacokinetic profiles of resveratrol. *Pharm. Res.* 2008, *25*, 2593–2600.

© 2014 WILEY-VCH Verlag GmbH & Co. KGaA, Weinheim

Supporting Information

Synthesis of pterostilbene-4'-sulfate (Pt-S)

Chlorosulfonic acid (0.128 g, 1.10 mmol, 5.0 eq.) in acetonitrile (0.5 mL) was added dropwise to a vigorously stirred solution of pterostilbene (Pt, 0.056 g, 0.22 mmol, 1.0 eq.) and pyridine (0.5 mL) in acetonitrile (2.0 mL) in a 50 mL conical centrifugation tube (Falcon^{TM} type) at -20 °C. The reaction mixture was allowed to warm to room temperature. After 16 h the resulting reaction mixture was concentrated to about 1.5 mL under a weak nitrogen stream and solutes were precipitated with diethyl ether (40 mL). The slurry was then centrifuged (2200 rpm, 5 minutes) and the solvent decanted. The residue (a pale yellow gel) was dissolved in the minimum amount of acetonitrile and precipitation was repeated. The resulting solid was dissolved in 2 mL of water/methanol 1:1 and applied to a column (1.5 cm × 15.0 cm) of cation-exchange resin (Dowex 50WX8, K^+ form, 10 g) and eluted with water. Fractions containing the desired product (identified by UV-detection on TLC) were combined and purified by reverse phase preparative HPLC using an ACE 5 AQ (150 mm × 21.2 mm) column and a flow rate of 17 mL/min (eluents: ACN and H_2O; from 10 to 60% ACN in 20 minutes; detection at 300 nm). Fractions containing the desired product were lyophilized to afford Pt-S as a bright white solid (0.062 g, 75%).

Purity (HPLC/UV) ≥ 99%.

^{1}H NMR (500 MHz, DMSO) δ 7.50 (d, *J* = 8.6 Hz, 2H), 7.23 (d, *J* = 16.4 Hz, 1H), 7.18 (d, *J* = 8.6 Hz, 2H), 7.06 (d, *J* = 16.4 Hz, 1H), 6.76 (d, *J* = 2.0 Hz, 2H), 6.39 (t, *J* = 2.0 Hz, 1H), 3.78 (s, 6H). ^{13}C NMR (126 MHz, DMSO) δ 161.11, 153.79, 139.79, 132.23, 129.04, 127.50, 127.47, 120.97, 104.70, 100.19, 55.65.

HRMS (ESI-): *m/z* 335.0589 $[M-H]^-$, calcd for $C_{16}H_{15}O_6S$:.335.0595.

Quantification of analytes in blood and tissue samples

The concentration of Pt or Pt-S in the original sample [A] was determined as follows:

$$[\mathbf{A}] = \frac{[A]_m}{[IS]_m} \times [IS]_{spike} \times \frac{\text{Recovery IS}}{\text{Recovery A}} =$$

$$= \frac{\text{Area}_{A,m}}{\alpha_A} \times \frac{\alpha_{IS}}{\text{Area}_{IS,m}} \times \frac{\text{Area}_{IS,spike}}{\alpha_{IS}} \times \frac{1}{R_{A/IS}} =$$

$$= \frac{\text{Area}_{A,m}}{\alpha_A} \times \frac{\text{Area}_{IS,spike}}{\text{Area}_{IS,m}} \times \frac{1}{R_{A/IS}}$$

Where:

- $[A]_m$ and $[IS]_m$ are the concentrations of analyte (A) or internal standard (IS), respectively, measured in the final/treated sample;
- $[IS]_{spike}$ is the known concentration of IS in a solution of H_2O:ACN, 1:1 spiked with the same amount of IS as in the sample before treatment;
- $\text{Area}_{A,m}$ and $\text{Area}_{IS,m}$ are the HPLC peak area of the analyte or internal standard, respectively, measured in the final/treated sample;
- $\text{Area}_{IS,spike}$ is the HPLC peak area of IS, measured in the spiked H_2O:ACN solution;
- α_A and α_{IS} are the slopes of the calibration curves for A or IS, respectively, which correlates HPLC peak area with concentrations;
- $R_{A/IS}$ is the ratio of recovery yields of A and IS, previously determined from samples spiked with known amounts of both A and IS (see below and Table 1).

We can arguably assume that 1 g of tissue corresponds to 1 mL volume, and thus the concentration of analyte per gram of tissue lysate (nmol/g) can be approximated to concentration in μM units (i.e., nomol/mL).

Recovery yields

To establish the recovery yields of Pt and Pt-S from blood and organs, the protocols for the treatment of blood or tissues were applied to samples spiked with a known amount of Pt or Pt-S.

Recoveries of Pt, Pt-S and internal standard were determined as follows:

$$\mathbf{R_{A/IS}} = \frac{\text{Recovery A}}{\text{Recovery IS}} =$$

$$= \frac{[A]_m}{[A]_{spike}} \times \frac{\text{Final volume}}{\text{Initial volume}} \Big/ \frac{[IS]_m}{[IS]_{spike}} \times \frac{\text{Final volume}}{\text{Initial volume}} =$$

$$= \frac{\text{Area}_{A,m}}{\alpha_A} \times \frac{\alpha_A}{\text{Area}_{A,spike}} \Big/ \frac{\text{Area}_{IS,m}}{\alpha_{IS}} \times \frac{\alpha_{IS}}{\text{Area}_{IS,spike}} =$$

$$= \frac{\text{Area}_{A,m}}{\text{Area}_{A,spike}} \times \frac{\text{Area}_{IS,spike}}{\text{Area}_{IS,m}}$$

Where:

- $[A]_{spike}$ is the known concentration of the analyte (A) in a solution of H_2O:ACN, 1:1 spiked with the same amount of A as in the sample before treatment;
- $\text{Area}_{A,spike}$ is HPLC peak area of A, measured in the spiked H_2O:ACN solution.

All the other abbreviations are the same as described for analyte quantification in blood and tissue samples (see above).

Supporting Information Table 1. Comparison of pharmacokinetic data for resveratrol (Resv) and pterostilbene (Pt).

					Tissue levels (nmol/g)[a]					
Compound, dose and route of administration	**Ref.**	**Analyte**	**Time**	*Notes*	**Brain**	**Lungs**	**Liver**	**Kidneys**	**Testes**	**Heart**
Resv 88 µmol/kg, oral	[57]	Resv	5-10 min	t_{max}	0.11 ± 0.05	0.81 ± 0.24	0.45 ± 0.11	0.06 ± 0.02	-	-
Resv 220 µmol/kg, oral	[55]	Resv	2 h	Sampling time; no kinetics	< 1	< 1	0	0	-	0
		Resv-metabolites (mainly glucuronide)	2 h		< 1	< 1	1 ± 0.3	4 ± 0.7	-	< 1
Resv 66 µmol/kg, i.v.	[44]	Resv	1,5 h	Sampling time; no kinetics	0.17 ± 0.04	1.13 ± 0.34	0.38 ± 0.05	1.45 ± 0.35	0.05 ± 0.01	-
		Resv-glucuronide	1,5 h		0	0.28 ± 0.02	0.58 ± 0.09	2.91 ± 0.19	0.70 ± 0.03	-
		Resv-sulfate	1,5 h		0.04 ± 0.1	0.42 ± 0.10	0.11 ± 0.02	0	0.23 ± 0.01	-
Resv 438 µmol/kg, oral	[58]	Resv	15 min	t_{max}	0.13 ± 0.02	1.66 ± 0.71	3.14 ± 0.81	2.53 ± 0.55	-	2.25 ± 0.40
Pt 88 µmol/kg, oral	*This work*	Pt	2 h	t_{max}	10.5 ± 7.0	6.8 ± 4.4	39.7 ± 14.2	18.5 ± 12.2	4.2 ± 3.0	6.1 ± 4.2
		Pt-S	2 h	t_{max}	2.7 ± 1.4	34.7 ± 24.8	207.6 ± 119.8	88.3 ± 52.2	6.4 ± 3.7	18.5 ± 12.4

a) some data were deduced from published graphs.

Chapter 4

New natural amino acid-bearing prodrugs boost pterostilbene's oral pharmacokinetic and distribution profile

(submitted European Journal of Pharmaceutics and Biopharmaceutics)

Michele Azzolini[1,2,#], Andrea Mattarei[3,#], Martina La Spina[1], Michele Fanin[3], Giacomo Chiodarelli[3], Matteo Romio[3], Mario Zoratti[1,2], Cristina Paradisi[3], Lucia Biasutto[1,2,*]

[1] University of Padova, Department of Biomedical Sciences, Viale G. Colombo 3, 35121 Padova, Italy

[2] CNR Neuroscience Institute, Viale G. Colombo 3, 35121 Padova, Italy

[3] University of Padova, Department of Chemical Sciences, Via F. Marzolo 1, 35131 Padova, Italy

[#] These Authors contributed equally to this work and share first authorship

*Corresponding Author:
CNR Neuroscience Institute
c/o Dept. Biomedical Sciences
Viale G. Colombo 3
35121 Padova
Tel.: ++39 0498276483; FAX; ++39 0498276040;
e-mail: lucia.biasutto@cnr.it

Abstract

The biomedical effects of the natural phenol pterostilbene are of great interest but its bioavailability is negatively affected by the phenolic group in position 4' which is an ideal target for the conjugative enzymes of phase II metabolism. We report the synthesis and characterization of prodrugs in which the hydroxyl moiety is reversibly protected as a carbamate ester linked to the N-terminus of a natural amino acid. Prodrugs comprising amino acids with hydrophobic side chains were readily absorbed after intragastric administration to rats. The Area Under the Curve for pterostilbene in blood was optimal when prodrugs with isoleucine or β-alanine were used. The prodrug incorporating isoleucine was used for further studies to map distribution into major organs. When compared to pterostilbene itself, administration of the isoleucine prodrug afforded increased absorption, reduced metabolism and higher concentrations of pterostilbene, sustained for several hours, in most of the organs examined. Experiments using Caco-2 cells as an in vitro model for human intestinal absorption suggest that the prodrug could have promising absorption profiles also in humans; its uptake is partly due to passive diffusion, and partly mediated by H^+-dependent transporters expressed on the apical membrane of enterocytes, such as PepT1 and OATP.

Introduction

Resveratrol (3,4',5-trihydroxystilbene), a natural polyphenol, has enormous biomedical potential. In addition to the many reports of positive effects on major syndromes such as cancer and metabolic disease (for recent reviews see [1, 2]), benefits have also been observed or suggested against such conditions as, e.g., acne [3, 4], caries [5], H. pylori-induced pathologies [6, 7], osteoporosis [8, 9], allergy [10], macular degeneration of the retina [11, 12], fatigue [13]. The mechanisms of resveratrol action [14-17] include SIRT1 [18] and AMPK activation and downregulation of mTOR and NF-kB, significantly overlapping those proposed for berberine [19, 20] and aspirin (salicylate) [21-25].

While most attention has been focused on resveratrol, other natural stilbenoids may actually possess analogous or even more marked bioactivities. Piceatannol (3,3',4',5-tetrahydroxy-t-stilbene), a plant-made compound as well as an animal metabolite of resveratrol, is believed to have anti-inflammatory, anti-diabetes, immune system-modulating and anti-cancer properties and marked favorable effects on the cardiovascular system (revs.: [26, 27]). Pinosylvin (3,5-dihydroxystilbene) also antagonizes inflammation

and oxidative stress [28-30] and exhibits anti-metastatic and anti-proliferative action [31, 32]. Pterostilbene (3,5-dimethoxy-4'-hydroxystilbene) (revs.: [33-35]) may be the most investigated resveratrol analogue. It shows remarkable antineoplastic activity [36-40], it is anti-inflammatory [41, 42], neuroprotective [43, 44], and it ameliorates the symptoms of metabolic syndrome [45]. Among the mechanisms underlying these effects is the ability of pterostilbene to inhibit the inducible forms of P450 enzymes responsible for the hydroxylation of polycyclic aromatic hydrocarbons [46] – which generates carcinogenic metabolites - as well as cyclooxygenases (especially COX-1) [47] and thus prostaglandin synthesis. Pterostilbene was also reported to induce autophagy [38, 48], activate the Nrf2 pathway [49-51], activate eNOS [52] and upregulate PPARα [53]. Its higher lipophilicity may be a key factor in allowing it to reach higher brain levels than resveratrol [54]. In turn, these higher levels may explain the efficacy of pterostilbene in ameliorating the symptoms of cognitive aging [55] and anxiety [56].

The efficacy of resveratrol and its analogues is however limited by the conjugative metabolism they undergo during absorption from the intestine and in the liver (e.g., for resveratrol: [57-61]; for pterostilbene: [62]). We are exploring one of the possible strategies to overcome this obstacle, namely the development of prodrugs in which the principal sites of metabolic conjugation - the phenolic functions - are reversibly protected by a structure comprising a suitably reactive bond system, which upon lysis will regenerate the free hydroxyl group, and moieties imparting desirable properties to the construct [63-65]. A promising bond system is the carbamate ester, already utilized in various precursors of phenolic drugs [66-70]. We have synthesized and tested resveratrol carbamate prodrugs in which the N-atom of the carbamate moiety carries a methyl and an hydrophilic group, namely butyl-glucosyl or PEG-350 [65]. The rates at which these constructs hydrolyze to regenerate the free hydroxyl group are however too low for them to be of practical use as prodrugs. N-monosubstituted carbamate esters are expected to hydrolyze more rapidly in physiological conditions [71]. We thus moved to this type of linkage [72] and tested resveratrol derivatives bearing at each hydroxyl hydrophilic groups such as methoxy-oligo(ethylene glycol)s [73], galactosyl or glyceryl [74]. These constructs proved to regenerate the parent compound with suitable kinetics, but their hydrophilicity limited absorption by diffusion through the intestinal wall. No evidence was found for an active transport mediated by intestinal sugar transporters [74]. In a quest for assistance by membrane carriers we turned to amino acid and peptide transport systems, and to natural amino acids as promoieties [75].

Amino acid transporters constitute a vast subdivision of the superfamily of membrane transporters [76-78]. It includes heterodimeric amino acid transporters (HATs) and proton amino acid co-transporters (PATs), whose representatives in rat intestine include LAT1/2 (L-type amino acid transporter 1/2) [79] and PAT1/2 [80]. Both have relatively broad specificity, and have been exploited for the transport/absorption of prodrugs, with LAT1/2 being especially useful for permeation of the blood brain barrier.

We reasoned that help may be also (or alternatively) provided by relatively low-specificity peptide permeases of the intestinal wall, which have been classified into a few families [81, 82]. Possibly the most relevant system may be the 4-member proton-coupled oligopeptide transporter family (SLC15A1-4) (revs.: [81-89]), predominantly expressed in the small intestine and kidneys, which mediates the uptake of di/tripeptides –normally derived from the hydrolysis of proteins – and of a variety of non-peptides. Some poorly absorbed drugs have been modified into peptidomimetic prodrugs targeting these transporters, in particular PepT1 (SLC15A1), to improve oral bioavailability (e.g.: [90-93]; revs: [94, 95]).

Despite the low specificity of the system (a desirable characteristic for our purposes), modeling studies have identified some features conferring to substrates of PepT1 a high affinity for the transporter [88, 96, 97]. As may have been expected, for dipeptides these include a free N-terminus α-amino group in the L configuration, a peptide bond and an acidic C-terminal group (i.e. a carboxy group). A hydrophobic side chain is desirable. We thus planned a prodrug in which these features could be presented to the transporter, at the same time maintaining the carbamate linkage to the pterostilbene kernel and insuring the safety of hydrolysis products.

Organic Anion Transporting Polypeptides (OATPs; SLCOs) [81, 98, 99] are a third transport system that might be exploited by amino acidic carbamoyl prodrugs for intestinal absorption. OATP-1A2 (SLCO1A2) and OATP-2B1 (SLCO2B1) are the OATP family members expressed in the apical membrane of enterocytes in human small intestine (orthologs are present in rats [100]); their substrates include bile acids, steroid conjugates, thyroid hormones, anionic peptides and drugs such as pravastatin or fexofenadine.

Amino acid derivatives of resveratrol had limited success: absorption of the prodrugs was unsatisfactory, possibly because of their hydrophilicity and of their extended structure [75]. Prodrugs carrying only one protective group of this sort would obviously be less ramified and bulky than the corresponding resveratrol trisubstituted derivatives, and may be expected to be handled more easily by membrane carriers. We thus tested the same approach with pterostilbene. Pterostilbene differs from resveratrol only for the presence of

two methoxy groups, rather than two hydroxyls, in positions 3 and 5 of the A ring (Figure 1). The hydroxyl group was connected via a carbamoyl linkage with the α-amino group of several different amino acids thus obtaining a small library of pterostilbene prodrugs. The prodrugs have been characterized with regard to their stability in solution at physiologically relevant pH values and in rat blood, and to their blood pharmacokinetic profile. The Pt derivative incorporating isoleucine was then used for further pharmacokinetic analysis, and the distribution in several organs of prodrug, Pt and Pt-sulfate was studied as a function of time after its intragastric administration. The results show the effectiveness of the combined presence of the carbamoyl functionality and of amino acid promoieties in boosting pterostilbene bioavailability. Experiments with the human intestinal cell line Caco-2 suggest the involvement of both peptide and organic anion (but not amino acid) transporters – in addition to passive transmembrane diffusion - in the uptake of these prodrugs.

Results and Discussion

The new prodrugs developed in this work are shown in Figure 1. Their synthesis, hydrolysis and blood pharmacokinetics are described next, followed by distribution studies in the rat. To understand how these prodrugs are absorbed, and to address possible species differences, the final section describes an investigation into the mechanisms of membrane permeation by the prodrug using a human *in vitro* model for intestinal absorption.

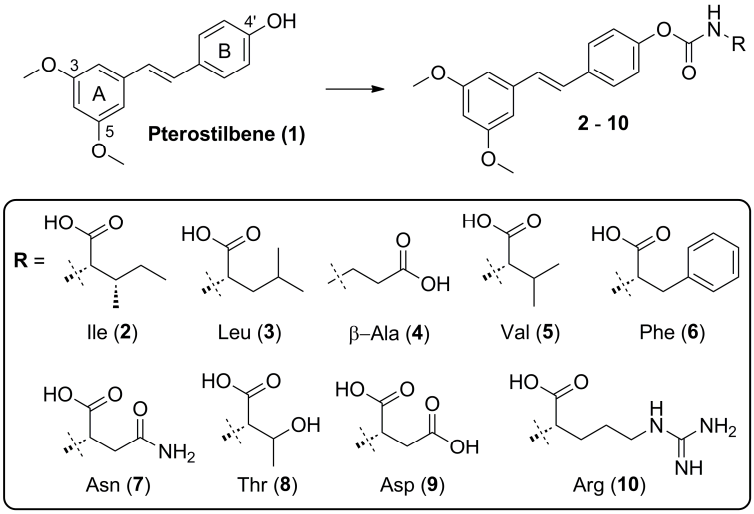


Fig.1: Pterostilbene (1) and N-monosubstituted carbamate amino acidic pterostilbene prodrugs (2 – 10).

Synthesis. The synthesis of compounds **2** – **10** (Fig. 1) was carried out by a two-step procedure as shown in Figure 2. In the first step the N-terminus amino group of a *tert*-butyl protected amino acid was activated by reaction with bis(4-nitrophenyl) carbonate (bis-PNPC). The activated 4-nitrophenyl urethane was then allowed to react in a one-pot procedure with pterostilbene (**1**) to obtain the *tert*-butyl protected N-monosubstituted amino acidic pterostilbene conjugate (**11** – **19**) (see Supplementary Experimental Procedures online). In the second step of the synthesis cleavage of the *tert*-butyl ester-protecting group on the amino acid moiety led to the desired product in good yield (**2** – **10**).

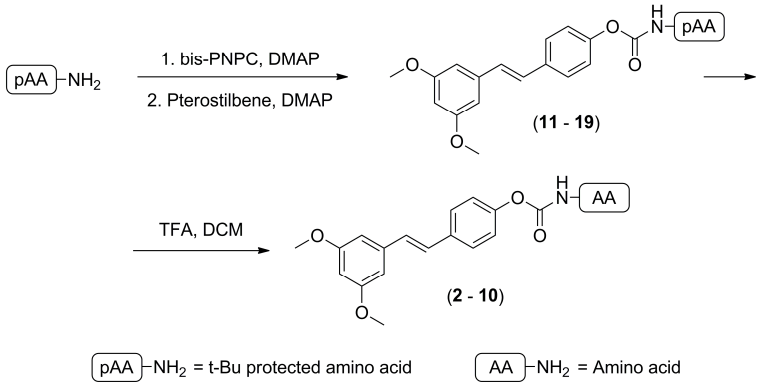


Fig.2: Synthesis of N-monosubstituted carbamate amino acidic pterostilbene prodrugs (2 – 10).

Hydrolysis studies. Besides being readily absorbed, prodrug candidates should also withstand the pH conditions of stomach and intestine to ensure protection of the phenolic moiety during absorption, and regenerate the parent compound with suitable kinetics after entering systemic circulation. In agreement with previous results obtained with similar derivatives [74], compounds **2** – **10** turned out to be stable in acidic media (pH = 1; 24 h, 37°C); at pH 6.8, representing the pH of the first part of the intestine, hydrolysis was rather slow and depended somewhat on the substituent group: derivatives **7** and **8** hydrolyzed more rapidly than **3**, **6** and **9** (Table 1; see also Supplementary Figure S1 online).

As expected, the higher pH of blood in comparison to that of the PBS solution used (7.4 *vs.* 6.8, respectively) and the presence of esterase activities resulted in a higher rate of hydrolysis in blood than in PBS, with an increase of the pseudo-first-order rate constants by about one order of magnitude (Table 1; see also Supplementary Figure S2 online). Derivative **4** (with β-alanine) regenerated **1** with the fastest kinetics, while derivatives **3**, **6** and **9** exhibited the lowest reaction rates. Derivative **6,** which has a phenylalanine substituent, was affected the least by higher pH and hydrolytic enzymes, probably due to steric effects.

Table 1. **Observed pseudo-first-order hydrolysis rate constants of derivatives 2 – 10 in aqueous PBS 0.1 M at pH 6.8 and 37°C and in rat blood.** Rate constants were determined as best fit of the experimental data using the first-order exponential equation: $[C] = [C]_0 * e^{-kt}$. Values ± standard error are reported as obtained from the fit of all the available data.

Derivative	**$10^2 \times k$ (h^{-1}) in PBS 0.1 M, pH 6.8, 37°C**	**$10^2 \times k$ (h^{-1}) in rat blood, 37°C**
2	0.547 ± 0.008	28 ± 1
3	0.465 ± 0.005	5.9 ± 0.4
4	0.70 ± 0.06	96 ± 5
5	0.65 ± 0.02	11.4 ± 0.7
6	0.50 ± 0.04	2.5 ± 0.2
7	1.14 ± 0.06	17.4 ± 0.5
8	1.320 ± 0.007	13.1 ± 0.5
9	0.34 ± 0.04	3.4 ± 0.3
10	0.99 ± 0.02	31 ± 3

Blood pharmacokinetics. *In vitro* (pH = 1 and pH = 6.8) and *ex vivo* (blood) stability profiles of derivatives **2** – **10** indicated their suitability for use as prodrugs of pterostilbene. We therefore proceeded to determine their pharmacokinetic profiles administering 88 µmoles/Kg b.w. by gavage. The results are shown in Figure 3, and are discussed by class of substituent group.

*1. Amino acids with hydrophobic side chain as promoieties (derivatives **2 – 6**).* Derivatives **2** – **6** were rapidly and extensively absorbed by the intestine after intragastric administration, reaching high concentrations in blood. As reported in Figure 3, compounds **2**, **3** and **5** showed C_{max} values around 100 µM (94 ± 49 µM, 113 ± 86 µM and 102 ± 36 µM, respectively). The C_{max}'s of compounds **4** and **6** were also high, but less so (50 ± 11 µM and 40 ± 50 µM respectively).

Compounds **2, 3** and **5** have a t_{max} in blood of 2 hours. Their level was sustained for at least 8 hours, then it dropped to almost zero after 24h. Pterostilbene (**1**) and its major metabolite, pterostilbene-4'-sulfate (**1-sulfate**), formed in all cases. The t_{max} for derivative **4**, with a ß-alanine substituent, was in the interval 0.5 - 2 hours; its levels then decreased rapidly. The high rate of hydrolysis (Table 1) and the rapid and consistent formation of **1-**

sulfate suggest that this compound is also well absorbed, but it rapidly hydrolyzes to produce **1**, which is subsequently sulfated. **6**, with phenylalanine, behaved similarly, but after reaching its peak the concentration in blood declined somewhat more slowly.

*2. Amino acids with polar uncharged side chains as promoieties (derivatives **7** and **8**).* Compared to the previously discussed compounds, the concentrations attained by these two derivatives in blood were very low. **7** reached 0.8 µM after 30 minutes, while **8** peaked at 5.7 µM after 10 minutes and then rapidly decreased. In the case of **7** no other species were detected, while **8** yielded traces of **1-sulfate** (Figure 3).

*3. Amino acids with electrically charged side chains as promoieties (derivatives **9** and **10**).* Administration of **9** and **10** led to very low concentrations of the derivatives in blood (1.4 µM after 10 minutes and 0.7 µM after 2 hours, respectively). **1** and **1-sulfate** were detected in mere traces only after administration of **9**.

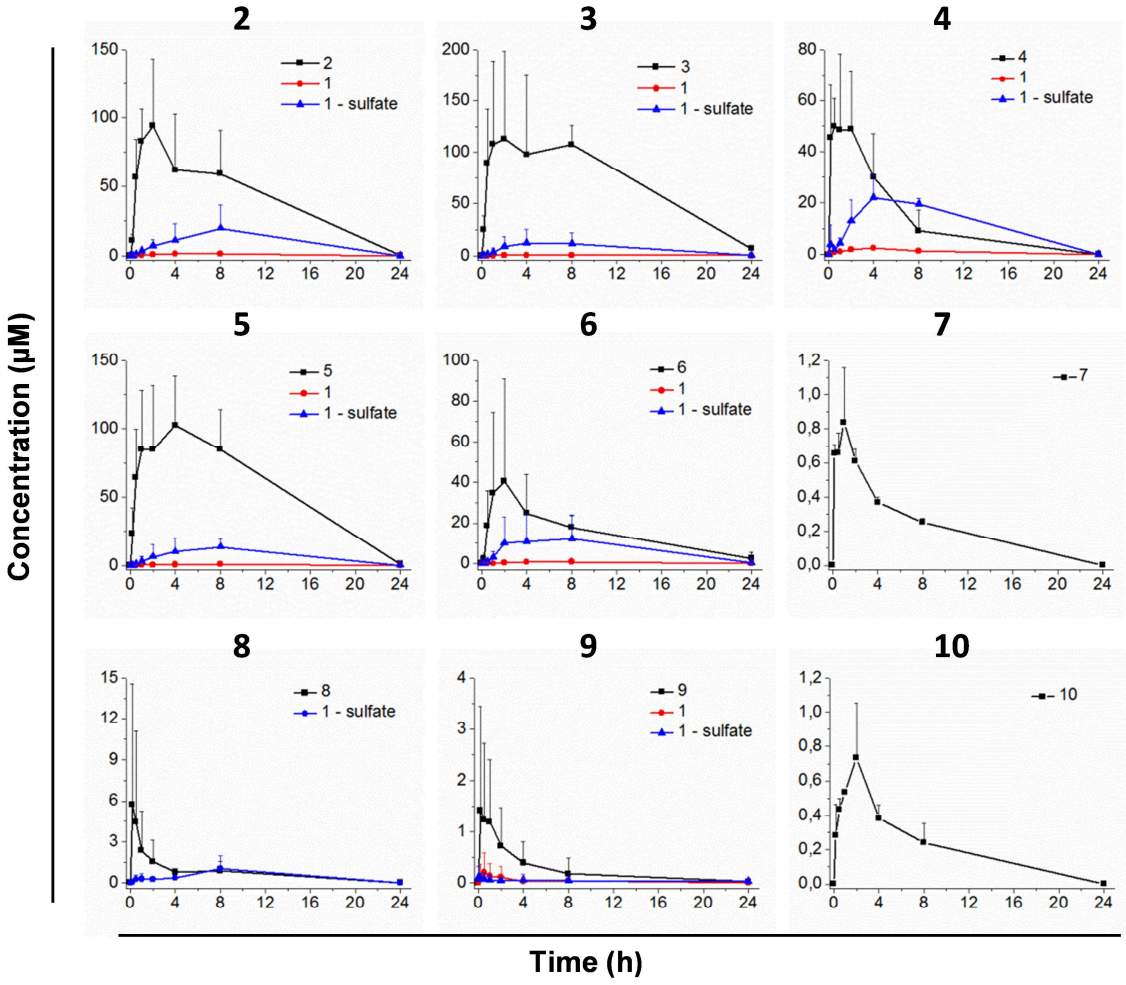


Fig.3: Blood pharmacokinetic profile after oral administration of derivatives 2 – 10. Data represent average values + standard deviation (an error bar of the same size in the negative direction is also implied but not shown for graphic clarity). N = 3 in all cases.

This analysis clearly indicates that compounds bearing amino acids with hydrophobic side chain as promoieties (**2** – **6**) give the best results. The Area Under the Curve ($AUC_{0\text{-}24h}$) parameter gives a quantitative idea of the results. The $AUC_{0\text{-}24h}$ of the total amount of pterostilbene-derived species after administration of derivatives **2** to **6** was definitely higher compared to that resulting from administration of **1** as such (Fig. 4). In contrast, derivatives **7** – **10** turned out not to be convenient prodrugs of Pt, at least if our administration protocol is used.

While the $AUC_{0\text{-}24h}$ of **1-sulfate** originating from prodrugs **2** – **6** was similar in all cases, the relative contribution of **1** and of the derivatives themselves depended strongly on the specific prodrug administered (Figure 4 A,B). Derivatives **2**, **3** and **5** afforded the highest values of overall $AUC_{0\text{-}24h}$. The highest $AUC_{0\text{-}24h}$ for **1** was produced upon administration of **2** (the isoleucine derivative) and **4** (the β-alanine derivative).

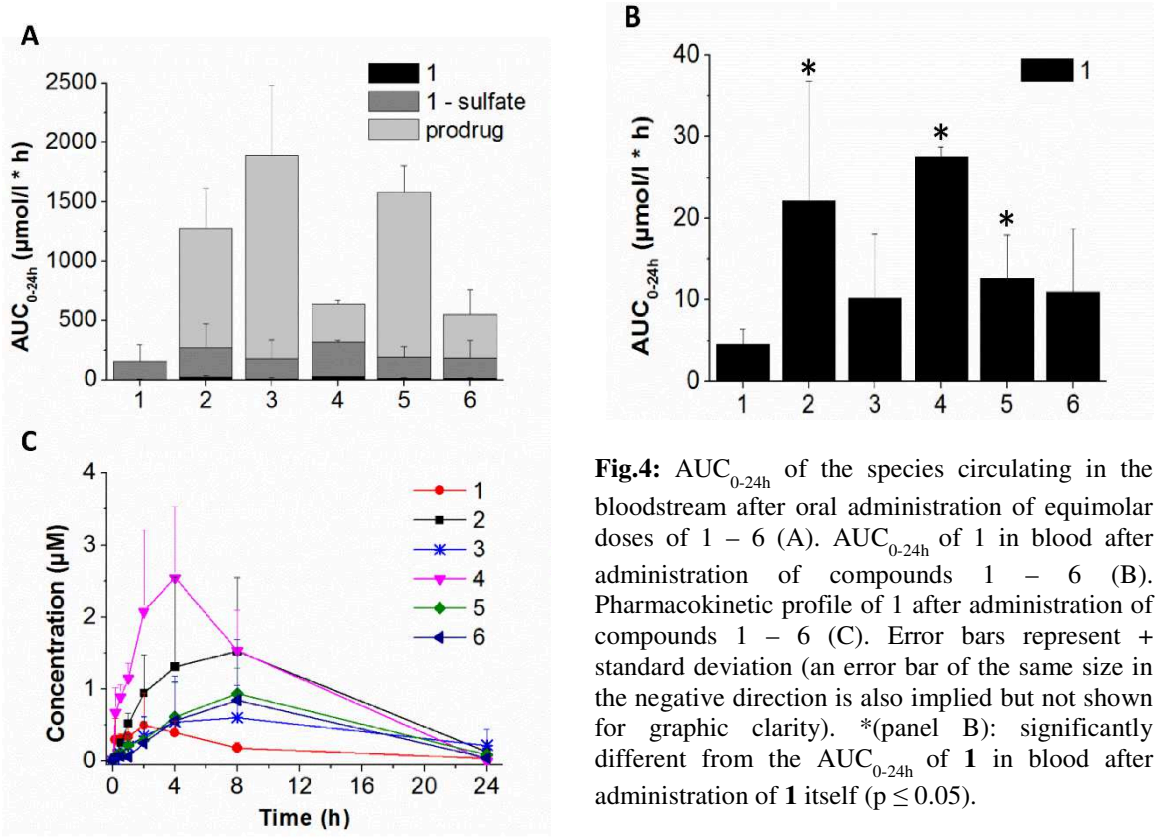


Fig.4: $AUC_{0\text{-}24h}$ of the species circulating in the bloodstream after oral administration of equimolar doses of 1 – 6 (A). $AUC_{0\text{-}24h}$ of 1 in blood after administration of compounds 1 – 6 (B). Pharmacokinetic profile of 1 after administration of compounds 1 – 6 (C). Error bars represent + standard deviation (an error bar of the same size in the negative direction is also implied but not shown for graphic clarity). *(panel B): significantly different from the $AUC_{0\text{-}24h}$ of **1** in blood after administration of **1** itself ($p \leq 0.05$).

We intend prodrugs as a tool to increase the levels of the parent compound in the body. Blood cannot be considered as fully representative of the body in terms of the levels of **1**, **1-sulfate** and of our derivatives since its aqueous character makes it much more attractive for hydrophilic compounds than for lipophilic ones [54]. We therefore carried out an analysis of the organ distribution of compound **2**, the isoleucine conjugate.

Distribution of derivative 2 into major organs. We wished to compare the distribution of **2** and the products arising from it with the results obtained by administering the parent compound, **1** [54]. The same experimental approach used in ref. [54] was therefore adopted, and the same organs analyzed. The recovery yield of **2** was satisfactory for all the organs examined (see Supplementary Table S1 online).

Blood analysis was repeated as a control for the experiment. Levels of **2**, **1** and **1-sulfate** were comparable to those observed in the blood pharmacokinetics study.

Derivative **2** was the major species observed in most of the organs examined (Fig. 5 and Fig. 6A), exceptions being the brain and skeletal muscles. **1** and **1-sulfate** concentrations varied depending on the tissue examined.

1 was the predominant species in the brain, reaching 20 nmoles/g 8 hours after the administration of the prodrug. Notably, in brain the levels of **1** remained above 10 nmoles/g approximately from 4 to 10 hours after administration. **1** was also present at appreciable levels in the other organs, with concentrations comprised between 10 and 20 nmoles/g in most cases (except blood), peaking around 8 hours after administration.

1-sulfate was present at high levels in the liver and kidneys (C_{max} approximately 60 and 25 nmoles/g, respectively) while in the brain, testes and skeletal muscle its levels were low (C_{max} approximately 0.5, 3 and 2 nmoles/g, respectively).

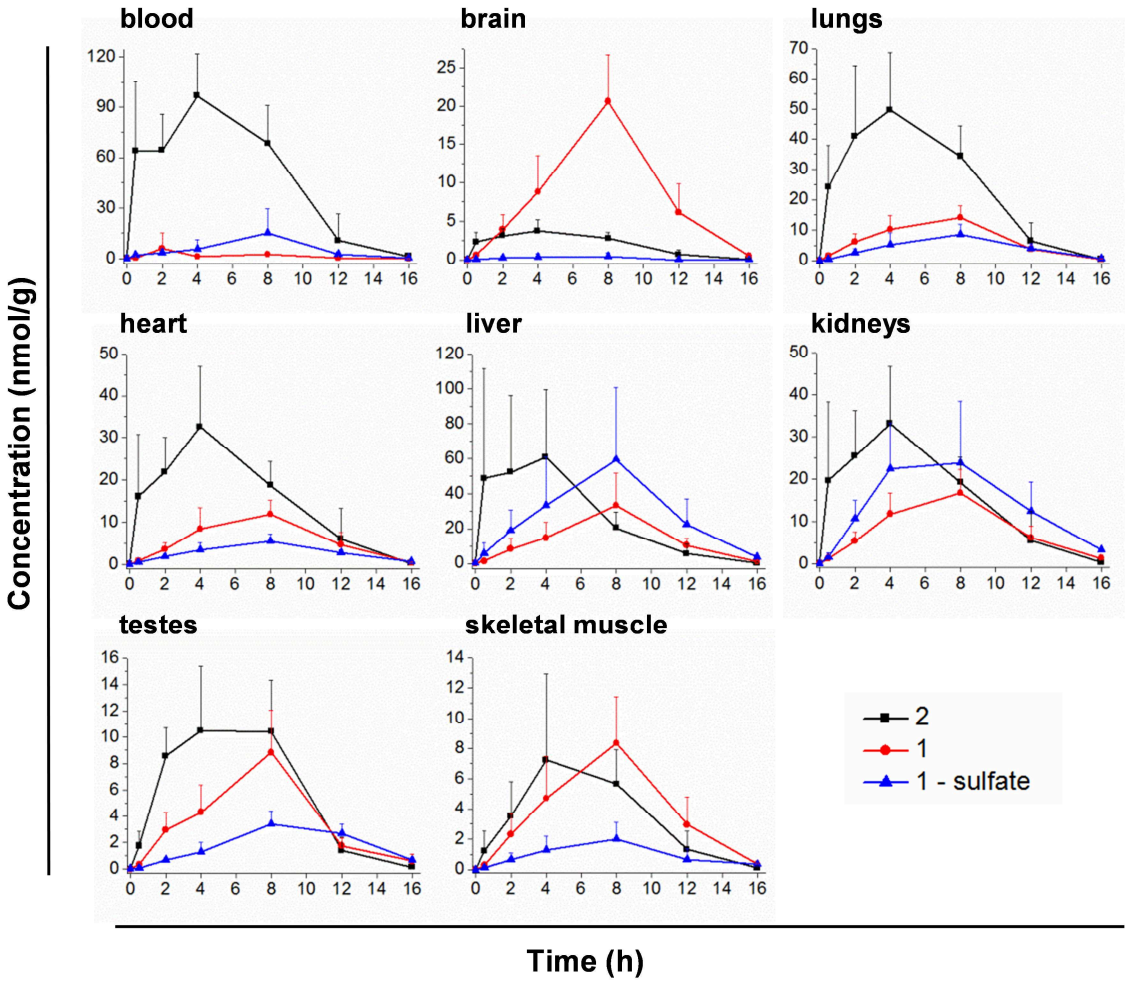


Fig.5: Concentration versus time profiles of derivative 2, 1 and 1-sulfate in blood and tissues. A single intragastric dose of **2** (88 µmoles/kg body weight) was administered to rats at time 0. Reported are mean values + standard deviation. N ≥ 3.

AUC comparison (Fig. 6B) indicates that by administering prodrug **2** we obtained a consistent increase in the $AUC_{0\text{-}16h}$ of **1** in most of the organs examined. Minor differences were found in the kidneys, lungs and blood, while the AUC doubled in the brain, heart, testes and skeletal muscle. In the liver the $AUC_{0\text{-}16h}$ of **1** was similar in the two cases.

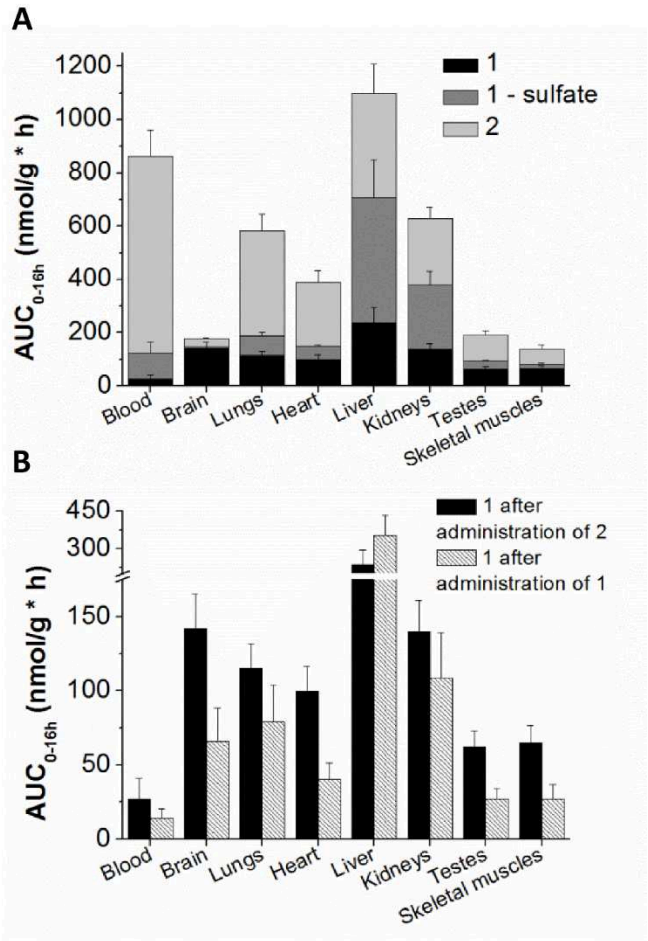


Fig.6: $AUC_{0\text{-}16h}$ of the species found in the indicated organs after oral administration of 2 (A). Comparison of the $AUC_{0\text{-}16h}$ obtained for 1 after administration of 1 (grey bars)[54] or after administration of derivative 2 (black bars) (B).

Following ingestion, compounds are absorbed by the intestine and funneled through the systemic circulation to the liver. This might explain why administration of **2** results in a lower $AUC_{0\text{-}16h}$ of **1-sulfate** in the liver: while by administering **1** all the absorbed phenol is filtered in the hepatocyte network, by administering **2** hepatic clearance concerns to a large extent the prodrug, in which the hydroxyl is still protected. **1** will reach the liver only after being generated by hydrolysis of **2**, which is distributed in the body. Presumably as a consequence of this lower production of metabolite in the liver, the $AUC_{0\text{-}16h}$ for **1-sulfate** shows in all cases a decrease when the prodrug, rather than **1**, is administered (see Supplementary Figure S3 online). The increased $AUC_{0\text{-}16h}$ of **1** in the brain seems to be due to the higher circulating levels of **1** after administration of the prodrug rather than to a good permeation of the blood brain barrier by **2**, since the levels of the latter in the brain were particularly low.

Absorption mechanisms of derivative 2. The high circulating and tissue levels obtained after administration of prodrug **2** prompted an investigation into the mechanisms involved in its absorption. The presence of a carboxylic group (which can be ionized at physiological pH) and the carbamate ester bond, in fact, render **2** more polar and hydrophilic than **1**, which is expected to permeate biological membranes by passive diffusion; the involvement of active transport systems was thus plausible.

Transepithelial transport and cellular uptake of derivative **2** were studied using differentiated Caco-2 cell monolayers, a well-established *in vitro* model to investigate intestinal absorption of drugs [101-103]. In particular, Caco-2 express candidate transporters that may have an impact in the absorption of **2** (i.e., PepT1 [102-104], OATP-2B1 [102-104] and LAT1/2 [79]) and, despite species differences, have orthologs expressed in rats [79, 100, 105]. Since Caco-2 is a human cell line, these experiments may also predict if the promising results obtained with rats might be of some relevance also for humans.

Permeation of **2** was pH-dependent: cell uptake and transepithelial transport increased when the pH of the compartment in which it was placed (the "loading compartment") was 6.0 instead of 7.4 (Fig. 7A,B). This behavior may be due to an increase of the undissociated (i.e. having the protonated carboxyl group) fraction of **2** at slightly acidic pH values, with the consequent facilitation of passive diffusion across membranes. However, the involvement of H^+-dependent transporter(s) in the apical side of the monolayer must also be considered, since in transport experiments the amount of **2** that crossed the monolayer was maximized when the derivative was loaded at pH 6.0 and on the apical side (Fig. 7B, blue trace); if **2** was loaded on the basolateral side using the same pH conditions (pH 6.0 in the donor chamber; pH 7.4 in the acceptor one), a lower permeation was observed (Fig. 7B, green trace).

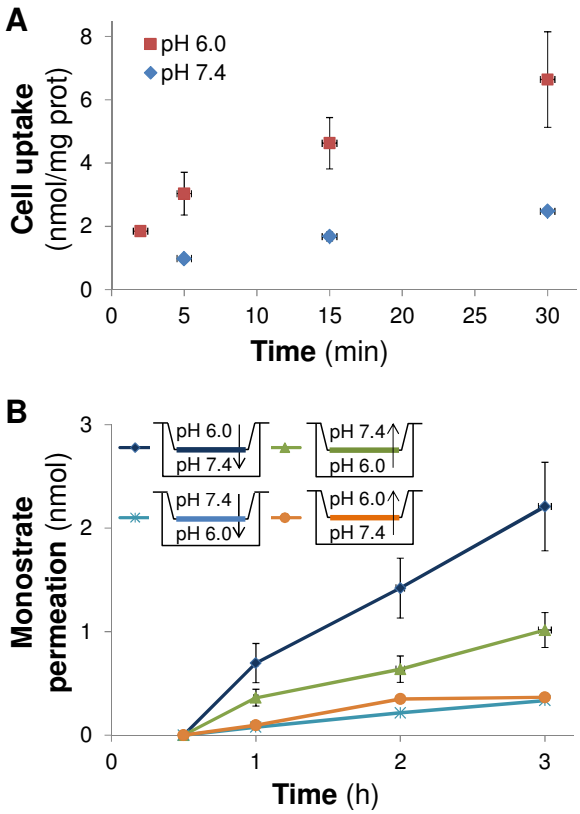


Fig.7: Uptake of 2 (10 µM) by Caco-2 cells at pH 6.0 and 7.4 (A). Transport of 2 across Caco-2 monolayers (B); the pH of apical (upper) and basolateral (lower) compartments and the direction of the transport were as indicated in the figure with reference to the experimental configuration. A 10 µM solution of 2 was placed in the compartment from which the arrow originates. Reported are mean values ± standard deviation. N ≥ 3.

The involvement of active transport systems was confirmed by experiments in the presence of well-known substrates of the candidate transporters [81, 100]: GlySar (a PepT1 substrate), Isoleucine (a substrate for LAT1 and LAT2), and Estrone-3-sulfate (E-3-S; a substrate for OATPs). The mixture of these substrates was able to competitively inhibit cellular uptake of **2**, but only if **2** was loaded on the apical side of the monolayer (see Supplementary Figure S4 online). When used individually, GlySar and E-3-S were both able to inhibit the uptake of **2**, while Isoleucine was not (Fig. 8); we can thus conclude that **2** is likely to be a substrate for PepT1 and OATP transporters (OATP-2B1 is the main isoform expressed in Caco-2 cells [102, 104, 106]).

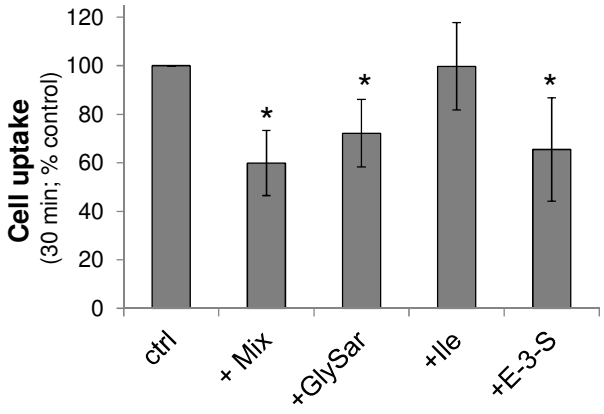


Fig.8: Effect of the substrates for PepT1, LAT and OATP on the uptake of 2 by Caco-2 cells. Cell monolayers were exposed to a 10 µM solution of 2 (in HBSS, pH 6.0) for 30 min, in the absence or in the presence of the indicated substrates. Mix: GlySar (10 mM) + Ile (1 mM) + E-3-S (2 mM). Reported are mean values ± standard deviation. N ≥ 3. *: significantly different compared to the control ($p < 0.05$).

Uptake experiments performed with HeLa cells, which are known to have very low levels of transporters such as PepT1 and OATPs [102], confirmed that both passive diffusion and transporters are involved (see Supplementary Figure S5 online).

Conclusions

Carbamoyl bond-based amino acid prodrugs of pterostilbene have been shown to be effective in increasing the natural compound bioavailability.

The stability in media mimicking gastric and intestinal pH of all the synthesized derivatives is high, ensuring protection in the gastrointestinal tract. At the same time all undergo hydrolysis in blood, at a moderate rate suitable for their use as prodrugs. From a practical point of view this means that when orally administered they can pass intact through the stomach and the intestine and, if absorbed, they can be distributed in the body through the blood and finally regenerate the natural compound in the organs. Blood pharmacokinetics in rats showed that prodrugs comprising amino acids with hydrophobic side chains (**2** - **6**) provide a marked advantage over unmodified pterostilbene, both in terms of overall absorption and of the levels of pterostilbene in blood.

The isoleucine conjugate (**2**) was selected for studies of its distribution in organs as a function of time. By administering the prodrug to rats we obtained increased absorption, consistent reduction of metabolism and higher concentrations of pterostilbene, sustained

for several hours, in most of the organs examined. The uptake of the prodrug was efficient also in an *in vitro* model of intestinal absorption (human Caco-2 cells). Both passive diffusion and transporter-mediated uptake are involved in the absorption of **2**.
Of note, the regeneration of the active molecule from these prodrugs is accompanied by the formation of innocuous/beneficial side products, namely CO_2 (i.e. bicarbonate) and a natural amino acid. We can then conclude that hydrophobic side chain amino acid N-monosubstituted carbamate ester derivatives of pterostilbene constitute a class of potentially useful prodrugs of this natural product, and possibly of other phenolic compounds.

Methods

Chemistry. *Materials and Instrumentations.* Pterostilbene was purchased from Waseta Int. Trading Co. (Shangai, P.R.China). Other starting materials and solvents were obtained from Wonda Science, Sigma Aldrich, Fluka & Riedel-de Haen, Carlo Erba Reagenti, Iris Biotech, Cambridge Isotope Laboratories Inc., Acros Organics, Prolabo, Merck-Novabiochem, J.T. Baker, and were used as received.
TLCs were run on silica gel supported on plastic (Macherey-Nagel Polygram® SIL G/UV254, silica thickness 0.2 mm) and visualized by UV detection using a Spectroline NMS-240 lamp. Purifications were performed by flash chromatography on silica gel (Macherey-Nagel 60, 230-400 mesh granulometry, 0.040-0.063 mm) under air pressure or by the automated chromatography system BÜCHI Sepacore® flash system X10. Mass spectrometry analyses were performed by Agilent Technologies MSD SL Trap equipped with an electrospray source and ion trap analyzer. A Phenomenex® Gemini 3u 110A column was used for HPLC-ESI/MS separations. NMR spectra were recorded with a Bruker AC 200F spectrometer operating at 200 MHz (for ^{1}H-NMR) and 50 MHz (for ^{13}C-NMR), or a Bruker AV300 FT-NMR UltraShield operating at 300 MHz (for ^{1}H-NMR) and 75 MHz (for ^{13}C-NMR), or a Bruker AVII500 UltraShield operating at 500 MHz (for ^{1}H-NMR) and 126 MHz (for ^{13}C-NMR).

Synthesis. Details on synthesis and characterization of the new synthesized derivatives can be found in the Supplementary Experimental Procedures online.

HPLC-UV Analysis. Samples (2 µl) were analyzed by HPLC-UV (1290 Infinity LC System, Agilent Technologies) using a reverse phase column (Zorbax RRHD Eclipse Plus C18, 1.8 µm, 50 x 2.1 mm i.d.; Agilent Technologies) and a UV diode array detector (190 - 500 nm). Solvents A and B were water containing 0.1% trifluoroacetic acid (TFA) and acetonitrile, respectively. The gradient for B was as follows: 10% (0.5 min) then from 10% to 100% in 5 min; the flow rate was 0.6 mL/min. The eluate was preferentially monitored at 286, 300 and 320 nm (corresponding to absorbance maxima of the internal standard, derivatives/metabolites and pterostilbene, respectively). The column compartment was maintained at 35°C.

Animals. Adult male Wistar rats (approximately 400 g body weight and 3 months old) from the facility of the Department of Biomedical Sciences were used for pharmacokinetic experiments. All experiments involving animals were performed after approval by the University of Padova Ethical Committee for Experimentation on Animals (CEASA) (Permit Number: 80/2011) and by the Italian Ministry of Health, and with the supervision of the Central Veterinary Service of the University of Padova, in compliance with Italian Law DL 116/92, embodying UE Directive 86/609.

Hydrolysis studies. The chemical stability of all new compounds was tested in aqueous media approximating gastric (0.1 N HCl, NormaFix) and intestinal (0.1 M PBS buffer, pH 6.8) pH values. A 5 µM solution of the compound was prepared from a 5 mM stock solution in DMSO, and incubated at 37°C for 24 hours; samples withdrawn at different times were analyzed by HPLC-UV. Non-linear curve fitting was performed using Origin 8.0 data analysis software; the hydrolysis reaction rate constants (k) of the starting compounds were calculated through interpolation of data with the equation for pseudo-first order reactions: $[C] = [C]_0 * e^{-kt}$, where: $[C\ ]$: concentration of the compound; $[C\ ]_0$: concentration of the compound at the initial time t_0; t: time.

Hydrolysis in blood. Rats were anesthetized and blood was withdrawn from the jugular vein, and transferred into heparinized tubes. Blood samples (1 mL) were spiked with compound (5 µM; dilution from a 5 mM stock solution in DMSO), and incubated at 37°C for 4 hours (the maximum period allowed by blood stability). Aliquots were taken after 10 min, 30 min, 1 h, 2 h and 4 h and treated as described below. Cleared blood samples were finally subjected to HPLC-UV analysis.

Blood Sample Treatment and Analysis. Before starting the treatment, 4,4'-dihydroxybiphenyl was added as internal standard to a carefully measured blood volume (25 µM final concentration). Blood was then stabilized with a freshly-prepared 10 mM solution of ascorbic acid (0.1 vol) and acidified with 0.6 M acetic acid (0.1 vol); after mixing, an excess of acetone (4 vol) was added, followed by sonication (2 min) and centrifugation (12,000 *g*, 7 min, 4°C). The supernatant was finally collected and stored at -20°C. Before analysis, acetone was allowed to evaporate at room temperature using a Univapo 150H (UniEquip) vacuum concentrator centrifuge, and up to 40 µL of CH_3CN were added to precipitate residual proteins. After centrifugation (12,000 *g*, 5 min, 4°C), cleared samples were directly subjected to HPLC-UV analysis.

The recovery yields of pterostilbene and its metabolite have been reported previously [54]. The recovery yields of the new prodrugs were obtained following the same protocol and are reported in Supplementary Table S1 online. Briefly, the recovery yield of each analyte was calculated as the ratio of the amount recovered to that of recovered internal standard. Knowledge of these ratios allowed us to determine the amount of analyte in a blood/organ sample after measuring the recovery of the internal standard (see [54, 107]). Since sample treatment includes an evaporation/concentration step, LOD and LOQ were determined relatively to the analytical part of the method (HPLC-UV analysis). The prodrugs have the same absorption coefficient as pterostilbene itself within experimental error: LOD and LOQ were thus the same as for pterostilbene (i.e., 0.05 and 0.15 µM, respectively), and quantification of the analytes in blood samples was done using the calibration curve determined for pterostilbene ($y = 4.96\ x$, where y is the peak area at the maximum absorption wavelength and x is the concentration in µM units), taking into account the recovery ratio [54].

Blood pharmacokinetics. Derivatives **2** – **10** were administered to overnight-fasted male rats as a single intragastric dose (88 µmol/Kg, dissolved in 250 µl DMSO). Blood samples were obtained by the tail bleeding technique: before drug administration, rats were anesthetized with isoflurane and the tip of the tail was cut off; blood samples (80-100 µL each) were then taken from the tail tip at different time points after drug administration. Blood was collected in heparinized tubes, kept in ice and treated as described above (blood sample treatment and analysis) within 10 min.

Distribution of derivative 2 into major organs. The organ distribution profile of derivative **2** was determined as described in [54]. Briefly, after a single intragastric oral administration of the derivative (same procedure as for blood pharmacokinetic determinations) animals were anesthetized with isoflurane and sacrificed (N = 3 or 4 for each time point). Blood was collected in heparinized tubes, kept in ice and treated as described above within 10 min. Brain, lungs, heart, liver, kidneys, testes and skeletal muscles (soleus, gastroctemius and anterior tibialis) were explanted, weighed and immediately frozen in liquid nitrogen. 1 g of thawed tissue was mixed with 1 mL of D-PBS (Euroclone), and homogenized with a motorized polypropylene pestel (Sigma, for brain and testes) or with an Ultra-Turrax T25 homogenizer (Janke & Kunkel, for all other tissues). 200 mg of tissue homogenate were transferred into a vial and spiked with the internal standard (4,4'-dihydroxybiphenyl, dilution from a 50× stock solution in acetonitrile, 25 nmol/g tissue final concentration). 10 µL of a freshly-prepared 10 mM solution of ascorbic acid, 10 µL of 4.35 M acetic acid, and 500 µL of acetone were added. Samples were vortexed (2 min), sonicated (2 min) and then centrifuged (12,000 g, 7 min, 4°C). An accurately measured portion of the supernatant was finally collected and stored at -20°C. Further processing and analysis was carried out as described above for blood samples.

Recovery yields of **1** and **1-sulfate** from the organs are those reported in [54]. The recovery yield of **2** from the organs was determined following the same procedure adopted for **1** and **1-sulfate**. Briefly, 1 g of tissue (from an untreated animal) was mixed with 1 mL of PBS containing 5 nmoles of **2** (dilution from a 100× stock solution in DMSO), and homogenized. 200 mg aliquots of the homogenate were then taken and processed as described above. Recoveries of **2** from the organs are listed in Supplementary Table S1 online.

AUC calculation. The Area Under the Curve (AUC) values were calculated using the trapezoidal rule. Note that different sampling time profiles were adopted for blood and organ pharmacokinetics (Fig.s 3 and 5, respectively). AUC values referring in both cases to blood but obtained with the two different protocols are therefore not comparable.

Cell culture. Caco-2 cells were routinely cultured in Dulbecco's Modified Eagle's medium (DMEM) (GIBCO) supplemented with 10% fetal bovine serum (Life Technologies) and penicillin/streptomycin (100 U/mL and 0.1 mg/mL, respectively) at

37°C in a humidified atmosphere with 5% CO_2. For uptake and transport studies, cells were seeded on 12-well plates (3.8 cm^2 growth area) or onto cell culture polyethylene terephthalate inserts (BD Falcon; pore size 0.4 µm, 4.2 cm^2 growth area), respectively, at a density of 3×10^5 cells/cm^2. The medium was replaced with fresh one every two days. Cells were grown for 9-11 or 19-22 days before uptake or transport experiments, respectively.

Uptake studies. Cells were grown for 9-11 days; they were washed twice (10 min each, 37°C) with HBSS; the medium was then replaced with 1 mL HBSS (pH 7.4 or 6.0 with 10 mM HEPES or 10 mM MES, respectively) containing 10 µM derivative **2**, alone or in the presence of 10 µM **1** and/or Pept1, LAT1 and OATP substrates (10 mM GlySar; 1 mM Isoleucine; 2 mM Estrone-3-sulfate, respectively). After the desired incubation period, the medium was collected, and cell monolayers were washed three times with PBS containing 2 µM Cyclosporin A. Cells were lysed with 40 µl of water, then they were collected, and 40 µl Acetone added; after 2 min sonication, the cell lysate was centrifuged (12000*g*, 5 min). Supernatants were collected and stored at -20°C until HPLC-UV analysis (see above). Total protein content of cell pellets (resuspended in 200 µL SDS 2%) was quantified with the BCA assay (Sigma Aldrich), using BSA as standard for calibration.

Transport studies. Both sides of the cell monolayer were washed three times with HBSS (two quick washings and the last one with 20 minutes incubation, 37°C). Bidirectional transport (apical-to-basolateral and basolateral-to-apical) of derivative **2** (and pterostilbene) was measured by sampling at different times after compound loading, using different pH conditions in the donor and receiver sides (see Results for details; HBSS was at pH 7.4 or 6.0 with 10 mM HEPES or 10 mM MES, respectively). At the end of the experiment (3h), both apical and basolateral solutions were collected; cell monolayers were washed, treated and analyzed as described for uptake studies (see above).

Statistics. Significance in comparisons was assessed using the Wilcoxon Rank Test.

References

1. Novelle, M.G., et al., *Resveratrol supplementation: Where are we now and where should we go?* Ageing Res Rev, 2015. **21**: p. 1-15.
2. Park, E.J. and J.M. Pezzuto, *The pharmacology of resveratrol in animals and humans.* Biochim Biophys Acta, 2015. **1852**(6): p. 1071-113.
3. Coenye, T., et al., *Eradication of Propionibacterium acnes biofilms by plant extracts and putative identification of icariin, resveratrol and salidroside as active compounds.* Phytomedicine, 2012. **19**(5): p. 409-12.
4. Fabbrocini, G., et al., *Resveratrol-containing gel for the treatment of acne vulgaris: a single-blind, vehicle-controlled, pilot study.* Am J Clin Dermatol, 2011. **12**(2): p. 133-41.
5. Kwon, Y.R., et al., *Bioactivity-guided separation of anti-acidogenic substances against Streptococcus mutans UA 159 from Polygonum cuspidatum.* Oral Dis, 2010. **16**(2): p. 204-9.
6. Lv, G., et al., *AMP-activated protein kinase activation protects gastric epithelial cells from Helicobacter pylori-induced apoptosis.* Biochem Biophys Res Commun, 2014. **453**(1): p. 13-8.
7. Zaidi, S.F., et al., *Effect of resveratrol on Helicobacter pylori-induced interleukin-8 secretion, reactive oxygen species generation and morphological changes in human gastric epithelial cells.* Biol Pharm Bull, 2009. **32**(11): p. 1931-5.
8. Mobasheri, A. and M. Shakibaei, *Osteogenic effects of resveratrol in vitro: potential for the prevention and treatment of osteoporosis.* Ann N Y Acad Sci, 2013. **1290**: p. 59-66.
9. Tou, J.C., *Resveratrol supplementation affects bone acquisition and osteoporosis: Pre-clinical evidence toward translational diet therapy.* Biochim Biophys Acta, 2015. **1852**(6): p. 1186-94.
10. Okada, Y., et al., *Dietary resveratrol prevents the development of food allergy in mice.* PLoS One, 2012. **7**(9): p. e44338.
11. Bola, C., H. Bartlett, and F. Eperjesi, *Resveratrol and the eye: activity and molecular mechanisms.* Graefes Arch Clin Exp Ophthalmol, 2014. **252**(5): p. 699-713.
12. Nagineni, C.N., et al., *Resveratrol Suppresses Expression of VEGF by Human Retinal Pigment Epithelial Cells: Potential Nutraceutical for Age-related Macular Degeneration.* Aging Dis, 2014. **5**(2): p. 88-100.
13. Wu, R.E., et al., *Resveratrol protects against physical fatigue and improves exercise performance in mice.* Molecules, 2013. **18**(4): p. 4689-702.
14. Bhullar, K.S. and B.P. Hubbard, *Lifespan and healthspan extension by resveratrol.* Biochim Biophys Acta, 2015. **1852**(6): p. 1209-18.
15. Britton, R.G., C. Kovoor, and K. Brown, *Direct molecular targets of resveratrol: identifying key interactions to unlock complex mechanisms.* Ann N Y Acad Sci, 2015. **1348**(1): p. 124-33.
16. Han, G., et al., *Anti-tumor effects and cellular mechanisms of resveratrol.* Drug Discov Ther, 2015. **9**(1): p. 1-12.
17. Kulkarni, S.S. and C. Canto, *The molecular targets of resveratrol.* Biochim Biophys Acta, 2015. **1852**(6): p. 1114-23.
18. Cao, D., et al., *Structural basis for allosteric, substrate-dependent stimulation of SIRT1 activity by resveratrol.* Genes Dev, 2015. **29**(12): p. 1316-25.
19. Gomes, A.P., et al., *Berberine protects against high fat diet-induced dysfunction in muscle mitochondria by inducing SIRT1-dependent mitochondrial biogenesis.* Biochim Biophys Acta, 2012. **1822**(2): p. 185-95.
20. Li, W., et al., *Berberine regulates AMP-activated protein kinase signaling pathways and inhibits colon tumorigenesis in mice.* Mol Carcinog, 2015. **54**(10): p. 1096-109.
21. Din, F.V., et al., *Aspirin inhibits mTOR signaling, activates AMP-activated protein kinase, and induces autophagy in colorectal cancer cells.* Gastroenterology, 2012. **142**(7): p. 1504-15.e3.
22. Ford, R.J., et al., *Metformin and salicylate synergistically activate liver AMPK, inhibit lipogenesis and improve insulin sensitivity.* Biochem J, 2015. **468**(1): p. 125-32.

23. Grahame Hardie, D., *AMP-activated protein kinase: a key regulator of energy balance with many roles in human disease.* J Intern Med, 2014. **276**(6): p. 543-59.
24. Kamble, P., et al., *Aspirin may promote mitochondrial biogenesis via the production of hydrogen peroxide and the induction of Sirtuin1/PGC-1alpha genes.* Eur J Pharmacol, 2013. **699**(1-3): p. 55-61.
25. Steinberg, G.R., M. Dandapani, and D.G. Hardie, *AMPK: mediating the metabolic effects of salicylate-based drugs?* Trends Endocrinol Metab, 2013. **24**(10): p. 481-7.
26. Piotrowska, H., M. Kucinska, and M. Murias, *Biological activity of piceatannol: leaving the shadow of resveratrol.* Mutat Res, 2012. **750**(1): p. 60-82.
27. Tang, Y.L. and S.W. Chan, *A review of the pharmacological effects of piceatannol on cardiovascular diseases.* Phytother Res, 2014. **28**(11): p. 1581-8.
28. Bauerova, K., et al., *Markers of inflammation and oxidative stress studied in adjuvant-induced arthritis in the rat on systemic and local level affected by pinosylvin and methotrexate and their combination.* Autoimmunity, 2015. **48**(1): p. 46-56.
29. Koskela, A., et al., *Pinosylvin-mediated protection against oxidative stress in human retinal pigment epithelial cells.* Mol Vis, 2014. **20**: p. 760-9.
30. Laavola, M., et al., *Pinosylvin and monomethylpinosylvin, constituents of an extract from the knot of Pinus sylvestris, reduce inflammatory gene expression and inflammatory responses in vivo.* J Agric Food Chem, 2015. **63**(13): p. 3445-53.
31. Park, E.J., et al., *Suppression of Src/ERK and GSK-3/beta-catenin signaling by pinosylvin inhibits the growth of human colorectal cancer cells.* Food Chem Toxicol, 2013. **55**: p. 424-33.
32. Park, E.J., et al., *Antimetastatic activity of pinosylvin, a natural stilbenoid, is associated with the suppression of matrix metalloproteinases.* J Nutr Biochem, 2012. **23**(8): p. 946-52.
33. Estrela, J.M., et al., *Pterostilbene: Biomedical applications.* Crit Rev Clin Lab Sci, 2013. **50**(3): p. 65-78.
34. McCormack, D. and D. McFadden, *Pterostilbene and cancer: current review.* J Surg Res, 2012. **173**(2): p. e53-61.
35. McCormack, D. and D. McFadden, *A review of pterostilbene antioxidant activity and disease modification.* Oxid Med Cell Longev, 2013. **2013**: p. 575482.
36. Dhar, S., et al., *Resveratrol and pterostilbene epigenetically restore PTEN expression by targeting oncomiRs of the miR-17 family in prostate cancer.* Oncotarget, 2015.
37. Hsiao, P.C., et al., *Pterostilbene simultaneously induced G0/G1-phase arrest and MAPK-mediated mitochondrial-derived apoptosis in human acute myeloid leukemia cell lines.* PLoS One, 2014. **9**(8): p. e105342.
38. Ko, C.P., et al., *Pterostilbene induce autophagy on human oral cancer cells through modulation of Akt and mitogen-activated protein kinase pathway.* Oral Oncol, 2015. **51**(6): p. 593-601.
39. Su, C.M., et al., *Pterostilbene inhibits triple-negative breast cancer metastasis via inducing microRNA-205 expression and negatively modulates epithelial-to-mesenchymal transition.* J Nutr Biochem, 2015. **26**(6): p. 675-85.
40. Wu, C.H., et al., *Targeting cancer stem cells in breast cancer: potential anticancer properties of 6-shogaol and pterostilbene.* J Agric Food Chem, 2015. **63**(9): p. 2432-41.
41. Lv, M., et al., *Pterostilbene attenuates the inflammatory reaction induced by ischemia/reperfusion in rat heart.* Mol Med Rep, 2015. **11**(1): p. 724-8.
42. Zhou, Y., et al., *Orally administrated pterostilbene attenuates acute cerebral ischemia-reperfusion injury in a dose- and time-dependent manner in mice.* Pharmacol Biochem Behav, 2015. **135**: p. 199-209.
43. Song, Z., et al., *Pterostilbene mediates neuroprotection against oxidative toxicity via oestrogen receptor alpha signalling pathways.* J Pharm Pharmacol, 2015. **67**(5): p. 720-30.
44. Hou, Y., et al., *Pterostilbene attenuates lipopolysaccharide-induced learning and memory impairment possibly via inhibiting microglia activation and protecting neuronal injury in mice.* Prog Neuropsychopharmacol Biol Psychiatry, 2014. **54**: p. 92-102.
45. Gomez-Zorita, S., et al., *Pterostilbene improves glycaemic control in rats fed an obesogenic diet: involvement of skeletal muscle and liver.* Food Funct, 2015. **6**(6): p. 1968-76.

46. Mikstacka, R., et al., *Inhibition of human recombinant cytochromes P450 CYP1A1 and CYP1B1 by trans-resveratrol methyl ethers.* Mol Nutr Food Res, 2007. **51**(5): p. 517-24.
47. Rimando, A.M., et al., *Cancer chemopreventive and antioxidant activities of pterostilbene, a naturally occurring analogue of resveratrol.* J Agric Food Chem, 2002. **50**(12): p. 3453-7.
48. Siedlecka-Kroplewska, K., et al., *Pterostilbene induces accumulation of autophagic vacuoles followed by cell death in HL60 human leukemia cells.* J Physiol Pharmacol, 2013. **64**(5): p. 545-56.
49. Bhakkiyalakshmi, E., et al., *Therapeutic potential of pterostilbene against pancreatic beta-cell apoptosis mediated through Nrf2.* Br J Pharmacol, 2014. **171**(7): p. 1747-57.
50. Chiou, Y.S., et al., *Pterostilbene is more potent than resveratrol in preventing azoxymethane (AOM)-induced colon tumorigenesis via activation of the NF-E2-related factor 2 (Nrf2)-mediated antioxidant signaling pathway.* J Agric Food Chem, 2011. **59**(6): p. 2725-33.
51. Sirerol, J.A., et al., *Topical treatment with pterostilbene, a natural phytoalexin, effectively protects hairless mice against UVB radiation-induced skin damage and carcinogenesis.* Free Radic Biol Med, 2015. **85**: p. 1-11.
52. Park, S.H., et al., *Pterostilbene, an Active Constituent of Blueberries, Stimulates Nitric Oxide Production via Activation of Endothelial Nitric Oxide Synthase in Human Umbilical Vein Endothelial Cells.* Plant Foods Hum Nutr, 2015. **70**(3): p. 263-8.
53. Rimando, A.M., et al., *Evaluation of PPARalpha activation by known blueberry constituents.* J Sci Food Agric, 2016. **96**(5): p. 1666-71.
54. Azzolini, M., et al., *Pharmacokinetics and tissue distribution of pterostilbene in the rat.* Mol Nutr Food Res, 2014. **58**(11): p. 2122-32.
55. Chang, J., et al., *Low-dose pterostilbene, but not resveratrol, is a potent neuromodulator in aging and Alzheimer's disease.* Neurobiol Aging, 2012. **33**(9): p. 2062-71.
56. Al Rahim, M., et al., *Anxiolytic action of pterostilbene: involvement of hippocampal ERK phosphorylation.* Planta Med, 2013. **79**(9): p. 723-30.
57. Azorin-Ortuno, M., et al., *Pharmacokinetic study of trans-resveratrol in adult pigs.* J Agric Food Chem, 2010. **58**(20): p. 11165-71.
58. Cottart, C.H., et al., *Resveratrol bioavailability and toxicity in humans.* Mol Nutr Food Res, 2010. **54**(1): p. 7-16.
59. Juan, M.E., M. Maijo, and J.M. Planas, *Quantification of trans-resveratrol and its metabolites in rat plasma and tissues by HPLC.* J Pharm Biomed Anal, 2010. **51**(2): p. 391-8.
60. Smoliga, J.M. and O. Blanchard, *Enhancing the delivery of resveratrol in humans: if low bioavailability is the problem, what is the solution?* Molecules, 2014. **19**(11): p. 17154-72.
61. Wenzel, E., et al., *Bioactivity and metabolism of trans-resveratrol orally administered to Wistar rats.* Mol Nutr Food Res, 2005. **49**(5): p. 482-94.
62. Kapetanovic, I.M., et al., *Pharmacokinetics, oral bioavailability, and metabolic profile of resveratrol and its dimethylether analog, pterostilbene, in rats.* Cancer Chemother Pharmacol, 2011. **68**(3): p. 593-601.
63. Biasutto, L., et al., *Improving the efficacy of plant polyphenols.* Anticancer Agents Med Chem, 2014. **14**(10): p. 1332-42.
64. Mattarei, A., et al., *Acetal derivatives as prodrugs of resveratrol.* Mol Pharm, 2013. **10**(7): p. 2781-92.
65. Mattarei, A., et al., *New water-soluble carbamate ester derivatives of resveratrol.* Molecules, 2014. **19**(10): p. 15900-17.
66. Ghosh, A.K. and M. Brindisi, *Organic carbamates in drug design and medicinal chemistry.* J Med Chem, 2015. **58**(7): p. 2895-940.
67. Hansen, J., N. Mørk, and H. Bundgaard, *Phenyl carbamates of amino acids as prodrug forms for protecting phenols against first-pass metabolism.* International Journal of Pharmaceutics, 1992. **81**(2): p. 253-261.
68. Igarashi, Y., et al., *Synthesis and evaluation of carbamate prodrugs of a phenolic compound.* Chem Pharm Bull (Tokyo), 2007. **55**(2): p. 328-33.

69. Mata, G., et al., *A carbamate-based approach to primaquine prodrugs: antimalarial activity, chemical stability and enzymatic activation.* Bioorg Med Chem, 2012. **20**(2): p. 886-92.
70. Savolainen, J., et al., *Synthesis and in vitro/in vivo evaluation of novel oral N-alkyl- and N,N-dialkyl-carbamate esters of entacapone.* Life Sci, 2000. **67**(2): p. 205-16.
71. Vacondio, F., et al., *Qualitative structure-metabolism relationships in the hydrolysis of carbamates.* Drug Metab Rev, 2010. **42**(4): p. 551-89.
72. Mattarei, A., et al., *New derivatives of resveratrol*. 2014, Google Patents: Europe.
73. Mattarei, A., et al., *N-Monosubstituted Methoxy-oligo(ethylene glycol) Carbamate Ester Prodrugs of Resveratrol.* Molecules, 2015. **20**(9): p. 16085-102.
74. Azzolini, M., et al., *Synthesis and Evaluation as Prodrugs of Hydrophilic Carbamate Ester Analogues of Resveratrol.* Mol Pharm, 2015. **12**(9): p. 3441-54.
75. Mattarei, A., et al., *Amino Acid Carbamates As Prodrugs Of Resveratrol.* Scientific Reports, 2015. **5**: p. 15216.
76. Fotiadis, D., Y. Kanai, and M. Palacin, *The SLC3 and SLC7 families of amino acid transporters.* Mol Aspects Med, 2013. **34**(2-3): p. 139-58.
77. Kanai, Y., et al., *The SLC1 high-affinity glutamate and neutral amino acid transporter family.* Mol Aspects Med, 2013. **34**(2-3): p. 108-20.
78. Steffansen, B., et al., *Intestinal solute carriers: an overview of trends and strategies for improving oral drug absorption.* Eur J Pharm Sci, 2004. **21**(1): p. 3-16.
79. Fraga, S., M.J. Pinho, and P. Soares-da-Silva, *Expression of LAT1 and LAT2 amino acid transporters in human and rat intestinal epithelial cells.* Amino Acids, 2005. **29**(3): p. 229-33.
80. Broberg, M., et al., *Function and expression of the proton-coupled amino acid transporter PAT1 along the rat gastrointestinal tract: implications for intestinal absorption of gaboxadol.* Br J Pharmacol, 2012. **167**(3): p. 654-65.
81. Estudante, M., et al., *Intestinal drug transporters: an overview.* Adv Drug Deliv Rev, 2013. **65**(10): p. 1340-56.
82. Smith, D.E., B. Clemencon, and M.A. Hediger, *Proton-coupled oligopeptide transporter family SLC15: Physiological, pharmacological and pathological implications.* Molecular Aspects of Medicine, 2013. **34**(2-3): p. 323-336.
83. Nielsen, C.U. and B. Brodin, *Di/tri-peptide transporters as drug delivery targets: Regulation of transport under physiological and patho-physiological conditions.* Current Drug Targets, 2003. **4**(5): p. 373-388.
84. Terada, T. and K. Inui, *Peptide transporters: Structure, function, regulation and application for drug delivery.* Current Drug Metabolism, 2004. **5**(1): p. 85-94.
85. Terada, T. and K. Inui, *Recent Advances in Structural Biology of Peptide Transporters.* Co-Transport Systems, 2012. **70**: p. 257-274.
86. Brandsch, M., *Transport of drugs by proton-coupled peptide transporters: pearls and pitfalls.* Expert Opinion on Drug Metabolism & Toxicology, 2009. **5**(8): p. 887-905.
87. Lyons, J.A., et al., *Structural basis for polyspecificity in the POT family of proton-coupled oligopeptide transporters.* Embo Reports, 2014. **15**(8): p. 886-893.
88. Newstead, S., *Molecular insights into proton coupled peptide transport in the PTR family of oligopeptide transporters.* Biochimica Et Biophysica Acta-General Subjects, 2015. **1850**(3): p. 488-499.
89. Freeman, H.J., *Clinical relevance of intestinal peptide uptake.* World J Gastrointest Pharmacol Ther, 2015. **6**(2): p. 22-7.
90. Cao, F., et al., *Propylene glycol-linked amino acid/dipeptide diester prodrugs of oleanolic acid for PepT1-mediated transport: synthesis, intestinal permeability, and pharmacokinetics.* Mol Pharm, 2013. **10**(4): p. 1378-87.
91. Gilzad-Kohan, M.H., K. Kaur, and F. Jamali, *The antiinflammatory action and pharmacokinetics of a novel glucosamine-based di-peptide aminosugar.* J Pharm Pharm Sci, 2013. **16**(2): p. 279-88.
92. Gilzad Kohan, H., K. Kaur, and F. Jamali, *Synthesis and characterization of a new Peptide prodrug of glucosamine with enhanced gut permeability.* PLoS One, 2015. **10**(5): p. e0126786.

93. Gupta, D., et al., *Increasing oral absorption of polar neuraminidase inhibitors: a prodrug transporter approach applied to oseltamivir analogue.* Mol Pharm, 2013. **10**(2): p. 512-22.
94. Brodin, B., et al., *Transport of peptidomimetic drugs by the intestinal Di/tri-peptide transporter, PepT1.* Pharmacol Toxicol, 2002. **90**(6): p. 285-96.
95. Zhang, Y., et al., *Prodrug design targeting intestinal PepT1 for improved oral absorption: design and performance.* Curr Drug Metab, 2013. **14**(6): p. 675-87.
96. Bailey, P.D., et al., *How to make drugs orally active: A substrate template for peptide transporter PepT1.* Angewandte Chemie-International Edition, 2000. **39**(3): p. 506-+.
97. Meredith, D., et al., *Modified amino acids and peptides as substrates for the intestinal peptide transporter PepT1.* European Journal of Biochemistry, 2000. **267**(12): p. 3723-3728.
98. Shugarts, S. and L.Z. Benet, *The role of transporters in the pharmacokinetics of orally administered drugs.* Pharm Res, 2009. **26**(9): p. 2039-54.
99. Tamai, I. and T. Nakanishi, *OATP transporter-mediated drug absorption and interaction.* Curr Opin Pharmacol, 2013. **13**(6): p. 859-63.
100. Roth, M., A. Obaidat, and B. Hagenbuch, *OATPs, OATs and OCTs: the organic anion and cation transporters of the SLCO and SLC22A gene superfamilies.* Br J Pharmacol, 2012. **165**(5): p. 1260-87.
101. Hidalgo, I.J., T.J. Raub, and R.T. Borchardt, *Characterization of the human colon carcinoma cell line (Caco-2) as a model system for intestinal epithelial permeability.* Gastroenterology, 1989. **96**(3): p. 736-49.
102. Ahlin, G., et al., *Endogenous gene and protein expression of drug-transporting proteins in cell lines routinely used in drug discovery programs.* Drug Metab Dispos, 2009. **37**(12): p. 2275-83.
103. Hilgendorf, C., et al., *Expression of thirty-six drug transporter genes in human intestine, liver, kidney, and organotypic cell lines.* Drug Metab Dispos, 2007. **35**(8): p. 1333-40.
104. Uchida, Y., et al., *Quantitative targeted absolute proteomics for 28 human transporters in plasma membrane of Caco-2 cell monolayer cultured for 2, 3, and 4 weeks.* Drug Metab Pharmacokinet, 2015. **30**(2): p. 205-8.
105. Herrera-Ruiz, D., et al., *Spatial expression patterns of peptide transporters in the human and rat gastrointestinal tracts, Caco-2 in vitro cell culture model, and multiple human tissues.* AAPS PharmSci, 2001. **3**(1): p. E9.
106. Hayeshi, R., et al., *Comparison of drug transporter gene expression and functionality in Caco-2 cells from 10 different laboratories.* Eur J Pharm Sci, 2008. **35**(5): p. 383-96.
107. Biasutto, L., et al., *Determination of quercetin and resveratrol in whole blood--implications for bioavailability studies.* Molecules, 2010. **15**(9): p. 6570-9.

Acknowledgments

This work was supported by grants from the Fondazione Cassa di Risparmio di Padova e Rovigo (CARIPARO) ("Developing a Pharmacology of Polyphenols"), from the Italian Ministry of the University and Research (PRIN n. 20107Z8XBW_004), and by the CNR Project of Special Interest on Aging.

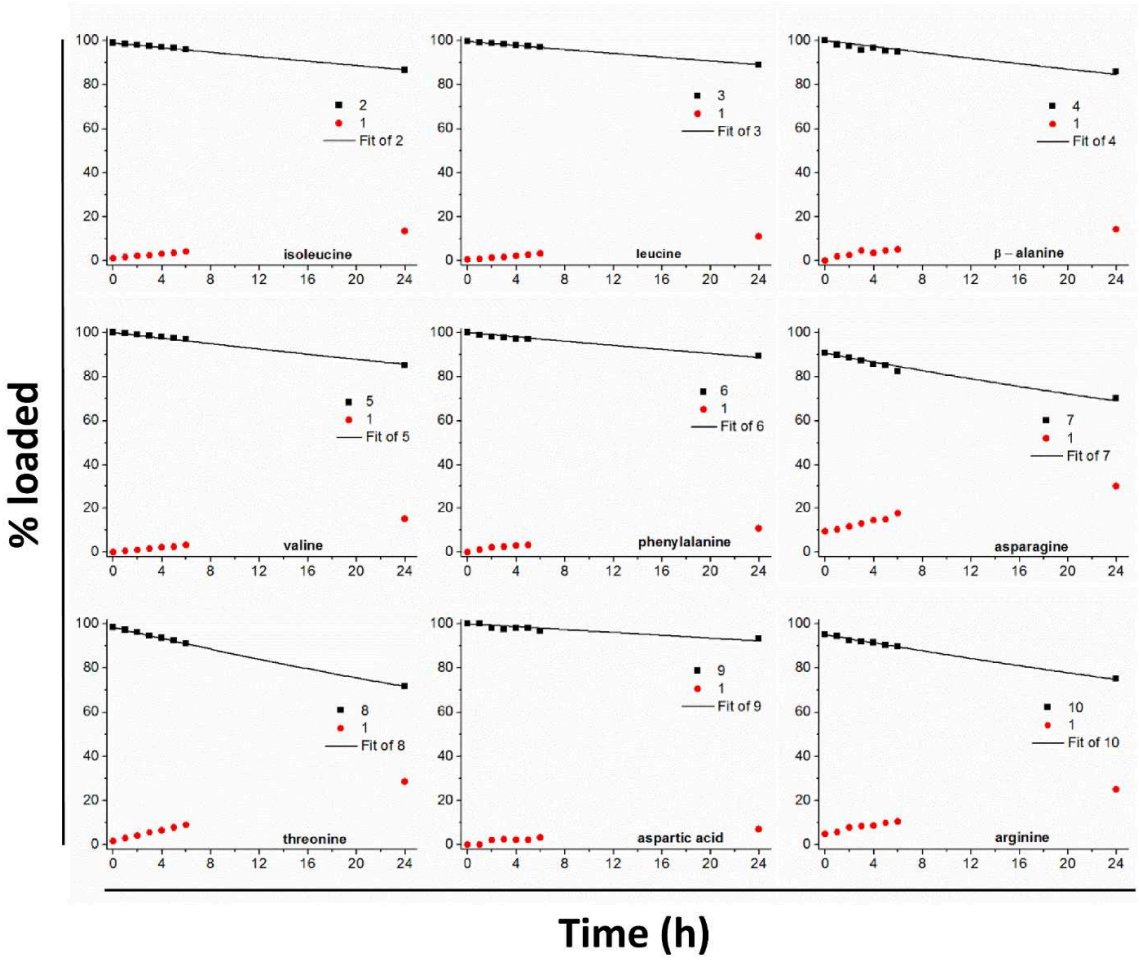
Author contribution

A.M., C.P., M.Z., L.B. designed the study and wrote the manuscript; A.M., M.F., G.C., M.R. carried out the syntheses; M.A., M.L.S. performed the hydrolysis studies and pharmacokinetics experiments. All authors reviewed the manuscript.

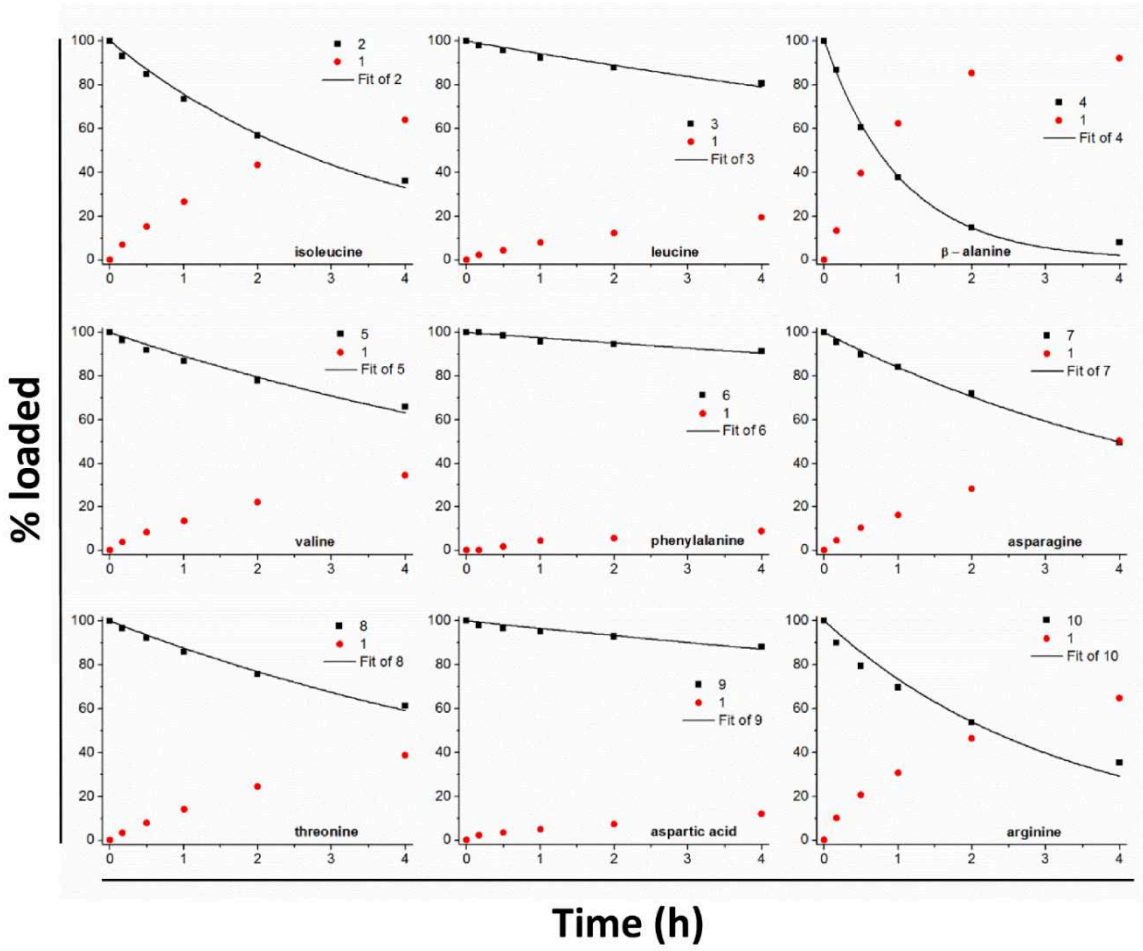
Additional Information

Competing financial interests: The authors declare they have no competing financial interests.

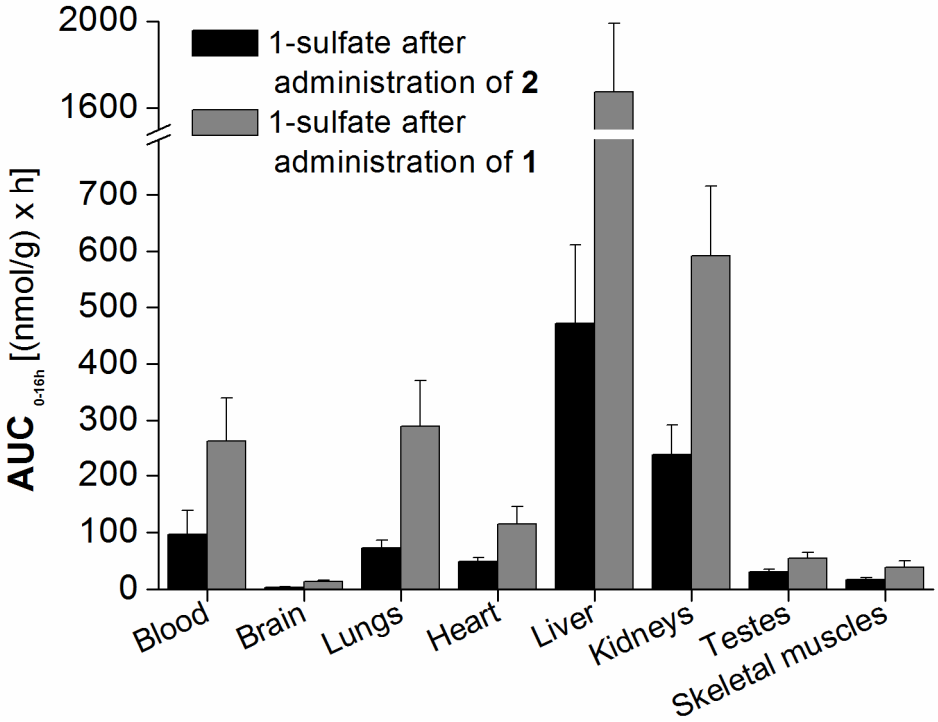
Supporting Information



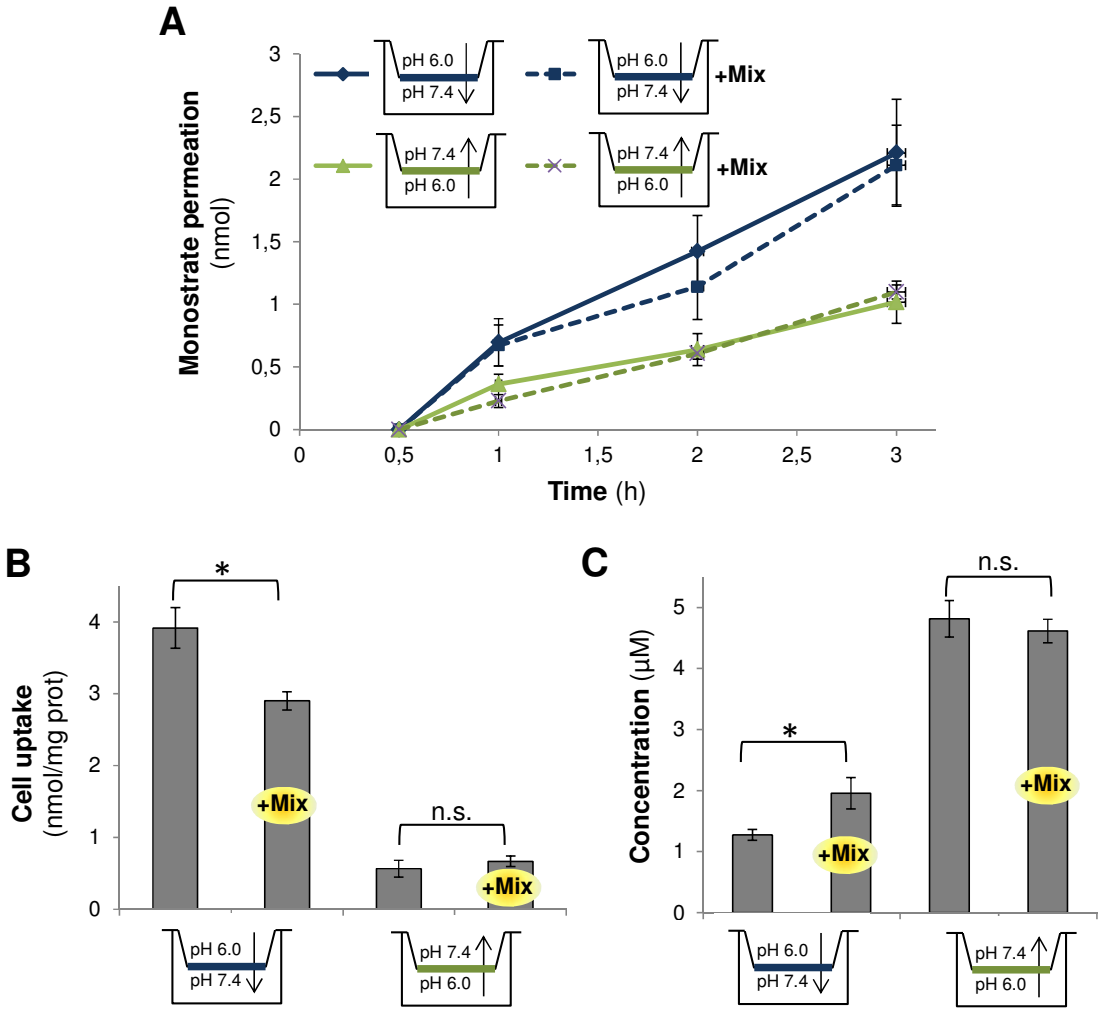
Supplementary Fig.S1: Hydrolysis of derivatives **2-10** in PBS 0.1M, pH 6.8, 37°C. Data are expressed as % of the initially loaded compound. A representative experiment. The fits are for pseudo-first order kinetics. Values ± standard error obtained from the fits of all available data are reported in Table 1, main text.



Supplementary Fig.S2: Hydrolysis or derivatives **2-10** in blood. Data are expressed as % of the initially loaded compound. A representative experiment. The fit is for pseudo-first order kinetics. Values ± standard error obtained from the fits of all available data are reported in Table 1, main text.



Supplementary Fig.S3: Comparison of the $AUC_{0\text{-}16h}$ obtained for **1**-sulfate after administration of **1** (grey bars; *Azzolini, M. et al, Mol Nutr Food Res 58, 2122-2132 (2014)*) or after administration of derivative **2** (black bars). Error bars represent + standard deviation (an error bar of the same size in the negative direction is also implied but not shown for graphic clarity).



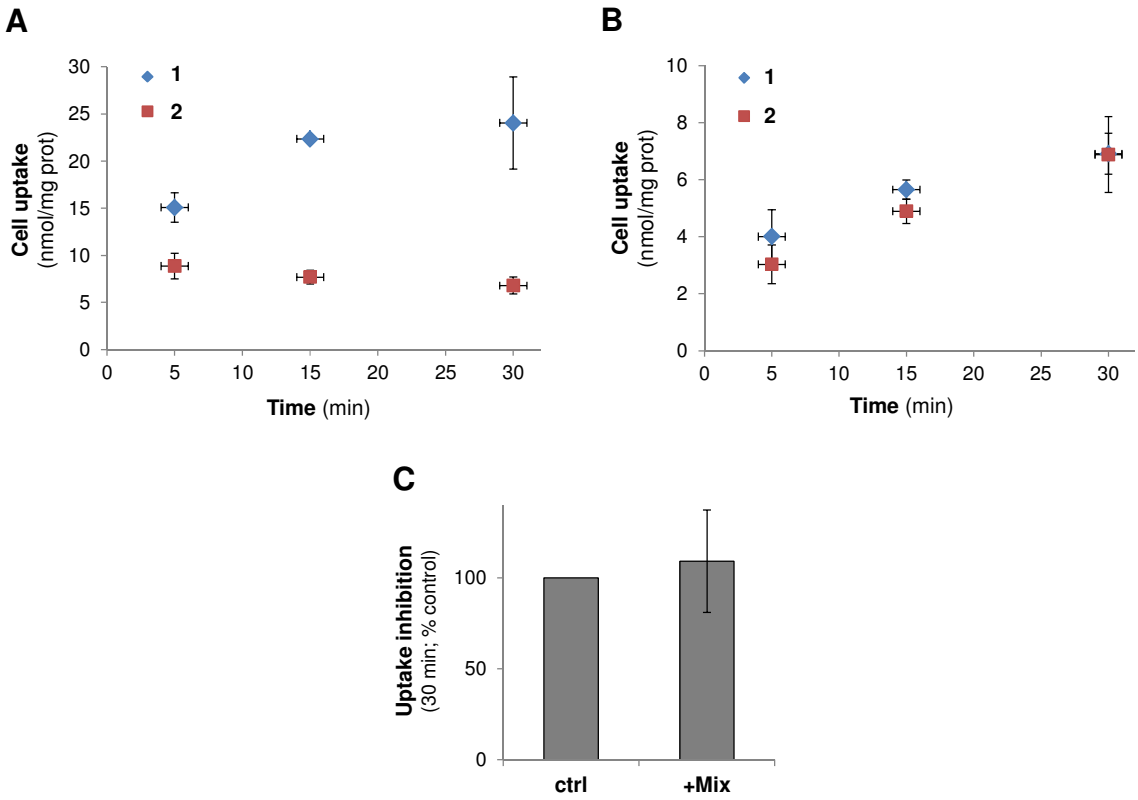
Supplementary Fig.S4: Effect of substrates of PepT1, LAT and OATP on the transport of **2** across Caco-2 monolayers. Amount of **2** in the receiver chamber as a function of time (A); cellular content of **2** at the end of the experiment (3h) (B). Amount of **2** remaining in the loading chamber at the end of the experiment (3h) (C). Cell monolayers were exposed to a 10 µM solution of **2**, loaded on the apical or basolateral side, as indicated, in the absence or in the presence of a mixture of GlySar, Ile and E-3-S (Mix). Reported are mean values ± standard deviation. N = 3. *: significantly different compared to the control ($p \leq 0.1$).

As shown in Supplementary Figure S4, the presence of PepT1, LAT and OATP substrates significantly decreased the amount of **2** taken up by Caco-2 cells (panel B); this was accompanied by an increase of **2** remaining in the loading compartment at the end of the experiment (panel C). Competitive inhibition was observed only if **2** was loaded on the apical side of the monolayer: this confirmed the involvement of transporters expressed on the apical side of the cells.

The presence of competitive substrates however did not significantly affect the amount of **2** reaching the acceptor compartment (panel A). Permeation of the cell monolayer implies

that **2** must cross both the apical and the basolateral membranes. While the candidate transporters are expressed in the apical side, they seem not to be expressed in the basolateral one. This implies that a transporter-mediated (substrate-sensitive) uptake takes place only at the apical membrane, while the passage of **2** through the basolateral one is by passive diffusion only. In addition, apical permeation of **2** is also largely mediated by passive diffusion (see main text and Figure S5 for details), which seems to emerge as the major rate determining factor in these experiments.

Further experiments to elucidate which specific transporters may be involved were thus performed looking at cellular uptake only.



Supplementary Fig.5: Comparison of the uptake of **2** and **1** by HeLa (A) and Caco-2 (B) cells. C: Effect of a mixture of PepT1, LAT and OATP substrates (Mix) on the uptake of **2** in HeLa cells. Cells were exposed to a 10 µM solution of **2** and **1** (in HBSS, pH 6.0) for the indicated times. Reported are mean values ± standard deviation. N ≥ 3.

HeLa cells are known to have very low levels of transporters such as PepT1 and OATPs (*Ahlin, G. et al. Drug Metab Dispos 37, 2275-2283 (2009)*). Comparing cell uptake of **2** and **1** in HeLa and Caco-2 cells, we can see that uptake of **2** is much lower than that of **1** in HeLa cells, but not in Caco-2 (Suppl. Fig. S5 A and B). A quantitative comparison between cells is not possible, since they have very different morphologies and thus a different surface exposed to the loading solution. Uptake experiments showed that HeLa cells are in any case able to take up **2**; however, this uptake is not sensitive to a mixture of competitive inhibitors for PepT1, LAT and OATP (Mix: GlySar, Ile and E-3-S) (Suppl. Fig. S5C). All these data confirm that **2** enters the cells both by passive diffusion (observed in both HeLa and Caco-2) and by active transport (observed only in Caco-2, and sensitive to GlySar and E-3-S).

Supplementary Table S1. Recovery ratios (analyte/internal standard) of derivatives **2-10** from blood (left column) and recovery ratios of derivative **2** from organs (right column).

Compound	Recovery ratio from blood *	Organ	Recovery ratio of 2 *
2	1.12 ± 0.09	**Brain**	0.93 ± 0.09
3	0.76 ± 0.07	**Lungs**	0.9 ± 0.1
4	0.70 ± 0.03	**Heart**	0.91 ± 0.09
5	0.89 ± 0.08	**Liver**	0.83 ± 0.06
6	0.85 ± 0.03	**Kidneys**	0.68 ± 0.08
7	0.71 ± 0.06	**Testes**	0.87 ± 0.09
8	0.71 ± 0.06	**Skeletal muscle**	0.96 ± 0.06
9	0.88 ± 0.05		
10	0.78 ± 0.03		

*Recovery ratios from blood and organs are given as mean values ± standard deviation. N ≥ 4 for each condition.

Supplementary Experimental Procedures

Synthesis of 4'-[N-(isoleucinyl)-carbamoyl]-pterostilbene (2).

4'-[N-(isoleucinyl-tert-butyl)]-pterostilbene (**11**): A solution of L-isoleucine-*tert*-butyl ester hydrochloride (0.50 g, 2.2 mmol, 1.0 eq) and dimethyl amino pyridine (DMAP, 1.1 g, 8.9 mmol, 4.0 eq) in anhydrous dichloromethane (DCM, 7 mL) was added dropwise to a solution of bis-(4-nitrophenyl) carbonate (PNPC) (0.71 g, 2.4 mmol, 1.1 eq) in anhydrous DCM (4.5 mL). The resulting mixture was stirred at 50 °C for 4 hours. Then, pterostilbene (0.75 g, 2.9 mmol, 1.3 eq) was added to the solution. The resulting mixture was stirred at 50°C overnight, and then it was diluted in DCM (100 mL) and extracted with HCl 0.5 M (2 × 100 mL). The organic layer was dried over $MgSO_4$ and filtered. The solvent was evaporated under reduced pressure and residues of 4-nitrophenol (PNP) and pterostilbene were eliminated by flash chromatography using petroleum ether/DCM/diethyl ether (DEE) (5:4:1) as eluent. Ile-OtBu-PNPC (the residual activated urethane) was removed by flash chromatography using petroleum ether:DEE (7:3) as eluent, to afford **11** (0.78 g, 74 % yield) as a colourless oil. MS-ESI (ion trap) = 470 m/z $[M + H]^+$; ^{1}H NMR (200 MHz, $CDCl_3$) δ (ppm) = 7.48 (d, J = 8.4 Hz, 2H), 7.19 – 6.82 (m, 4H), 6.66 (d, J = 2.0 Hz, 2H), 6.39 (m, 1H), 5.62 (m, 1H), 4.29 (m, 1H), 3.83 (s, 6H), 1.95 (m, 1H), 1.50 (m, 11H), 0.97 (m, 6H). ^{13}C NMR (50 MHz, $CDCl_3$) δ(ppm) = 170.91, 161.20, 154.31, 150.64, 139.40, 134.54, 128.45, 127.50, 121.90, 104.66, 100.17, 82.40, 58.82, 55.49, 38.50, 28.21, 25.30, 15.54, 11.88.

4'-[N-(isoleucinyl)-carbamoyl]-pterostilbene (**2**): Trifluoroacetic acid (TFA, 2.5 mL, 32.6 mmol, 40 eq) was added to a solution of **11** (0.38 g, 0.81 mmol, 1.0 eq) and triisopropylsilane (TIPS, 0.25 mL, 5 % v/v) in anhydrous DCM (2.5 mL). The mixture was stirred at 0 °C overnight. TFA and the solvent were evaporated off under reduced pressure. Toluene (2 × 5 mL) was then added and the solvent was stripped off under reduced pressure to remove traces of TFA. The residue was purified by flash chromatography using petroleum ether/acetone (7:3) as eluent, to afford **2** as a white solid (0.25 g, 76 % yield). MS-ESI (ion trap) = 414 m/z $[M + H]^+$; ^{1}H NMR (200 MHz, $CDCl_3$) δ (ppm) = 8.06 - 8.03 (m, 1H) 7.49 (d, J = 8.5 Hz, 2H), 7.04 (m, 4H), 6.66 (d, J = 1.9 Hz, 2H), 6.40 (m, 1H), 4.46 (m, 1H), 3.83 (s, 6H), 1.86 (m, 1H), 1.53-1.21 (m, 1H) 0.94-0.85 (m, 1H), 1.03 (m, 6H); ^{13}C NMR (50 MHz, $CDCl_3$) δ (ppm) = 176.02, 160.66, 154.11, 150.02, 138.93, 134.31, 128.42, 127.93, 127.11, 121.42, 104.27, 99.77, 58.05, 55.07, 37.53, 24.60, 15.25, 11.32.

Synthesis of 4'-[N-(leucinyl)-carbamoyl]-pterostilbene (3).

4'-[N-(leucinyl-tert-butyl)]-pterostilbene (**12**): A solution of L-leucine-*tert*-butyl ester hydrochloride (1.6 g, 7.2 mmol, 1.0 eq) and DMAP (3.5 g, 28.6 mmol, 4.0 eq) in anhydrous DCM (30 mL) was added dropwise to a solution of bis-(4-nitrophenyl) carbonate (0.71 g, 2.4 mmol, 1.1 eq) in anhydrous DCM (4.5 mL). The resulting mixture was stirred at 50 °C for 4 hours. Pterostilbene (2.4 g, 9.4 mmol, 1.3 eq) was then added to the solution. The resulting mixture was stirred at 50°C overnight, and then it was diluted in DCM (100 mL) and extracted with HCl 0.5 M (2 × 100 mL). The organic layer was dried over $MgSO_4$ and filtered. The solvent was evaporated under reduced pressure and residues of 4-nitrophenol (PNP) and pterostilbene were removed by flash chromatography using petroleum ether/DCM/DEE (5:4:1) as eluent. Contaminating PNPC-Leu-OtBu (the activated urethane) was eliminated by flash chromatography using petroleum ether:DEE (7:3) as eluent, to afford **12** (2.81 g, 77 % yield) as a colourless oil. MS-ESI (ion trap) = 470 m/z $[M + H]^+$; ^1H NMR ($CDCl_3$, 500 MHz) δ (ppm): 8,01 (d, 1H, J = 10.0 Hz), 7.47 (d, 2H, J = 5.3 Hz), 7.13 (d, 2H, J = 10.1 Hz), 6.93-7.06 (m, 2H), 6.66 (d, 2H, J = 2.2 Hz), 6.40 (t, 1H, J = 2.2 Hz), 4.32-4.36 (m, 1H), 3.80 (s, 6H), 1.75-1,83 (m, 1H), 1.55-1.70 (m, 2H), 1.50 (s, 9H), 0.98-1.00 (m, 6H); ^{13}C NMR ($CDCl_3$, 126 MHz) δ (ppm): 172.12, 160.94, 154.17, 150.47, 139.22, 134.37, 128.55, 128.22, 127.33, 121.75, 104.52, 100.00, 82.03, 55.27, 41.90, 27.97, 24.86, 22.82, 21.99.

4'-[N-(leucinyl)-carbamoyl]-pterostilbene (**3**): TFA (5.0 mL, 65.3 mmol, 43 eq) was added to a solution of **12** (0.80 g, 1.69 mmol, 1.0 eq) and triisopropylsilane (TIPS, 0.5 mL, 5 % v/v) in anhydrous DCM (5 mL). The mixture was stirred at 0 °C overnight. TFA and the solvent were evaporated under reduced pressure. Toluene (2 × 5 mL) was then added and the solvent was stripped off under reduced pressure to remove traces of TFA. The residue was purified by flash chromatography using petroleum ether/acetone (7:3) as eluent, to afford **3** as a white solid (0.51 g, 73 % yield). MS-ESI (ion trap) = 414 m/z $[M + H]^+$; ^1H NMR (500 MHz, $CDCl_3$) δ (ppm) = 7.47 (d, 2H, J = 10.1 Hz), 7.13 (d, 2H, J = 10.1 Hz), 6.94-7.06 (m, 2H), 6.66 (d, 2H, J = 2.2 Hz), 6.40 (t, 1H, J = 2.1 Hz), 4.43-4.48 (m, 1H), 3.82 (s, 6H), 1.72-1.84 (m, 2H), 1.61-1.67 (m, 1H), 0.98-1.00 (m, 6H); ^{13}C NMR (126 MHz, $CDCl_3$) δ (ppm) = 172.12, 160.94, 154.17, 150.47, 139.22, 134.37, 128.55, 128..22, 127.33, 121.75, 104.52, 100.00, 82.03, 55.27, 41.90, 27.97, 24.86, 22.82, 21.99.

Synthesis of 4'-[N-(ß-alanyl)-carbamoyl]-pterostilbene (4).

4'-[N-(ß-alanyl-tert butyl ester)-carbamoyl]-pterostilbene (**13**): A solution of ß-alanine-*tert*-butyl ester (0.50 g, 2.8 mmol, 1.0 eq) and DMAP (1.4 g, 11.1 mmol, 4.0 eq) in anhydrous DCM (10 mL) was added dropwise to a solution of bis-(4-nitrophenyl) carbonate (0.82 g, 2.8 mmol, 1.0 eq) in anhydrous DCM (5 mL). The resulting mixture was stirred at 50 °C for 4 hours. Pterostilbene (0.92 g, 3.6 mmol, 1.3 eq) was then added to the solution. The resulting mixture was stirred at 50°C overnight, and then it was diluted in DCM (100 mL) and extracted with HCl 0.5 M (2 × 100 mL). The organic layer was dried over $MgSO_4$ and filtered. The solvent was evaporated off under reduced pressure and the product was purified by flash chromatography using Chloroform/DEE/petroleum ether (5:1.5:3.5) as eluent, to afford **13** (0.90 g, 75 % yield) as a colourless oil. MS-ESI (ion trap) = 428 m/z $[M + H]^+$; ^1H NMR ($CDCl_3$, 500 MHz) δ (ppm): 7.50 (d, J = 8.5 Hz, 2H), 7.18 – 6.94 (m, 4H), 6.69 (d, J = 2.2 Hz, 2H), 6.42 (t, J = 2.1 Hz, 1H), 3.85 (s, 6H), 3.53 (m, 2H), 2.55 (t, J = 6.0 Hz, 2H), 1.51 (s, 9H); ^{13}C NMR ($CDCl_3$, 126 MHz) δ (ppm): 171.73, 160.99, 154.46, 150.57, 139.29, 134.37, 128.59, 128.33, 127.40, 121.79, 104.55, 100.03, 81.27, 55.37, 36.92, 35.34, 28.14.

4'-[N-(ß-alanyl)-carbamoyl]-pterostilbene (**4**): TFA (5.0 mL, 65.3 mmol, 34 eq) was added to a solution of **13** (0.83 g, 1.95 mmol, 1.0 eq) and triisopropylsilane (TIPS, 0.5 mL, 5 % v/v) in anhydrous DCM (5 mL). The mixture was stirred at 0 °C overnight. TFA and the solvent were evaporated off under reduced pressure. Toluene (2 × 5 mL) was then added and the solvent was stripped off under reduced pressure to remove traces of TFA. The residue was purified by flash chromatography using chloroform/acetone (7:3) as eluent, to afford **4** as a white solid (0.60 g, 83 % yield). MS-ESI (ion trap) = 372 m/z $[M + H]^+$; ^1H NMR (500 MHz, $CDCl_3$) δ (ppm) = 7.60 (d, J = 8.6 Hz, 2H), 7.20 (m, 4H), 6.79 (d, J = 2.1 Hz, 2H), 6.43 (t, J = 2.1 Hz, 1H), 3.79 (s, 6H), 3.31 (m, 2H), 2.49 (t, J = 7.0 Hz, 2H); ^{13}C NMR (126 MHz, $CDCl_3$) δ (ppm) = 172.72, 160.70, 154.21, 150.58, 139.11, 133.83, 128.14, 127.32, 121.98, 104.47, 99.90, 55.22, 39.52, 36.73, 33.97.

Synthesis of 4'-[N-(valinyl)-carbamoyl]-pterostilbene (5).

4'-[N-(valinyl-tert-butyl ester)-carbamoyl]-pterostilbene (**13**): A solution of valine-*tert*-butyl ester hydrochloride (1.0 g, 4.8 mmol, 1.0 eq) and DMAP (2.3 g, 19 mmol, 4.0 eq) in anhydrous DCM (20 mL) was added dropwise to a solution of bis-(4-nitrophenyl) carbonate (1.5 g, 4.8 mmol, 1.0 eq) in anhydrous DCM (10 mL). The resulting mixture was stirred at 50 °C for 4 hours. Pterostilbene (1.6 g, 6.1 mmol, 1.3 eq) was then added to the

solution. The resulting mixture was stirred at 50°C overnight, and then it was diluted in DCM (100 mL) and extracted with HCl 0.5 M (2 × 100 mL). The organic layer was dried over $MgSO_4$ and filtered. The solvent was evaporated off under reduced pressure and contaminating residual PNPC-Val-OtBu was eliminated by flash chromatography using Petroleum Ether/Acetone/DEE (7:1:2). The fraction collected was further purified from residual 4-nitrophenol by flash chromatography using Petroleum Ether/DCM/Acetone = (5:4:1). The solvent was evaporated off under reduced pressure to afford **14** (1.4 g, 73 % yield) as a pale yellow oil. MS-ESI (ion trap) = 456 m/z $[M + H]^+$; ^1H NMR ($CDCl_3$, 500 MHz) δ (ppm): 7.46 (d, 2H, J = 9.2 Hz), 7.14 (d, 2H, J = 10.1 Hz), 6.92-7.05 (m, 2H), 6.66 (d, 2H, J = 3.1 Hz), 6.40 (t, 1H, J = 3.1 Hz), 5.91 (t, 1H), 4.27-4.30 (m, 1H), 3.78 (s, 6H), 2.20-2.06 (m, 1H), 1.50 (s, 9H), 1.04-0.965 (m, 6H); ^{13}C NMR ($CDCl_3$, 126 MHz) δ (ppm): 170.86, 160.85, 154.36, 150.44, 139.12, 134.23, 128.43, 128.09, 127.22, 121.64, 104.43, 99.87, 81.96, 59.41, 55.11, 31.36, 27.89, 18.85, 17.34.

4'-[N-(valinyl)-carbamoyl]-pterostilbene (**5**): TFA (5.0 mL, 65.3 mmol, 41 eq) was added to a solution of **14** (0.72 g, 1.6 mmol, 1.0 eq) and TIPS (0.5 mL, 5 % v/v) in anhydrous DCM (5 mL). The mixture was stirred at 0 °C overnight. TFA and the solvent were evaporated off under reduced pressure. Toluene (2 × 5 mL) was then added and the solvent was stripped off under reduced pressure to remove traces of TFA. The residue was purified by flash chromatography using Petroleum Ether/Acetone (6:4) as eluent, to afford **5** as a white solid (0.45 g, 72 % yield). MS-ESI (ion trap) = 400 m/z $[M + H]^+$; ^1H NMR (500 MHz, $CDCl_3$) δ (ppm) = 7.49 (d, 2H, J = 10.1 Hz), 7.14 (d, 2H, J = 10.2 Hz), 6.95-7.07 (m, 2H), 6.66 (d, 2H, J = 3.1 Hz), 6.40 (t, 1H, J = 3.1 Hz), 5.57 (d, 1H, J = 10.1 Hz), 4.41-4.44 (m, 1H), 3.83 (s, 6H), 2.29-2.35 (m, 1H), 1.09 (d, 3H), 1.02 (d, 3H); ^{13}C NMR (126 MHz, $CDCl_3$) δ (ppm) = 176.44, 161.10, 154.82, 150.40, 139.36, 134.81, 128.91, 128.35, 127.27, 121.86, 104.72, 100.22, 59.14, 55.53, 31.23, 19.20 17.52.

Synthesis of 4'-[N-(phenylalanin)-carbamoyl]-pterostilbene (6).

4'-[N-(phenylalanyl tert-butyl ester)-carbamoyl]-pterostilbene (**15**): A solution of L-phenylalanine-*tert*-butyl ester hydrochloride (0.51 g, 2.0 mmol, 1.0 eq) and DMAP (1.0 g, 8.5 mmol, 4.3 eq) in anhydrous DCM (4 mL) was added dropwise to a solution of PNPC (0.63 g, 2.1 mmol, 1.1 eq) in anhydrous DCM (5 mL). The resulting mixture was stirred at 50°C for 4 hours. Pterostilbene (0.67 g, 2.59 mmol, 1.3 eq) was then added to the solution. The resulting mixture was stirred at 50°C overnight, and then it was diluted in DCM (100 mL) and extracted with HCl 0.5 M (3 × 100 mL). The organic layer was dried over $MgSO_4$

and filtered. The solvent was stripped off under reduced pressure and the product was purified by flash chromatography using Chloroform/Ethyl Acetate (99.5:0.5) as eluent to afford **15** as a colourless oil (0.64 g, 66 % yield). MS-ESI (ion trap): 504 m/z $[M + H]^+$; ^{1}H NMR (200 MHz, CDCl3) δ (ppm) = 7.52 (d, J = 8.6 Hz, 2H), 7.33 (m, 5H), 7.09 (m, 4H), 6.70 (d, J = 2.1 Hz, 2H), 6.44 (t, J = 2.1 Hz, 1H), 5.61 (m, 1H), 4.63 (m, 1H), 3.87 (s, 6H), 3.20 (m, 2H), 1.48 (s, 9H). ^{13}C NMR (75 MHz, CDCl3) δ (ppm) = 170.46, 161.12, 153.87, 150.54, 139.39, 136.08, 134.61, 129.68, 128.78, 128.61, 128.41, 127.50, 127.21, 121.87, 104.69, 100.18, 82.71, 55.49, 38.48, 31.01, 28.05.

4'-[N-(phenylalanyl)-carbamoyl]-pterostilbene (**6**): TFA (4.5 mL, 59.7 mmol, 54 eq) and TIPS (0.450 mL, 5 % v/v) were added to a solution of **15** (0.64 g, 1.3 mmol, 1.0 eq) in anhydrous DCM (4.5 mL). The mixture was stirred at 0 °C overnight. TFA and the solvent were evaporated off under reduced pressure. Toluene (2 × 5 mL) was then added and the solvent was stripped off under reduced pressure to remove traces of TFA. The residue was purified by flash chromatography using DCM/Acetone (97:3) + 1% AcOH as eluent. The product was dissolved in acetonitrile (ACN)/water (3:7) and it was lyophilized to afford **6** as a white solid (0.38 g, 67.4 % yield). MS-ESI (ion trap): 448 m/z $[M + H]^+$; ^{1}H NMR (500 MHz, DMSO) δ(ppm) = 8.31 (s, 1H), 8.19 (m, 1H), 7.57 (d, J = 8.6 Hz, 2H), 7.29 (m, 5H), 7.06 (m, 4H), 6.77 (d, J = 2.2 Hz, 2H), 6.41 (t, J = 2.2 Hz, 1H), 4.25 (m, 1H), 3.77 (s, 6H), 3.15 (m, 1H), 2.92 (m, 1H). ^{13}C NMR (126 MHz, DMSO) δ (ppm) = 173.42, 161.13, 154.68, 150.85, 139.52, 138.23, 134.34, 129.65, 128.72, 128.52, 127.78, 126.96, 122.19, 104.91, 100.37, 79.65, 56.16, 55.67, 36.97.

Synthesis of 4'-[N-(asparagyl)-carbamoyl]-pterostilbene (7).

4'-[N-(asparagyl-tert-butyl ester)-carbamoyl]-pterostilbene (**16**)**:** A solution of L-asparagine-*tert*- butyl ester hydrochloride (0.40 g, 1.8 mmol, 1.0 eq) and DMAP (0.89 g, 7.3 mmol, 4.0 eq) in anhydrous ACN (6 mL) and DCM (7 mL) was added dropwise to a solution of PNPC (0.57 g, 1.9 mmol, 1.0 eq) in anhydrous ACN (5 mL). The resulting mixture was stirred at -15 °C for 15 minutes. Pterostilbene (0.60 g, 2.4 mmol, 1.3 eq) was then added to the solution. The resulting mixture was stirred at -15 °C for 2 h and at r.t. overnight. The mixture was diluted in DCM (50 mL) and extracted with HCl 0.5 M (50 mL). The aqueous layer was further extracted with DCM (3 × 10 mL). The combined organic layers were dried over $MgSO_4$ and filtered. The solvent was stripped off under reduced pressure and the product was purified by flash chromatography using Ethyl acetate (EtOAc)/Petroleum Ether (8:2) as eluent to afford **16** as a colourless oil (0.58 g, 69 %

yield). MS-ESI = 493 m/z $[M + Na]^+$; ^1H NMR (300 MHz, $CDCl_3$) δ (ppm) = 7.47 (d, *J* = 8.5 Hz, 2H), 7.15 – 6.84 (m, 4H), 6.65 (d, *J* = 1.9 Hz, 2H), 6.39 (m, 2H), 5.87 (m, 2H) 4.49 (m,1H), 3.82 (s, 6H), 2.83 (m, 2H), 1.48 (s, 9H). ^{13}C NMR (75 MHz, $CDCl_3$) δ (ppm) = 172.50, 169.86, 161.10, 154.64, 150.53, 139.35, 134.65, 128.83, 128.35, 127.50, 121.92, 104.69, 100.19, 82.79, 77.16, 55.48, 51.51, 37.29, 27.99.

4'-[N-(asparagyl)-carbamoyl]-pterostilbene (**7**): TFA (6.2 mL, 80 mmol, 50 eq) kept at -15 °C was added dropwise to a stirred solution of **16** (0.76 g, 1.6 mmol, 1.0 eq) and TIPS (0.62 mL) (5 % v/v) in anhydrous DCM (6.2 mL) at -15 °C and the resulting solution was warmed to RT over 1 hour. The mixture was stirred at room temperature for a further 4 hours. TFA and the solvent were stripped off under reduced pressure. Toluene (2 × 5 mL) was then added and the solvent was stripped off under reduced pressure to remove traces of TFA. The residue was purified by flash chromatography using DCM/MeOH (97.5:2.5) + 1% AcOH, to afford **7** as a white solid (0.5 g, 76 % yield). MS-ESI (ion trap) = 415 m/z $[M + H]^+$; ^1H NMR (300 MHz, DMSO) δ (ppm) = 7.98 (m, 1H), 7.60 (d, *J* = 8.5 Hz, 2H), 7.34 – 6.88 (m, 4H), 6.78 (d, *J* = 1.7 Hz, 2H), 6.42 (m, 1H), 4.40 (m, 1H), 3.78 (s, 6H), 2.75 – 2.53 (m, 2H); ^{13}C NMR (75 MHz, DMSO) δ (ppm) = 172.90, 171.16, 160.68, 153.98, 150.47, 139.08, 133.89, 128.28, 128.09, 127.34, 121.79, 104.47, 99.92, 55.21, 50.84, 39.52, 36.66.

Synthesis of 4'-[N-(threonyl)-carbamoyl]-pterostilbene (8).

[N-(tert-butyl-threonyl-tert-butyl)-carbamoyl]-pterostilbene (**17**): A solution of *O-tert*-butyl threonine-*tert*-butyl ester (1.6 g, 6.9 mmol, 1.0 eq) and DMAP (3.4 g, 27.8 mmol, 4.0 eq) in THF (30 mL) was added dropwise to a solution of PNPC (2.1 g, 6.9 mmol, 1.0 eq) in THF (15 mL), and the mixture was stirred at room temperature for 3 hours. Pterostilbene (2.30 g, 9.0 mmol, 1.3 eq) was then added to the solution. The resulting mixture was stirred at 50°C overnight, and then it was diluted in DCM (100 mL) and extracted with HCl 0.5 M (3 × 100 mL). The organic layer was dried over $MgSO_4$ and filtered. The solvent was stripped off under reduced pressure and the product was purified by flash chromatography using Petroleum Ether/Acetone/DEE (8:1:1) as eluent to afford **16** as a colourless oil (2.69 g, 78 % yield). MS-ESI (ion trap): 513 m/z $[M + H]^+$; ^1H NMR ($CDCl_3$, 300 MHz) δ (ppm): 7.47 (d, 2H, J = 6.1 Hz), 7.155 (d, 2H, J = 9.2 Hz), 6.92-7.07 (m, 2H), 6.65 (d, 2H, J = 3.0 Hz), 6.39 (t, 1H, J = 3.1 Hz), 5.82 (d, 1H, J = 9.1 Hz), 4.23-4.26 (m, 1H), 4.12-4.16 (m, 1H), 3.80 (s, 6H), 1.49 (s, 9H), 1.27 (d, 3H, J = 6.2 Hz), 1.19 (s, 9H); ^{13}C NMR

($CDCl_3$, 300 MHz) δ (ppm): 169.85, 160.99, 154.92, 150.64, 139.27, 134.37, 128.29, 121.78, 104.55, 100.02, 82.04, 71.88, 67.17, 60.56, 55.28, 28.74, 28.08, 21.05.

4'-[N-(threonyl)-carbamoyl]-pterostilbene (**8**): TFA (5.0 mL, 65 mmol, 37 eq) maintained at -15 °C was added dropwise to a stirred solution of **17** (0.89 g, 1.8 mmol, 1.0 eq) and TIPS (0.5 mL) (5 % v/v) in anhydrous DCM (5 mL) kept at -15 °C and the resulting solution was warmed to RT over 1 hour. The mixture was then stirred at room temperature for a further 4 hours. TFA and the solvent were stripped off under reduced pressure. Toluene (2 × 5 mL) was then added and the solvent was stripped off under reduced pressure to remove traces of TFA. The residue purified by flash chromatography using DCM/MeOH (97.5:2.5) + 1% AcOH, to afford **8** as a white solid (0.5 g, 69 % yield). MS-ESI (ion trap) = 402 m/z $[M + H]^+$; ^{1}H NMR (DMSO, 300 MHz) δ (ppm): 7.54-7.62 (m, 3H), 7.06-7.31 (m, 4H), 6.78 (d, 2H, J = 3.1 Hz), 6.42 (t, 1H, J = 3.1 Hz), 4.12-4.19 (m, 1H), 4.00-4.04 (m, 1H), 3.78 (s, 6H), 1.16 (d, 3H, J = 6.1 Hz); ^{13}C NMR (75 MHz, DMSO) δ (ppm) = 171.97, 160.67, 154.85, 150.50, 159.07, 133.93, 128.18, 127.35, 121.85, 104.47, 99.92, 66.39, 60.23, 55.21, 20.42.

Synthesis of 4'-[N-(aspartic acid)-carbamoyl]-pterostilbene (9).

4'-[N-(aspartic acid di-tert-butyl ester)-carbamoyl]-pterostilbene (**18**): A solution of L-aspartic acid-di-*tert*-butyl ester hydrochloride (0.50 g, 1.8 mmol, 1.0 eq) and DMAP (0.84 g, 6.9 mmol, 3.8 eq) in anhydrous ACN (7.0 mL) was added dropwise to a solution of PNPC (0.58 g, 1.92 mmol, 1.1 eq) in anhydrous ACN (3 mL). The resulting mixture was stirred at 50 °C for 10 minutes. Pterostilbene (0.6 g, 2.3 mmol, 1.3 eq) was then added to the solution. The mixture was stirred at 50°C for 1 hour, and then it was diluted in DCM (100 mL) and extracted with HCl 0.1 M (100 mL); the aqueous layer was further extracted with DCM (3 × 100 mL). The combined organic layers were dried over $MgSO_4$ and filtered. The solvent was evaporated off under reduced pressure and the product was purified by flash chromatography using DCM/petroleum ether/acetone (5.5:4:0.5) as eluent to afford **18** as a colourless oil (0.58 g, 62 % yield). MS-ESI (ion trap) = 550 m/z $[M + Na]^+$; ^{1}H NMR (300 MHz, $CDCl_3$) δ (ppm) = 7.48 (d, *J* = 8.7 Hz, 2H), 7.18 – 6.88 (m, 4H), 6.66 (d, *J* = 2.2 Hz, 2H), 6.39 (t, *J* = 2.2 Hz, 1H), 6.06 (m, 1H), 4.50 (m, 1H), 3.82 (s, 6H), 2.87 (m, 2H), 1.47 (s, 18H). ^{13}C NMR (75 MHz, $CDCl_3$) δ (ppm) = 171.86, 171.28, 162.72, 155.96, 152.20, 141.00, 136.21, 130.37, 130.03, 129.11, 123.50, 106.28, 101.78, 84.26, 83.46, 57.45, 57.08, 52.83, 39.41, 29.83, 29.76, 29.68, 29.61.

4'-[N-(aspartic acid)-carbamoyl]-pterostilbene (**9**): TFA (3.4 mL, 44 mmol, 40 eq) at -15 °C was added dropwise to a stirred solution of **18** (0.58 g, 1.1 mmol, 1.0 eq) and TIPS (0.34 mL; 5 % v/v) in 3.4 mL of anhydrous DCM at 0 °C and the resulting solution was warmed to RT over 1 hour. The mixture was then stirred at room temperature for a further 4 hours. TFA and the solvent were stripped off under reduced pressure. Toluene (2 × 5 mL) was then added and the solvent was stripped off under reduced pressure to remove traces of TFA. The residue was purified by flash chromatography using Chloroform/MeOH (95:5) + 1% AcOH, to afford **9** as a white solid (0.33 g, 72 % yield). MS-ESI (ion trap) = 416 m/z $[M + H]^+$; ^{1}H NMR (300 MHz, DMSO) δ (ppm) = 8.10 (m, 2H), 7.60 (d, *J* = 8.2 Hz, 1H), 7.36 – 6.98 (m, 4H), 6.78 (m, 2H), 6.39 (m, 1H), 4.39 (m, 1H), 3.78 (s, 6H), 2.72 (m, 2H); ^{13}C NMR (75 MHz, DMSO) δ (ppm) = 172.33, 171.61, 160.66, 154.02, 150.42, 139.05, 133.92, 128.29, 128.06, 127.33, 121.77, 104.45, 99.91, 55.19, 50.68, 39.52, 36.06.

Synthesis of 4'-[N-(arginyl)-carbamoyl]-pterostilbene (10).

4'-[N-(arginyl-tert butyl-ester)-carbamoyl]-pterostilbene (**19**): A solution of L-arginine *tert* butyl ester di-hydrochloride (0.50 g, 1.7 mmol, 1.0 eq) and DMAP (0.42 g, 3.4 mmol, 2.0 eq) in anhydrous DCM (4 mL) was added dropwise to a solution of PNPC (0.52 g, 1.7 mmol, 1.0 eq) in anhydrous DCM (3 mL). The resulting mixture was stirred at -15°C for 5 hours. Then, a solution of pterostilbene (0.55 g, 2.1 mmol, 1.3 eq) and DMAP (0.21 g, 1.7 mmol, 1.0 eq) in anhydrous DCM (2 mL) was added to the solution. The resulting mixture was stirred at -15° C for two days and then diluted in EtOAc (100 mL) and extracted with HCl 0.5 M (100 mL). The aqueous layer was further extracted with EtOAc (3 × 100 mL). The combined organic layers were dried over $MgSO_4$ and filtered. The solvent was stripped off under reduced pressure and the product was purified by flash chromatography using DCM/MeOH (9:1) as eluent to afford **19** as a colourless oil (0.41 g, 48 % yield); MS-ESI = 513 m/z $[M+H]^+$; ^{1}H NMR (300 MHz, $CDCl_3$) δ = 7.43 (d, *J* = 8.2 Hz, 2H), 7.00 (m, 7H), 6.62 (m, 2H), 6.40 (m, 1H), 6.36 (m, 1H), 4.13 (m, 1H), 3.78 (s, 6H), 3.44 (s, 1H), 3.16 (m, 2H), 1.82 (m, 2H), 1.64 (m, 2H), 1.44 (s, 9H); ^{13}C NMR (75 MHz, $CDCl_3$) δ (ppm) = 171.27, 161.07, 157.50, 155.09, 150.38, 139.30, 134.74, 128.95, 128.20, 127.57, 121.99, 104.74, 100.19, 82.82, 77.16, 55.45, 54.36, 41.05, 28.18, 27.99.

4'-[N-(arginyl)-carbamoyl]-pterostilbene (**10**): TFA (3 mL, 39 mmol, 50 eq) at -15 °C was added dropwise to a stirred solution of **19** (0.41 g, 0.8 mmol, 1.0 eq) and TIPS (0.3 mL) (5 % v/v) in anhydrous DCM (3 mL) at -15 °C. The mixture was stirred at -15 °C for 3 hours

and then overnight at room temperature. TFA and the solvent were evaporated off under reduced pressure. Toluene (2 × 5 mL) was then added and the solvent was stripped off under reduced pressure to remove traces of TFA. The residue was purified by flash chromatography using DCM/MeOH (8:2) + 1% AcOH, to afford **10** as a white solid (0.27 g, 75 % yield). MS-ESI (ion trap) = 457 m/z $[M+H]^+$; ^{1}H NMR (300 MHz, DMSO) δ (ppm) = 8.11 (m, 1H), 7.89 (m, 1H), 7.60 (d, *J* = 8.5 Hz, 2H), 7.36 – 6.95 (m, 7H), 6.77 (d, *J* = 1.7 Hz, 2H), 6.41 (m, 1H), 4.02 (m, 1H), 3.78 (s, 6H), 3.15 (m, 2H), 1.81 (m, 2H), 1.62 (m, 2H); ^{13}C NMR (75 MHz, $CDCl_3$) δ 173.37, 160.69, 157.00, 154.34, 150.48, 139.07, 133.91, 128.29, 128.09, 127.38, 121.83, 104.48, 99.92, 55.22, 53.76, 39.52, 25.29.

Transcription Factor EB is a crucial transducer of the biochemical activity of the natural compound Pterostilbene

Abstract

Many natural compounds present to various extents in the human diet exhibit identifiable and potentially useful bioactivities in experiments and in some cases in statistical correlative studies. Among them, Pterostilbene (Pt) has drawn the attention of scientific community for its potential as a therapeutic/preventive agent in several sectors of health care and for its high bioavailability. Indeed, in rats Pt can reach micromolar concentrations in many organs after a single oral administration of 20 mg/Kg body weight.

Although the remarkable effects of this compound are widely recognized, much remains to be learned about its molecular mechanisms of action. Since it displays anti-proliferative, anti-obesity and neuro-protective effects, autophagy is thought to be one of them.

The master regulator of autophagy is Transcription Factor EB (TFEB). Its subcellular localization and activation depend on phosphorylation events mediated by the mammalian target of rapamycin complex1 (mTORC1) and Ca^{2+}-dependent phosphatase Calcineurin.

In view of the above, we set out:

1) To verify whether Pt and its two major metabolites (DiHydroPt and Pt-4-Sulfate), present in the body at high levels after polyphenol ingestion, may modulate TFEB activity and thus autophagy;
2) In case of positive response to the 1^{st} point, to check the signaling cascade upstream of TFEB migration

To this purpose, HeLa cells overexpressing TFEB-GFP were treated or not with the stilbenoids and monitored by confocal microscopy. RT-qPCR was performed to determine the expression levels of some TFEB target genes. Autophagy induction and the activation of some kinases that may regulate the transcription factor were evaluated by Western blotting. The implication of cAMP was also checked, by performing FRET-based experiments as well as HPLC/UV analyses.

Both Pt and DiHydroPt, in our system, caused the translocation to the nucleus of the transcription factor already at low, physiologically meaningful concentrations, but to a lesser extent than nutrients deprivation. Treatment with Pt or DiHydroPt also revealed an up-regulation of some selected TFEB target genes, while biochemical analyses supported the induction of autophagy showing an increase in the lipidation of LC3.

Pt induced an increase in cAMP levels that might partially account, through AMPK activation and consequent mTORC1 downregulation, for TFEB migration. Accordingly, Pt decreased the phosphorylation levels of S6, a mTORC1 target. On the contrary, the sulfated form was found to be ineffective. Our results, however, indicate that this pathway cannot fully account for the phenomenology. Therefore, we conclude that Pt enhances TFEB activity by modulating more than one signaling cascade. The involvement of reactive oxygen species and Ca^{2+} in the process is still under investigation. Using a superoxide probe and an anti-oxidant in *in vitro* experiments I have verified that treatment with Pt induces ROS production, which correlates with TFEB-GFP nuclear migration. Furthermore, inhibition of the Ca^{2+}-dependent phosphatase Calcineurin, known to dephosphorylate TFEB thus promoting its migration, antagonizes nuclear accumulation of the transcription factor, thus indicating a role – still to be confirmed – for Ca^{2+} signaling.

Introduction

Over the years, Pterostilbene (trans-3,5-dimethoxy-4-hydroxystilbene, Pt), a phenolic compound found in berries, has emerged for its health-promoting effects [1-3]. Furthermore, it is characterized by a higher bioavailability than most other plant polyphenols. Indeed, as reported by Azzolini et al. in 2014, methylation of two of the three hydroxyl groups on the stilbenic scaffold lends lipophilicity to the molecule, facilitates its intestinal absorption and provides a degree of protection from Phase II metabolism [4].

However Pt is not free of shortcomings a major one being that its molecular mechanisms of action have not been completely defined.

For a long time, natural polyphenols have been considered exclusively as anti-oxidants capable to directly scavenge free radicals or to chelate metal ions [5-9]. Instead, a huge amount of molecular investigations underpins the notion that they act mainly in a more “sophisticated” manner. In particular, they mediate the activity of key cellular “switches” turning on cellular defense systems such as the expression of enzymes counteracting oxidative stress or autophagy [10-16].

Several papers have reported that Pt up-regulates autophagy in different cell lines. [17-20]. Autophagy is a major evolutionary conserved catabolic pathway and is mainly controlled by Transcription Factor EB (TFEB) [21].
TFEB belongs to the family of the microphthalmia-associated transcription factors (MiTF) and it is responsible for the modulation of the expression of genes involved in lysosomal autophagy, lipophagy and fatty acids β-oxidation, sharing a 10bp palindromic motif called "coordinated lysosomal expression and regulation" (CLEAR), in their promoters [22-29].

The subcellular localization of this transcription factor is controlled by phosphorylation events. In the presence of nutrients, a complex formed by the lysosomal v-ATPase and small GTPases recruits and activates mTORC1 at the lysosomal surface. This latter, a metabolic sensor that consists of different subunits (mTOR itself, RAPTOR, MLST8, PRAS40 and DEPTOR) phosphorylates TFEB at serine 211 confining it in the cytosol through the interaction with 14-3-3 proteins. Conversely, in case of starvation or lysosomal stress, mTORC1 is inactivated [21, 30-33]. In this circumstance, the assembly and the activity of the heterodimer formed by Tuberous sclerosis proteins 1 and 2 (TSC1/2) are fundamental. TSC2, whose action is regulated by different kinases (e.g. AMPK activates it), is a GTPase activating protein (GAP) that when phosphorylated binds to the G protein Rheb. Upon this interaction, the molecule of GTP bound to Rheb is hydrolyzed to GDP and, therefore, it cannot anymore activate mTORC1 that detaches from lysosomal membranes. At the same time, lysosomal Ca^{2+} release occurs through the mucolipin1 channel. This leads to the activation of the Ca^{2+}-dependent phosphatase Calcineurin that dephosphorylates TFEB promoting its migration to the nucleus (**Fig.1**). [21, 33-35].

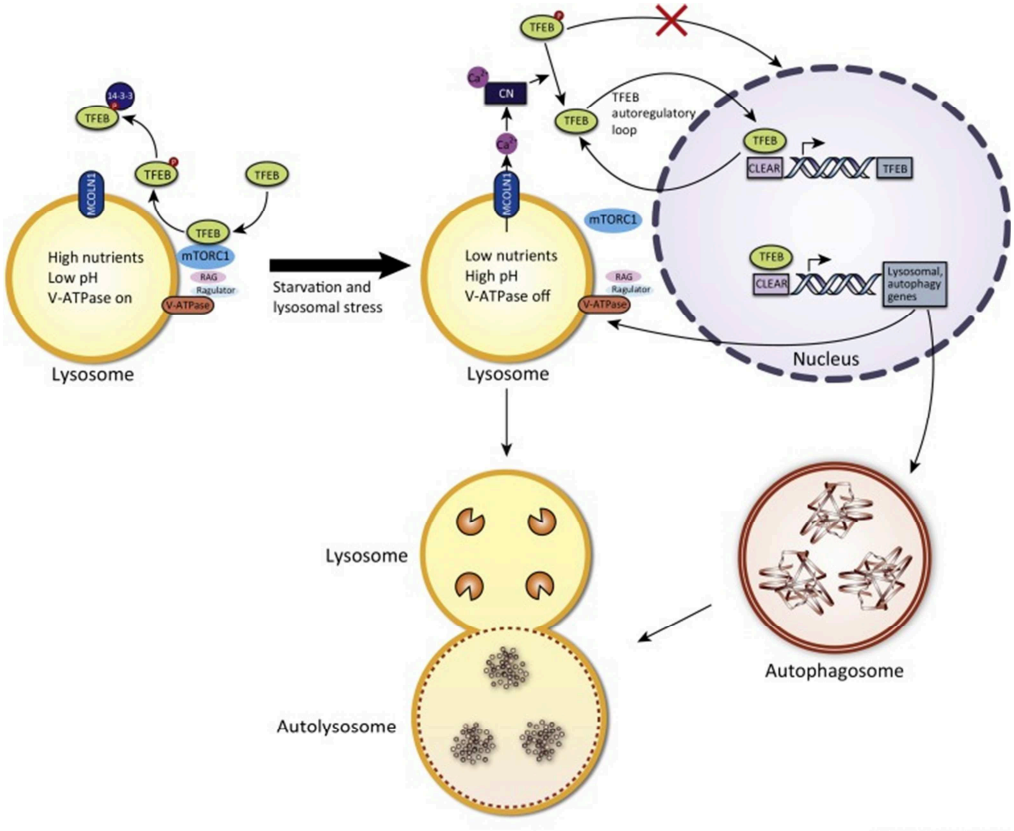


Fig.1: sketch of the "lysosome-to-nucleus pathway" from Martini-Stoica H. et al, 2016 [36].

Autophagy stimulation might underlie actions of Pt such as its capability to counteract obesity and metabolic disorders [37-41]. Both *in vitro* and *in vivo* studies indeed indicate that lipid droplets can be selectively sequestered in autophagosomes and delivered to lysosomes for degradation by acid lipases [42, 43]. Notably, as reported by Gómez-Zorita in 2014, Pt hinders fat accumulation in rats, fed with a highly caloric diet, by increasing the activity of AMP-activated protein kinase (AMPK) [44, 45]. This metabolic sensor, essential to cellular energy balance, has been known for a long time to inhibit mTORC1, in different contexts and through multiple mechanisms, and may be taken into account as a possible actor in the induction of TFEB migration and activation [46-48]. Accordingly, mice over-expressing TFEB in their liver have an elevated fatty acid catabolism as well as a high whole body energy expenditure and show a leaner phenotype if compared to Wild Type (WT) counterparts [25].

Furthermore, while the role of autophagy in tumoral cells is still matter of debate [49, 50], this process seems to be crucial in the preservation of cerebral plasticity [51-54]. Indeed, it has been reported that mice knock out (KO) for genes encoding key proteins of the autophagy core machinery undergo axonal degeneration and neuronal death [55, 56].

Alterations in autophagic flux may also lead to the accumulation of toxic protein aggregates and damaged organelles, typical hallmarks of aging and its related disorders [57-61]. Work carried out by Chang et al. in 2012 has demonstrated a considerable rescue in cognitive impairment in murine models of sporadic and aging-associated Alzheimer's disease following chronic administration of modest doses of Pt [62]. Remarkably these effects have been associated with an up-regulation of the peroxisome proliferator activated receptor alpha (PPARα) gene, a well-recognized TFEB target [25, 30, 63, 64].

Molecular processes behind cognition are extremely complex and many regulators are involved in their tune-up, one being the cAMP response elements binding protein (CREB) [65-67].

Recently, a new profile of this transcription factor has been outlined. In 2014, the research group of Prof. Kemper has reported that CREB, together with the fed-sensing nuclear farnesoid X receptor (FXR), defines a molecular axis resulting in the up-regulation of TFEB and its downstream autophagic genes at the hepatic level [68, 69]. This cross-talk might be likewise relevant elsewhere, e.g. for the maintenance of appropriate brain functionalities.

In light of these previous evidences, during my PhD program I wanted to address whether the TFEB transcription factor, as autophagy master regulator, might be an effector of Pt biomedical activities. Since this seemed to be the case, I investigated the signalling cascade(s) upstream of this phenomenon. Finally, since Pt, similarly to other polyphenols, is subjected to a considerable metabolism, so that metabolites are the main species present in the body after its ingestion, I checked the effectiveness of two Pt major metabolites in my experimental system.

Materials and methods

Chemicals: Pt was purchased from Waseta Int. Trading Co. (Shangai, P.R.China). Other starting reagents and solvents necessary for the chemical synthesis of metabolites were from Sigma-Aldrich.

Metabolites synthesis: This part of the work was performed by the group of Prof. Cristina Paradisi of the Department of Chemistry of the University of Padua. Pt-4'-Sulfate was synthesized as previously described in chapter 3, while DiHydroPt was prepared by

hydrogenation of the parent compound starting from the procedure reported by D.C. Rueda et al. in 2014 [70]. A solution of Pt (1mM) in absolute Ethanol (EtOH, 15 mL) was stirred under H_2 in the presence of 10% Palladium on carbon (Pd/C) for up to 6h. The reaction mixture was filtered over Celite to remove the catalyst and evaporated to dryness. The reaction residues were eliminated by flash column chromatography, using a Hexane/Ethyl acetate gradient, to afford target DiHydroPt (95% yield).

Cells Cultures: migration experiments were carried out in HeLa cells over-expressing a TFEB-GFP construct, kindly provided by Prof. Ballabio of TIGEM (Naples) and generated as described by Settembre et al., in 2012 [33]. They were cultured in high-glucose Dulbecco's Modified Eagle Medium (DMEM, Sigma-Aldrich) with phenol red, supplemented with 10% Fetal Bovine Serum (FBS, Euroclone). Their selection was maintained by adding Geneticin 418 (G418, 100μg/mL, Sigma-Aldrich) to the culture medium. One day prior the experiments, 200.000 cells were seeded in a glass coverslip (24mm diameter, BDH) and incubated overnight in DMEM supplemented with 10% of FBS at 37° C to allow adhesion. Before starting the treatment, the coverslip was mounted in an appropriate holder and adherent cells were gently rinsed with PBS (1X). Finally 1ml of Leibovitz's L-15 medium (without phenol red) was added. This strongly buffered medium is designed for supporting cell growth in low-CO_2 environments or without CO_2 equilibration, and therefore it was preferred over DMEM.
Western Blot, RT-qPCR analysis as well as mitochondrial mass measurement were performed in WT HeLa cells. They were grown following procedures similar to those adopted for engineered HeLa cells overexpressing the TFB-GFP chimera. In particular, one day prior to the experiment they were seeded into wells of multi-well plates (100.000/well in 12-well plates and 200.000/well in 6-well plates) and incubated with DMEM with 10% FBS. After about 6 hours, FBS and phenol red were removed to avoid interference during treatment with drugs.

Determination of TFEB-GFP migration to the nucleus: a LEICA SP2 confocal microscope was used to follow migration kinetics. The instrument was equipped with a thermostat (Medical System Corporation) set at 37°C. The light source was the emission from an Ar/HeNe laser at 488nm. TFEB migration was monitored for up to 3 hours after the addition of the desired compound. Images were taken through a 40X oil immersion objective every 15 minutes.

TFEB migration was measured as a fluorescence ratio nucleus/cytosol. ImageJ 1.48v (http://imagej.nih.gov/ij) software was used. A few circular fields (regions of interest, ROIs) were drawn within the area of the nuclear and cytosolic cross sections of a given cell and their mean pixel intensity reading was used for fluorescence ratio determinations. All ratios measured were combined to obtain a final average value of the TFEB-GFP nuclear/cytosolic concentration ratio for each time point. Numerosity (N) represents the number of cells analyzed.

Drugs and treatments: Treatments with Pt, DiHydroPt and Pt-4'-Sulfate were carried out at concentrations ranging from 1μM to 25μM. Additional drugs used were A769662 (Abcam, 25μM), Forskolin (Sigma-Aldrich, 25 μM) and IBMX (Abcam, 100μM), Cyclosporine A (CsA, Sigma-Aldrich 1μM), N-Acetyl-L-Cysteine (NAC, Sigma-Aldrich 1 and 10mM). All compounds were dissolved in sterile dimethyl sulfoxide (DMSO, Sigma-Aldrich). Stock solutions were prepared at 1000x the desired working solution concentration in order to fix the final DMSO percentage at 0.1% in all cases (including controls without drugs).

cAMP measurements: Cyclic nucleotide levels were measured by using the specific EPAC1-based FRET sensor H30 described by Ponsioen B. et al., in 2004 [71]. Briefly, WT HeLa cells seeded onto a glass coverslip, at 50-70% of confluence, were transiently transfected with the specific probes using the FuGENE-6 transfection reagent (Promega) according to manufacturer's instructions. Imaging experiments were performed 24-48 hours after transfection. Specifically, cells were maintained in Hepes-buffered Ringer-modified saline (125mM NaCl, 5mM KCl, 1mM Na_3PO_4, 1mM $MgSO_4$, 5.5mM glucose, 1mM $CaCl_2$ and 20mM Hepes, pH 7.5) at room temperature. Images were taken with an inverted microscope (IX50, 60x NA 1.4 oil immersion objective, Olympus), and acquired using custom-made software.
FRET fluctuations were measured as changes in the background-subtracted 480/545 nm fluorescence emission intensities on excitation at 430 nm and expressed as either R/R_0, where R is the ratio at time t and R_0 is the ratio at time = 0 s, or $\Delta R/R_0$ where $\Delta R = R-R_0$.

Phosphodiesterases (PDEs) activity assays: adherent cells were detached using trypsin (0.05%) and centrifuged (200g, 10 minutes, room temperature). Next they were rinsed with HBSS, re-suspended in an appropriate buffer (Tris-HCl 50mM, $MgCl_2$ 10mM, pH 8),

supplemented with protease inhibitor, at the final density of 3.000.000 cells/mL and sonicated (three times, 10 seconds/each). cAMP to a final concentration of 100µM was added to the lysate. 150 µL samples of the suspension were collected at 0, 10, 30 and 60 minutes after cAMP addition, boiled for 2 minutes and centrifuged at 12000g for 5 minutes. Finally, the supernatant was collected and analyzed with a HPLC/UV (1290 Infinity LC System, Agilent Technologies) by using a reverse phase column (Zorbax RRHD Eclipse Plus C18, 1.8 µm, 50 x 2.1 mm i.d.; Agilent Technologies) and a UV diode array detector (190-500 nm). Solvents A and B were water containing 0.1% trifluoroacetic acid (TFA, Sigma-Aldrich) and acetonitrile (CAN, Sigma Aldrich), respectively. The gradient for B was as follows: 1% for 1 minute, and then from 1% to 100% in 2 minutes. The flow rate was 0.5 mL/min. The eluate was preferentially monitored at 254 nm.

Western blots: Cells were lysed in RIPA buffer supplemented with fresh proteases and phosphatases inhibitors cocktails 2 and 3 (Sigma-Aldrich). Then, the lysate was kept in ice for 30 minutes, in order to achieve the total brakeage of cell membranes, and centrifuged (12000g, 20min, 4° C). The resulting supernatant was collected and stored at -80° C. Protein content was estimated with the Bradford or BCA assays. Prior to electrophoresis, samples were supplemented with sample buffer (1X: 62.5mM Tris-HCl pH 6.8, 2% SDS, 10% glycerol, 50mM DTT, 0.02% bromophenol blue) and heated for 5 minutes. Pre-cast Bis-Tris gels (NUPAGE, Invitrogen) at different percentages of acrylamide were used depending on the molecular weight of the proteins of interest. After electrophoretic separation, proteins were transferred to PVDF membranes (Pall Corporation). Next, the membranes were saturated with 5% BSA (Sigma-Aldrich) at room temperature for 1 hour and incubated with primary antibodies overnight at 4° C. The following day, the membranes were washed with TBS Tween 0.1% (TBST) and incubated with IRDye 680RD or 700DX secondary antibodies (LICOR). Finally, they were washed one more time before detection with the Odissey Imaging System (LICOR).
Antibodies against the following proteins were used: LC3B (Cell Signaling, Rb, monoclonal, 1:1000); phospho-S6 (Cell Signaling Ser235/236, Rb, monoclonal, 1:1000); phospho-CREB (Cell Signaling, Rb, monoclonal, 1:1000); β-Actin (Cell Signaling, Ms, monoclonal, 1:5000).

RT-qPCR analyses: Total RNA was extracted from cells using TRIzol (Invitrogen). Reverse transcription was performed by using the SuperScriptVILO cDNA synthesis Kit

(Invitrogen). Reaction mix tubes were shaken and incubated first at 25° C for 10 minutes and then at 42° C for 60 minutes. Finally the reaction was arrested by heating at 85° C for 5 minutes. The expression levels of lysosomal TFEB target genes were measured.
All primers were purchased from Sigma-Aldrich. Primer sequences were as follows:

β-Actin (*Actb*): Fw CTCTTCCAGCCTTCCTTCCT; Rv AGCACTGTGTTGGCGTACAG

Transcription Factor EB (*tfeb*): Fw CCAGAAGCGAGAGCTCACAGAT; Rv TGTGATTGTCTTTCTTCTGCC

ATPase H^+ Transporting lysosomal V1 subunit H (*ATPase6V1H*) Fw GGAAGTGTCAGATGATCCCCA; Rv CCGTTTGCCTCGTGGATAAT

Cathepsin F (*ctsf*): Fw ACAGAGGAGGAGTTCCGCACTA; Rv GCTTGCTTCATCTTGTTGCC

Mucolipin 1 (*mcoln1*): Fw: TTGCTCTCTGCCAGCGGTACTA; Rv GCAGTCAGTAACCACCATCGG

Tripeptidyl Peptidase 1 (*tpp1*): Fw GATCCCAGCTCTCCTCAATACG; Rv GCCATTTTTGCACCGTGT

Peroxisome Proliferator-Activated receptor γ Coactivator 1α (*ppargc1a*) Fw: AAACAGCAGCAGACAAATGC; Rv TTGGTTTGGCTTGTAAGTGTTGTG

IQ Syber Green Supermix (Biorad) was exploited as detection system. DDCt value was calculated between the controls and the treated samples. Lastly, the fold change was calculated using $2^{(-DDCt)}$. β-Actin was used as reference gene.

FACS analyses of mitochondrial content: WT HeLa cells were detached, centrifuged (200g, 10 minutes) and stained with Acrydine Orange 10-nonyl Bromide (NAO, Sigma-Aldrich) at a final concentration of 2μM in DMEM (no phenol red, no FBS; incubation in darkness at 37°C, 30 minutes). Finally, they were re-suspended in HBSS. A Beckton Dickinson II flow cytometer was used and 10000 events were counted for each measurement.

ROS measurements: one day prior to the experiment, 200.000 WT HeLa cells were seeded onto a glass coverslip, similarly to the migration experiments, with DMEM supplemented with 10% of FBS and incubated at 37° C. The following day, the coverslip was mounted in an appropriate holder. Cells were gently rinsed with PBS (1X) and next

loaded with 1μM MitoSOX Red (Invitrogen), in the presence of 0.8μM CsH, at 37° C for 30 minutes in the darkness. MitoSOX fluorescence increase kinetics were followed for up to 90 minutes with a LEICA SP2 confocal microscope. Excitation was at 500–520 nm, and fluorescence was collected at $\lambda > 570$ nm. Images were captured every 30 minutes.
ImageJ 1.48v software was used for measurements. ROIs were drawn following the cell perimeter and their relative fluorescence intensity was followed over the captured time points.

Statistical analyses: TWO-WAY ANOVA analysis for repeated measures as a function of time and treatment was performed as statistical test in migration and ROS measurement experiments to compare drug efficacies versus vehicle (DMSO) or the effects of different compounds with respect to each other. Dunnett's or Tukey's correction were applied, respectively. All available analogous experimental results (TFEB-GFP migration or Mitosox fluorescence measurements) were included in a single statistical test. Statements about the significance of observed differences with respect to control are based on these analyses. When using Western Blot or RT-qPCR the efficacy of Pt or DiHydroPt was evaluated by applying Kruskal-Wallis' non-parametric test, with Dunn's correction, and ONE-WAY ANOVA respectively. GraphPad Prism 7.02 software was used in all cases.

Results and discussion

1. Pt stimulates TFEB nuclear translocation.

In order to verify whether Pt may induce TFEB translocation from the cytosol to the nucleus, HeLa cells overexpressing a TFEB-GFP construct [33] were treated with the compound. As positive control for our experimental system, we chose incubation with HBSS. This medium allows the preservation of the pH and the osmotic balance, provides water and essential organic ions, but contains no amino acids. Therefore, it rapidly leads to mTORC1 detachment from lysosomal membranes and its inhibition. As a consequence, TFEB is no longer phosphorylated and may migrate to the nucleus.
As hypothesized, Pt 25μM induced a consistent migration of TFEB but with slower kinetics than those observed under nutrient deprivation conditions. Indeed, while starved cells show a maximal TFEB nuclear localization within 1 hour, Pt acts more progressively. Conversely, the addition of DMSO, used as vehicle, had no effects (**Fig.2**).

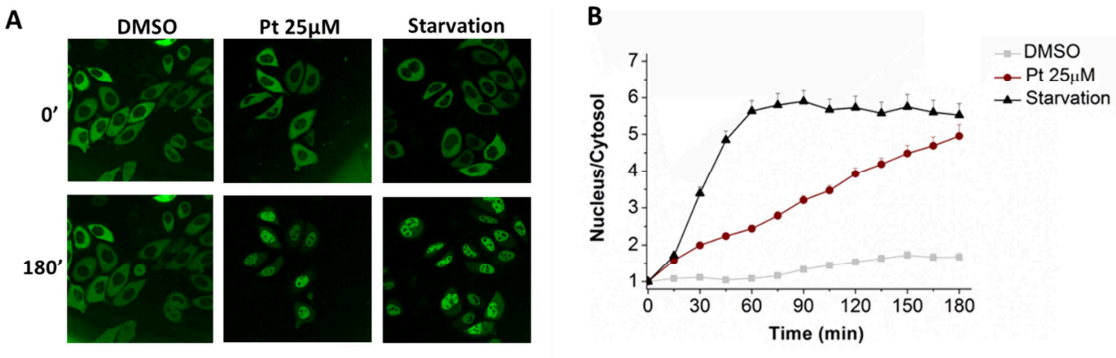


Fig.2 Pt induces TFEB nuclear translocation. (**A):** Representative images of HeLa cell over-expressing the TFEB-GFP chimera prior or following three hours treatments as indicated. (**B):** The kinetics of migration were faster in the case of HBSS-induced starvation than upon addition of Pt 25µM. A statistically significant difference with respect to control (DMSO) was reached at 30 minutes both for incubation with HBSS ($p \leq 0.0001$) and addition of Pt in Leibovitz's medium ($p \leq 0.05$). N ≥ 27; Error bars reported as standard error of the mean (SEM).

Pt concentrations in the 25µM range are however difficult to reach *in vivo*. Our previous pharmacokinetic analysis in rats showed that Pt can reach such levels only in some organs, such as the liver and the kidneys, following a moderate oral administration (chapter 3) [4]. Thus, we sought to define the effects of more physiologically relevant doses such as 1 and 10µM. As shown in **Fig.3** both concentrations drave the transcription factor into the nuclei of cells. While Pt 10µM was about as effective as Pt 25µM, lower TFEB nucleus/cytosol ratios were measured at all times upon exposure to Pt 1µM.

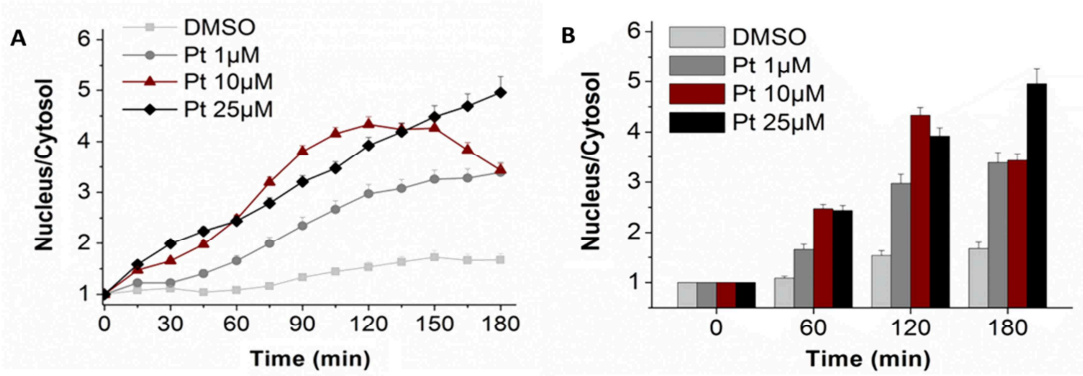


Fig.3 Pt triggers TFEB nuclear translocation already at low and physiologically meaningful concentrations. (**A,B**): While Pt 10µM is as potent as Pt 25µM, Pt 1µM is slightly less effective. Statistical analyses show that treatment with Pt 10µM or Pt 1µM caused a significant difference with respect to control at 45 ($p \leq 0.05$) or 75 minutes ($p \leq 0.05$) respectively. Significance of the divergence was reached at 30 minutes in the case of Pt 25µM vs Pt 1µM ($p \leq 0.001$); at 45 minutes for Pt 10µM vs Pt 1µM ($p \leq 0.05$); at 90 minutes for Pt 25µM vs Pt 10µM ($p \leq 0.05$). N ≥ 27; Error bars indicate SEM.

2. Evaluation of the efficacy of the major metabolites of Pt.

Notoriously, phenolic compounds are subjected to an intense metabolism. Particularly, their free hydroxyl group(s) represent preferential sites of action for phase II enzymes mediating conjugative reactions such as sulfation and glucuronidation. We reported that Pt-4'-Sulfate is the major Pt metabolite in rats and that following an oral administration of pharmacological doses of Pt its concentrations are higher compared to those of the parent compound in each organ tested, with the only exception of the brain (chapter 3) [4]. Pt may undergo other metabolic transformations by gut microbiota, such as reduction of the characteristic stilbenic double bound resulting in the formation of DiHydroPt. Consequently, metabolites are the main species in the body after a polyphenol's ingestion.

This high rate of metabolic transformations led several authors to propose that the beneficial actions ascribed to the phenolic compounds might actually be accounted for by their metabolites [72-76]. In light of this, we addressed the effectiveness of Pt-4'-Sulfate and DiHydroPt, in our experimental system. As they have been reported to be present at high concentrations in the organs and in the intestine respectively, we tested these molecules only at 25μM.

Interestingly, as shown in **Fig.4**, DiHydroPt triggered the nuclear migration of the transcription factor. However, the kinetics indicate an effectiveness comparable to that of Pt 1μM. On the other hand, the sulfated form was almost ineffective and induced only a small shift of TFEB to the nucleus, if any.

A possible explanation for these behaviors might be found in the different chemical properties of these molecules. Indeed, while DiHydroPt is relatively apolar and can passively diffuse through cell membranes, the negatively charged sulfate has an elevated hydrophilicity that confines it outside the cells.

These results may underpin epidemiological studies that link consumption of polyphenols to a lower risk of colon cancer [77-83].

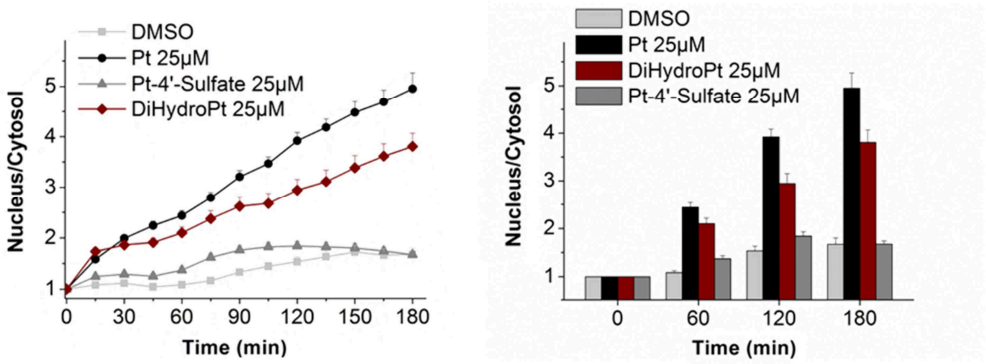


Fig.3 Activity of the major Pt metabolites. (**A,B**): While DiHydroPt formed by intestinal bacterial flora perturbs TFEB distribution, Pt-4'-Sulfate is almost ineffective. TWO-WAY ANOVA analyses show that the reduced form causes a statistically relevant difference vs control at 45 minutes ($p \leq 0.05$). The divergence between the effects of Pt vs Pt-4'-Sulfate becomes significant at 30 minutes ($p \leq 0.01$); the difference in the effect of DiHydroPt vs Pt-4'-Sulfate is significant at 30 minutes ($p \leq 0.05$); Pt vs DiHydroPt at 90 minutes ($p \leq 0.05$). $N \geq 27$; Error bars reported as SEM.

3. Pt induces autophagy onset.

As previously mentioned, Transcription Factor EB plays a pivotal role in the regulation of autophagic and lysosomal genes. Furthermore, it can also sustain its own expression [25].

As just mentioned, our experiments showed that both Pt and DiHydroPt can trigger TFEB migration to the nucleus.

To confirm their capability to affect the activation of the autophagy master regulator, we decided to measure the expression levels of the TFEB gene itself following treatment with these stilbenoids. These analyses were carried at one day post the addition of the compounds to WT HeLa cells in their culture media since transcriptional events usually take a relatively long time. Moreover, we wanted to verify that the effects we observed were not limited to the TFEB-GFP expressing cell line. The effectiveness of Pt-4'-Sulfate was not assessed given that it did not alter the cellular localization of the transcription factor.

In agreement with migration experiments, RT-qPCR analysis (**Fig.5**) showed that Pt and DiHydroPt significantly up-regulated the TFEB transcript. Remarkably, this effect was again observed also at low doses of Pt.

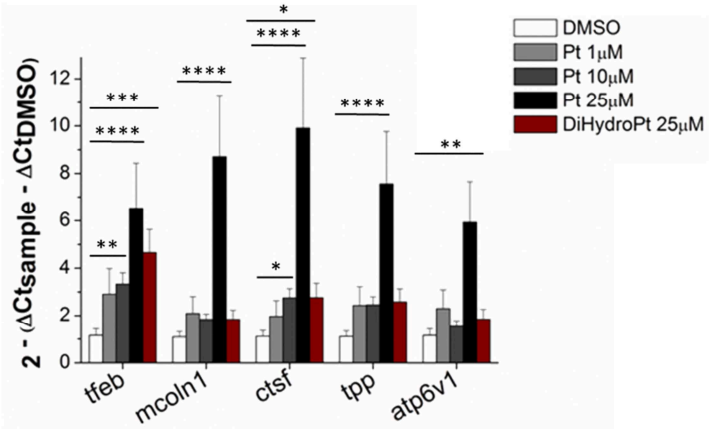


Fig. 5: both Pt and DiHydroPt enhance the expression of TFEB and its target genes. Pt 25μM showed the most potent effect. ONE-WAY ANOVA analyses, applying Tukey's correction. N ≥ 5; Error notation: +SEM. Bar extremities correspond to the columns to be compared; asterisks denote significance: * ≤ 0.05; ** ≤ 0.01; *** ≤ 0.001; **** ≤ 0.0001.

Furthermore, we also checked the expression levels of some TFEB target genes. Particularly, we selected those genes whose transcripts, according to the work of Prof. Ballabio and collaborators, were the most strongly up-regulated following TFEB overexpression such as: *mcoln1* (encoding an endosomal/lysosomal channel), *atp6v1* (encoding a subunit of a lysosomal proton pump), *tpp1* and *ctsf* (encoding two proteolytic enzymes).

As reported in **Fig. 5**, all of them were up-regulated by treatment with both Pt and DiHydroPt. However, Pt 25 μM was the specie and the concentration most notably effective.

Finally, in order to verify autophagy onset, we looked at microtubule-associated protein1 light chain 3 (LC3). Following its translation, LC3 is proteolytically cleaved resulting in the LC3I form with a carboxy-terminal exposed glycine. Upon autophagy induction, this amino-acidic residue is conjugated to the highly lipophilic phosphatidylethanolamine moiety to generate LC3II (also known as LC3B). This phosphatidylethanolamine group, in turn, allows the integration of the protein into lipid membranes at the autophagosome. Therefore, LC3II is widely recognized as an autophagic marker.

Western blot analysis revealed an increase in the lipidation levels of LC3 in WT HeLa cells already after 9 hours of treatment with Pt, confirming its pro-autophagic role (**Fig.6**). Analyses aimed to assess the efficacy of the reduced form are still ongoing.

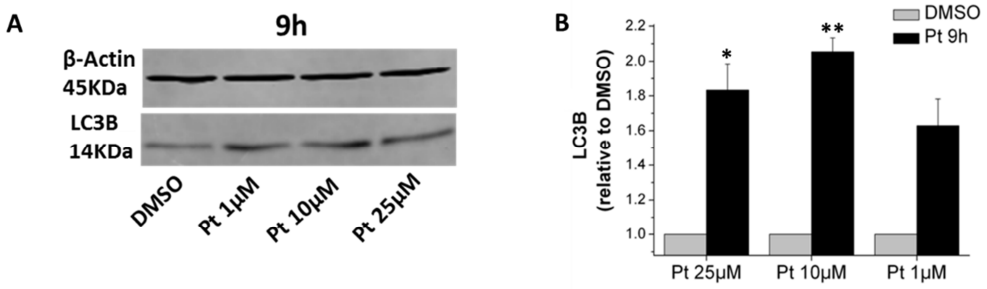


Fig.6: Pt treatment triggers autophagy onset. (**A,B**): Western blot and relative quantification of the lipidated form of LC3 protein. Statistical analysis, performed with Kruskal-Wallis' non-parametric test applying Dunn's correction, shows significance of the treatment with Pt 10μM vs DMSO ($p \leq 0.001$) and of Pt 25μM vs DMSO ($p \leq 0.05$). Reported are mean values +SEM; $N \geq 3$.

Overall, these experiments suggest that Pt triggers two parallel events. On the one hand, it promotes the engulfment of the material selected to be degraded; on the other, through the activation of transcription factor EB, enhances a transcriptional program able to sustain its elimination in the lysosomes.

4. Molecular mechanisms underlying TFEB migration.

4.1. Pt inhibits mTORC1:

Having established that Pt promotes TFEB activation as well as autophagy, next I turned to investigating the molecular mechanism underlying these phenomena. We first looked at mTORC1, as key cellular energy sensor.

When cells have adequate nutrients availability and proper growth factors, this kinase blocks autophagy by retaining TFEB in the cytosol and activates protein synthesis by promoting the activity of ribosomal protein S6. Conversely, in absence of nutrients, mTORC1 is turned off. At the same time, TFEB is activated and can stimulate lysosomal degradation of macromolecules to provide energy to cells, while translation is arrested as S6 is no longer phosphorylated.

Western Blot analysis of S6 revealed a time-dependent reduction of the phosphorylation levels of this protein by Pt 25μM in WT HeLa cells (**Fig.7 A, B**).

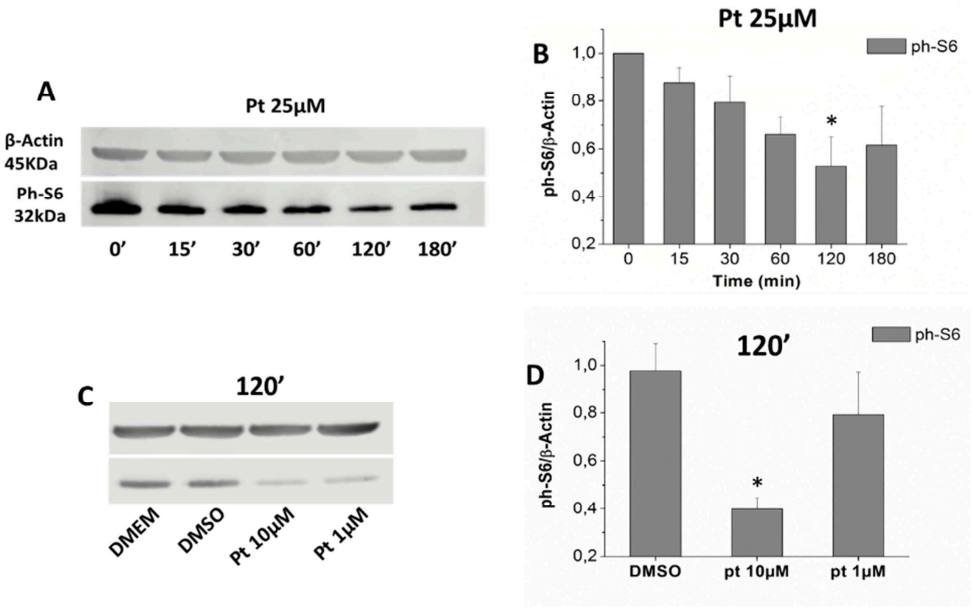


Fig. 7: Western blot analysis of ph-S6 ribosomal protein. (**A**,**B**) Pt progressively reduces the phosphorylation level of this mTORC1 target with maximal inhibition after 2 hours ($p \leq 0.05$). (**C**, **D**) While Pt 25μM and 10μM had a similar effect ($p \leq 0.05$ at 2h vs control), Pt 1μM was less effective. Kruskal-Wallis' non-parametric test applying Dunn's correction. Reported are mean values +SEM; $N \geq 4$.

Since this effect was maximal 2 hours after the beginning of the treatment, we decided to test lower doses of Pt only at this time point. In agreement with migration experiments, while Pt 10μM was about as effective as Pt 25μM, Pt 1μM was less powerful, inducing only a faint dephosphorylation of S6 (**Fig.7 C, D**).

While these results do not exclude an action on Calcineurin, they suggest that Pt stimulates, at least partially, TFEB nuclear migration by hindering the phosphorylation of the transcription factor by mTORC1.

4.2 The involvement of cAMP and its downstream signaling:

A key role in the regulation of mTORC1 activity is played by AMPK. It has been already reported that Pt enhances the activity of this kinase in a different context [44]. However, the modalities by which this phenomenon occurs have not been completely illustrated.

AMPK is canonically up-regulated following an increase in AMP/ATP ratio that provokes a conformational change of the γ subunit accompanied by exposure of the active site (on the α subunit) to the action of activating kinase LKB1.

In 2012 Park and colleagues observed the indirect activation of AMPK by Resveratrol (Rv) a non-methylated analogue of Pt. This was ascribed to an increase in cAMP and the downstream enhancement of an EPAC1-CamKKβ axis [84].

AMPK, in turn, can inhibit mTORC1 by phosphorylating either TSC2 or RAPTOR [85, 86].

Considering the structural similarity of Rv and Pt, it is logical to postulate that the same molecular processes might intervene for both molecules. Therefore, we checked whether Pt could provoke an increase in cAMP.

To this end, we used two different methods. First, we examined CREB through biochemical analyses. The phosphorylation levels of this transcription factor may be indicative of the cAMP level in cells, given that it is mainly activated by protein kinase A (PKA), a "front-line effector" of the cyclic nucleotide.

As shown in **Fig.8**, Western Blot analyses reported a rapid increment in the phosphorylation levels of CREB, with a maximal effect reached within 1 hour from the beginning of the treatment, suggesting an increase in cAMP.

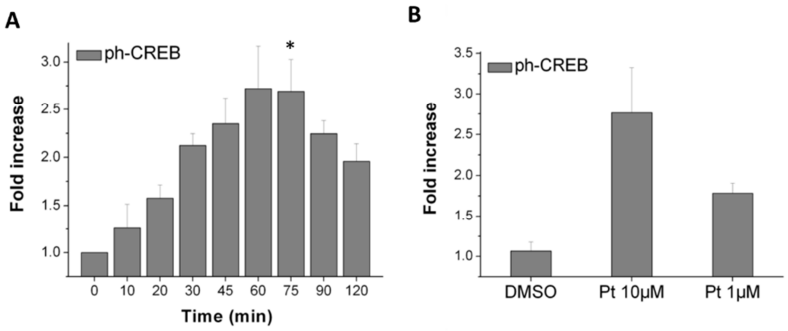


Fig.8: Western Blot of ph-CREB. (**A,B**): Kruskal-Wallis' non-parametric test applying Dunn's correction shows that maximally significant phosphorylation levels were reached 75 minutes after the administration of Pt to WT HeLa cells, in culture medium ($p = 0.0374$).

However, in addition to PKA, further regulators may promote CREB activity. Therefore, we resorted (in collaboration with Dr. Giulietta Di Benedetto of the National Research Council Institute of Neuroscience, Padua) to a second approach: a direct determination of the amount of [87] in HeLa cells under conditions of interest by taking advantage of the H30 FRET sensor. This was engineered with an EPAC1 molecule sandwiched between cyan- and yellow fluorescent proteins (respectively representing the donor and the acceptor). Following the binding of the intracellular second messenger, EPAC1 undergoes a conformational change resulting in the unfolding of the construct. As a consequence, there is no longer energy transfer between the two fluorophores. Thus, increases in cAMP concentrations can be followed as a drop in FRET.

Experiments performed in HeLa cells transiently transfected with EPAC1-based FRET sensor confirm that Pt, even at low and physiologically relevant doses, may provoke a rapid increase in the concentration of the cAMP (**Fig.9**). However, the subsequent additions of Forskolin 25µM (a pan-activator of Cyclases) and IBMX 100µM (a broad-spectrum inhibitor of PDEs), used as experimental controls, caused further larger increases.

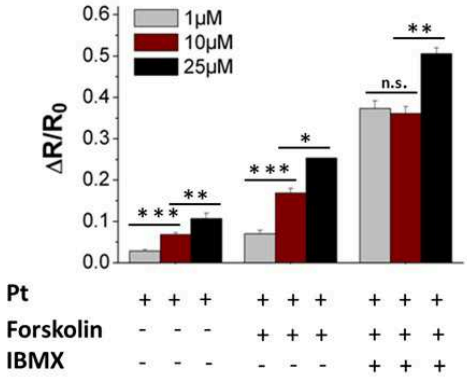


Fig.9: FRET-based measurement of cAMP. Pt induced a concentration-dependent increase in the amount of this second messenger. Forskolin and IBMX added afterwards provoked further increments.

These observations indicate that Pt at the concentrations used cannot fully modulate the activities of these classes of enzymes. Furthermore, the data do not allow discerning between an action on Adenyl Cyclases or on PDEs or both.

Since Rv has been reported to be an inhibitor of PDEs by Park et al., in 2012 [84], we checked whether Pt could behave analogously. Thus, we developed an assay for determining PDE activity. cAMP (100µM) was added to unfractionated cell lysates, without other additions or in the presence of IBMX (100 µM), or Pt (25 µM). The decrease of cyclic nucleotide concentration was monitored via periodic sampling and HPLC/UV analysis.

As shown in **Fig.10A**, while cAMP was hydrolysed in the control samples or in the presence of Forskolin (a further control) a much more modest reduction of the concentration of the cyclic nucleotide took place in the presence of IBMX, suggesting that cAMP was stable under the experimental conditions in the absence of PDE activity. Pt at the concentration of 25µM provoked a lesser reduction in the rate of hydrolysis. Application of the paired *t*test statistical analysis indicates that the difference between control and 25µM Pt is significant ($p < 0.05$) at least for the 30-minutes data set, with

inhibition of cAMP hydrolysis by the phenolic compound corresponding to about 30% of that caused by IBMX at that time (**Fig.10B**).

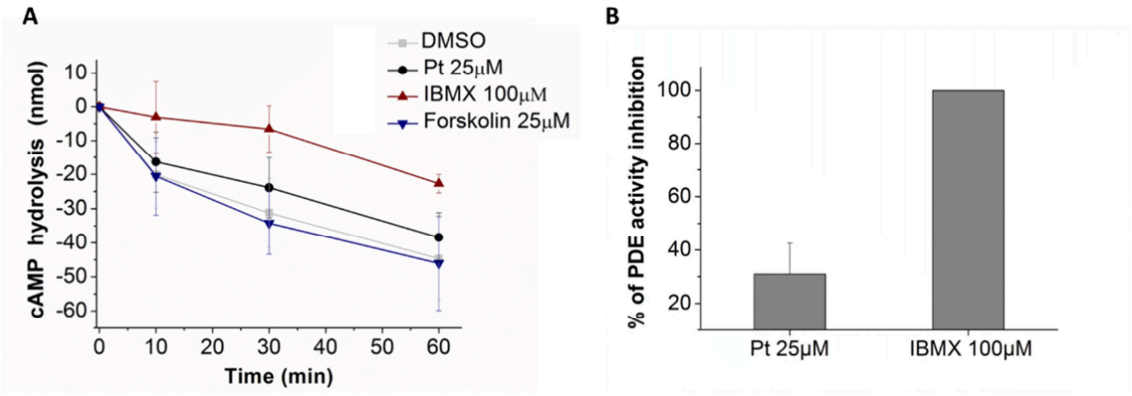


Fig.10: HPLC/UV analyses of cAMP. (**A,B**): the amount of cAMP in the samples was higher in the presence of Pt if compared to DMSO at all time points. However, Pt was less potent than IBMX as PDE inhibitor. The inhibition afforded by IMBX 100μM was taken as 100%. N = 6. Error bars reported as standard deviation.

Although these results are preliminary and need to be further confirmed, they suggest that Pt may promote cAMP increase through the inhibition of PDEs.

Finally, we wondered whether TFEB migration from the cytosol to the nucleus might be due to the increase in intracellular levels of cAMP and to the downstream activation of AMPK. HeLa TFEB-GFP cells were thus treated with IBMX 100μM or A769662 25μM (an AMPK activator). Although both molecules were used at the concentrations known to strongly inhibit PDEs and activate AMPK respectively, interestingly, they induced a weaker migration of the transcription factor to the nucleus if compared to that observed with Pt (**Fig.11**).

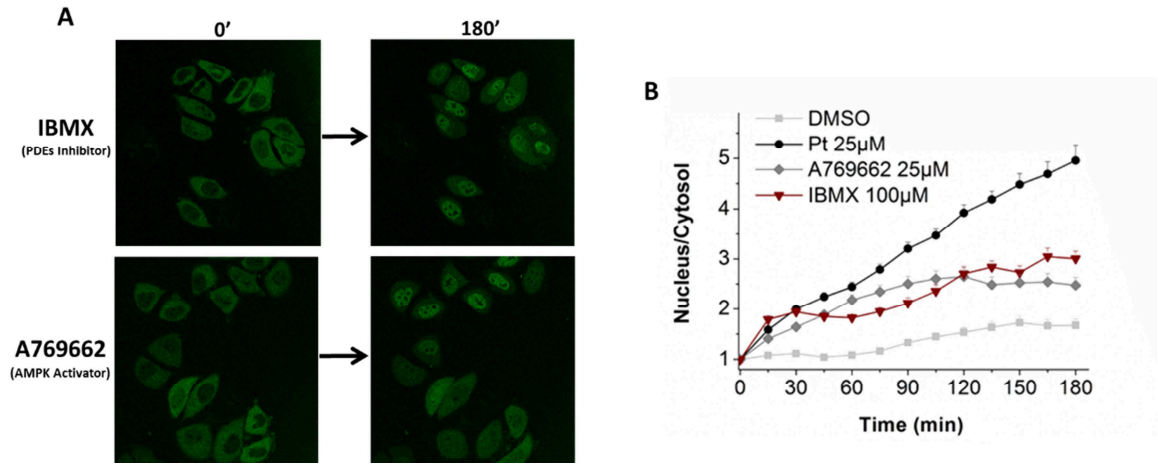


Fig.11: The cAMP-AMPK-mTORC1 axis accounts only partially for TFEB nuclear translocation. (**A**): Representative images of HeLa cells over-expressing TFEB-GFP prior and after treatment with IBMX or A769662. (**B**): Both drugs induce a weaker TFEB translocation if compared to Pt. While A769662 treatment reaches a statistically relevant difference with respect to DMSO at 45minutes ($p \leq 0.05$), IBMX does so only at 120 minutes ($p \leq 0.01$). At 60 minutes Pt vs IBMX: $p \leq 0.05$; at 90 minutes Pt vs A769662: $p \leq 0.001$. TWO-WAY ANOVA analyses for repeated measures as a function of time and treatment, applying Dunnett's correction. N ≥ 20; Error bars reported as +SEM.

While these data do not exclude a direct action of Pt on AMPK or mTORC1, they suggest that:

1) TFEB nuclear migration induced by the phenolic compound is partly downstream of cAMP, but
2) the PDEs-AMPK-mTORC1 axis is not the only and obligatory signaling cascade initiated by Pt in triggering TFEB nuclear translocation

These points are further considered in the Discussion section.

5. ROS generation by Pt - an alternative to drive TFEB to the nucleus.

As mentioned above, natural polyphenols were primarily defined anti-oxidant agents. However, it has been demonstrated that, depending on conditions, they may also promote the generation of ROS [7-9].

The capability of reactive oxygen species to act as second messenger and to regulate a variety of physiological process has been known for a long time. Multiple connections between ROS and autophagy have been also documented [88-94]. However, the mechanisms by which these unstable molecules promote the catabolic process are still largely unknown.

In 2016, Zhang et al. [95, 96] have reported that ROS production may trigger TFEB migration and autophagy through a mechanism independent of mTORC1. More in detail,

they showed that both exogenous and mitochondrial endogenous ROS oxidize the mucolipin1 channel in the lysosomal membranes. The occurrence of this oxidation favours the channel adopting a constitutively-open state. This results in Ca^{2+} release from lysosomal stores and consequently in the activation of the phosphatase Calcineurin. This, in turn, dephosphorylates TFEB allowing its nuclear translocation and autophagy onset.

As seen, the enhancement of cAMP downstream signalling, resulting in the inhibition of mTORC1, cannot fully account for the migration of TFEB to the nucleus induced by Pt, suggesting that another mechanism contributes importantly to this phenomenon. In light of this, we wanted to verify the possibility of ROS production by Pt and whether these species could mediate the nuclear translocation of the autophagy master regulator.

In order to test this hypothesis, first we incubated WT HeLa cells with the Mitosox probe, an indicator of superoxide generation. Following the generation of this radical specie, Mitosox is oxidized and becomes highly fluorescent upon binding to nucleic acids. Therefore, it can be easily visualized by fluorescence microscopy. Next, we treated Mitosox pre-loaded cells with Pt and followed them by confocal microscopy.

As shown in **Fig.12**, the phenolic compound induced a dose-dependent increase in the fluorescence intensity of this probe, indicating ROS production in WT HeLa cells. Pt 10µM caused a higher production of superoxide and with faster kinetics than Pt 1µM. Pre-incubation of cells with NAC 1mM, an antioxidant capable to increase the intracellular pool of free radical scavengers, markedly reduced reactive species production. As expected, the vehicle, DMSO, had no effect.

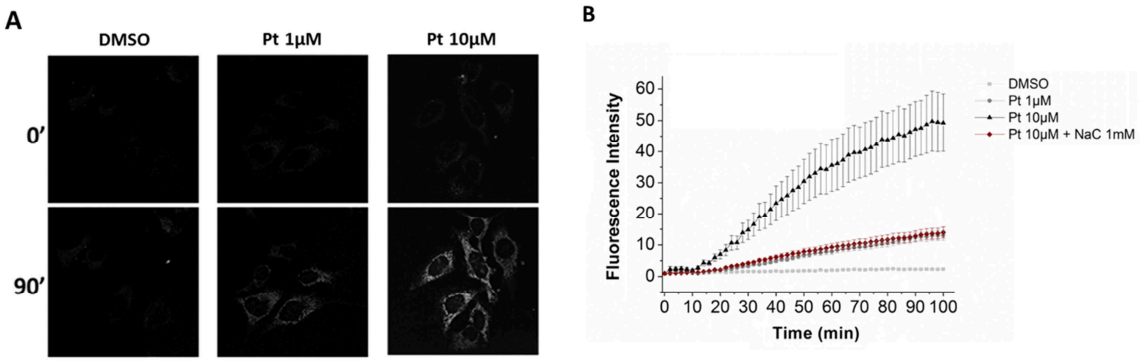


Fig. 12: ROS production induced by Pt. (**A**): representative images of WT HeLa cells, loaded with the Mitosox probe, with or without treatment with Pt at the indicated concentrations and time. (**B**): if compared to DMSO, the statistically relevant ROS generation induced by Pt 10µM ($p \leq 0.05$ at 24 minutes) is drastically reduced by pre-incubation of cells with NAC 1mM. At 24 minutes, Pt 10µM vs Pt 1µM: $p \leq 0.05$; at 36 minutes, Pt 10µM vs Pt 10µM + NAC 1mM: $p \leq 0.05$. ROS production was quantified as the mean value of Mitosox fluorescence intensity. N ≥ 32; Error bars: ± SEM

As next step, we looked at the migration of TFEB triggered by Pt in HeLa cells over-expressing the chimeric construct, following their 1hour pre-incubation with NAC 10mM. As shown in **Fig.13**, NAC reduced TFEB nuclear translocation to about 50% of that caused by the polyphenol alone, as measured 120 minutes after its addition, when accumulation is almost maximal.

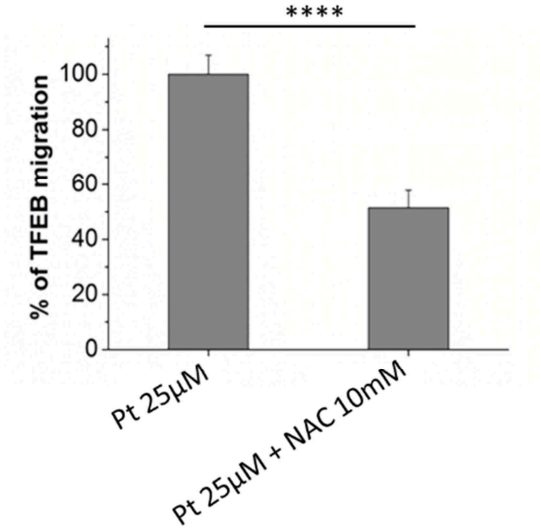


Fig.13: NAC antagonizes Pt-induced TFEB migration to the nucleus. The accumulation induced by Pt 25µM (nuclear/cytoplasmic fluorescence ratio at 2 hours) was taken as 100%. NAC + Pt vs Pt *t*test yields $p = < 0.0001$. $N \geq 37$. Error bars: +SEM.

In light of the above, we moved to evaluate the role of Calcineurin in our experimental conditions. To this end, we turned to the use of Cyclosporin A (CsA). This drug, clinically employed as immunosuppressive agent, comprises of a binding site for cyclophilins, proteins showing peptidyl prolyl isomerase activity. Among cyclophilins, the isoform A interacts with the phosphatase Calcineurin, inhibiting it. Thus, we evaluated the effect of CsA in combination with Pt in TFEB-GFP expressing HeLa cells. In agreement with our previous results, **Fig.14** shows that after 120 minutes, the presence of CsA 1µM reduced Pt-induced TFEB nuclear translocation by about 50%.

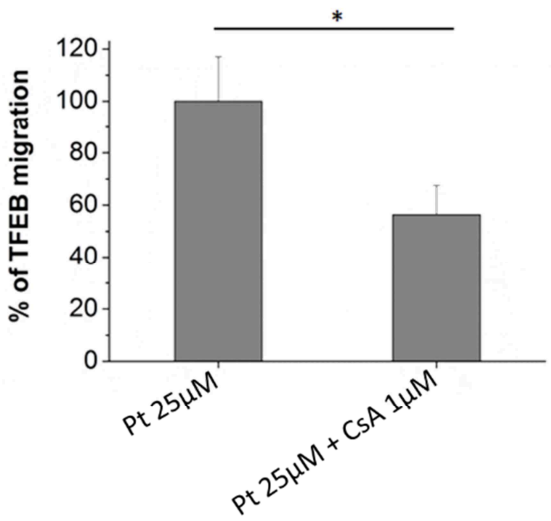


Fig.14: Cyclosporin A antagonizes Pterostilbene-induced TFEB nuclear migration. The accumulation (nuclear/cytoplasmic fluorescence ratio) induced by Pt 25µM at 2 hours was taken as 100%. CsA + Pt vs Pt *t*test yields $p = < 0.016$. N ≥ 35. Error bars: +SEM.

However, this part of the project is still incomplete and needs further investigations to:

1. evaluate the effectiveness of Pt metabolites in ROS production
2. verify whether a cytosolic Ca^{2+} increase does occur after Pt addition and
3. if so, whether it might be downstream of ROS production

6. Pt promotes mitochondrial biogenesis.

The term autophagy generally refers to the selective elimination of dysfunctional macromolecules and organelles.

As main ROS source, mitochondria are continuously subjected to an intensive oxidative stress that damages them. Since they participate in many major metabolic processes, old and impaired mitochondria need to be replaced by new and perfectly functioning organelles.

Among the endogenous and the exogenous factors that may stimulate mitochondrial biogenesis, transcriptional co-activator peroxisome proliferator-activated receptor gamma co-activator 1α (PGC-1α) has been one of the most intensively investigated. The molecular mechanisms behind its activation are still controversial and not completely defined; however, the metabolic sensor AMPK, together with SIRT1, seems to have a crucial role. The consensus view is that a site-specific phosphorylation by AMPK promotes its

subsequent deacetylation by SIRT1. This, in turn, allows the achievement of the protein's full stability.

In the previous paragraph, I showed that the natural compounds Pt and DiHydroPt promote TFEB migration partly through the upstream activation of AMPK. This evidence suggested to me that Pt, at the same time, might promote mitochondrial biogenesis ensuring a good quality control of these organelles.

To verify this hypothesis, we first measured, by RT-qPCR, the expression levels of *ppargc1a*, the gene encoding for PGC-1α in WT HeLa cells after 24 hours of treatment. As expected, both molecules significantly up-regulated this transcript (**Fig.15**) further confirming their capability to activate AMPK.

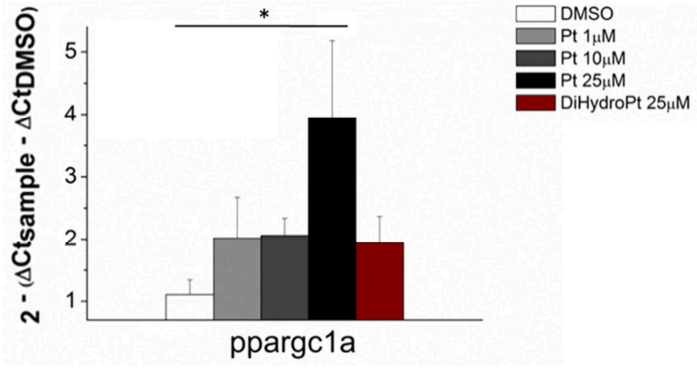


Fig.15: RT-qPCR analysis of ppargc1a. Both Pt and DiHydroPt increase transcription levels of this gene. Bar extremities correspond to the columns to be compared; asterisk denotes significance ($p = 0.015$). ONE-WAY ANOVA analysis, applying Tukey's correction. $N \geq 3$; Error bars: +SEM.

Next, we verified whether this effect could be transduced into an increment of mitochondrial mass. Therefore, we looked at mitochondrial content in living cells through flow cytometry analyses using Nonyl Acridine Orange (NAO).

NAO is a non-toxic fluorescent dye which selectively binds to cardiolipin, an important structural component of the mitochondrial inner membrane, and acts therefore as mitochondrial marker [97].

Fig.16 reports that Pt, at the concentration of 10 μM, induces a positive shift in the median fluorescent intensity of NAO-stained cells, as measured by FACS (see Materials and Methods), already one day post the beginning of the treatment. This effect was significantly more pronounced after 48 hours of treatment, denoting an increase in mitochondrial mass by roughly 40%. The increment of mitochondrial biogenesis has been

also promoted by using Pt 1μM but to a lesser extent if compared to that observed at higher dose and it required a longer exposure to the drug.

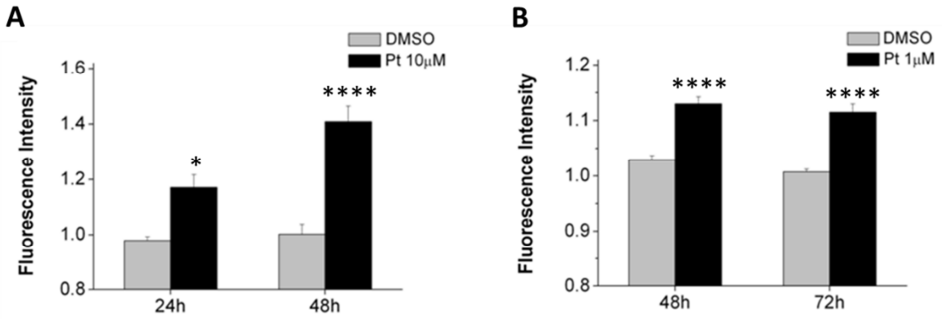


Fig.16: FACS measurements of mitochondrial mass in WT HeLa cells. (**A,B**). Pt induced a time- and concentration dependent increase in NAO signal. TWO-WAY ANOVA analysis for repeated measures as a function of time and treatment, applying Bonferroni's correction. Reported are mean values +SEM; N ≥ 4.

Altogether, these experiments suggest that Pt acts as a remarkable modulator of mitochondrial turn-over.

Conclusions

The anti-proliferative, anti-obesity and neuro-protective effects ascribed to Pt lead to hypothesize that this molecule might stimulate autophagy.

The occurrence of this process by this molecule had been already reported in several papers; however, the underlying molecular mechanisms had not been yet outlined.

With this work, one of the few performed at physiologically relevant concentrations, we not only confirm the pro-autophagic role of this compound but, most importantly, we identified transcription factor EB, the autophagy master regulator, as fundamental transducer of the actions of Pt. Indeed, at least *in vitro*, this polyphenol induces TFEB translocation to the nuclei of HeLa cells overexpressing a TFEB-GFP chimera as well as the up-regulation of TFEB transcript in WT HeLa cells.

Moreover, we qualified DiHydroPt, the product of the reduction of the stilbenic double bond by colonic flora, as active metabolic specie in our experimental system, while no effects were reported by treating cells with Pt-4'-Sulfate, a phase II metabolite.

Both DiHydroPt and its parent compound also up-regulated the expression of PGC-1α, the main promoter of mitochondrial biogenesis. This effect was accompanied, in the case of Pt, by an increase in mitochondrial mass. Thus, this natural compound may finely balance the two opposite phenomena, ensuring a good quality control of mitochondria, whose

maintenance is essential to prevent the onset of various pathologies and for the promotion of healthy aging [87, 98-101].

In agreement with the migration of TFEB, we report a Pt-induced reduction of the activity of mTORC1. This effect has been ascribed to the upstream activation of AMPK by cAMP. FRET based experiments indeed showed modest increases in the cellular amount of this second messenger following treatment with the natural polyphenol. However, this signalling cascade seems to be only partially responsible for the observed TFEB behaviour. In fact, near-maximal activation of AMPK or inhibition of PDEs using A769662 and IBMX respectively provoked a weaker TFEB-GFP nuclear migration than that elicited by Pt. Therefore, Pt enhances the activity of this transcription factor by modulating more than one cellular pathway.

Zhang and colleagues recently reported that MCOLN1/TRPML1 channel may promote Ca^{2+} release from lysosomal stores and Calcineurin-dependent TFEB migration in response to ROS generation [95, 96]. While this part of my work needs further investigations, Pt increases ROS in WT HeLa cells. ROS detection by MitoSOX is significantly reduced by pre-treatment with NAC. Moreover, both the buffering of reactive species and the inhibition of Calcineurin using CsA slacken TFEB nuclear translocation. This may therefore well represent an alternative manner by which our phenol promotes the activity of the autophagy master regulator.

In summary, my PhD research has clarified one of the mechanisms accounting for the biomedical activities of Pt and strengthens the possibility of using this natural compound as an adjuvant in the treatment or prevention of several human conditions.

References

1. Estrela, J.M., et al., *Pterostilbene: Biomedical applications.* Crit Rev Clin Lab Sci, 2013. **50**(3): p. 65-78.
2. Kosuru, R., et al., *Promising therapeutic potential of pterostilbene and its mechanistic insight based on preclinical evidence.* Eur J Pharmacol, 2016. **789**: p. 229-43.
3. McCormack, D. and D. McFadden, *Pterostilbene and cancer: current review.* J Surg Res, 2012. **173**(2): p. e53-61.
4. Azzolini, M., et al., *Pharmacokinetics and tissue distribution of pterostilbene in the rat.* Mol Nutr Food Res, 2014. **58**(11): p. 2122-32.
5. Biasutto, L., I. Szabo, and M. Zoratti, *Mitochondrial effects of plant-made compounds.* Antioxid Redox Signal, 2011. **15**(12): p. 3039-59.
6. Eghbaliferiz, S. and M. Iranshahi, *Prooxidant Activity of Polyphenols, Flavonoids, Anthocyanins and Carotenoids: Updated Review of Mechanisms and Catalyzing Metals.* Phytother Res, 2016. **30**(9): p. 1379-91.
7. Mileo, A.M. and S. Miccadei, *Polyphenols as Modulator of Oxidative Stress in Cancer Disease: New Therapeutic Strategies.* Oxid Med Cell Longev, 2016. **2016**: p. 6475624.
8. Khan, H.Y., et al., *Plant polyphenol induced cell death in human cancer cells involves mobilization of intracellular copper ions and reactive oxygen species generation: a mechanism for cancer chemopreventive action.* Mol Nutr Food Res, 2014. **58**(3): p. 437-46.
9. Khan, H.Y., et al., *A prooxidant mechanism for the anticancer and chemopreventive properties of plant polyphenols.* Curr Drug Targets, 2012. **13**(14): p. 1738-49.
10. Park, S., *Polyphenol Compound as a Transcription Factor Inhibitor.* Nutrients, 2015. **7**(11): p. 8987-9004.
11. Chu, A.J., *Antagonism by bioactive polyphenols against inflammation: a systematic view.* Inflamm Allergy Drug Targets, 2014. **13**(1): p. 34-64.
12. Murakami, A. and K. Ohnishi, *Target molecules of food phytochemicals: food science bound for the next dimension.* Food Funct, 2012. **3**(5): p. 462-76.
13. Li, W., X. Mei, and Y.Y. Tu, *Effects of tea polyphenols and their polymers on MAPK signaling pathways in cancer research.* Mini Rev Med Chem, 2012. **12**(2): p. 120-6.
14. Kang, N.J., et al., *Polyphenols as small molecular inhibitors of signaling cascades in carcinogenesis.* Pharmacol Ther, 2011. **130**(3): p. 310-24.
15. Das, S. and D.K. Das, *Anti-inflammatory responses of resveratrol.* Inflamm Allergy Drug Targets, 2007. **6**(3): p. 168-73.
16. Sang, S., et al., *Redox properties of tea polyphenols and related biological activities.* Antioxid Redox Signal, 2005. **7**(11-12): p. 1704-14.
17. Ko, C.P., et al., *Pterostilbene induce autophagy on human oral cancer cells through modulation of Akt and mitogen-activated protein kinase pathway.* Oral Oncol, 2015. **51**(6): p. 593-601.
18. Chen, R.J., et al., *Chemopreventive effects of pterostilbene on urethane-induced lung carcinogenesis in mice via the inhibition of EGFR-mediated pathways and the induction of apoptosis and autophagy.* J Agric Food Chem, 2012. **60**(46): p. 11533-41.
19. Zhang, L., et al., *Pterostilbene, a natural small-molecular compound, promotes cytoprotective macroautophagy in vascular endothelial cells.* J Nutr Biochem, 2013. **24**(5): p. 903-11.

20. Chakraborty, A., et al., *Long term induction by pterostilbene results in autophagy and cellular differentiation in MCF-7 cells via ROS dependent pathway.* Mol Cell Endocrinol, 2012. **355**(1): p. 25-40.
21. Napolitano, G. and A. Ballabio, *TFEB at a glance.* 2016. **129**(13): p. 2475-81.
22. Palmieri, M., et al., *Characterization of the CLEAR network reveals an integrated control of cellular clearance pathways.* Hum Mol Genet, 2011. **20**(19): p. 3852-66.
23. Settembre, C. and A. Ballabio, *Lysosome: regulator of lipid degradation pathways.* Trends Cell Biol, 2014. **24**(12): p. 743-50.
24. Settembre, C., et al., *Signals from the lysosome: a control centre for cellular clearance and energy metabolism.* Nat Rev Mol Cell Biol, 2013. **14**(5): p. 283-96.
25. Settembre, C., et al., *TFEB controls cellular lipid metabolism through a starvation-induced autoregulatory loop.* Nat Cell Biol, 2013. **15**(6): p. 647-58.
26. Settembre, C. and A. Ballabio, *TFEB regulates autophagy: an integrated coordination of cellular degradation and recycling processes.* Autophagy, 2011. **7**(11): p. 1379-81.
27. Settembre, C., et al., *TFEB links autophagy to lysosomal biogenesis.* Science, 2011. **332**(6036): p. 1429-33.
28. Sardiello, M., et al., *A gene network regulating lysosomal biogenesis and function.* Science, 2009. **325**(5939): p. 473-7.
29. Sardiello, M. and A. Ballabio, *Lysosomal enhancement: a CLEAR answer to cellular degradative needs.* Cell Cycle, 2009. **8**(24): p. 4021-2.
30. Laplante, M. and D.M. Sabatini, *Regulation of mTORC1 and its impact on gene expression at a glance.* J Cell Sci, 2013. **126**(Pt 8): p. 1713-9.
31. Martina, J.A. and R. Puertollano, *Rag GTPases mediate amino acid-dependent recruitment of TFEB and MITF to lysosomes.* J Cell Biol, 2013. **200**(4): p. 475-91.
32. Martina, J.A. and R. Puertollano, *RRAG GTPases link nutrient availability to gene expression, autophagy and lysosomal biogenesis.* Autophagy, 2013. **9**(6): p. 928-30.
33. Settembre, C., et al., *A lysosome-to-nucleus signalling mechanism senses and regulates the lysosome via mTOR and TFEB.* Embo j, 2012. **31**(5): p. 1095-108.
34. Medina, D.L. and A. Ballabio, *Lysosomal calcium regulates autophagy.* Autophagy, 2015. **11**(6): p. 970-1.
35. Medina, D.L., et al., *Lysosomal calcium signalling regulates autophagy through calcineurin and TFEB.* Nat Cell Biol, 2015. **17**(3): p. 288-99.
36. Martini-Stoica, H., et al., *The Autophagy-Lysosomal Pathway in Neurodegeneration: A TFEB Perspective.* Trends Neurosci, 2016. **39**(4): p. 221-34.
37. Maixner, N., et al., *Transcriptional Dysregulation of Adipose Tissue Autophagy in Obesity.* Physiology (Bethesda), 2016. **31**(4): p. 270-82.
38. Stienstra, R., et al., *Autophagy in adipose tissue and the beta cell: implications for obesity and diabetes.* Diabetologia, 2014. **57**(8): p. 1505-16.
39. Chen, C.F., Y.D. Li, and Z. Xu, *[Chemical principles and bioactivities of blueberry].* Yao Xue Xue Bao, 2010. **45**(4): p. 422-9.
40. Rimando, A.M., et al., *Pterostilbene, a new agonist for the peroxisome proliferator-activated receptor alpha-isoform, lowers plasma lipoproteins and cholesterol in hypercholesterolemic hamsters.* J Agric Food Chem, 2005. **53**(9): p. 3403-7.
41. Manickam, M., et al., *Antihyperglycemic activity of phenolics from Pterocarpus marsupium.* J Nat Prod, 1997. **60**(6): p. 609-10.
42. Singh, R., et al., *Autophagy regulates lipid metabolism.* Nature, 2009. **458**(7242): p. 1131-5.

43. Singh, R., et al., *Autophagy regulates adipose mass and differentiation in mice.* J Clin Invest, 2009. **119**(11): p. 3329-39.
44. Gomez-Zorita, S., et al., *Pterostilbene, a dimethyl ether derivative of resveratrol, reduces fat accumulation in rats fed an obesogenic diet.* J Agric Food Chem, 2014. **62**(33): p. 8371-8.
45. Gomez-Zorita, S., et al., *Pterostilbene improves glycaemic control in rats fed an obesogenic diet: involvement of skeletal muscle and liver.* Food Funct, 2015. **6**(6): p. 1968-76.
46. Yao, F., M. Zhang, and L. Chen, *5'-Monophosphate-activated protein kinase (AMPK) improves autophagic activity in diabetes and diabetic complications.* Acta Pharm Sin B, 2016. **6**(1): p. 20-5.
47. Luo, Z., M. Zang, and W. Guo, *AMPK as a metabolic tumor suppressor: control of metabolism and cell growth.* Future Oncol, 2010. **6**(3): p. 457-70.
48. Shaw, R.J., *LKB1 and AMP-activated protein kinase control of mTOR signalling and growth.* Acta Physiol (Oxf), 2009. **196**(1): p. 65-80.
49. Yang, Z.J., et al., *The role of autophagy in cancer: therapeutic implications.* Mol Cancer Ther, 2011. **10**(9): p. 1533-41.
50. Morselli, E., et al., *Anti- and pro-tumor functions of autophagy.* Biochim Biophys Acta, 2009. **1793**(9): p. 1524-32.
51. Komatsu, M., et al., *Essential role for autophagy protein Atg7 in the maintenance of axonal homeostasis and the prevention of axonal degeneration.* Proc Natl Acad Sci U S A, 2007. **104**(36): p. 14489-94.
52. Garza-Lombo, C. and M.E. Gonsebatt, *Mammalian Target of Rapamycin: Its Role in Early Neural Development and in Adult and Aged Brain Function.* Front Cell Neurosci, 2016. **10**: p. 157.
53. Bockaert, J. and P. Marin, *mTOR in Brain Physiology and Pathologies.* Physiol Rev, 2015. **95**(4): p. 1157-87.
54. Pani, G., *Neuroprotective effects of dietary restriction: Evidence and mechanisms.* Semin Cell Dev Biol, 2015. **40**: p. 106-14.
55. Xi, Y., et al., *Knockout of Atg5 delays the maturation and reduces the survival of adult-generated neurons in the hippocampus.* Cell Death Dis, 2016. **7**: p. e2127.
56. Fekadu, J. and A. Rami, *Beclin-1 Deficiency Alters Autophagosome Formation, Lysosome Biogenesis and Enhances Neuronal Vulnerability of HT22 Hippocampal Cells.* Mol Neurobiol, 2016. **53**(8): p. 5500-9.
57. Shen, D.N., et al., *Autophagy in synaptic development, function, and pathology.* Neurosci Bull, 2015. **31**(4): p. 416-26.
58. Button, R.W., S. Luo, and D.C. Rubinsztein, *Autophagic activity in neuronal cell death.* Neurosci Bull, 2015. **31**(4): p. 382-94.
59. Heras-Sandoval, D., et al., *The role of PI3K/AKT/mTOR pathway in the modulation of autophagy and the clearance of protein aggregates in neurodegeneration.* Cell Signal, 2014. **26**(12): p. 2694-701.
60. Son, J.H., et al., *Neuronal autophagy and neurodegenerative diseases.* Exp Mol Med, 2012. **44**(2): p. 89-98.
61. Xilouri, M. and L. Stefanis, *Autophagy in the central nervous system: implications for neurodegenerative disorders.* CNS Neurol Disord Drug Targets, 2010. **9**(6): p. 701-19.
62. Chang, J., et al., *Low-dose pterostilbene, but not resveratrol, is a potent neuromodulator in aging and Alzheimer's disease.* Neurobiol Aging, 2012. **33**(9): p. 2062-71.

63. Joassard, O.R., et al., *Regulation of Akt-mTOR, ubiquitin-proteasome and autophagy-lysosome pathways in response to formoterol administration in rat skeletal muscle.* Int J Biochem Cell Biol, 2013. **45**(11): p. 2444-55.
64. Ghosh, A., et al., *Activation of peroxisome proliferator-activated receptor alpha induces lysosomal biogenesis in brain cells: implications for lysosomal storage disorders.* J Biol Chem, 2015. **290**(16): p. 10309-24.
65. Kandel, E.R., *The molecular biology of memory: cAMP, PKA, CRE, CREB-1, CREB-2, and CPEB.* Mol Brain, 2012. **5**: p. 14.
66. Sakamoto, K., K. Karelina, and K. Obrietan, *CREB: a multifaceted regulator of neuronal plasticity and protection.* J Neurochem, 2011. **116**(1): p. 1-9.
67. Silva, A.J., et al., *CREB and memory.* Annu Rev Neurosci, 1998. **21**: p. 127-48.
68. Manley, S. and W. Ding, *Role of farnesoid X receptor and bile acids in alcoholic liver disease.* Acta Pharm Sin B, 2015. **5**(2): p. 158-67.
69. Seok, S., et al., *Transcriptional regulation of autophagy by an FXR-CREB axis.* Nature, 2014. **516**(7529): p. 108-11.
70. Rueda, D.C., et al., *Identification of dihydrostilbenes in Pholidota chinensis as a new scaffold for GABAA receptor modulators.* Bioorg Med Chem, 2014. **22**(4): p. 1276-84.
71. Ponsioen, B., et al., *Detecting cAMP-induced Epac activation by fluorescence resonance energy transfer: Epac as a novel cAMP indicator.* EMBO Rep, 2004. **5**(12): p. 1176-80.
72. Del Rio, D., G. Borges, and A. Crozier, *Berry flavonoids and phenolics: bioavailability and evidence of protective effects.* Br J Nutr, 2010. **104 Suppl 3**: p. S67-90.
73. Bolca, S., T. Van de Wiele, and S. Possemiers, *Gut metabotypes govern health effects of dietary polyphenols.* Curr Opin Biotechnol, 2013. **24**(2): p. 220-5.
74. Ozdal, T., et al., *The Reciprocal Interactions between Polyphenols and Gut Microbiota and Effects on Bioaccessibility.* Nutrients, 2016. **8**(2): p. 78.
75. Stevens, J.F. and C.S. Maier, *The Chemistry of Gut Microbial Metabolism of Polyphenols.* Phytochem Rev, 2016. **15**(3): p. 425-444.
76. Tomas-Barberan, F.A., M.V. Selma, and J.C. Espin, *Interactions of gut microbiota with dietary polyphenols and consequences to human health.* Curr Opin Clin Nutr Metab Care, 2016. **19**(6): p. 471-476.
77. Sun, Y., et al., *Identification of pinostilbene as a major colonic metabolite of pterostilbene and its inhibitory effects on colon cancer cells.* Mol Nutr Food Res, 2016. **60**(9): p. 1924-32.
78. Wawszczyk, J., et al., *In vitro evaluation of antiproliferative and cytotoxic properties of pterostilbene against human colon cancer cells.* Acta Pol Pharm, 2014. **71**(6): p. 1051-5.
79. Nutakul, W., et al., *Inhibitory effects of resveratrol and pterostilbene on human colon cancer cells: a side-by-side comparison.* J Agric Food Chem, 2011. **59**(20): p. 10964-70.
80. Paul, S., et al., *Dietary intake of pterostilbene, a constituent of blueberries, inhibits the beta-catenin/p65 downstream signaling pathway and colon carcinogenesis in rats.* Carcinogenesis, 2010. **31**(7): p. 1272-8.
81. Sancho, M. and N. Mach, *[Effects of wine polyphenols on cancer prevention].* Nutr Hosp, 2014. **31**(2): p. 535-51.
82. Brown, E.M., et al., *Mechanisms underlying the anti-proliferative effects of berry components in in vitro models of colon cancer.* Curr Pharm Biotechnol, 2012. **13**(1): p. 200-9.

83. Rudolf, E., H. Andelova, and M. Cervinka, *Polyphenolic compounds in chemoprevention of colon cancer - targets and signaling pathways.* Anticancer Agents Med Chem, 2007. **7**(5): p. 559-75.
84. Park, S.J., et al., *Resveratrol ameliorates aging-related metabolic phenotypes by inhibiting cAMP phosphodiesterases.* Cell, 2012. **148**(3): p. 421-33.
85. Gwinn, D.M., et al., *AMPK phosphorylation of raptor mediates a metabolic checkpoint.* Mol Cell, 2008. **30**(2): p. 214-26.
86. Mihaylova, M.M. and R.J. Shaw, *The AMPK signalling pathway coordinates cell growth, autophagy and metabolism.* Nat Cell Biol, 2011. **13**(9): p. 1016-23.
87. Campos, J.C., et al., *Mitochondrial Quality Control in Cardiac Diseases.* Front Physiol, 2016. **7**: p. 479.
88. Huang, J., G.Y. Lam, and J.H. Brumell, *Autophagy signaling through reactive oxygen species.* Antioxid Redox Signal, 2011. **14**(11): p. 2215-31.
89. Santin, Y., et al., *Oxidative Stress by Monoamine Oxidase-A Impairs Transcription Factor EB Activation and Autophagosome Clearance, Leading to Cardiomyocyte Necrosis and Heart Failure.* Antioxid Redox Signal, 2016. **25**(1): p. 10-27.
90. Liu, G.Y., et al., *ROS activates JNK-mediated autophagy to counteract apoptosis in mouse mesenchymal stem cells in vitro.* Acta Pharmacol Sin, 2015. **36**(12): p. 1473-9.
91. Zhang, L., et al., *Redox signaling: Potential arbitrator of autophagy and apoptosis in therapeutic response.* Free Radic Biol Med, 2015. **89**: p. 452-65.
92. Chen, Y., M.B. Azad, and S.B. Gibson, *Superoxide is the major reactive oxygen species regulating autophagy.* Cell Death Differ, 2009. **16**(7): p. 1040-52.
93. Li, L., Y. Chen, and S.B. Gibson, *Starvation-induced autophagy is regulated by mitochondrial reactive oxygen species leading to AMPK activation.* Cell Signal, 2013. **25**(1): p. 50-65.
94. Rodney, G.G., R. Pal, and R. Abo-Zahrah, *Redox regulation of autophagy in skeletal muscle.* Free Radic Biol Med, 2016. **98**: p. 103-12.
95. Zhang, X., et al., *MCOLN1 is a ROS sensor in lysosomes that regulates autophagy.* Nat Commun, 2016. **7**: p. 12109.
96. Zhang, X., L. Yu, and H. Xu, *Lysosome calcium in ROS regulation of autophagy.* Autophagy, 2016. **12**(10): p. 1954-1955.
97. Kaewsuya, P., N.D. Danielson, and D. Ekhterae, *Fluorescent determination of cardiolipin using 10-N-nonyl acridine orange.* Anal Bioanal Chem, 2007. **387**(8): p. 2775-82.
98. Shoshan, M., *On mitochondrial metabolism in tumor biology.* Curr Opin Oncol, 2016.
99. Amigo, I., et al., *Mitochondrial form, function and signalling in aging.* Biochem J, 2016. **473**(20): p. 3421-3449.
100. Cai, Q. and P. Tammineni, *Alterations in Mitochondrial Quality Control in Alzheimer's Disease.* Front Cell Neurosci, 2016. **10**: p. 24.
101. Hang, L., J. Thundyil, and K.L. Lim, *Mitochondrial dysfunction and Parkinson disease: a Parkin-AMPK alliance in neuroprotection.* Ann N Y Acad Sci, 2015. **1350**: p. 37-47.

Chapter 6

Pterostilbene partially rescues the phenotype of CollagenVI dystrophic zebrafish morphants

Abstract

Pterostilbene (trans-3,5-dimethoxy-4'-hydroxystilbene, Pt) is a natural compound found primarily in blueberries and in grapevines. A remarkable number of studies suggests that this molecule manifests preventive and therapeutic properties against a vast range of human diseases such as neurological, cardiovascular and metabolic disorders. An anti-proliferative action of Pt, of obvious oncological interest, has also been reported.

These multiple beneficial effects stem not only from the redox properties of Pt, which are not particularly remarkable, but also, and mainly, from the modulation of the activities of enzymes and/or transcription factors.

For instance, our *in vitro* investigations have shown that Pt triggers the migration to the nucleus and activity of transcription factor EB (TFEB), the main regulator of autophagy (Chapter 5).

CollagenVI (ColVI) is a filamentous protein of the extracellular matrix conferring mechanical support to muscle cells. Mutations in genes encoding for ColVI α-chains lead to the onset of muscular disorders such as Bethlem myopathy and Ulrich congenital muscular dystrophy. Both of them are characterized by dysfunctional mitochondria whose accumulation is boosted, importantly, by defective autophagic flux. As a consequence, muscular fibers undergo apoptotic cell death. Currently, no pharmacological therapies are available for treating these pathologies. Zebrafish is a promising new tool for the study of genetic disorders as well as for drug screening. Recently, a zebrafish model of ColVI-related myopathies reflecting the human phenotype has been generated by taking advantage of a morpholino antisense oligonucleotide expression repressor.

As Pt shows a pro-autophagic role, I decided to verify its effectiveness in this animal model characterized by severe locomotor impairments and alterations in the structure of muscular fibers.

For this purpose, ColVI knock-down zebrafish embryos were incubated with Pt for 24 hours and then locomotor activities and myofiber structure were analyzed.

The recording of spontaneous movements as well as touch-evoked escape responses and birefringence analysis showed that this molecule significantly rescues both movement abnormalities and alteration in the myofiber organization of morphants.
According to our *in vitro* data, Pt treatment also significantly increased the expression of a mCherry protein under control of cAMP responsive elements (CRE), in a zebrafish transgenic line, denoting the activation of the cAMP signal. Although further investigations need to be performed, we can conclude that Pt might mediate both *in vitro* and *in vivo* the same molecular mechanisms leading to the amelioration of the phenotype of ColVI knock-down embryos.

Introduction

Pterostilbene, a bio-medically active plant phenol present in the human diet, is a good candidate as a natural health promoter since its bioavailability is higher than that of most other plant (poly)phenols [1-14]. However, its molecular mechanisms of action are still only sketchily defined, hindering an adequate exploitation of its therapeutic potential.
In vitro investigations I described in the previous chapter underpin the idea that Pt triggers autophagy by up-regulating the activity of TFEB, the master regulator of the process.
Autophagy plays a fundamental role in the maintenance of cellular homeostasis [15-17]. Indeed, this catabolic pathway not only provides energy to cells in case of nutrient deprivation but also promotes the clearance of damaged organelles [18-20].
Impairments of autophagic flux and the accumulation of altered organelles, particularly mitochondria, are involved in the pathogenesis of a variety of degenerative diseases including Bethlem myopathy and Ulrich congenital muscular dystrophy [21-27]. Although the latter is more severe than the former, both of them are caused by mutations of CollagenVI (ColVI) [28].
ColVI is a filamentous protein of the extracellular matrix composed of three different chains α1, α2 and α3, encoded by three different genes (COL6A1, COL6A2 and COL6A3) [29, 30].
The synthesis process as well as the first steps of chain assembly, leading to tetramers, take place within fibroblasts and muscle cells [21]. Then, tetramers are secreted in the surrounding environment and they organize in higher structural complexes. The resulting fibrils confer mechanical support to muscular cells by making structural connections with the basal lamina [28, 31].

However, mutated ColVI molecules are not properly built up, leading to alterations in muscle fiber structure. Then, the concentration of Ca^{2+} in the cytoplasm is increased and larger-than-usual amounts of this ion are taken up by the sarcoplasmic reticulum and mitochondria. The overload of Ca^{2+} in mitochondria triggers the opening of the permeability transition pore. Consequently, cristae undergo remodeling and cytochrome c is released outside the organelles promoting caspase activation and apoptosis [21, 32-34]. In addition, the defective formation of autophagosomes exacerbates these effects progressively leading to muscles wasting and a dystrophic phenotype [21]. Muscular weakness and joint contractures are the main physical hallmarks of the pathologies [27, 34].

Despite recent advances in our understanding of the pathophysiology of these myopathies, much remains to be clarified. Indeed, the exact mechanism by which the structural impairment of the extracellular matrix affects intracellular Ca^{2+} levels inside muscle cells is still unknown. Moreover, to date, no effective therapeutic treatments exist.

Limited access to the biopsies of patients considerably hinders further investigations and drug screening.

Thus, researchers strongly depend on animal models mirroring the human diseases. Generally, the use of rodents is preferred because of the high homology percentage with the human genome. Moreover they are manageable and highly prolific.

Several years ago, ColVIa1 knock out (KO) mice have been generated. In the absence of the α1 chain, ColVI fibrils cannot assembly and these animals completely lack ColVI. Nevertheless, ColVI KO mice display only a mild phenotype without muscular weakness and fibrosis [32]. Moreover, no progression of the pathology has been reported, as is the case instead in humans.

Lately, zebrafish (*Danio rerio*) has become a new tool to study genetic diseases [35-37]. Although there are obvious differences between fish and humans and a lower degree of identity with the human genome, zebrafish exhibits many advantages. First, this species is characterized by an elevated fecundity. Large numbers of eggs are produced per mating. Second, zebrafish embryogenesis is rapid. The entire body plan is established by 24 hours post fertilization (hpf) and organogenesis is mostly completed by 96 hpf. Embryos and larvae also show a high transparency that allows the visualization and monitoring of tissues and internal organs *in vivo* by simple optical microscopy [37]. Moreover, silencing genome techniques, such as morpholino, CRISPR-CAS9, TALEN and ZFN, can be easily applied to zebrafish.

On the basis of literature reports, morpholino-mediated silencing is actually the best strategy to obtain zebrafish models with a strong phenotype of ColVI-related muscle dystrophies [38].

“Morpholino” is a synthetic modified antisense oligonucleotide. Like DNA/RNA, it has nucleobases; however, the deoxyribose backbone is substituted by morpholine rings linked through phosphorodiamidate groups.

Unlike other antisense oligonucleotide-based technologies, such as siRNA, a morpholino does not cause degradation of its target sequence. Instead, it acts by "sterically blocking" the translational start site of the target mRNA. Additionally, it can be designed to interfere with mRNA splicing or to protect mRNAs from microRNA-mediated turn-over [39].

To be effective, the morpholino is injected directly into zebrafish eggs at one- to four-cell stage to obtain the overall silencing of the target gene. Due to the short half-life of morpholinos all phenotypical analyses must be performed within three days.

As we reported that Pt induces autophagy *in vitro*, we wanted to test its effectiveness in a zebrafish model of ColVI-related myopathies. Moreover, since we ascribed, partially, this pro-autophagic role to an increase in cAMP intracellular concentrations, we verified whether a similar phenomenon might occur also *in vivo*, by taking advantage of a zebrafish cAMP reporter line. Usage of zebrafish transgenic reporter lines to study molecular signaling cascades is currently increasing [40].

Materials and methods

Zebrafish and embryos maintenance: adult WT and 6XCRE fish were maintained in the facility of the University of Padua in tanks containing aerated, 28.5° C thermostatted saline water according to standard protocols. Fish were kept in a regimen of 14 hours of light alternated by 10 hours in the dark. For mating, males and females selected from the general sex-segregated population were placed within a special tank in the afternoon. The following morning they were allowed to start courtship, which ended with egg deposition and fecundation. The eggs were collected and kept in fish water (0.5mM NaH_2PO_4, 0.5mM $NaHPO_4$, 0.2mg/L methylene blue, 3mg/L “instant ocean sea salt”, Istant ocean) at 28.5° C.

Generation of Tg (6XCRE:nlsmCherry) lines: In Prof. F. Argenton's laboratory, a cassette containing six multimerized cAMP responsive elements (- 5' TGACGTCA 3' -) was inserted upstream of a rabbit β-globulin minimal promoter. These repeated elements (6XCRE) were then cloned in a 5'-entry vector, following the manufacturer's guidelines (Invitrogen Multisite Gateway System).
The resulting Gateway 5'-entry vector was recombined with a middle entry vector containing a nlsmCherry reporter gene, pMEvector (pME-nlsmCherry), a 3'-entry vector containing the SV40-polyA sequence (p3E-polyA) and Tol2 final destination vector. 25-50pg of the resulting vector were co-injected together with 25pg of *in vitro* synthesized Tol2 Transposase mRNA into one-cell WT embryos. Mosaic transgenic fish were selected at approximately 24hpf for fluorescence expression and raised to the adult stage for screening. Positive founders were selected for the fluorescence level of their offspring.

Injection with antisense morpholino: To knock down ColVI we took advantage of an exon 9 morpholino, previously designed by Telfer et al. in 2010, targeting zebrafish ColVIa1 mRNA leading to translation of a truncated, dominant negative, version of the ColVIa1 chain. Embryos from zebrafish WT incrosses were injected with the morpholino at 1-4 cell stage using a WPI pneumatic PicoPump PV820 injector. Morpholino was injected at the concentration of 0.1mM, corresponding to about 4ng per embryo.

Drug treatments: zebrafish embryos were dechorionated at 20hpf and then incubated at 28° C with drugs until the time of observation in Petri dishes. Pt (Waseta Int. Trading Co. Shangai, P.R.China), DiHydroPt and Pt-4'-Sulfate (synthetized by the group of Prof. Cristina Paradisi of the University of Padua) were used at concentrations ranging from 0.05 to 25μM and were dissolved in fish water without methylene blue. Stock solutions were prepared 1000x the desired working solutions in order to fix the final DMSO at 0.1% in all cases (including controls).

Motor activity test: Spontaneous coiling rate was recorded as the number of events observed in 15 seconds for each embryo at 24hpf using a light microscope. For the touch escape response assay, we observed the ability of embryos to escape after being touched with a small tip at 48hpf. Individuals were classified into four groups according to their ability to escape: 3. normal (corresponding to normal swimming motility); 2. motor

impairments (embryos with minor motility abnormalities); 1. only coiling events (embryos circling without the ability to escape) and 0. paralyzed (embryos with no motility).

Birefringence assay: Muscle birefringence was analyzed by exploiting muscle fibers anisotropy. Briefly, fish were anesthetized with tricaine (160µg/mL) and placed on a glass slide. Two polarizing filters were used. The first filter polarizes light of the stereomicroscope (Leica M165FC). This polarized ray is refracted by anisotropic muscles. The second filter (analyzer) is finally twisted to detect the angle of refracted light until the muscular fibers become maximally brilliant.

Image J analysis: We calculated the density integrated area of birefringence using ImageJ software, as described by Berger et al., in 2012. Birefringence values $\geq 2 \times 10^6$ (typical of WT individuals) were rated as normal, values between 2×10^6 and 1×10^6 were considered as an indication of mild disease and values $\leq 1 \times 10^6$ were rated as an indication of severe myopathy.
Similarly, the cAMP/CREB signal was measured by calculating the integrated area of fluorescent pixels from whole embryos.

Statistical analyses: the efficacy of Pt treatment with respect to DMSO in recovering motor abilities and myofibers structure of ColVI exon9 morphants has been evaluated by applying the *t*test.

Results and discussion

1. Toxicity: dose - response effects.

To assess the toxicity of Pt in zebrafish we first treated WT embryos with progressively increasing concentrations of the compound and, after 24 hours, we evaluated their motility by performing touch-evoked escape response assays (**Fig.1**). The embryos were attributed to four different classes according to their ability to escape (see Materials and Methods). As a readout we calculated the percentage of embryos per class.

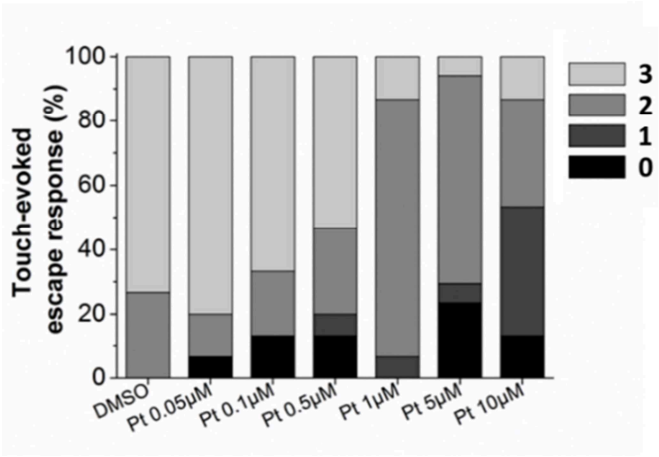


Fig.1: Touch-evoked escape response of WT zebrafish embryos treated with increasing concentrations of Pt. N ≥ 15.

As shown in **Fig.1**, we observed a direct correlation between concentration and abnormalities in the locomotor activities. Moreover, zebrafish embryos treated with concentrations not less than 5µM were notably underdeveloped. Therefore, we did not use these higher doses in subsequent experiments.

2. Morphant zebrafish locomotor activities tests.

To knock down ColVIa1, we injected zebrafish eggs with a morpholino specifically directed against the exon 9 splicing region. This results in the in-frame deletion of the N-terminal region of the ColVIa1 triple helical domain and severe phenotypical abnormalities as in humans. To verify whether Pt could induce a recovery of these impairments, we incubated injected embryos (morphants), with different doses of the phenolic compound ranging from 0.05 to 1µM, at 20hpf. At this stage of development, zebrafish are still confined within the chorion. Since this transparent membrane is almost impermeable, it acts as a barrier to the entry of molecules. Thus, to promote the action of our compound, we dechorionated embryos, mechanically, by using two needles. We then observed spontaneous movements. They consist in alternating tail coils, beginning at about 17hpf and are completely independent of sensory stimulation. Instead, they are driven by the activities in the spinal cord.

Treatment with Pt fully restored spontaneous coiling events at a concentration of 1µM while lower doses were not effective. Similarly, the vehicle (DMSO) did not induce any rescue (**Fig.2**).

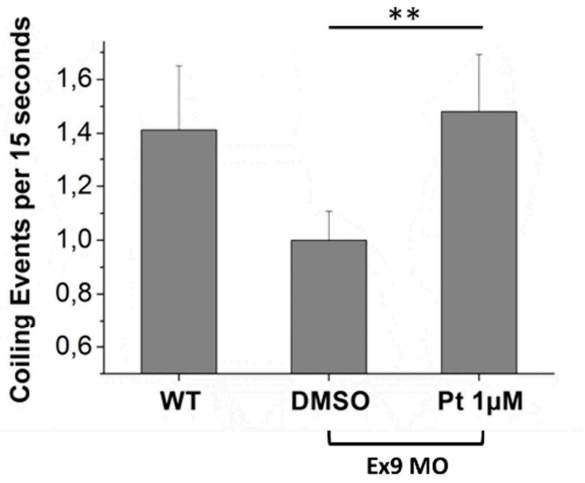


Fig.2. Spontaneous coiling events of ColVI morphant zebrafish. Pt 1µM, after 3 hours, completely eliminated the deficit of spontaneous movements. WT: untreated (no morpholino, no Pt) embryos. Reported are mean values +SEM. N ≥ 100; Pt vs DMSO *t*test yields $p = 0.007$.

As embryogenesis advances, spontaneous movements progressively disappear. When skeletal muscles complete their development, zebrafish embryos show new motor behaviors. In short, they become reactive to mechanical stimuli and respond with strong tail coils generated by rapid trunk contractions.

To further verify the efficacy of Pt on the locomotor activities of ColVI morphants, we also assessed their ability to escape, as described, at 48hpf.

Touch evoked responses improved after treatment with Pt 1µM. Indeed, as shown in **Fig.3**, this phenolic compound induced an increase in the percentages of fish showing either only mild impairments or normal phenotypes.

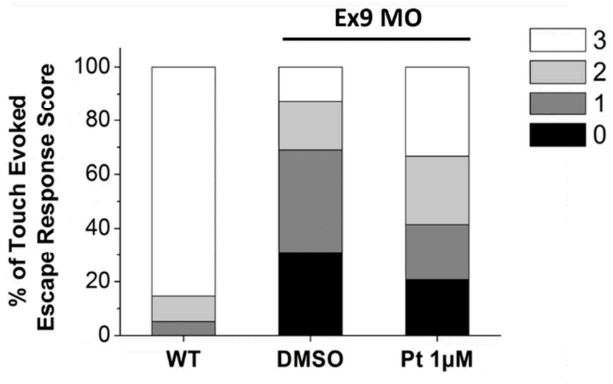


Fig.3: Touch-evoked response assay. Pt 1µM increased the percentage of fish showing mild or normal phenotypes. Responses were evoked by touching 48 hpf embryos with a tip. N ≥ 70. $p = 0.0007$ (*t*test) for Pt vs DMSO.

Finally, we checked the structure of muscle fibers by performing the birefringence test, which exploits muscle anisotropy.

In agreement with the recovery of locomotor activities, Pt 1µM induced a partial but significant rescue of myofiber structure (**Fig.4A** and **B**).

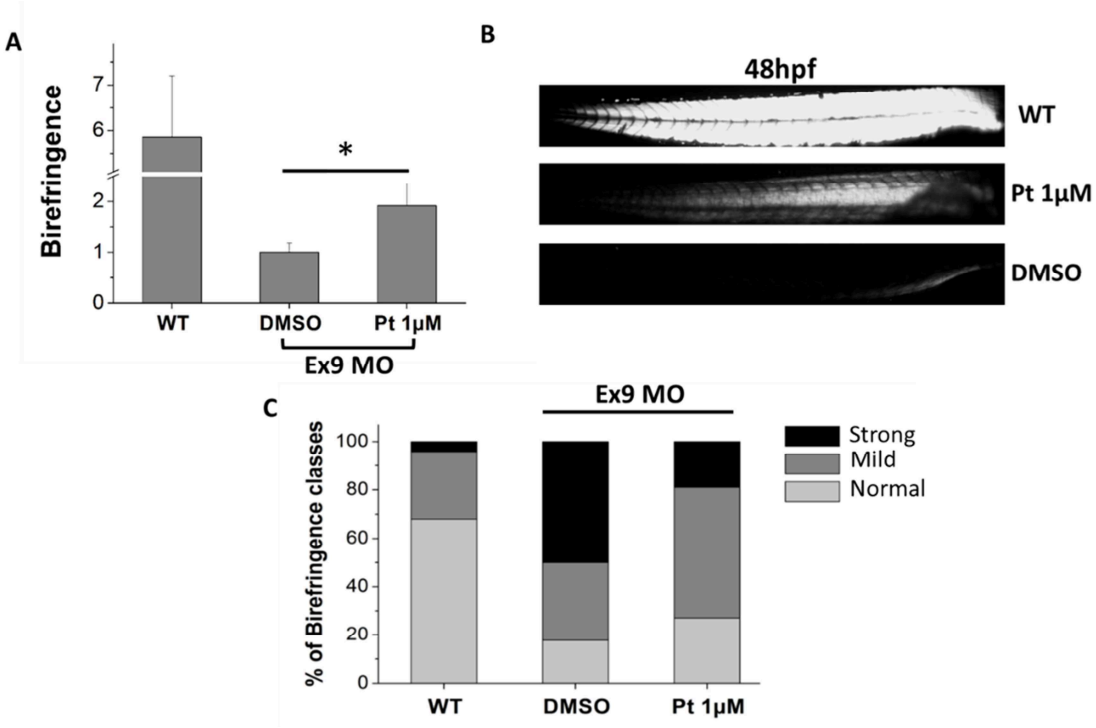


Fig.4: Birefringence assay. (**A**): Pt 1µM induced a significant increase in birefringence of morphants at 48hpf. Pt vs DMSO (*t*test): $p = 0.016$. Reported are mean values +SEM. N ≥ 60. (**B**) Representative images from WT fish or exon 9 morphants after treatment with Pt or DMSO. (**C**) The percentage of fish showing a strong phenotype of ColVI-related myopathy was considerably reduced by 1µM Pt.

Particularly, taking into account fish showing both normal and mild phenotypes, we observed a rescue of about 35% if compared to DMSO (**Fig.4C**). Even though we do not have yet direct evidence of autophagy occurrence, altogether these results strongly support the hypothesis that Pt might promote the recovery of the normal phenotype in these morphants by eliminating dysfunctional mitochondria and stimulating the biogenesis of new healthy organelles. Further analysis needs to be performed.

3. Pt activates cAMP/CREB signaling in zebrafish.

Our previous data suggest that the *in vitro* effects of Pt, at least in part, derive from an increase in cAMP concentration and the downstream activation of AMPK. Hereafter, I will describe initial investigations carried out in zebrafish to demonstrate that this mechanism of action might operate also *in vivo*.

To evaluate whether an increase in cAMP could be reproduced in zebrafish, we first exploited a zebrafish transgenic reporter line in which a gene encoding for a mCherry protein is placed under the control of cAMP responsive elements (CRE). This transgenic animal has been generated by the group of Prof. Natascia Tiso of the Dept. of Biology of the University of Padova, and has been used with her permission and help. As shown in **Fig.5A** and **B**, treatment of these embryos with Pt significantly intensified the fluorescence of their whole body reflecting an increase in cAMP levels and thus the activation of cAMP response elements binding protein (CREB). Notably, this occurs at the concentration of 1µM already reported to promote an amelioration of the ColVI dystrophy phenotype of morphant zebrafish.

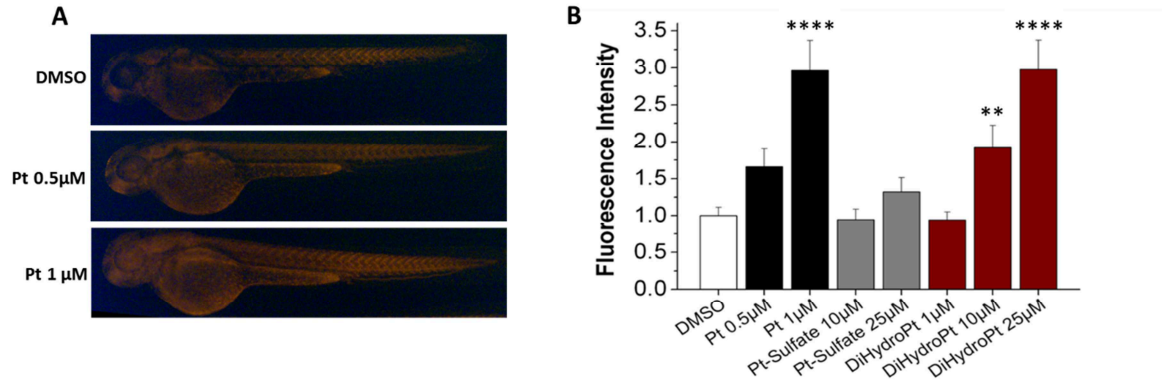


Fig.5: CREB zebrafish transgenic reporter line. (**A**): Pt increased the expression of a mCherry protein under the control of cAMP responsive elements. (**B**): While Pt-4'-Sulfate 25µM was ineffective, DiHydroPt 25µM was approximately as effective as Pt 1µM. ONE-WAY ANOVA statistical test, performed applying Tukey's correction shows that: Pt 1µM vs DMSO $p < 0.0001$; Pt 0.5µM vs Pt 1µM $p = 0.0061$; DiHydroPt 10µM vs DMSO $p = 0.0043$; DiHydroPt 25µM vs DMSO $p < 0.0001$; Pt-4'-Sulfate 10µM vs DiHydroPt 10µM $p = 0.017$; Pt-4'-Sulfate 10µM vs DiHydroPt 25µM $p < 0.0001$; Pt-4'-Sulfate 25µM vs DiHydroPt 25µM $p < 0.0001$; DiHydroPt 1µM vs DiHydroPt 10µM $p = 0.0023$; DiHydroPt 1µM vs DiHydroPt 25µM $p < 0.0001$; DiHydroPt 10µM vs DiHydroPt 25µM $p = 0.0011$. Reported are mean values +SEM. $N \geq 11$. Other comparisons did not reveal statistically significant differences.

Additionally, we tested the efficacy of Pt major metabolites DiHydroPt (produced by intestinal flora) and Pt-4'-Sulfate (a phase II metabolite). In cultured cells, while the sulfated form was almost ineffective, DiHydroPt showed an activity comparable to that of the parent compound but required higher concentrations. Similarly, DiHydroPt 1µM did

not induce any increase in the fluorescence intensity of the mCherry reporter protein. Instead, at the concentration of 25µM it was about as effective as Pt 1µM. Once again Pt-4'-Sulfated had only a slight effect, if any (**Fig.5B**).

Experiments aimed to confirm the activation of cAMP downstream signaling are still ongoing and are too preliminary to be reported here.

Conclusions and further perspectives

Previous studies have demonstrated that defective autophagy has a crucial role in the pathogenesis of muscles dystrophies.

Even though the experiments I reported above do not directly investigate the autophagic pathway, all results we obtained show that Pt ameliorates the phenotype of the zebrafish model of ColVI related myopathies, supporting (but of course not proving) its pro-autophagic action.

In vitro data suggest that Pt promotes TFEB activity in part through the up-regulation of the cAMP-AMPK axis. Accordingly, we observed an enhanced expression of a mCherry reporter protein under control of cAMP responsive elements by the phenolic compound in a zebrafish transgenic line.

To confirm the potential therapeutic effect of this natural molecule in ColVI myopathies, and to ascribe it (or not) to TFEB-mediated autophagy, we are planning to perform biochemical analyses for mitophagic markers as well as to further investigate cAMP downstream signaling.

Moreover, we plan to take advantage of stable ColVI mutants under development in the Department of Biomedical Sciences using CRISPR-CAS9 technology, to extend our analysis to adult zebrafish and to overcome the transient character of morpholino action.

References

1. Azzolini, M., et al., *Pharmacokinetics and tissue distribution of pterostilbene in the rat.* Mol Nutr Food Res, 2014. **58**(11): p. 2122-32.
2. Kosuru, R., et al., *Promising therapeutic potential of pterostilbene and its mechanistic insight based on preclinical evidence.* Eur J Pharmacol, 2016. **789**: p. 229-43.
3. Gomez-Zorita, S., et al., *Pterostilbene improves glycaemic control in rats fed an obesogenic diet: involvement of skeletal muscle and liver.* Food Funct, 2015. **6**(6): p. 1968-76.
4. Poulose, S.M., et al., *Effects of pterostilbene and resveratrol on brain and behavior.* Neurochem Int, 2015. **89**: p. 227-33.
5. Bhakkiyalakshmi, E., et al., *Anti-hyperlipidemic and anti-peroxidative role of pterostilbene via Nrf2 signaling in experimental diabetes.* Eur J Pharmacol, 2016. **777**: p. 9-16.
6. Fu, Z., et al., *Effects of piceatannol and pterostilbene against beta-amyloid-induced apoptosis on the PI3K/Akt/Bad signaling pathway in PC12 cells.* Food Funct, 2016. **7**(2): p. 1014-23.
7. Guo, L., et al., *Pterostilbene inhibits hepatocellular carcinoma through p53/SOD2/ROS-mediated mitochondrial apoptosis.* Oncol Rep, 2016.
8. Zhang, Y. and Y. Zhang, *Pterostilbene, a novel natural plant conduct, inhibits high fat-induced atherosclerosis inflammation via NF-kappaB signaling pathway in Toll-like receptor 5 (TLR5) deficient mice.* Biomed Pharmacother, 2016. **81**: p. 345-55.
9. Guo, Y., et al., *Restoration of sirt1 function by pterostilbene attenuates hypoxia-reoxygenation injury in cardiomyocytes.* Eur J Pharmacol, 2016. **776**: p. 26-33.
10. Feng, Y., et al., *Pterostilbene Inhibits the Growth of Human Esophageal Cancer Cells by Regulating Endoplasmic Reticulum Stress.* Cell Physiol Biochem, 2016. **38**(3): p. 1226-44.
11. Dong, J., H. Guo, and Y. Chen, *Pterostilbene induces apoptosis through caspase activation in ovarian cancer cells.* Eur J Gynaecol Oncol, 2016. **37**(3): p. 342-7.
12. Siedlecka-Kroplewska, K., et al., *Pterostilbene induces accumulation of autophagic vacuoles followed by cell death in HL60 human leukemia cells.* J Physiol Pharmacol, 2013. **64**(5): p. 545-56.
13. Pan, Z., et al., *Identification of molecular pathways affected by pterostilbene, a natural dimethylether analog of resveratrol.* BMC Med Genomics, 2008. **1**: p. 7.
14. Liu, Y., et al., *Pterostilbene exerts antitumor activity against human osteosarcoma cells by inhibiting the JAK2/STAT3 signaling pathway.* Toxicology, 2013. **304**: p. 120-31.
15. Voos, W., et al., *Protein quality control at the mitochondrion.* Essays Biochem, 2016. **60**(2): p. 213-225.
16. Paronetto, M.P., I. Passacantilli, and C. Sette, *Alternative splicing and cell survival: from tissue homeostasis to disease.* 2016.
17. Dengjel, J. and H. Abeliovich, *Roles of mitophagy in cellular physiology and development.* Cell Tissue Res, 2016.
18. Ntsapi, C. and B. Loos, *Caloric restriction and the precision-control of autophagy: A strategy for delaying neurodegenerative disease progression.* Exp Gerontol, 2016. **83**: p. 97-111.
19. Stipanuk, M.H., *Macroautophagy and its role in nutrient homeostasis.* Nutr Rev, 2009. **67**(12): p. 677-89.
20. Redmann, M., V. Darley-Usmar, and J. Zhang, *The Role of Autophagy, Mitophagy and Lysosomal Functions in Modulating Bioenergetics and Survival in the Context*

of Redox and Proteotoxic Damage: Implications for Neurodegenerative Diseases. Aging Dis, 2016. **7**(2): p. 150-62.
21. Grumati, P., et al., *Autophagy is defective in collagen VI muscular dystrophies, and its reactivation rescues myofiber degeneration.* Nat Med, 2010. **16**(11): p. 1313-20.
22. Grumati, P., et al., *Autophagy induction rescues muscular dystrophy.* Autophagy, 2011. **7**(4): p. 426-8.
23. Grumati, P., et al., *Physical exercise stimulates autophagy in normal skeletal muscles but is detrimental for collagen VI-deficient muscles.* Autophagy, 2011. **7**(12): p. 1415-23.
24. Angelin, A., et al., *Mitochondrial dysfunction in the pathogenesis of Ullrich congenital muscular dystrophy and prospective therapy with cyclosporins.* Proc Natl Acad Sci U S A, 2007. **104**(3): p. 991-6.
25. Angelin, A., P. Bonaldo, and P. Bernardi, *Altered threshold of the mitochondrial permeability transition pore in Ullrich congenital muscular dystrophy.* Biochim Biophys Acta, 2008. **1777**(7-8): p. 893-6.
26. Bertini, E. and G. Pepe, *Collagen type VI and related disorders: Bethlem myopathy and Ullrich scleroatonic muscular dystrophy.* Eur J Paediatr Neurol, 2002. **6**(4): p. 193-8.
27. Allamand, V., et al., *ColVI myopathies: where do we stand, where do we go?* Skelet Muscle, 2011. **1**: p. 30.
28. Bernardi, P. and P. Bonaldo, *Mitochondrial dysfunction and defective autophagy in the pathogenesis of collagen VI muscular dystrophies.* Cold Spring Harb Perspect Biol, 2013. **5**(5): p. a011387.
29. Chu, M.L., et al., *Sequence analysis of alpha 1(VI) and alpha 2(VI) chains of human type VI collagen reveals internal triplication of globular domains similar to the A domains of von Willebrand factor and two alpha 2(VI) chain variants that differ in the carboxy terminus.* Embo j, 1989. **8**(7): p. 1939-46.
30. Chu, M.L., et al., *Mosaic structure of globular domains in the human type VI collagen alpha 3 chain: similarity to von Willebrand factor, fibronectin, actin, salivary proteins and aprotinin type protease inhibitors.* Embo j, 1990. **9**(2): p. 385-93.
31. Schessl, J., Y. Zou, and C.G. Bonnemann, *Congenital muscular dystrophies and the extracellular matrix.* Semin Pediatr Neurol, 2006. **13**(2): p. 80-9.
32. Irwin, W.A., et al., *Mitochondrial dysfunction and apoptosis in myopathic mice with collagen VI deficiency.* Nat Genet, 2003. **35**(4): p. 367-71.
33. Zulian, A., et al., *Forty years later: Mitochondria as therapeutic targets in muscle diseases.* Pharmacol Res, 2016. **113**(Pt A): p. 563-573.
34. Zulian, A., et al., *NIM811, a cyclophilin inhibitor without immunosuppressive activity, is beneficial in collagen VI congenital muscular dystrophy models.* Hum Mol Genet, 2014. **23**(20): p. 5353-63.
35. Lieschke, G.J. and P.D. Currie, *Animal models of human disease: zebrafish swim into view.* Nat Rev Genet, 2007. **8**(5): p. 353-67.
36. Zon, L.I. and R.T. Peterson, *In vivo drug discovery in the zebrafish.* Nat Rev Drug Discov, 2005. **4**(1): p. 35-44.
37. Chakraborty, C., et al., *Zebrafish: a complete animal model for in vivo drug discovery and development.* Curr Drug Metab, 2009. **10**(2): p. 116-24.
38. Telfer, W.R., et al., *Zebrafish models of collagen VI-related myopathies.* Hum Mol Genet, 2010. **19**(12): p. 2433-44.
39. Blum, M., et al., *Morpholinos: Antisense and Sensibility.* Dev Cell, 2015. **35**(2): p. 145-9.

40. Lee, O., J.M. Green, and C.R. Tyler, *Transgenic fish systems and their application in ecotoxicology.* Crit Rev Toxicol, 2015. **45**(2): p. 124-41.

Chapter 7

Pterostilbene improves cognitive performance in aged rats: a mechanistic pilot study

Summary

Pterostilbene (trans-3,5-dimethoxy-4'-hydroxystilbene, Pt) is a natural polyphenol mainly existing in blueberries and grapevines. Interest in this compound has been affirmed in recent years as it shows an array of biomedical activities similar to those of its non-methylated analogue, Resveratrol (Rv). Furthermore, its higher bioavailability represents an additional advantage.

Several studies have reported that aged rats, fed a diet containing Pt, underwent an amelioration of cognitive functions demonstrating the capability of this molecule to counteract deleterious effects caused by aging in the nervous system. However, no insights about the underlying molecular mechanisms have been provided.

Investigations I performed with cultured cells during my PhD program have shown that Pt may increase the intracellular cAMP concentration leading to the activation of transcription factor CREB. These observations have been confirmed in a zebrafish cAMP reporter line.

CREB is known since far back to be involved in memory consolidation as it promotes neurogenesis in the dentate gyrus of the hippocampus of adult individuals.

In light of this, we began a pilot *in vivo* study aimed to evaluate the behavioral effects of Pt in aged animals characterized by a mild cognitive impairment and to verify the impact, if any, of the treatment on the phosphorylation (i.e., activity) of CREB in the hippocampus. To this purpose, 18-month-old rats were subjected to cognitive tests to establish the "baseline", then chronically fed Pt for 20 consecutive days, tested again and sacrificed. The dentate gyrus, the hippocampus and the prefrontal and perirhinal cortices were then collected and RT-qPCR and/or western blot analyses were performed on ph-CREB and a few other proteins potentially involved in remodeling. Additionally, mitochondrial content was assessed as these organelles are essential to provide energy during synaptic remodeling processes and are believed to play a role in cognitive decline.

The scores reached in behavioral tests by treated animals indicate that Pt administration improved their performance and positively affected memory consolidation. CREB activity

tends to be up-regulated in the hippocampus, however, the low numerosity in this preliminary analysis did not allow the achievement of statistical significance.
Importantly, the dentate gyrus seems to be the cerebral region most affected by treatment with Pt as suggested by the positive correlations between the mean values of ph-CREB or BDNF expression in this region and the scores obtained by the animals in the Tmaze test. Similar results were obtained when assessing mitochondrial mass. No effects could be reliably observed in the remaining cerebral areas we examined.
Concluding, our results, although preliminary, are encouraging and confirm that the activities Pt displays *in vitro* may represent relevant mechanisms of action *in vivo*, to be taken into account for an appropriate exploitation of its therapeutic potential.

Introduction

It is widely recognized that an appropriate nutrition may favor a healthy aging [1, 2]. An elevated intake of fruits and additional plant-derived foods seems to preserve brain plasticity and to protect from the progressive cognitive decline associated with aging and neurodegenerative disorders [3-7]. This is mainly attributed to the presence of bioactive components and their properties. In this regard, polyphenols, and in particular flavonoids and the stilbene Resveratrol (trans-3,4,5-tryhydroxystilbene, Rv) have attracted much attention [8-10].
The neuroprotective role of polyphenols may be mainly ascribed to their inter-connected anti-inflammatory and anti-oxidant properties.
For a long time, these natural compounds have been considered to act as direct scavengers of free radicals, but this has now been recognized to be of only minor relevance *in vivo*. A considerable amount of research has led to the conclusion that they may reduce the production of free radicals by inhibiting the activities of several enzymatic families such of NADPH and xanthine oxidases [11]. Moreover, under specific conditions, polyphenols act as mild pro-oxidants to elicit positive, beneficial responses from cells [12, 13] such as the activation of the Nrf2-ARE signaling pathway, well-documented in neuronal cell lines [14]. The transcription factor Nrf2 is usually retained in the cytosol because of an inhibitory binding to the protein Keap1 that promotes its degradation through the ubiquitin-proteasome system (UPS). Instead, in case of a pronounced oxidative stress, Keap1 detaches from Nrf2 allowing its migration to the nucleus. Here, it binds to the anti-oxidant responsive elements (ARE) and drives the expression of detoxifying enzymes such as

NAD(P)H quinone oxidoreductase 1 (NQO1), heme oxygenase 1 (HMOX1), glutamate-cysteine ligase (GCL) and glutathione S transferases (GSTs) [14, 15].

Nrf2 is not the only transcription factor whose activity is modulated by phenolic compounds. Indeed, some of them may also antagonize the activation of NF-kB, the master regulator of the inflammatory process [16-18]. Like Nrf2, NF-kB is usually confined outside the nucleus by the interaction with the protein IkB. However, upon binding of pro-inflammatory mediators to membrane receptors, IkB kinase (IKK) is activated and phosphorylates IkB promoting its degradation by the proteasome and the nuclear translocation of NF-kB [19, 20]. As a consequence, the expression of pro-inflammatory genes occurs.

However, even in hindering neuro-inflammation polyphenols may act by multiple mechanisms. Indeed, they can prevent both the release of cytokines or chemokines by activated resident immune cells (astrocytes and microglia) and their binding to surface receptors leading to the activation of neuronal cell death pathways (involving p38 and JNK) [18, 21]. Polyphenols may also act *a priori*, counteracting the inducers of inflammation such as protein aggregates, typical hallmarks of neurodegenerative disorders, promoting their elimination through UPS or autophagic pathways or preventing the formation of noxious higher-order aggregates by amyloidogenic proteins (Aβ, α-synuclein, and tau) [22-25].

Secondarily, the benefits of phenolic compounds in the nervous system have been associated to their neurotrophic properties. Indeed, many of them competitively mime the action of neurotrophins such as BDNF, NGF, NT3 and NT4 binding to several transmembrane receptors such as tropomyosin receptors kinase (TrK) [26, 27]. Upon their activation, intracellular signaling cascades get started culminating in neurite growth and in the establishment of new synapses. Thus, gene expression and protein synthesis take place. Finally, polyphenols can up-regulate enzymes involved in the synthesis of neurotrophic factors as well as modulate the expression of TrK receptors [14, 28-34].

The implementation of polyphenols' effects reported above strictly depends on their bioavailability and brain accessibility.

Recently, Pterostilbene (trans-3,5-dimethoxy-4'-hydroxystilbene) has gained the attention of the scientific community for its salutary actions largely overlapping those of its non-methylated analogue, Rv. However, the former seems to be more effective than the latter. We performed pharmacokinetic analysis of Pt in organs of rats, reporting higher levels of

the compound than those reached by Rv after administration of an equimolar dose, which might account for the superior effectiveness (chapter 3) [35]. Notably, unlike other organs, the brain revealed an elevated amount of non-metabolized Pt.

Pt seems to positively affect memory in adults. Indeed, several studies have reported that it improves the abilities of rodents showing sporadic and age-related neurodegenerative disorders in performing specific behavioral tests [36]. The molecular mechanisms underlying these effects have not been fully elucidated.

Memory formation is a very complex phenomenon. Information is initially stored as short-term memory that persists, at most, only several hours. To generate a prolonged and stable memory (long-term memory), consolidation processes are required [37]. They mainly comprise *de novo* gene expression and proteins synthesis and therefore rely on the activities of different transcription factors. Among them, cAMP responsive elements binding protein (CREB) has been demonstrated to play a central role [38].

CREB affects cognitive process and memory consolidation by promoting adult hippocampal neurogenesis that mainly takes place in the sub-granular zone of the dentate gyrus. [38-40]. Its activation depends on phosphorylation at serine 133. This post-translational modification is mainly ascribed to protein kinase A (PKA) upon an increase in cAMP. MAPK and Ca^{2+}-CaMKIV pathways may modulate the phosphorylation level of CREB (ph-CREB) as well. Moreover, its action is strongly supported by CREB binding protein (CBP). This is an acetyl-transferase enzyme recruited and bound by ph-CREB itself, that masks positive charges of lysine residues in histone “tails”. In this manner, the interactions with the negative charges of DNA are prevented, the chromatin acquires an unfolded structure and becomes accessible to the transcription factor. In the absence of this process, its activation would be irrelevant.

In addition to the up-regulation of gene expression and protein synthesis, the phenomenon of memory consolidation is accompanied by an increment of mitochondrial biogenesis. These organelles, as main producers of ATP, are necessary to provide energy for fundamental cellular processes involved in neurite outgrowth such as cytoskeletal remodeling, membrane turnover and transport of various protein cargos [41] underlying the establishment of new synaptic connections. Conversely, a reduction in mitochondrial turn-over is associated with the cognitive decline of aging and neurodegenerative disorders and may be ascribed to alterations in degradative pathways such as autophagy.

My *in vitro* investigations, described in chapter 5 of this thesis, have shown that Pt induces CREB activation. This has been confirmed in a zebrafish transgenic line (chapter n. 6). At

the same time, experiments I performed with cultured cells suggest this stilbene can stimulate pgc-1α-dependent mitochondrial biogenesis as well as autophagy.
In light of this, in collaboration with Prof. Nicoletta Berardi and the research group of Dr. Alessandro Sale (Institute of Neuroscience, CNR, Pisa), we set up a study aimed at evaluating whether a chronic administration of Pterostilbene could ameliorate cognitive performance in aged rats manifesting a mild cognitive impairment and at assessing molecular modifications at both transcriptional and translational levels, if any.
The results I report hereafter are still incomplete but substantially promising.

Materials and methods

Animal handling and treatments: all procedures met the requirements of the Italian Ministry of Health (Laws 116/92 and 26/214) and European Community Council (Directives 86/609/EEC and 210/63/UE).
9 male and 6 female 18-months-old Long-Evans rats were housed in the facility of the Institute of Neuroscience (Pisa) under a 12-hour light regimen. Food and water were provided *ad libitum.*
Rats were subdivided into treated and untreated groups; females and males were equally distributed. Animals belonging to the treated group received for 20 consecutive days a 22.5 mg/kg dose of Pt (Waseta Int. Trading Co., Shangai, P.R. China) (the molar equivalent of 20 mg/kg of Resveratrol) in a palatable jelly prepared as described by Zhang Lei ([42]; materials were from commercial shops) twice a day. Instead, animals of the "control" group received "unloaded" jelly.
Drug incorporation in jelly was preferred over addition in food or water to provide Pt since, as reported by Zhang et al., 2011 [42], it ensures a controlled administration and does not cause stress to animals.
To manufacture the jelly, two different solutions were prepared in parallel:

1) Grated Parmigiano cheese was blended with commercial mineral water (ratio 1:2) under stirring for 30 minutes; then the mix was filtered in order to obtain a savory liquid
2) Lyophilized jelly (PaneAngeli) was re-hydrated with mineral water at room temperature for 10 minutes; following re-hydration, the jelly was liquefied by heating at 55-60° C under stirring for 10 minutes

Finally, the two solutions were mixed to obtain a homogenous solution. Pt was added to the mixture for the treated group. The difference in the average weight of male and female animals was taken into account in calculating the concentration of Pt needed to provide the desired dose of about 22.5 mg/kg body weight in each 500µL jelly portion. The preparate was further stirred and aliquoted into a 48 well-plate (500µl) and stored at 4° C. Before the beginning of the Pt treatment, animals were handled daily to avoid neophobia. Rats promptly learned to eat jellies voluntarily since they were attracted by their flavor.
The cognitive performance of the animals was evaluated both prior and after 20 days of jelly administration, carrying out the Tmaze, object recognition and object in context tests (described below). As their execution requires several days, vehicle jellies were provided to all animals for the entire duration of baseline assessment of the performance to avoid loss of interest in the flavor. Similarly, we prolonged the administration of "unloaded" and "loaded" jellies to untreated and treated animals respectively, during the period of final evaluation (about two weeks) to sustain the effect of Pt, if any.
After the final round of behavioral tests, the animals were sacrificed under anesthesia (Isoflurane). The brain was quickly removed and dentate gyrus, hippocampus and prefrontal and perirhinal cortices were dissected. Each specimen was immediately placed in a sealed vial, rapidly frozen by immersion in a bath of isopentane and dry ice and stored at -80° C.

Tmaze: the Tmaze test was carried out adapting the protocol reported by Dominguez G et al., in 2014 [43]. Briefly, animals were placed at the bottom of a T-shape box for ten successive trials at 90 seconds intervals. Each time the animal chose and entered the arm opposite to the one examined during the previous trial was classified as an alternation response. The alternation rate was calculated by considering the nine successive trials, and expressed as the mean of the arm alternation. To avoid olfactory suggestions, the cage was washed with water and ethanol after each trial.

Object recognition test (ORT): this behavioral test was carried out using a polyvinyl chloride (PVC) square arena, with black walls and white floor, and cubical plastic objects that differed for the visual patterns lining the walls of the cube. The experimental protocol was set up according to the guidelines described by Ennaceur and Delacour [44]. The entire assessment consisted of three consecutive sections: 1) habituation phase; 2) sample phase; 3) test phase

1) Rats were placed in the empty arena for 5 minutes in order to familiarize with the apparatus and test room;
2) After 24 hours, each animal was placed in the arena again, exposed to two identical objects for 5 minutes and returned to its own cage;
3) Finally, after 1 or 24 hours, the rats were placed back in the arena for a third time and exposed to either a familiar object (an object identical to those seen in the sample phase) or a novel object, located in the same positions as in the sample phase, for 5 minutes. Specifically, the novel object for one-half of the animals, treated or untreated, represented the familiar object for the remaining half for each retention time interval. The couples of objects used for the two sessions, 1 or 24 hours, differed.

The time spent by each animal exploring the objects was recorded and a discrimination index was calculated as described below (see measurements and statistics part). Box and objects were cleaned up between trials to avoid interference by olfactory suggestions.

Object in context test (OCT): The protocol used was similar to that previously described by De Rosa et al. in 2005 [45]. Unlike the object recognition test, it took advantage of two different PVC arenas differing by shape (circular and square). One furthermore presented horizontal white stripes on the black walls and a floor covered by rough Plexiglas while the other had gray walls and the floor was made by smooth Plexiglas. The first and second arenas represented respectively experimental condition A and experimental condition B. The assessment consisted in determining the animals' sensitivity to a change in context for a given object.

In this case, two 5 minute-long habituation phases were carried out during which rats were exposed to both conditions A and B. The two habituation phases were followed by four sample phases and one test phase, each lasting 3 minutes. The recovery period within the sample phases was 3 minutes long while there were five minutes of interval between the last sample phase and the test phase (the habituation phase was started two days before the test phase).

During the four sample phases, two objects were positioned in adjacent corners of the arena. Specifically, objects A_1 and A_2 were placed in environment A during phases 1 and 4 while objects B_1 and B_2 were placed in environment B during phases 2 and 3. Finally, the test phase took place in the same environment of sample phase 4, but object A_2 was replaced by object B_2 so that only one object was in the same environment as in the sample

phase. To avoid any confounding preference for context A or context B, half of the animals started the sample phase in environment A with object A_1 and A_2 and finished the assessment in the same environment with objects A_1 and B_2 and *vice versa*. Habituation and samples phases will be referred to as a single training period in the results section.

Measurements and Statistics: The mean of the arm alternations has been calculated as evaluation criterion for the Tmaze experiments. The preference to enter one arm rather than the other one was compared across groups (treated and untreated) with the Mann-Whitney statistical test.

For the statistical analysis of the results of ORT and OCT, the parameter taken into account was the time spent exploring the objects. The exploration of an object was defined as directing the nose to the object at a distance of < 2 cm and touching it with the nose. Turning around, climbing over, or sitting on the object were not considered. Animals were excluded if their exploration time was < 3 seconds in the sample phase. Similarly, they were discarded if the time exploring familiar and new objects was < 1 second in the test phase. A discrimination index (DI) was calculated, both for ORT and OCT, as the difference between the time spent exploring new and old objects divided by the total time spent exploring the objects [$(n - f)/(f + n)$, where n represents new and f represents familiar]. The total time spent exploring each object was recorded and compared across different groups (treated and untreated), through the Mann-Whitney statistical test. The scores obtained by the same set of animals, prior to and after administration of the jellies, were compared by applying Wilcoxon's statistical test.

RT-qPCR and Western Blot: Total RNA and proteins were extracted from dentate gyrus, hippocampus, prefrontal cortex and perirhinal cortex of both treated and untreated groups of animals following TRIzol® (Invitrogen) extraction methods, according to the manufacturer's instructions.

For retrotranscription, reaction mix tubes, each containing 100ng of RNA, were mixed and incubated first at 25° C for 10 minutes. Next, they were incubated at 42° C for 60 minutes. Finally the reaction was arrested by heating at 85° C for 5 minutes. All samples were simultaneously processed to reduce experimental variability. In order to measure the expression levels of genes of interest, specific primers were designed using Primer3input (http://bioinfo.ut.ee/primer3-0.4.0/primer3/) or Primer Blast NCBI

(http://www.ncbi.nlm.nih.gov/tools/primer-blast/) or taken from already published sequences (for *gapdh* and *bdnf*: [46]).

Primer sequences were as follows:

Glyceraldehyde 3-phosphate dehydrogenase (*gapdh*): Fw ATCACCATCTTCCAGGAGCG; Rv GATGGCATGGACTGTGGTCA

Meis homeobox 1 (*meis1*): Fw GCACAGGTGACGATGATGAC; Rv GAAGGATGGTGAGTCCCGTA

Desmoplakin (*dsp*): Fw CACTCCCAGTCTTCACAGCA; Rv TTTCTCCAGGTCCCACAATC

Brain-derived neurotrophic factor (*bdnf*): Fw ATAGGAGACCCTCCGCAA; Rv CTGCCATGCATGAAACACTT

RT-qPCR was carried out in a 96-well IQ5 Thermal Cycler (BioRad) and each sample was measured in duplicate. IQ Syber Green Supermix (Biorad) was used as detection system. Normalization was performed using the ΔC_T method. GAPDH was used as reference gene.
For Western blot analyses, protein samples were supplemented with sample buffer (1X: 62.5mM Tris-HCl pH 6.8, 2% SDS, 10% glycerol, 50mM DTT, 0.02% bromophenol blue) and heated for 5 minutes. Pre-cast Bis-Tris gels (NUPAGE, Invitrogen) at different percentages of acrylamide were used depending on the molecular weight of the proteins of interest. After electrophoretic separation, proteins were transferred to PVDF membranes (Pall Corporation). Next, the membranes were saturated with 5% BSA (Sigma-Aldrich) at room temperature for 1 hour and incubated with primary antibodies, overnight at 4° C. The following day, membranes were washed with TBS Tween 0.1% (TBST) and incubated with IRDye 680RD or 700DX secondary antibodies (LICOR). Finally, there were washed three more times before detection with the Odissey Imaging System (LICOR).
Antibodies against the following proteins were used: LC3B (Cell Signaling, Rb, monoclonal, 1:1000); phospho-CREB (Cell Signaling, Rb, monoclonal, 1:1000); β-Actin (Cell Signaling, Ms, monoclonal, 1:5000). VDAC1/porin (Abcam, Ms, monoclonal 1µg/mL).

Results

1. Behavioral tests

As mentioned in the introduction, the phenomena of memory formation and consolidation in adults, resulting from the action of transcription factors such as CREB, predominantly occur in the dentate gyrus of the hippocampus [38-40]. Therefore, we chose specific behavioral tests that could reflect the activities in this area of the brain, such as the Tmaze and OCT. While the latter is strictly dependent on hippocampal function, the former and its variants may also be used to evaluate other activities of the nervous system.

Aging, in addition to affecting memory, significantly impairs other functions in the nervous system. Since this is a preliminary study, we decided to extend our investigations to two main areas (perhirinal and prefrontal cortices) in order to evaluate the broad-spectrum effects of Pt on cognitive processes. The ORT has been considered as a method to evaluate their functionalities.

The baseline evaluation revealed that all 18-month-old rats homogeneously presented a mild age-related impairment of cognitive functions.

- **Tmaze:** this test provides an index of working memory involved in holding transient information in mind and in its manipulation [47-49]. In this trial, animals could voluntarily decide the arm of the T-shape box to explore. Rodents with impaired memory are expected to achieve a lower arm alternation score than controls.

  While treated animals reported a score similar to that recorded before Pt administration, untreated animals remarkably underwent a deterioration in performing this task, suggesting that the phenolic compound played a role in preserving cognitive function (**Fig.1**).

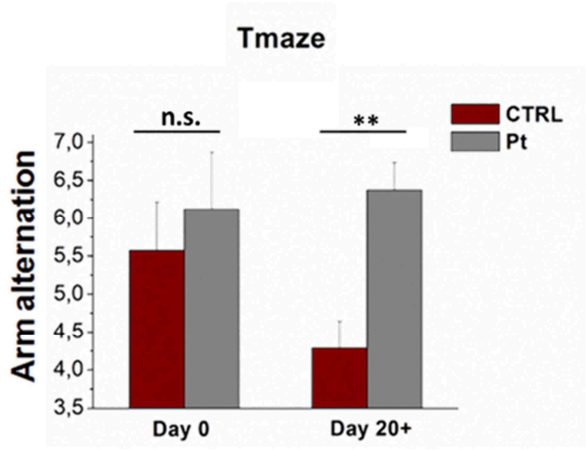


Fig.1: the working memory of treated animals is remarkably more efficient than that of control animals. Mann-Withney's test was applied as statistical analysis to compare the baseline and final behavioral evaluations. After 20 days, $p = 0.0025$ by comparing scores obtained by treated rats with those reached by control animals. Wilcoxon's test was also used to compare both treated and untreated animal prior to and after administration of the jellies, but no statistical differences were found. $N \geq 7$; Error bars represent standard error of the mean (SEM).

- **Object in context test:** this kind of test is specific for the assessment of memory consolidation [50-53]. It was performed twice, at 1 and 24 hours after a training period (see Materials and Methods). Importantly, to avoid recollection of the previous test, objects used in the first session differed from those used in the second one. As shown in **Fig.2**, Pt treatment turned out to be effective and in both tests allowed animals to obtain a higher score. Conversely, untreated rats maintained a behavioral deficit similar to that reported during the baseline evaluation.

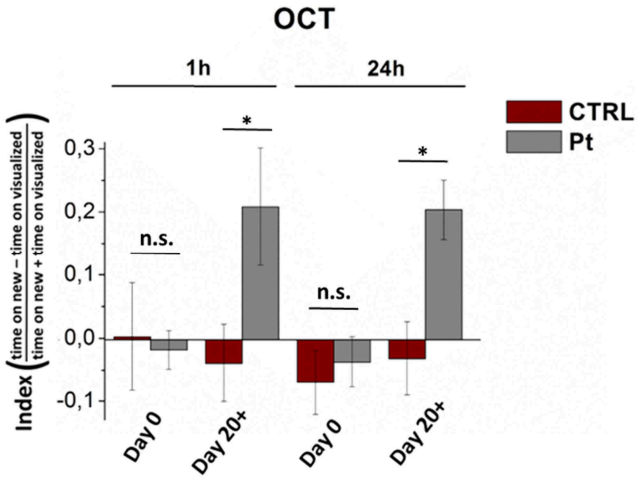


Fig.2: The object in context test was carried out 1 and 24 hours after two preliminary phases. 20 consecutive days of Pt treatment positively affected the performance of rats and the consolidation of short-term memory. Mann-Withney's test applied to comparing treated rats with control animals shows significant differences both 1h (p = 0.0379) and 24h (p = 0.02) after the habituation and sample phases. Wilcoxon's test was used to compare treated and untreated rats prior to and after the administration of the jellies. By comparing scores obtained by treated rats after 20 days of Pt administration with the scores reached by the same animals during the baseline evaluation, during the session carried out 24h after the preliminary phases, p = 0.0078. N ≥ 7; error bars represent SEM.

- **Object recognition test:** this test aimed to assess spatial memory relative to environmental representations [50, 54, 55]. Like OCT, it was performed twice, 1 and 24 hours after a training session and gave similar results. Indeed, animals chronically treated with Pt explored the new object more if compared to those belonging to the control group in both cases (**Fig.3**).

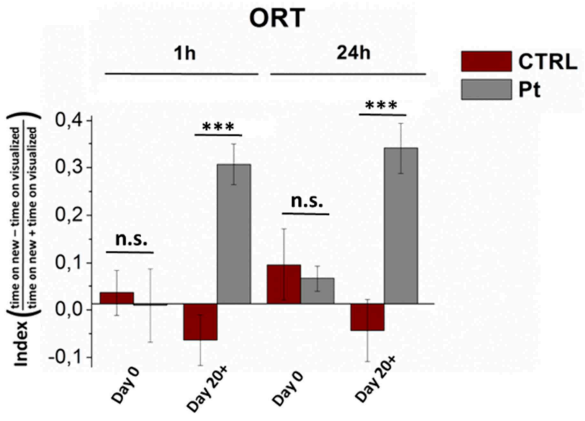


Fig.3: object recognition test. Pt treatment allowed aged rats to reach higher scores in both sessions of this task. Mann-Withney's test reveals statistically relevant differences between treated and untreated animals after the Pt administration period both at 1h (p = 0.0003) and 24h (p = 0.0006) after the habituation and sample phases. Wilcoxon's statistical test was performed to compare scores obtained by treated or untreated animal prior to and after administration of the jellies. The scores obtained by rats following Pt treatment (24h after the preliminary phases) differ significantly (p = 0.0156) from the scores obtained by the same animals during the baseline evaluation. N ≥ 7; Error bars represent SEM.

2. Dentate gyrus dissection accuracy control

The behavioural analyses confirmed that Pt may rescue deficit in cognitive functions of old rats. Before further proceeding with investigations, we checked the accuracy of the dentate gyrus isolation. This cerebral area is wrapped up by the surrounding anatomical structures and especially by the residual hippocampus. As a consequence, its dissection is markedly difficult. Hereafter in reporting the results with the term "hippocampus" I refer to the excised cerebral tissue containing the hippocampus minus the dentate gyrus.

We measured the expression levels of *dsp* and *meis1* genes, molecular markers of the dentate gyrus and the hippocampus respectively [56].

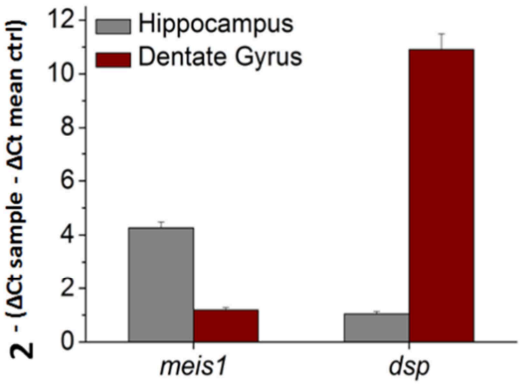


Fig.4: RT-qPCR of dentate gyrus and hippocampal markers. Each bar represents the average of 15 animals. Error bars reported as SEM.

As shown in **Fig.4** mRNA levels of the *dsp* gene were considerably higher in the samples supposed to be the dentate gyrus while they were irrelevant in the hippocampal fraction of the whole set of animals and *vice versa* the *meis1* transcript was more abundant in the remaining hippocampal tissue. This indicates that the dissection was appropriately performed.

3. Is CREB involved in memory consolidation of aged rats?

To verify whether the activity of the transcription factor CREB could account for the amelioration of cognitive functions by Pt, we adopted a double approach.

First, we looked at its phosphorylation levels in both dentate gyrus and hippocampal samples by Western blot. Although statistical significance was not reached due to the low numerosity, as shown in **Fig.5,** the mean value of ph-CREB was higher in animals chronically treated with Pt if compared to untreated animals in both areas of the brain.

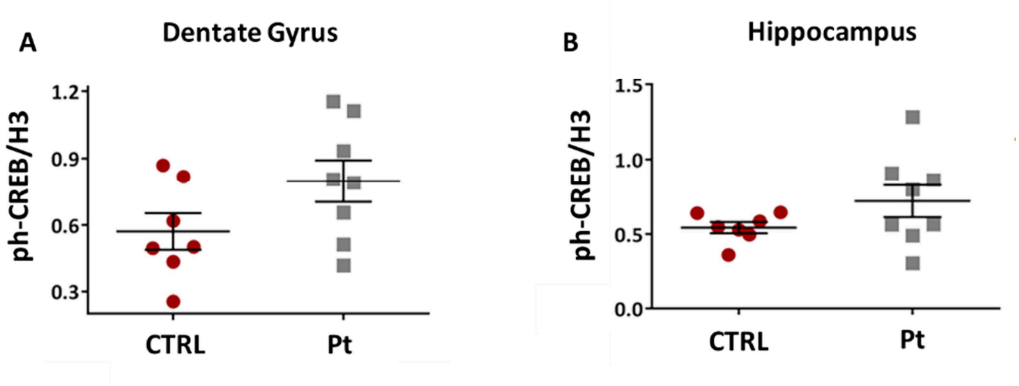


Fig.5: Western blot analyses of ph-CREB. **A** and **B**: Pt treatment seems to stimulate the activation of the transcription factor mainly in the dentate gyrus of 18-month-old rats rats.

Interestingly, this difference was more evident in the dentate gyrus. Indeed, a positive correlation has been found between the scores reported by each animal in the Tmaze test and its ph-CREB levels in the dentate gyrus but not in the hippocampus (**Fig.6**).

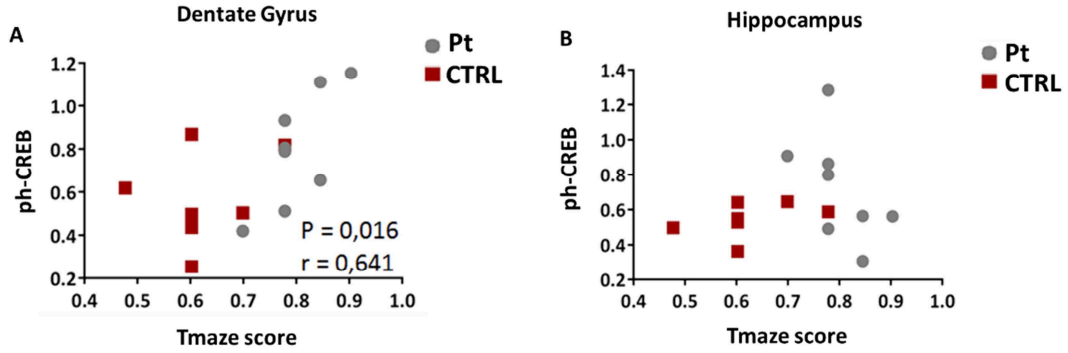


Fig6: Correlations between the scores in the Tmaze behavioral test and CREB phosphorylation levels (normalized to Histone 3) in the Dentate gyrus (**A**) and in the hippocampus (**B**).

Second, we measured by qPCR the mRNA levels of BDNF, a widely recognized CREB target gene [57, 58]. In agreement with the previous results, the mean level of transcription of this neurotrophin was slightly higher in the dentate gyrus of animals treated with Pt if compared to that in untreated animals (**Fig.7A**).

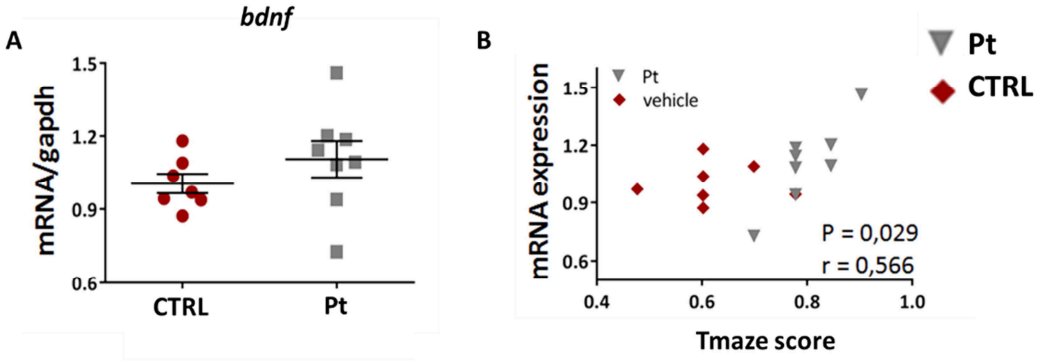


Fig.7. (**A**): mean values BDNF mRNA in the dentate gyrus of old animals. Again, these are higher in treated animals and positively correlate with the score in the Tmaze test (**B**).

Also in this case, we found a positive correlation between the score reached in the Tmaze behavioural test by each animal and the relative amounts of BDNF mRNA in the dentate gyrus (**Fig.7B**). Conversely, no differences have been observed in the hippocampus.

Finally, looking for evidence of neuronal plasticity, we considered postsynaptic density protein 95 (PSD95) [59]. PSD95, a "scaffold" protein, is known to play an important role in the stabilization of modifications of synaptic structures, underlying functional activity-related changes, such as memory formation and consolidation [60].

Somewhat surprisingly, the levels of this protein, measured by Western blot, were however similar in the dentate gyrus of treated and untreated animals (data not shown).

All the investigations I just described have been carried out in parallel also on prefrontal and perirhinal cortices samples. However, Pt treatment seemed to have no effect in these areas of the brain. I therefore decided to limit the analysis to the dentate gyrus and residual hippocampus.

4. Pt treatment induces an increment in mitochondrial mass but apparently not in autophagy

Although not yet statistically relevant, our preliminary data lead us to speculate that Pt might promote neurogenesis with the establishment of new synaptic connections. Thus, it is credible to assume that these processes are accompanied by an increment in mitochondria content, as these organelles are the main cellular suppliers of energy [41].

We carried out Western blot analyses for porin1, a protein of the mitochondrial outer membrane often used as mitochondrial marker. As expected, the amount of porin1 (normalized to histone 3, taken as reference housekeeping protein) was higher in the dentate gyrus of the rats which had received Pt than in that of untreated animals. (**Fig.8 A**).

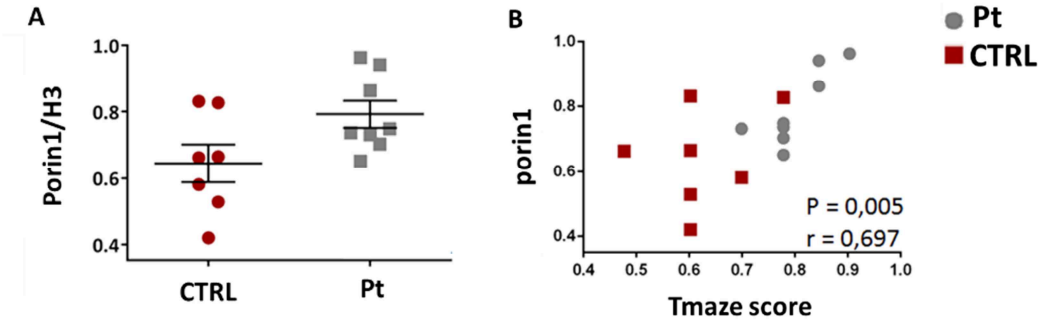


Fig.8. (**A**): mean values of porin1 expression in the dentate gyrus of old animals. (**B**): Plots displaying the direct correlation with the scores in the Tmaze test.

Once again, a direct correlation seems to exist between porin1 levels and the scores obtained in the Tmaze test (**Fig.8B**). No effect of Pt was detected in the hippocampus (data not shown).

On the contrary, autophagy seemed to be unaffected by Pt treatment. I was also unable to uncover evidence for a stimulation of autophagy by Pt in this experimental system. Indeed, no significant differences in the lipidation levels of LC3, used as indicative parameter of the occurrence of this degradative pathway [61], were observed (data not shown; on this point however please see the Discussion).

Discussion and future perspectives

Although incomplete, our results have confirmed that Pt ameliorates cognitive deficits in old rats by positively affecting memory consolidation. RT-qPCR and Western blot analyses suggest that these effects might be associated to the stimulation of CREB activity and, consequently, rearrangements in the neuronal architecture.

I may propose a comment on the plots correlating the levels of a biochemical parameter (CREB phosphorylation, BDNF mRNA and porin1 levels) and the performance in the Tmaze test (Fig.s 6, 7, 8). A positive correlation seems evident if one considers the plots obtained after treatment (grey symbols), while no such correlation is apparent in the plots of the data obtained from untreated rats. Why should a correlation be lacking in this latter case? I do not have a definite answer, but the reason might have to do with the cooperation of multiple molecular factors to set the level of cognitive performance, which certainly is not determined by the status of a single protein. In untreated animals, some of these factors may be in a favourable state and others in an unfavourable one, resulting in a poor

correlation of overall performance with any given factor. Pt administration may act to correlate at least those of these factors which are under the control of, let's say, ph-CREB. Thus, depending on factors such as, for example, the exact age of the rat, the extent of absorption of Pt from the gastrointestinal tract, the power of Phase II metabolism in each individual, the exact time elapsed from cognitive testing to sacrifice, in one case the upregulation of ph-CREB might have been stronger than in another. Genes downstream of ph-CREB, such as BDNF, would consequently be upregulated more strongly in the former case than in the second. The stronger or weaker coordinated modulation of multiple factors at once would now be expected to have a measurable stronger or weaker effect on cognitive performance, resulting in a recognizable correlation (the former rat would have been expected to perform better than the latter in testing).

We did not observe a difference in PSD95 levels between treated and untreated animals. A possible explanation for this result may be reconduced to the inedaquecy of the method used. Western blot allows only an overall quantitative assessment. It cannot provide information on protein location. Thus, any synaptic remodelling not involving a change in the amount of PSD95 would have gone undetected. Immunohistochemistry procedures will be considered for future analyses. Alternatively, PSD95 might not represent an effector of Pt and this natural compound might esplicate its action by orchestrating other scaffold proteins.

Among a variety of biological processes, aging significantly perturbs mitochondrial biogenesis, leading to drastic consequences for the organisms. Because of cellular homeostasis, it is reasonable to deduce that if biogenesis of mitochondria is not sustained also their degradation may be hindered, with a resulting high proportion of poorly functioning organelles. Our results show that animals treated with Pt tend to have a higher mitochondrial content and agree with our previous investigations, performed in cultured cells, denoting the ability of the natural compound to up-regulate PGC-1α, as assessed at the 24-hour time point. Nevertheless, we did not find evidence of autophagy up-regulation *in vivo*, suggesting that this process might be irrelevant in this context. This is rather surprising in view of the *in vitro* results and also because autophagy induction has been indicated as the mechanism responsible for the cognitive improvement afforded by spermidine in various models [62-64]. It should be noted however that LC3B lipidation was assessed after 20 days of Pt administration. By that time mitophagy might have been stimulated, eliminating defective mitochondria, only to be down-regulated once the mitochondrial population had returned to a normal level of efficiency. In future work it

may therefore be worthwhile to assess autophagy in Pt-receiving animals as a function of time.

Somewhat analogous considerations may actually apply to the determinations of ph-CREB. The phosphorylation of any protein is a dynamic process, and the levels of phosphoprotein may vary rather rapidly (for ph-CREB *in vitro* in our system see chapter 5, Fig. 8). In future work we may therefore want to define more precisely kinetic aspects *in vivo*.

Interestingly, most differences at the molecular level have been found specifically in the dentate gyrus, one of the cerebral region most affected by age. As next aim, in addition to improving statistics by adding more animals to the various experimental groups, we will try to understand why these effects are restricted to this area. Phosphodiesterase-1b has been found to be highly expressed in the dentate gyrus [65]. As demonstrated by Park et al. in 2012, Rv competitively inhibits several classes of PDEs [66]. Considering the high structural analogy with Pt, it is logical to suppose that the two molecules may show similar properties. Indeed, I also obtained indications of inhibition of overall PDE activity by Pt (chapt. 5, Fig. 10), and FRET-sensor based analyses suggest that it is able to increase cAMP concentration thorugh inhibition of PDEs. Thus, the elevated expression of PDE-1b and the dentate gyrus-restricted action of Pt may be interlinked.

References

1. Fontana, L. and L. Partridge, *Promoting health and longevity through diet: from model organisms to humans.* Cell, 2015. **161**(1): p. 106-18.
2. Harmell, A.L., D. Jeste, and C. Depp, *Strategies for successful aging: a research update.* Curr Psychiatry Rep, 2014. **16**(10): p. 476.
3. Miller, M.G. and B. Shukitt-Hale, *Berry fruit enhances beneficial signaling in the brain.* J Agric Food Chem, 2012. **60**(23): p. 5709-15.
4. Pribis, P. and B. Shukitt-Hale, *Cognition: the new frontier for nuts and berries.* Am J Clin Nutr, 2014. **100 Suppl 1**: p. 347s-52s.
5. Subash, S., et al., *Neuroprotective effects of berry fruits on neurodegenerative diseases.* Neural Regen Res, 2014. **9**(16): p. 1557-66.
6. Murphy, T., G.P. Dias, and S. Thuret, *Effects of diet on brain plasticity in animal and human studies: mind the gap.* 2014. **2014**: p. 563160.
7. Cirmi, S., et al., *Neurodegenerative Diseases: Might Citrus Flavonoids Play a Protective Role?* Molecules, 2016. **21**(10).
8. Orhan, I.E., et al., *Flavonoids and dementia: an update.* Curr Med Chem, 2015. **22**(8): p. 1004-15.
9. Kulkarni, S.S. and C. Canto, *The molecular targets of resveratrol.* Biochim Biophys Acta, 2015. **1852**(6): p. 1114-23.
10. Vauzour, D., *Effect of flavonoids on learning, memory and neurocognitive performance: relevance and potential implications for Alzheimer's disease pathophysiology.* J Sci Food Agric, 2014. **94**(6): p. 1042-56.
11. Stepanic, V., et al., *Selected attributes of polyphenols in targeting oxidative stress in cancer.* Curr Top Med Chem, 2015. **15**(5): p. 496-509.
12. Zheng, L.F., et al., *DNA damage induced by resveratrol and its synthetic analogues in the presence of Cu (II) ions: mechanism and structure-activity relationship.* Free Radic Biol Med, 2006. **41**(12): p. 1807-16.
13. Bayele, H.K., E.S. Debnam, and K.S. Srai, *Nrf2 transcriptional derepression from Keap1 by dietary polyphenols.* Biochem Biophys Res Commun, 2016. **469**(3): p. 521-8.
14. Moosavi, F., et al., *Modulation of neurotrophic signaling pathways by polyphenols.* Drug Des Devel Ther, 2016. **10**: p. 23-42.
15. Kansanen, E., et al., *The Keap1-Nrf2 pathway: Mechanisms of activation and dysregulation in cancer.* Redox Biol, 2013. **1**: p. 45-9.
16. Vendrame, S. and D. Klimis-Zacas, *Anti-inflammatory effect of anthocyanins via modulation of nuclear factor-kappaB and mitogen-activated protein kinase signaling cascades.* Nutr Rev, 2015. **73**(6): p. 348-58.
17. Basu, A., et al., *Strawberry as a functional food: an evidence-based review.* Crit Rev Food Sci Nutr, 2014. **54**(6): p. 790-806.
18. Chu, A.J., *Antagonism by bioactive polyphenols against inflammation: a systematic view.* Inflamm Allergy Drug Targets, 2014. **13**(1): p. 34-64.
19. De Luca, F., *Role of Nuclear Factor Kappa B (NF-kappaB) in Growth Plate Chondrogenesis.* Pediatr Endocrinol Rev, 2016. **13**(4): p. 720-30.
20. Mitchell, S. and J. Vargas, *Signaling via the NFkappaB system.* 2016. **8**(3): p. 227-41.
21. Hoensch, H. and R. Oertel, *[Anti-inflammatory effects of tea-flavonoids].* Dtsch Med Wochenschr, 2012. **137**(51-52): p. 2738-40.
22. Ushikubo, H., et al., *3,3',4',5,5'-Pentahydroxyflavone is a potent inhibitor of amyloid beta fibril formation.* Neurosci Lett, 2012. **513**(1): p. 51-6.
23. Meng, P., et al., *Carnosic acid attenuates apoptosis induced by amyloid-beta 1-42 or 1-43 in SH-SY5Y human neuroblastoma cells.* Neurosci Res, 2015. **94**: p. 1-9.

24. Stefani, M. and S. Rigacci, *Beneficial properties of natural phenols: highlight on protection against pathological conditions associated with amyloid aggregation.* Biofactors, 2014. **40**(5): p. 482-93.
25. Macedo, D., et al., *(Poly)phenols protect from alpha-synuclein toxicity by reducing oxidative stress and promoting autophagy.* Hum Mol Genet, 2015. **24**(6): p. 1717-32.
26. Jang, S.W., et al., *A selective TrkB agonist with potent neurotrophic activities by 7,8-dihydroxyflavone.* Proc Natl Acad Sci U S A, 2010. **107**(6): p. 2687-92.
27. Yu, Q., et al., *Protection of spiral ganglion neurons from degeneration using small-molecule TrkB receptor agonists.* J Neurosci, 2013. **33**(32): p. 13042-52.
28. Chai, L., et al., *Scutellarin and caffeic acid ester fraction, active components of Dengzhanxixin injection, upregulate neurotrophins synthesis and release in hypoxia/reoxygenation rat astrocytes.* J Ethnopharmacol, 2013. **150**(1): p. 100-7.
29. Xu, S.L., et al., *Flavonoids induce the synthesis and secretion of neurotrophic factors in cultured rat astrocytes: a signaling response mediated by estrogen receptor.* Evid Based Complement Alternat Med, 2013. **2013**: p. 127075.
30. Souza, L.C., et al., *Flavonoid Chrysin prevents age-related cognitive decline via attenuation of oxidative stress and modulation of BDNF levels in aged mouse brain.* Pharmacol Biochem Behav, 2015. **134**: p. 22-30.
31. Pan, M., et al., *Effects of genistein and daidzein on hippocampus neuronal cell proliferation and BDNF expression in H19-7 neural cell line.* J Nutr Health Aging, 2012. **16**(4): p. 389-94.
32. Zhang, F., et al., *Resveratrol promotes neurotrophic factor release from astroglia.* Exp Biol Med (Maywood), 2012. **237**(8): p. 943-8.
33. Zhang, F., et al., *Resveratrol Produces Neurotrophic Effects on Cultured Dopaminergic Neurons through Prompting Astroglial BDNF and GDNF Release.* Evid Based Complement Alternat Med, 2012. **2012**: p. 937605.
34. Liu, R., et al., *The anti-amnesic effects of luteolin against amyloid beta(25-35) peptide-induced toxicity in mice involve the protection of neurovascular unit.* Neuroscience, 2009. **162**(4): p. 1232-43.
35. Azzolini, M., et al., *Pharmacokinetics and tissue distribution of pterostilbene in the rat.* Mol Nutr Food Res, 2014. **58**(11): p. 2122-32.
36. Chang, J., et al., *Low-dose pterostilbene, but not resveratrol, is a potent neuromodulator in aging and Alzheimer's disease.* Neurobiol Aging, 2012. **33**(9): p. 2062-71.
37. Kida, S. and T. Serita, *Functional roles of CREB as a positive regulator in the formation and enhancement of memory.* Brain Res Bull, 2014. **105**: p. 17-24.
38. Kandel, E.R., *The molecular biology of memory: cAMP, PKA, CRE, CREB-1, CREB-2, and CPEB.* Mol Brain, 2012. **5**: p. 14.
39. Silva, A.J., et al., *CREB and memory.* Annu Rev Neurosci, 1998. **21**: p. 127-48.
40. Sakamoto, K., K. Karelina, and K. Obrietan, *CREB: a multifaceted regulator of neuronal plasticity and protection.* J Neurochem, 2011. **116**(1): p. 1-9.
41. Cheng, A., Y. Hou, and M.P. Mattson, *Mitochondria and neuroplasticity.* ASN Neuro, 2010. **2**(5): p. e00045.
42. Zhang, L., *Voluntary oral administration of drugs in mice.* 2011.
43. Dominguez, G., et al., *Rescuing prefrontal cAMP-CREB pathway reverses working memory deficits during withdrawal from prolonged alcohol exposure.* Brain Struct Funct, 2014.
44. Ennaceur, A. and J. Delacour, *A new one-trial test for neurobiological studies of memory in rats. 1: Behavioral data.* Behavioural Brain Research, 1988. **31**(1): p. 47-59.

45. De Rosa, R., et al., *Intranasal administration of nerve growth factor (NGF) rescues recognition memory deficits in AD11 anti-NGF transgenic mice.* Proc Natl Acad Sci U S A, 2005. **102**(10): p. 3811-6.
46. Hasan, M.R., et al., *Effect of HDAC inhibitors on neuroprotection and neurite outgrowth in primary rat cortical neurons following ischemic insult.* Neurochem Res, 2013. **38**(9): p. 1921-34.
47. Diamond, A., *Executive functions.* Annu Rev Psychol, 2013. **64**: p. 135-68.
48. Thomas, S.A., *Neuromodulatory signaling in hippocampus-dependent memory retrieval.* Hippocampus, 2015. **25**(4): p. 415-31.
49. Shoji, H., et al., *T-maze forced alternation and left-right discrimination tasks for assessing working and reference memory in mice.* J Vis Exp, 2012(60).
50. Balderas, I., C.J. Rodriguez-Ortiz, and F. Bermudez-Rattoni, *Consolidation and reconsolidation of object recognition memory.* Behav Brain Res, 2015. **285**: p. 213-22.
51. Barker, G.R. and E.C. Warburton, *When is the hippocampus involved in recognition memory?* J Neurosci, 2011. **31**(29): p. 10721-31.
52. Preston, A.R. and H. Eichenbaum, *Interplay of hippocampus and prefrontal cortex in memory.* Curr Biol, 2013. **23**(17): p. R764-73.
53. Frick, K.M., *Epigenetics, oestradiol and hippocampal memory consolidation.* J Neuroendocrinol, 2013. **25**(11): p. 1151-62.
54. Silingardi, D., et al., *ERK pathway activation bidirectionally affects visual recognition memory and synaptic plasticity in the perirhinal cortex.* Front Behav Neurosci, 2011. **5**: p. 84.
55. Balderas, I., C.J. Rodriguez-Ortiz, and F. Bermudez-Rattoni, *Retrieval and reconsolidation of object recognition memory are independent processes in the perirhinal cortex.* Neuroscience, 2013. **253**: p. 398-405.
56. Hagihara, H., et al., *Dissection of hippocampal dentate gyrus from adult mouse.* J Vis Exp, 2009(33).
57. Panja, D. and C.R. Bramham, *BDNF mechanisms in late LTP formation: A synthesis and breakdown.* Neuropharmacology, 2014. **76 Pt C**: p. 664-76.
58. Leal, G., D. Comprido, and C.B. Duarte, *BDNF-induced local protein synthesis and synaptic plasticity.* Neuropharmacology, 2014. **76 Pt C**: p. 639-56.
59. Sheng, M. and C. Sala, *PDZ domains and the organization of supramolecular complexes.* Annu Rev Neurosci, 2001. **24**: p. 1-29.
60. Meyer, D., T. Bonhoeffer, and V. Scheuss, *Balance and stability of synaptic structures during synaptic plasticity.* Neuron, 2014. **82**(2): p. 430-43.
61. Barth, S., D. Glick, and K.F. Macleod, *Autophagy: assays and artifacts.* J Pathol, 2010. **221**(2): p. 117-24.
62. Gupta, V.K., et al., *Restoring polyamines protects from age-induced memory impairment in an autophagy-dependent manner.* Nat Neurosci, 2013. **16**(10): p. 1453-60.
63. Sigrist, S.J., et al., *Spermidine-triggered autophagy ameliorates memory during aging.* Autophagy, 2014. **10**(1): p. 178-9.
64. Marino, G., et al., *Caloric restriction mimetics: natural/physiological pharmacological autophagy inducers.* Autophagy, 2014. **10**(11): p. 1879-82.
65. Lein, E.S., X. Zhao, and F.H. Gage, *Defining a molecular atlas of the hippocampus using DNA microarrays and high-throughput in situ hybridization.* J Neurosci, 2004. **24**(15): p. 3879-89.
66. Park, S.J., et al., *Resveratrol ameliorates aging-related metabolic phenotypes by inhibiting cAMP phosphodiesterases.* Cell, 2012. **148**(3): p. 421-33.

Abbreviations:

ACN: acetonitrile (CH_3CN)

AMPK: 5'-adenosine monophosphate (AMP)-activated protein kinase

ARE: antioxidant response element

ATP: Adenosine triphosphate

AUC: area under the curve

BDNF: brain-derived neurotrophic factor

BSA: bovine serum albumin

CaMK: Ca^{2+}/Calmodulin-dependent protein kinase

cAMP: cyclic AMP

CBP: CREB binding protein (also called CREBBP)

C_{max}: maximal concentration

ColVI: collagen VI

COX: cyclooxygenase

CREB: cAMP response element-binding protein

CRISPR-CAS9: clustered regularly interspaced short palindrome repeats-CRISPR associated protein 9 nuclease

CsH: cyclosporine H

DEPTOR: domain-containing mTOR-interacting protein

DI: discrimination index

DMSO: dimethyl sulfoxide

EPAC: exchange protein activated by cAMP

EtOAc: ethyl acetate

EtOH: ethanol

GAPDH: Glyceraldehyde 3-phosphate dehydrogenase

GCL: glutamate-cysteine ligase

GFP: green fluorescence protein

GSTs: glutathione S transferases

JNK: c-Jun N-Terminal kinase

H30-FRET: epac-H30 Fluorescence Resonance Energy Transfer

HBSS: Hank's balanced salt solution

HMOX1: heme oxygenase 1

HPF: hours post fertilization

HPLC/UV: high performance liquid chromatography/UV

IBMX: 3-isobutyl-1-methylxanthine

IkB: inhibitor of kappa B

IKK: IκB kinase

LAT: L-type aminoacids transporter

LKB: liver kinase B

LC3: Microtubule-associated protein 1A/1B-light chain 3

LOX: lypoxygenases

MAPK: mitogen-activated protein kinases

MLST8: mammalian lethal with SEC13 protein 8

mTORC1: mammalian target of rapamycin complex 1

NADP: nicotinamide adenine dinucleotide phosphate

NF-kB: nuclear factor kappa B

NMR: nuclear magnetic resonance

NGF: nerve growth factor

NT3: neurotrophin 3

NT4: neurotrophin 4

NQO1: dihydronicotinamide riboside quinone reductase 1

Nrf2/Keap1: nuclear factor erythroid 2 [NF-E2]-related factor 2/Kelch-like erythroid cell-derived protein with CNC homology [ECH]-associated protein 1

OCT: object in context test

ORT: object recognition test

Pd/C: palladium/carbon

PEG: polyethylenglicol

PDE: phosphodiesterase

PGC-1α: peroxisome proliferator-activated receptor gamma coactivator 1-alpha

PKA: protein kinase A

PRAS: proline-rich AKT substrate

PSD95: postsynaptic density protein 95

PPAR: peroxisome proliferator-activated receptor

Pt: Pterostilbene

RAPTOR: regulatory-associated protein of mTOR

RIPA: radio immune assay (buffer)

ROI: regions of interest

ROS: reactive oxygen species

RT-qPCR: quantitative reverse transcription PCR

Rv: Resveratrol

SEM: standard error of the mean

S6: ribosomal protein S6

TALEN: transcription activator-like effector nuclease

TBS(T): tris buffered saline (Tween)

TFA: trifluoroacetic acid

TFEB: transcription factor EB

TrkB: tropomyosin-related kinase receptor B

TSC: tuberous sclerosis protein

UPS: ubiquitine proteasome system

ZNF: zinc finger nuclease

Ringraziamenti

Finita la lettura di una tesi di dottorato in biologia cellulare credo emerga chiaramente la complessità di ogni organismo vivente e quanto, ancor di più, lo siano i meccanismi molecolari che ne permettono il suo funzionamento. Ritengo tuttavia che ciascuno di noi non sia costituito solo da atomi, molecole, cellule e tessuti. Noi tutti viviamo principalmente di sentimenti ed emozioni. Così, quasi alla fine di questo mio percorso, desidero ringraziare coloro i quali, nel corso di questi anni, mi hanno regalato in un modo o nell'altro forti sensazioni, e chi ha contribuito alla mia crescita lavorativa.

Un primo grazie va al Dott. Mario Zoratti, per le possibilità che mi ha dato e per la professionalità con la quale mi ha guidata in un ambiente di lavoro sereno come pochi. A Lui va tutta la mia stima.

Grazie alla Dott.ssa Lucia Biasutto, altrettanto preziosa per la mia formazione scientifica per la Sua preparazione e competenza.

Grazie a Lino, compagno di un'avventura che vorrei potesse non finire mai. Grazie per le risate, gli scherzi, i giochi e soprattutto per avermi spronata a credere in me stessa ed aver tirato fuori il meglio di me. Senza te oggi non sarei quel che sono.

Grazie a Manu e Lù per l'affetto e la pazienza che mi hanno dimostrato. Non è necessario avere gli stessi gruppi sanguigni per essere sorelle, perché questo è ciò che voi rappresentate per me. A voi auguro un futuro radioso e pieno delle più grandi soddisfazioni.

Grazie a Cisco, per riuscire a capire "*quando rido senza muovere il mio viso o piango senza un grido*", per essere sempre al mio fianco e non abbandonarmi mai.

Grazie a mamma e papà, per avermi insegnato a camminare a testa alta ricordandomi sempre di essere umile. Insieme a Ciccio, in questi anni di lontananza, siete sempre riusciti a far pervenire il vostro amore e non una sola sera è passata senza che i miei occhi si addormentassero immaginando di essere a casa.

Grazie di cuore ad Antonio, al quale dedico la mia tesi e persona che più di ogni altra ha permesso che tutto ciò si realizzasse. "*Non accadrà mai, comunque si svolga la nostra vita, che nel momento in cui tu mi chiami mi trovi sorda al tuo appello. Mai!*"

Infine, grazie a tutti coloro i quali hanno contribuito alla realizzazione di questo progetto: la Prof. Cristina Paradisi, la Prof. Natascia Tiso ed il Prof. Paolo Bernardi ed i loro rispettivi gruppi di ricerca dell'Università degli Studi di Padova. La Prof. Nicoletta Berardi

ed il Dott. Alessandro Sale dell'Università degli Studi di Firenze e dell'Istituto di Neuroscienze del Consiglio Nazionale delle Ricerche insieme ai loro collaboratori.
Scriveva William Shakespeare: "*siamo fatti della stessa sostanza di cui sono fatti i sogni*".
Uno dei miei, si è appena avverato.